MUSCLE ENERGETICS AND AGEING IN THE CONTEXT OF

RYR1 VARIANTS

Katie Mhairi Nicoll Baines

Submitted in accordance with the requirements for the degree of Doctor

of Philosophy

University of Leeds

Faculty of Biological Sciences

School of Biomedical Sciences

April 2017

Declaration

The candidate confirms that the work submitted is their own and that appropriate credit has been given where reference has been made to the work of others.

This copy has been supplied on the understanding that it is copyright material and that no quotation from the thesis may be published without proper acknowledgement.

The right of Katie Nicoll Baines to be identified as Author of this work has been asserted by her in accordance with the Copyright, Designs and Patents Act 1988.

Acknowledgements

The nature of the work carried out in this project has provided me with the opportunity to work in a number of laboratories and with a lot of fantastic people. My home for the last four years has been the Leeds MH Unit. The staff in the Leeds MH Unit have provided a lot of support throughout my PhD. Professor Phil Hopkins, head of the unit, provided funding to carry out the gene expression chapter, and was an invaluable resource of knowledge on all things relating to patients and anaesthesia. He also made it possible for me to attend the ARS, EMHG and AUA conferences to have the opportunity to present my work. Miss Catherine Daly must be acknowledged for her tireless patience when dealing with my Database queries and ensuring that the lab runs so smoothly. Dr Dorota Miller taught me how to do TaqMan assays, RNA extraction and reverse transcription and provided the Affymetrix data for chapter 3. Miss (soon to be Dr) Lois Gardner, was a truly a stellar office-mate, she fuelled my tea addiction and listened to me vent my frustrations. Finally, and most importantly, I must express the utmost gratitude to my supervisor Dr Marie-Anne Shaw. She has provided unfailing support throughout my entire 4 years at Leeds. Dr Shaw has always been there to discuss my project and help me work through issues that have arisen. I have so much appreciation for the effort that she put into improving my abilities as a scientist.

For the work carried out in chapter 2 I was based in Professor Ian Hope's lab. Ian personally took the time to teach me how to handle *C. elegans* and I must thank him for his patience and support in helping me learn the principles of recombineering and genetic crosses involving hermaphrodites. Towards the end of my time in the Hope

lab, the group expanded and I have had the pleasure of working alongside Rob, David, Elpi, Brittany and Celia. I am particularly excited to see how Brittany and Celia's work progresses in continuing what I started.

I also spent time working with Dr John Boyle in the school of Biomedical Sciences, carrying out the work in chapter 4. I must thank him for starting the experimental elements of this work and providing me with ongoing lab support and advice on the respirometry protocol. The rest of my PhD research was carried out in the Askew lab in Sport and Exercise Science, to achieve the work that makes up chapter 5 of this thesis. Dr Graham Askew, as my co-supervisor, was invaluable in the building of the thermopile apparatus and showed me everything about how it works. He also carried out a number of the dissections on mice (thanks go to Pierce Mullen from the Deuchars lab for supplying the leg muscles from old mice) used to obtain preliminary data for this project. I must also thank the other lab members, Tom, Laura, Alex and Roger for their additional support with this work and just being generally hilarious and wonderful all the time.

The sheer volume of data in chapter 3 provided a number of analytical challenges for me. With help from Dr Alastair Droop, I was able to streamline the process and have learnt a lot about coding in R. Advice from Dr Josie Hayes was also essential in determining the predictive models and input from Dr Richard Gunton enabled me to understand the loop function in R.

I might never have been a PhD student at Leeds had it not been for the Anatomy Demonstrating Studentship that I was awarded that provided me with the support to

Abstract

In aged muscle, from humans and mice, the ryanodine receptor (RyR1) is leaky, leading to increased levels of resting Ca^{2+} in the myoplasm. This is also a feature of skeletal muscle disorders caused by variants in RyR1 such as malignant hyperthermia (MH), central core disease (CCD), exertional heat illness (EHI) and late-onset axial myopathy (LOAM). Elevated Ca^{2+} is damaging to mitochondria, leading to production of reactive oxygen and nitrogen species associated with MH susceptibility to inhalational anaesthetics. Mice with Ryr1 variants show premature muscle ageing and highlight the cycle of inefficient calcium handling and oxidative damage to mitochondria that impairs skeletal muscle energetics. *Caenorhabditis elegans* models of MH CCD EHI and LOAM variants, both homozygous and heterozygous forms, showed increased sensitivity to halothane. Altered caffeine sensitivity was evident in MH and CCD models, and at very high concentrations in EHI models. Strains with RyR1 variants exhibit age-related accelerated myosin disorganisation. Whole genome Affymetrix arrays revealed genes and pathways correlated with skeletal muscle ageing and MH. Of additional genes of interest investigated *UNC13, CASQ1, ORAI1, MCU* and *MICU1* showed altered expression with age. Array data from blood has been used to identify a signature for MH susceptibility. There is loss of mitochondrial membrane integrity and alteration in mitochondrial number in MH. New apparatus, capable of quantifying heat produced during muscle contraction, has enabled calculation of skeletal muscle efficiency. Preliminary data indicates that there was loss of skeletal muscle efficiency in aged muscle from wild type mice. This work provides new information on the role of *RYR1* variants in skeletal muscle ageing and the importance of calcium handling in muscle energetics.

List of abbreviations

ADP	Adenosine diphosphate
AIC	Akaike information criterion
AICAR	5-aminoimidazole-4-carboxamide ribonucleoside
ALS	Amyotrophic lateral sclerosis
ATP	Adenosine triphosphate
bp	base pair
B2M	Beta-2-microglobulin
CALM1	Calmodulin 1
CAPN3	Calpain 3
CASQ1	Calsequestrin 1
CAV1	Caveolin 1
$Ca_v1.1$	Alpha subunit of the DHPR
CCD	Central core disease
cDNA	Complementary deoxyribonucleic acid
CHCT	Caffeine/halothane contracture test
CHERP	Calcium homeostasis endoplasmic reticulum protein
CRU	Calcium release unit
DHPR	Dihydropyrine receptor
DMD	Duchenne muscular dystrophy
DMSO	Dimethyl sulfoxide
dNTPs	Deoxyribonucleotide triphosphates
DTNA	Dystrobrevin alpha

EC	Excitation contraction
ECCE	Excitation-coupled calcium entry
EDL	Extensor digitorum longus
EHI	Exertional heat illness
EHS	Exertional heat stroke
EMHG	European malignant hyperthermia group
ER	Endoplasmic reticulum
ETC	Electron transport chain
FCR	Flux control ratio
FDB	Flexor digitorum brevis
GAPDH	Glyceraldehyde 3-phosphate dehydrogenase
GFP	Green fluorescent protein
GOI	Gene of interest
GTEx	Genotype-tissue expression
HPRT1	Hypoxanthine-guanine phosphoribosyltransferase
HSPA4	Heat-shock protein 4
INM	Institute of Naval Medicine
IVCT	*In vitro* contracture test
kb	kilobase
KCNA1	Potassium voltage-gated channel
LASSO	Least Absolute Shrinkage and Selection Operator
LB	Lysogeny broth
LOAM	Late onset axial myopathy
MCU	Mitochondrial Calcium Uniporter
MH	Malignant hyperthermia

MHE	Malignant hyperthermia equivocal
MHN	Malignant hyperthermia normal/negative
MHS/MHShc	Malignant hyperthermia susceptible
MHSc	Malignant hyperthermia susceptible for caffeine
MHSh	Malignant hyperthermia susceptible for halothane
MHS-	Malignant hyperthermia susceptible with no causative mutation in *RYR1*
MHS+	Malignant hyperthermia susceptible with causative mutation in *RYR1*
MICU1	Mitochondrial induced calcium uptake protein 1
NFKB1	Nuclear factor Kappa B1
NGM	Nematode Growth Medium
NGS	Next generation sequencing
NIH	National Institutes of Health
NSLB	No-salt lysogeny broth
OXPHOS	Oxidative Phosphorylation
PCR	Polymerase chain reaction
qPCR	quantitative real-time polymerase chain reaction
RAD	Ras-related associated with diabetes
REM2	Ras-like GTP binding protein
RIN	RNA integrity number
RNS	Reactive nitrogen species
ROS	Reactive oxygen species
RPRL0	Ribosomal protein, large P0
RYR1	Ryanodine receptor isoform 1
SLC24A37	Solute carrier family 24A, member 37

SERCA	Sarco(endo)plasmic reticulum calcium ATPase
SOB	Super optimal broth
SOCE	Store operated calcium entry
SR	Sarcoplasmic reticulum
STIM1	Stromal interactin molecule 1
TBP	TATA-binding protein
TRPC3	Transient receptor protein 3
TPRC6	Transient receptor protein 6
T-tubule	Transverse tubule
UV	Ultra violet

Table of Contents

List of Figures

Chapter 2: A *Caenorhabditis elegans* model for studying *RYR1* variants and muscle ageing

List of Tables

Chapter 4: Basal oxidative phosphorylation and expression of genes implicated in mitochondrial dysfunction in malignant hyperthermia and in the context of ageing

Chapter 5: Development of a system for quantifying the effect of age on skeletal muscle energetics

1   General Introduction

It is estimated that by 2050 there will be over 1.5 billion people in the world over the age of 65, almost 1 billion more than in 2010 (United Nations, 2012). In the UK, between 1974 and 2014 the number of adults aged 75-84 years increased by 43% (Office for National Statistics, 2015). This increase in the size of our ageing population stimulates the need to better understand the underlying mechanisms of the ageing process so that in future we may better serve the needs of this population and provide the means to offset the physical and economic consequences of ageing.

Skeletal muscle comprises almost half of the human body mass and is vital for movement (Tyrovolas *et al.*, 2016). Sarcopenia, or skeletal muscle ageing, is a key component of the ageing process in humans. Deterioration of skeletal muscle has a considerable impact on human health and maintenance of skeletal muscle strength is considered of key importance for healthy ageing (McLeod *et al.*, 2016). Loss of mobility in particular is cited as one of the primary determinants of needing nursing home care in the US (Lang *et al.*, 2010). According to an estimate by the UK Department of Health the average cost of providing health services to people aged 85 and over is 3 times greater than for a person aged 65-74 years (House of Commons, 2015). A better understanding of the components of muscle ageing will provide greater chance of offsetting these costs to the UK and world economies.

Sarcopenia is characterised by degeneration of skeletal muscle whereby there is a reduction in mass, total aerobic capacity and the functional capacity of the muscle is

noticeably weakened (Nair, 2005; Lang *et al.*, 2010). These alterations in functional capacity or muscle quality cannot be simply explained by loss of muscle quantity but by examining a number of cellular processes such as denervation, mitochondrial dysfunction, inflammatory and hormonal changes as well as changes in muscle strength and rates of fatigue.

The decline in muscle mass begins at the fourth decade of life (Lexell *et al.*, 1988; Lindle *et al.*, 1997; Short *et al.*, 2004). As well as decreasing muscle mass with age, loss of muscle strength due to increased age also occurs as a result of decreased muscle-specific force (muscle force per cross-sectional area) (Delbono, 2002). Loss of muscle power and force with age have been well established in humans, with cross-sectional studies reporting declines of 20-40% knee extension strength comparing age groups of 20-40 and 70-90 years, with losses of greater than 50% in individuals over the age of 90 (Murray *et al.*, 1985). Similar losses in strength have been reported in elbow extension and grip (Doherty, 2003). Longitudinal studies have also highlighted the relationship between age and the loss of muscle power, citing declines of between 12 and 18% over the course of 10 years (Hughes *et al.*, 2001).

Factors implicated in the loss of contractile function, therefore compromising the energetic capacity of skeletal muscle, that occurs with age in humans, include:

- Decreased acto-myosin force and lowered cross-bridge stability (Lowe *et al.*, 2002)

- Defective excitation-contraction (EC) coupling (Payne & Delbono, 2004)

- Reduced capacity for regulation of Ca^{2+} levels (Weisleder *et al.*, 2006; Zhao *et al.*, 2008)

Age-related mitochondrial dysfunction (Rooyackers *et al.*, 1996) The metabolic cost of locomotion is increased in old adults compared to young adults (Mian *et al.*, 2006; Ortega & Farley, 2007). This increased cost results in muscle fatigue and therefore could be related to the higher incidence of falls in the elderly, the main cause of injury in over 70s. Low levels of activity are a major predictor of mortality (United Nations, 2007). This introduction will outline the process of EC coupling and mechanisms of calcium handling in skeletal muscle such as the role of calsequestrin, and store operated calcium entry, with particular focus on the role of the ryanodine receptor (RyR), the relationship between muscle disorders linked to *RYR1* variants and skeletal muscle ageing as well as the connection between calcium handling and mitochondrial function/dysfunction.

1.1 Calcium handling in skeletal muscle

Regulation of intracellular calcium levels is involved in a number of cellular processes such as cell growth, mitochondrial function and muscle contraction (Berridge *et al.*, 2000; Fill & Copello, 2002). The large difference in calcium concentration between the cytosol (~100nM in most cells) and sites of calcium storage, endo/sarcoplasmic reticulum (ER/SR) (1-3mM in most cells), in conjunction with slow cytoplasmic diffusion rate make cells able to efficiently elevate local cytosolic calcium levels necessary for triggering biological processes (Berridge *et al.*, 2000).

1.1.1 Excitation contraction coupling

The process of EC coupling describes the conversion of an electrical stimulus into a mechanical response (Sandow, 1952) and is vital for muscle force production. It is the link between the depolarisation of the myocyte surface membrane *via* acetylcholine-

mediated propagation of an action potential at the neuromuscular junction and Ca^{2+} release from the sarcoplasmic reticulum (SR). It is dependent upon interaction between the L-type Ca^{2+} channel, the dihydropyridine receptor (DHPR), and the ryanodine receptor 1 (RyR1) channel (Ozawa, 2011). In skeletal muscle, transmission of the voltage sensor signal occurs through a protein-protein interaction between RyR1 and the II-III loop of the α_1 subunit of the dihydropyridine receptor (Ozawa, 2011) (Figure 1.1). This depolarisation-induced activation of RyR1 results in a ten-fold increase in intracellular free calcium concentration.

DHPR is a surface membrane, voltage-gated cation channel comprising four repeats of six membrane-spanning domains. In skeletal muscle this protein contains α-1, α-2/δ, β, γ subunits (Figure 1.1A). It is the α-1 subunit of the DHPR that is believed to play an important role in the process of transmitting the signal. This subunit is embedded in the membrane and contains the Ca^{2+} ion channel, the dihydropyridine binding site and the voltage sensor for EC coupling (Dolphin, 1999; Ahern $et\ al.$, 2001). More recently, it has also been indicated in the control of skeletal muscle mass and morphogenesis (Piétri-Rouxel $et\ al.$, 2010). The isoform of the α-1 subunit expressed in skeletal muscle is $Ca_{V1.1}$ (also known as α_{1S}). EC coupling is found to be absent in myocytes that do not express the DHPR α-1 subunit, providing evidence that this subunit is the voltage sensor essential for EC coupling (Adams $et\ al.$, 1990). Activation of RyR1, via its interaction with the DHPR, causes the channels to open and permit the influx of calcium ions from the SR to the myoplasm, unbinding the calcium ions from calsequestrin (CASQ1) (Figure 1.1B).
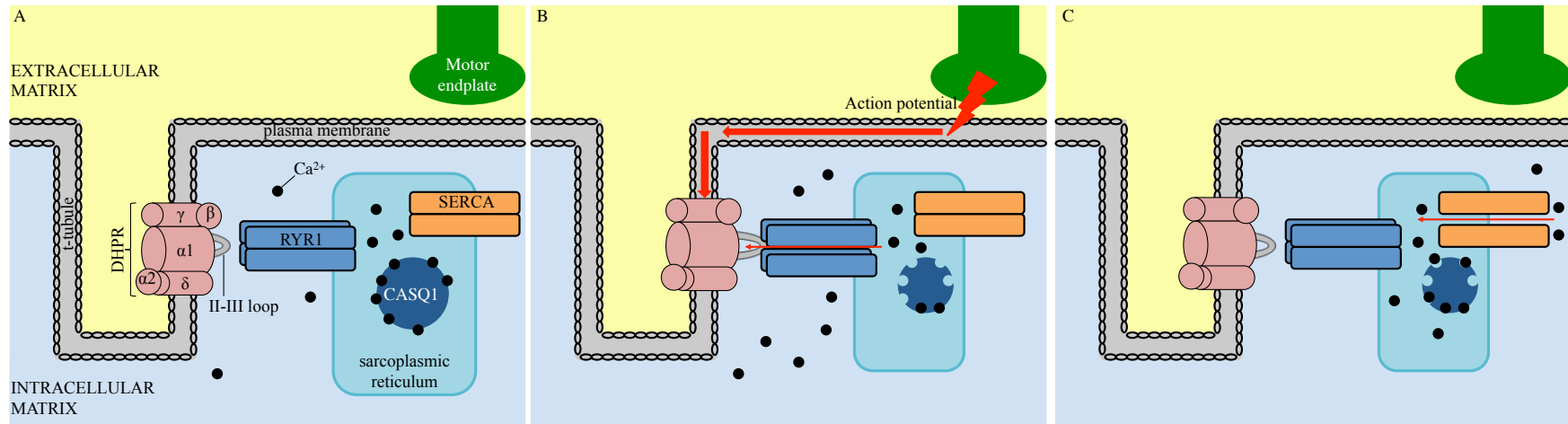
Figure 1.1 Diagram of EC coupling in skeletal muscle cell, depicting interaction between DHPR and RyR1 with calcium release from the SR. A: skeletal muscle in a relaxed state. Intracellular calcium levels are low, most is stored in the SR. B: an action potential is triggered at the motor endplate: the signal is transmitted along the plasma membrane to the t-tubule where it stimulates the DHPR. This results in interaction with RYR1 *via* the II-III loop triggering release of calcium from the SR (calcium is unbound from CASQ1) and leads to muscle contraction. C: the sarco(endo)plasmic reticulum ATPase (SERCA) pump actively transports calcium back into the SR, muscle contraction ends and calcium binds to CASQ1 again. Adapted from (Meissner & Lu, 1995; Lanner *et al.*, 2010)

1.1.2 Calsequestrin

Calsequestrin has a high storage capacity for Ca^{2+}, 40-50 moles of Ca^{2+} per mole of calsequestrin, and low binding affinity, which allows the rapid release and binding of Ca^{2+} (Royer & Ríos, 2009; Sanchez *et al.*, 2012). In normal muscle calsequestrin is always in equilibrium with the SR luminal $[Ca^{2+}]$. This allows the rapid release of large volumes of Ca^{2+} from the SR to drive muscle contraction during EC coupling (MacLennan & Wong, 1971). Calsequestrin does not have a specific calcium-binding site. Instead it structured as an electronegative net to which pairs of Ca^{2+} ions bind (Wang *et al.*, 1998). As SR luminal $[Ca^{2+}]$ rises calsequestrin has the ability to increase its binding capacity by sequentially dimerising and then polymerising which results in the formation of negatively charged pockets into which more Ca^{2+} ions can bind. At normal resting concentration of SR calcium (around 1mM), calsequestrin is present predominantly in the monomeric form (Beard *et al.*, 2004).

1.1.3 Cross-bridge cycling

Once calcium has been released into the myoplasm from the SR, following EC coupling, it binds to troponin alongside the actin filaments (Figure 1.2A) pulling the tropomyosin away from the myosin binding sites on the neighbouring actin filaments (Figure 1.2B).

6
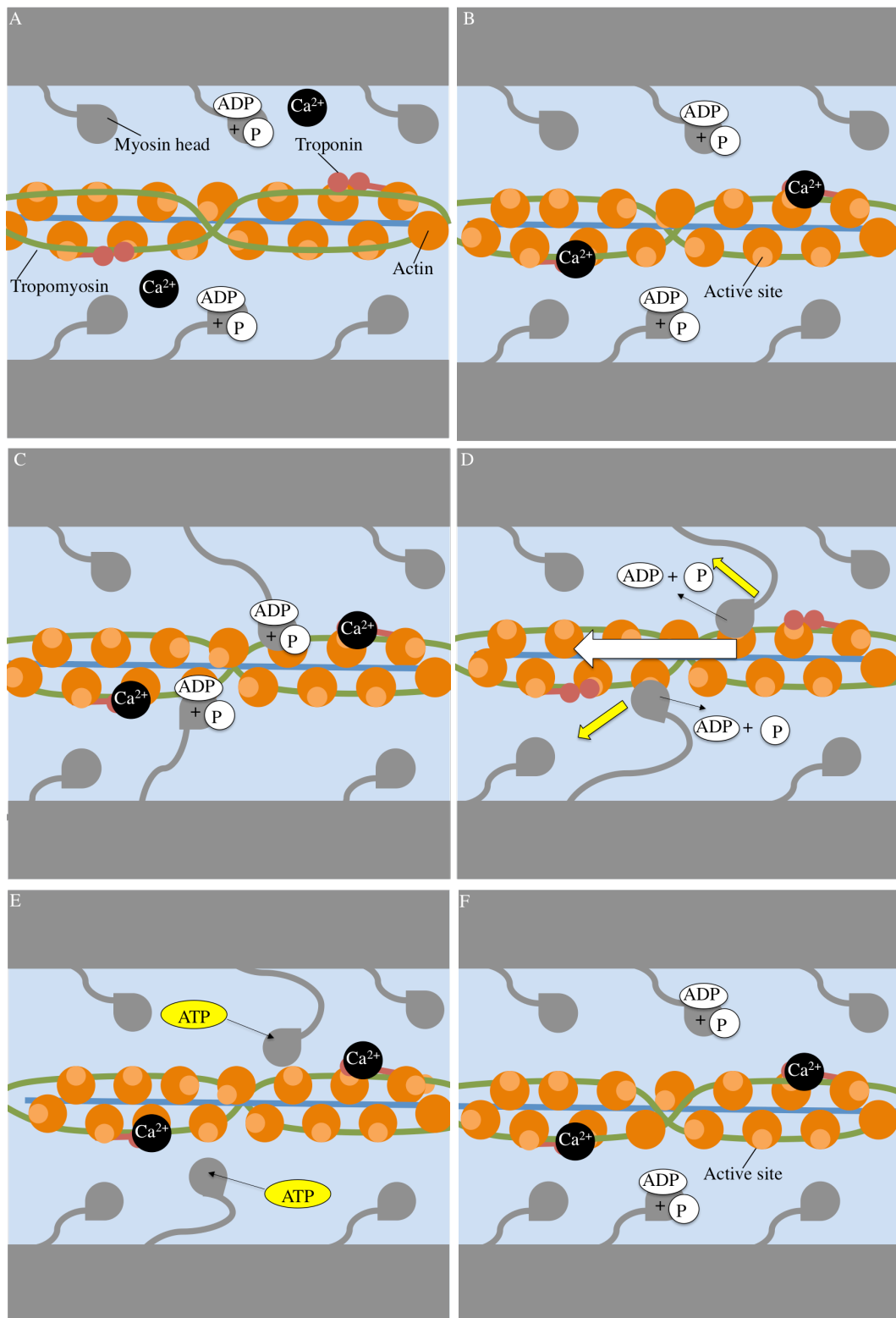
Figure 1.2 Utilisation of calcium and ATP during cross-bridge formation in skeletal muscle. A: Calcium is present in the overlap zone in the sarcomere, myosin in charged position, actin binding sites covered by tropo-myosin complex B: Calcium binds to troponin, weakening the troponin-tropomyosin complex and revealing the active sites on actin C: Myosin binds to actin forming cross-bridges, D: Energy stored in myosin head is released and the myosin head changes position. E: When ATP binds to the myosin head the actin-myosin bond is broken, the active site exposed and able to form another cross bridge F: Free myosin head splits ATP into ADP + P, released energy forces the myosin head back into charged position. Adapted from (Fitts, 2008; England & Loughna, 2013).

This uncovers the myosin cross-bridge binding sites on the actin filaments. Through the process of ATP hydrolysis and calcium cycling, myosin will now cycle through attached and detached states to actin (Figure 1.2A-F). This is known as 'cross bridge cycling'. If enough force develops to exceed the load, a concentric contraction is initiated whereby the muscle produces force during shortening.

During this contraction the interaction of actin and myosin results in the movement of actin towards the centre of the sarcomere, this contraction of the sarcomere will remain in a state of rigor unless sufficient ATP is present to bind to myosin. Simultaneously, calcium ions are actively pumped back into the SR by the sarco/endoplasmic reticulum calcium ATPase (SERCA) and they rebind to calsequestrin. This results in the troponin complex returning to its blocking position as it is no longer bound to calcium and tropomyosin returns to a position that covers the binding sites on actin. Cessation of cross-bridge cycling causes the sarcomeres to lengthen.

Alterations in the process of cross-bridge cycling are implicated in muscle disorders (Guellich *et al.*, 2014) and it was been speculated that deterioration of specific features of this cycle could contribute to muscle ageing (Brooks & Faulkner, 1988). It is clear that availability of ATP is an essential part of this process, therefore mitochondrial defects may have a role in muscle ageing. The mechanism of calcium handling in skeletal muscle is also complex, involving a number of interacting proteins.

The contractile elements of mammalian skeletal muscle, that utilise the calcium made available through EC coupling, are arranged in a striated pattern. Thin (comprised of actin, troponin and tropomyosin) and thick (comprised of myosin) filaments are

regularly spaced, comprising the sarcomere: the functional unit of muscle. A sarcomere is defined as the regions between two Z-lines at which the actin molecules are bound. One sarcomere contains an A-band where the thick and thin filaments overlap, a central M-line where the thick filaments meet and an I-band where there are only thin filaments (Figure 1.3).

RELAXED
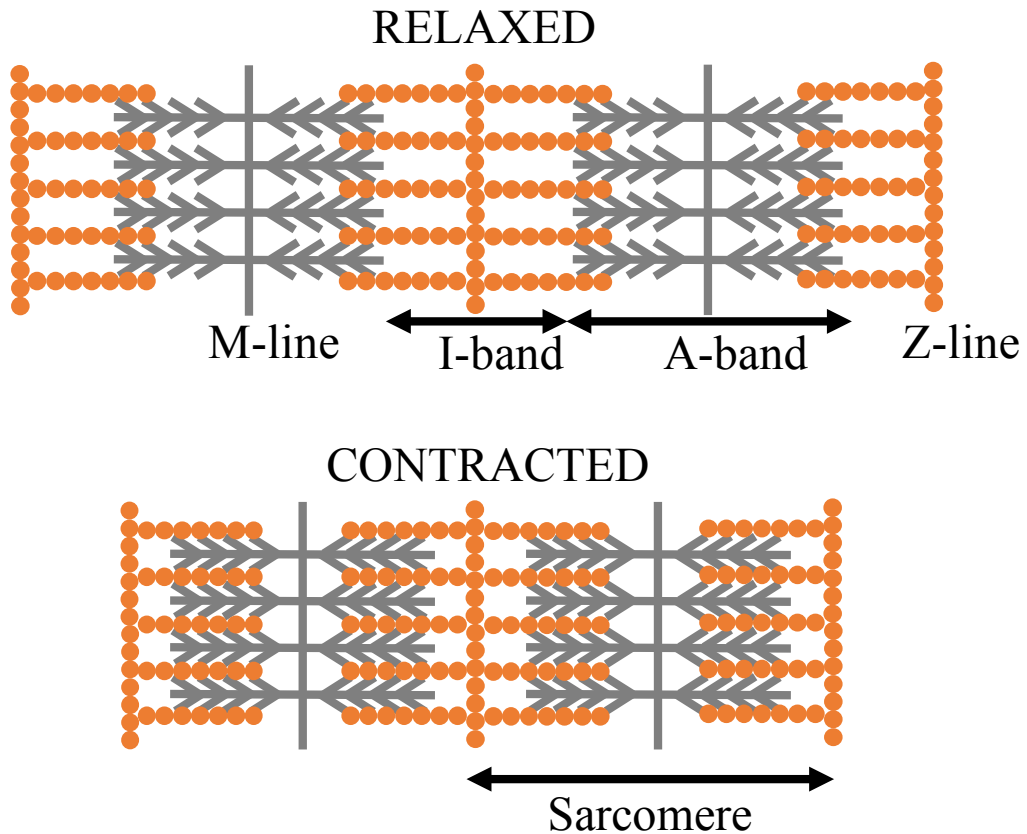
CONTRACTED

Figure 1.3 Schematic representation of skeletal muscle ultra-structure. Thick filaments are coloured grey; thin filaments are coloured orange. Adapted from (England & Loughna, 2013).

During contraction, the thin filaments slide over the thick filaments shortening the I-band. The availability of calcium ions and adenosine triphosphate (ATP) is essential to this process.

1.1.4 Store Operated Calcium Entry

Store operated calcium entry (SOCE) is the mechanism by which extracellular calcium can enter a skeletal muscle cell. It was first examined as the major process of calcium influx in non-excitable cell types such as lymphocytes (Feske *et al.*, 2006; Feske, 2007), with identification of stromal interactin molecule 1 (STIM1), located in the intracellular compartment, (Liou *et al.*, 2005) and calcium release-activated calcium channel protein 1 (Orai1), located in the plasma membrane, proteins as the main components of this process.

SOCE has been observed in neurones, cardiac muscle, smooth muscle (Paraekh & Putney, 2005) and skeletal muscle (Pan *et al.*, 2002; Launikonis *et al.*, 2003; Launikonis & Rios, 2007). Recent work has conclusively shown the importance of both STIM1 and Orai1 for SOCE function in skeletal muscle and showed that knock-down of either STIM1 or Orai1 does not compromise EC-coupling suggesting that the two processes are molecularly distinct (Lyfenko & Dirksen, 2008). In addition to Orai1, STIM1 has also been shown to interact with transient receptor potential cation (TRPC) channel proteins, suggesting that they may also have a role in SOCE (Rosenberg *et al.*, 2004; Sampieri *et al.*, 2005) (Figure 1.4A-C).
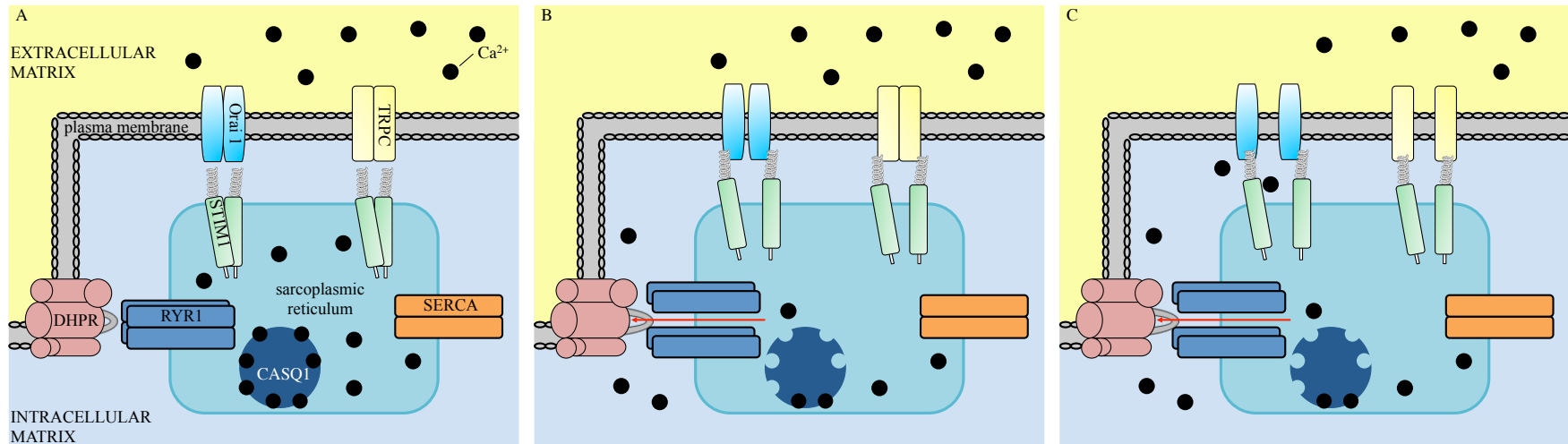
Figure 1.4 Proposed model for SOCE in skeletal muscle. A: At rest Orai1 and TRPC proteins are present within the plasma membrane of the myocyte, STIM1 proteins are located in throughout the SR. B: Depletion of calcium stores in the SR triggers the rearrangement of STIM1 channels close to the plasma membrane to allow interaction with Orai1 and TRPC. C: interaction of STIM1 and Orai1 or TRPC allows for entry of calcium from the extracellular matrix. Image devised based on information from (Lewis, 2007; Lyfenko & Dirksen, 2008; Kiviluoto *et al.*, 2011).

Expression of *STIM1* and *ORAI1* are high in skeletal muscle and depletion of the corresponding proteins is associated with skeletal myopathy (Stiber *et al.*, 2008; Vig *et al.*, 2008). These skeletal myopathies are characterised by loss of muscle fibre integrity, progressive muscle instability and structural abnormalities of the sarcomere (Völkers *et al.*, 2012). SOCE has also been found to be severely compromised in aged mouse skeletal muscle, indicating its role in the diminished capacity for calcium homeostasis associated with muscle ageing (Zhao *et al.*, 2008).

1.1.5 The Ryanodine Receptor

RyRs are the primary calcium release channel in striated muscle, first identified by Campbell and colleagues due to their high binding affinity with the plant alkaloid ryanodine (Campbell *et al.*, 1987). They comprise a family of poorly selective cation channels, which exhibit a slight preference towards divalent ions over monovalent ones (Lindsay *et al.*, 1991; Tinker *et al.*, 1992). Due to this poor selectivity, the channel is able to rapidly efflux large volumes of ions from the SR during EC coupling (see section 1.1.1 for full details). Mammals have 3 isoforms of RyR, which are found in different tissue types. RyR1 is found predominantly in skeletal muscle, RyR2 in cardiac muscle and RyR3 is found in the majority of tissue types but at relatively low expression levels compared to the other isoforms (Fill & Copello, 2002).

RYR1 was first cloned in 1990 and mapped onto chromosome 19q13.2 with a transcript of approximately 15,117 nucleotides (MacKenzie *et al.*, 1990). The gene contains 106 exons with alternative splicing possible at exons 70 and 83 and the full-length protein is composed of 5038 amino acid residues. The RyR1 protein comprises four identical monomers with a combined mass of ~550kDa forming the largest known ion channel (Hamada *et al.*, 2002).

Ca^{2+} regulation of RyR1 is achieved through binding of the ion to either the high-affinity divalent binding site (A-site) or the low-affinity divalent binding site (I-site). When Ca^{2+} occupies the A-site, the channel is activated, and when it occupies the I-site, it is inhibited (Meissner, 1994). The structure of RyRs consists of cytoplasmic and transmembrane regions, with the cytoplasmic region being responsible for sensing interactions with ions such as calcium (Meissner, 1994; Lanner *et al.*, 2010).

Until 2015, the highest resolution reconstruction for an intact RyR1 was 9.6Å (Serysheva *et al.*, 2008). While this provided information regarding the dimensions of the protein and approximated promotor boundaries it was not capable of isolating secondary structural elements or key domains (Zalk *et al.*, 2015). In early 2015, three groups independently exceeded this. The structure of the rabbit RyR1 has been solved at a resolution of 6.8Å, providing information regarding the calcium binding domain and demonstrating that it functions as a conformational switch that changes the shape of the channel to gate it (Efremov *et al.*, 2015). This result is supported by another study that also showed a unique domain within the transmembrane helices that suggests a mechanism for channel gating by calcium (Zalk *et al.*, 2015). The structure was also reported in complex with the folding chaperone FKBP12 at a resolution of 3.8Å and identified three previously unidentified domains: central, handle and helical (Yan *et al.*, 2015).

Pharmacological agents can also affect the function of RyR1. Ryanodine, the plant alkaloid after which the channel is named, affects channel function in a concentration-dependent manner. At nM concentrations ryanodine locks RyR1 in a half open state leading to massive muscle contractions whereas at μM concentrations it closes the

channel causing paralysis (Buck *et al.*, 1992). Caffeine, which has a low binding affinity to RyR1, causes conformational changes in the channel making it more sensitive to activation by calcium and voltage (Sitsapesan & Williams, 1990).

Progressive oxidation of the skeletal muscle ryanodine receptor occurs with increasing age resulting in a leaky channel that is therefore less efficient at the process of calcium handling (Jimenez-Moreno *et al.*, 2008; Andersson *et al.*, 2011). Leaky skeletal muscle ryanodine receptors are also a feature of myopathies caused by variants in *RYR1* (Cully & Launikonis, 2016). Increased calcium leak causes increased ROS production that in turn will result in oxidative damage to RyR1 (Andersson *et al.*, 2011; Görlach *et al.*, 2015).

1.2   RYR1 variants and associated myopathies

Human muscle disorders where myocyte calcium regulation is disrupted, such as MH, CCD, EHI and LOAM have been attributed to mutations in *RYR1* (Tong *et al.*, 1997; McCarthy *et al.*, 2000; Bouchama & Knochel, 2002; Robinson *et al.*, 2002; Robinson *et al.*, 2006; Jungbluth *et al.*, 2009; Nishio *et al.*, 2009; Loseth *et al.*, 2013).

1.2.1   Malignant Hyperthermia

MH is a pharmacogenetic disorder whereby volatile inhalational anaesthetics trigger a potentially lethal hypermetabolic reaction in susceptible individuals. The incidence of MH is difficult to estimate. Based on data from incidences of reactions during anaesthesia in North America it ranges from 1:5000, to 1:50000-100000 anaesthesias (Rosenberg *et al.*, 2007). However when factoring diagnostic and genetic data this estimate could be as high as 1:2000 (Monnier *et al.*, 2002).

The first case was documented in 1962, when a previously healthy 21 year old underwent surgery to repair a fractured tibia and fibula (Denborough *et al.*, 1962). Having reported to his surgeons that members of his family died during surgery under ether induced anaesthesia; the surgery went ahead using halothane instead. However, 10 minutes into the operation the patient began to exhibit the classical symptoms of what would become recognised as an MH reaction. Halothane application was removed and cooling procedures implemented resulting in recovery of the patient soon after.

The definition of an MH crisis has since been characterised to include a number of clinical features: masseter spasm, tachypnoea and tachycardia, increased temperature, generalised muscle rigidity, raised creatine kinase, rhabdomyolysis, hyperkalaemia, hypoxaemia and if not treated promptly an MH crisis is fatal (Hopkins, 2000; Rosenberg *et al.*, 2007). Onset of an MH episode can occur at any time during or immediately after anaesthesia. Hyperthermia occurs relatively late during an episode and can progress quicker than 1°C every 2.5 minutes reaching a maximum temperature of approximately 44°C, resulting in catastrophic and fatal organ failure. If untreated the high muscle metabolism can lead to hypoxia resulting in acidosis of body fluids (Nelson, 1990). As the episode progresses myocytes die when ATP levels are depleted and membrane integrity is compromised (Rosenberg *et al.*, 2007). This results in rhabdomyolysis, the breakdown of muscle fibres, releasing potassium and myoglobin into the blood, which cause hyperkalaemia, hepatic and renal failure and eventually death. An MH crisis does not necessarily include all the aforementioned symptoms and the severity can also vary greatly between patients. This is partly related to the duration of anaesthesia, type of anaesthetic used and inter-patient variability whereby

some individuals have reported normal reactions to anaesthesia on multiple occasions prior to displaying an MH reaction.

The symptoms of an MH episode are attributed to dysregulation of calcium handling in skeletal muscle (Hopkins, 2000). Approximately 70% of individuals suffering from MH exhibit a mutation in *RYR1* (Robinson *et al.*, 2006). These mutations make the RyR1 channel open more easily and close more slowly in response to certain chemical stimuli, such as halothane and caffeine. During an MH episode calcium homeostasis of the SR is disrupted. Inhalational anaesthetics trigger RyR1 and it opens without neural stimulation. This results in flooding of the myoplasm with Ca^{2+} resulting in uncontrolled muscle contraction. SERCA is constitutively activated and its activity increases as the cell attempts to re-establish the gradient across the SR membrane. The RyR1 channel is fixed in an open state making the action of SERCA futile (Robinson *et al.*, 2006). The increase in myocyte Ca^{2+} concentration also causes the up-regulation of mitochondrial ATP-synthase to supply the SR calcium pumps with ATP and results in the muscle entering a hypermetabolic state (Territo *et al.*, 2001).

It is important to note that manifestation of an MH reaction is not always consistent. There are documented cases of patients undergoing general anaesthesia on more than one occasion, prior to having an MH reaction and no common factor has been found that can explain this phenomenon (Halsall *et al.*, 1979). It is therefore essential that susceptibility to MH is based on a clear diagnostic test.

The primary method of diagnosing MH susceptibility is through the use of *in vitro* contracture testing (IVCT), procedures for which have been developed by the

European Malignant Hyperthermia Group (EMHG) (Ording *et al.*, 1997) and the North American Malignant Hyperthermia Group (NAMHG) (Larach, 1989). The NAMHG refer to their test as the caffeine halothane contracture test (CHCT). Both the IVCT and CHCT measure the contractile response of patients' muscle biopsies to halothane and caffeine. The CHCT diagnoses a patient as susceptible (MHS) when they exhibit a positive response to either trigger agent. Until May 2013 an MHS diagnosis under EMHG guidelines was given when both of the trigger agents provide a positive result and an MHN result if there is no response to the trigger agents, but with the addition of a third diagnosis; MH equivocal (MHE) when only one of the triggers provided a positive response. This third classification is primarily of interest for research purposes as it demonstrates complexity in the IVCT response. For diagnostic purposes, MHE=MHS. Following the 2013 EMHG conference it was decided that the 'equivocal' diagnosis would no longer be used as it is considered confusing and uninformative to patients. Nomenclature now used by the Leeds MH unit stipulates whether the test has resulted in an MHS (susceptible to both halothane and caffeine), an MHSh (susceptible to just halothane), an MHSc (susceptible to just caffeine, very rare) or an MHN (not susceptible to either trigger agent).

The protocol for the IVCT uses a viable muscle biopsy obtained from the *vastus medialis* muscle. The muscle is placed in a chamber containing oxygenated Krebs Hensleit solution, maintained at a temperature of 37°C. Static tests are performed on the muscle where it is exposed to increasing concentrations of a trigger agent: 0.25mM to 32mM caffeine and 0.5% to 2% v/v halothane. The successive concentration is added after the specimen has reached a contracture plateau from the previous stimulation (Figure 1.5A&B).

A dynamic halothane test is also executed, whereby the muscle specimen is exposed to the same incremental concentrations of halothane but they are added following cycles of contraction at a rate of 4mm/minute for 90 seconds. A diagnosis of MH susceptible (MHS) is defined by a sustained contracture of 0.2g at or below 2mM caffeine or 2% halothane for all tests. If this level of contracture is not reached, then the diagnosis is MH normal (MHN). The IVCT requires an invasive surgical procedure to retrieve the muscle tissue for testing, and can only be carried out at specialist test centres (Leeds is the UK testing centre for MH). It is considered to have a high diagnostic sensitivity: 99% (95% confidence interval 94.8-100%) and a satisfactory specificity of 93.6% (95% confidence interval 89.2-96.5%) (Ording *et al.*, 1997). The CHCT has a sensitivity of 97% (95% confidence interval 84-100%) and a specificity of 78% (95% confidence interval 69-85%) (Allen *et al.*, 1998).
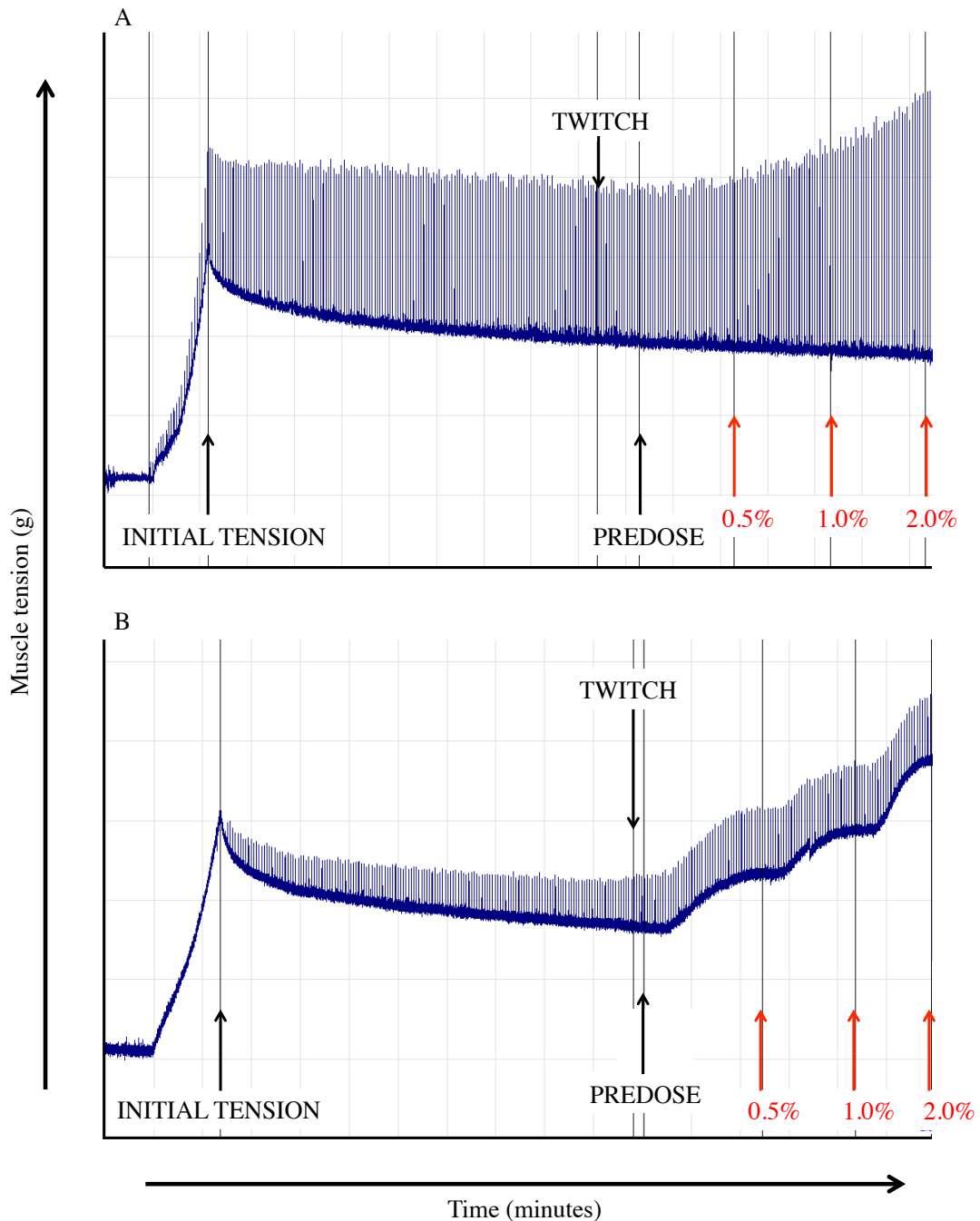
Figure 1.5 Example traces from halothane IVCT. A: Example of a trace from a muscle sample that tested negative for MH. For the range of halothane concentrations administered no increase in muscle tension is observed, B: Example trace from a muscle sample that tested positive for MH. Upon addition of 0.5% halothane muscle tension rises and continues to do so across the range of concentrations applied.

The first MH related *RYR1* mutation was identified in 1990 and early studies found that MH associated mutations clustered in three regions of the gene: the C-terminal, N-terminal and central regions (McCarthy *et al.*, 1990). It was thought that mutations primarily occurred in these regions. However, it now appears that the mutations are

spread more evenly through the gene and these hotspots were identified due to screening bias as researchers focussed their work on the regions where the MH associated mutations were first located (Robinson *et al.*, 2006). To date, 35 causative mutations in *RYR1* have been identified, where functional analysis of these variants has indicated that they are causative of MH (EMHG, 2016). Aside from the *RYR1* variants there have been three functionally characterised mutations in the *CACNA1S* gene, which encodes the α-1 subunit of DHPR (Carpenter *et al.*, 2009a; EMHG, 2016). These 35 variants are just the ones functionally characterised, there are in excess of 100 familial mutations that have been identified at the Leeds MH Unit that have yet to be functionally characterised.

In the UK, *RYR1* variants are implicated in MH susceptibility in over 70% of pedigrees and these are inherited in an autosomal dominant manner (Sambuughin *et al.*, 2005). There is noted discordance between IVCT phenotype and *RYR1* genotype, exemplified by the incidence of MHS mutation negative and MHN mutation positive patients. Robinson and colleagues conducted a study in European MH families which found that in individuals who lack the *RYR1* mutation, their relatives still test MHS 2.5% of the time (Robinson *et al.*, 2003b). This discordancy indicates that MH may not be a single gene disorder and there is evidence to suggest the existence of modifier loci that may be causative of MH (Robinson *et al.*, 2000; Robinson *et al.*, 2003a). However, with the advent of next generation sequencing (NGS), many cases of discordancy are explained for example by the presence of two *RYR1* variants in a family that was previously only screened for known familial variants or functionally characterised mutations (Fiszer *et al.*, 2015).

Due to the rapid depletion of SR Ca^{2+} levels during an MH episode, it has been recently hypothesised that SOCE may also play a role in the manifestation of MH (Duke *et al.*, 2010). Evidence to support this was derived from patient muscle biopsies, indicating that SR Ca^{2+} depletion during an MH episode triggers SOCE. STIM1 was shown to have an important role in this process and this sustained SOCE may contribute to the pathological increase in calcium concentration in an MH episode (Duke *et al.*, 2010). CASQ1 may also play a role in MH due to its role as in calcium storage and as a luminal calcium sensor. It has recently been shown to inhibit SOCE by preventing the interaction between STIM1 and Orai1 (Wang *et al.*, 2015). Therefore, there is increasing evidence for the role of additional mechanisms in the pathophysiology of MH.

1.2.2 Central Core Disease

In addition to MH, *RYR1* variants have found to be implicated in central core disease (CCD). CCD, first described in 1956, is a congenital myopathy that presents with progressive proximal muscle weakness (Shy & Magee, 1956). The National Organization for Rare Diseases (NORD) cites that the exact incidence and prevalence of CCD is unknown, but that it is believed to be the most common form of congenital myopathy and estimates occurrence at 6:100000 live births (NORD, 2015). Diagnosis of CCD requires histological evidence of the presence of well-defined areas that lack mitochondria together with muscle weakness (Quinlivan *et al.*, 2003). Type 1 fibres exhibit cores that arise from unstructured myofibrils that are lacking in mitochondria (Zhou *et al.*, 2007; Jungbluth, 2007) (Figure 1.6).
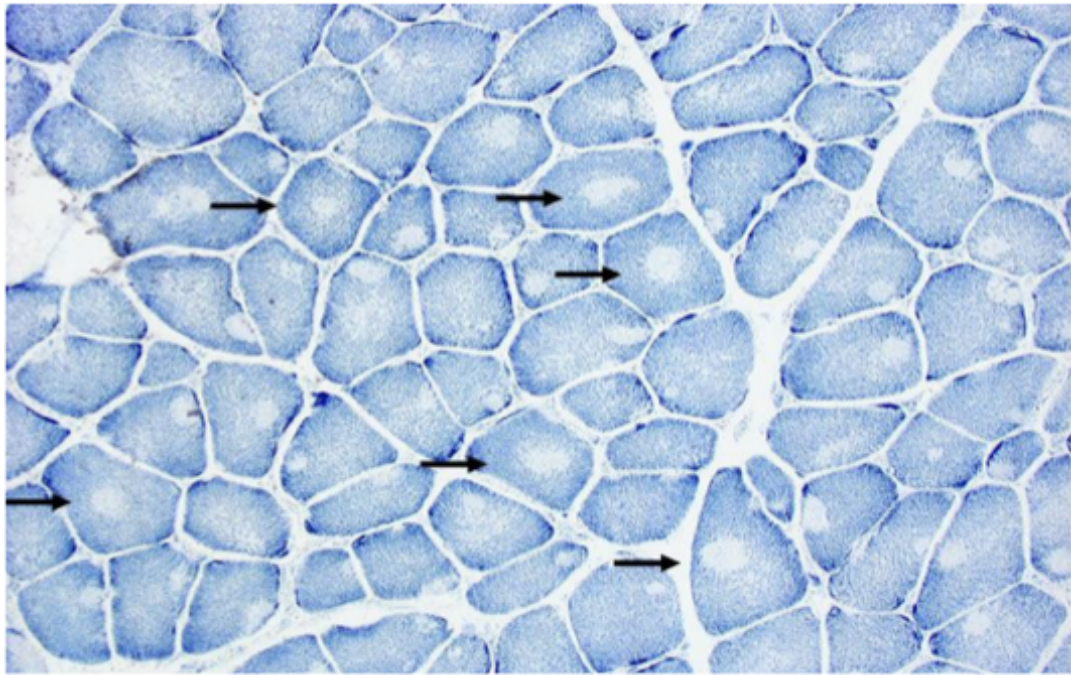
Figure 1.6 Histological appearance of central core disease Transverse section from *rectus femoris* muscle. Stained type 1 fibres exhibit cores that are well marked (⟶) (Jungbluth, 2007).

Common clinical features of CCD include lower limb weakness and muscle atrophy, though a wide spectrum of severity in symptoms is also observed, with many patients exhibiting no symptoms despite the presence of cores while others exhibit acute muscle weakness. In the majority of cases the disease is not progressive, or progresses very slowly (NORD, 2015).

There is overlap between MH and CCD with mutations implicated in MH also being implicated in CCD, and individuals with such mutations displaying a more severe MH phenotype (Robinson *et al.*, 2002). The mutations implicated in CCD, as with MH, are associated with elevated resting calcium due to passive leak through RyR1. In patients with CCD it is apparent that this leak is stronger thus resulting in the altered muscle phenotypes in the absence of anaesthesia (Tong *et al.*, 1997). Like MH, inheritance of CCD is most commonly reported as displaying autosomal dominant inheritance (Monnier *et al.*, 2000; Monnier *et al.*, 2001). However, there is evidence

indicating that inheritance may be recessive in some families (Ferreiro *et al.*, 2002; Jungbluth *et al.*, 2002).

Initial *RYR1* mutation screening of CCD patients focused on specific 'hot spot' regions of the gene, indicating that 47-67% of patients were found to carry *RYR1* mutations (Monnier *et al.*, 2001; Davis *et al.*, 2003; Shepherd *et al.*, 2004). However later work that has sequenced the entirety of *RYR1* indicates that more than 90% of patients may express variants along the entire length of the gene (Wu *et al.*, 2006). 31 *RYR1* variants are implicated in MH and CCD, and a further 29 only implicated in CCD to date since these variants have not been associated with susceptibility to MH (Robinson *et al.*, 2006). In these examples, the proposed mechanism for causing CCD is termed 'EC uncoupling' (Dirksen & Avila, 2002). In brief, the resting calcium level in the myoplasm is elevated due to leaky RyR1 channels, and calcium release upon depolarisation of the muscle membrane cannot occur due to depleted calcium stores and lack of coupling between the DHPR and RyR1.

1.2.3   Exertional Heat Illness

There have been reports of apparently 'awake' MH episodes unrelated to anaesthesia causing deaths of young and physically fit individuals (Bouchama & Knochel, 2002). Anyone can experience hyperthermia in hot, humid environments or during sustained vigorous exercise, but there is evidence to suggest that some people appear to be predisposed to it (Davis *et al.*, 2002; Nishio *et al.*, 2009). The death of three special forces soldiers from exertional heat illness (EHI) while on selection in 2013 has highlighted the lack of understanding regarding the diagnosis and treatment of this potentially fatal condition (Morris, 2015; BBC NEWS, 2015). These fatalities were

ruled a consequence of gross failures by the Ministry of Defence (Brown, 2015). The Institute of Naval Medicine (INM), the UK military heat illness centre, estimates an annual incidence of over 500 cases of heat illness, with 145 referred to the INM for heat tolerance testing (Ministry of Defence, 2013). Information regarding the epidemiology of EHI in the general population is limited, but has been reported as one of the leading causes of death in young athletes (Maron *et al.*, 2009) indicating that under the right stressful conditions this condition may be quite common.

The link between MH and EHI was first proposed in 1991, when two members of the armed forces that suffered cases of EHI were classified as MHS by the IVCT, along with their relatives (Hopkins *et al.*, 1991). There are also clear phenotypic similarities in the symptoms of the two conditions. These phenotypic similarities are supported by genetic data, specifically the case of a 12-year-old boy where his MH history could be linked to an EHI reaction. After surviving an MH reaction during general anaesthesia, the boy later died several months later following an episode of EHI during a game of football. Genetic analysis of the boy and members of his family revealed the RyR1 R163C variant, previously implicated in MH and shown to be causative of the condition in functional experiments (Tong *et al.*, 1997; Yang *et al.*, 2003).

Some but not all individuals reported to have had episodes of EHI have subsequently tested susceptible for MH with the IVCT (Hopkins, 2007; Capacchione & Muldoon, 2009). This evidence, in addition to the similarity in symptomology, has laid the foundation for a link between the two conditions. In an EHI attack the increased body temperature results in the RyR1 allowing greater calcium leakage into the myoplasm. This stimulates the formation of reactive nitrogen species (RNS) which cause S-

nitrosylation of RyR1 further activating the channel leading to increased muscle metabolism which generates more heat, establishing a positive feedback loop which, if left uninterrupted, can cause death (Carsana, 2013). This increased body temperature can induce a range of symptoms; from mild muscle weakness and nausea to severe metabolic acidosis and rhabdomyolysis and is often coupled with significant central nervous system dysfunction, ranging from confused behaviour to acute loss of consciousness, coma and death (Capacchione & Muldoon, 2009).

1.2.4 Late-onset axial myopathy

'Axial myopathy' is a non-specific term for the disorders of skeletal muscle that relate to the axial musculature. Patients with these conditions may develop contracture of the spine, dropped head syndrome and camptocormia (bent spine) (Mahjneh *et al.*, 2002). Camptocormia is also a feature of Parkinson's disease, especially in the advanced stages as well as a range of neuromuscular disorders (Azher & Jankovic, 2005). Patients with LOAM exhibit a range of symptoms such as lumbar hyperlordosis, scapular winging and camptocormia with one unifying feature - the onset occurs between the ages of 30 and 70 years, hence the term 'late-onset axial myopathy'. The symptoms are in contrast to those witnessed in early onset axial myopathies where most changes occur in the anterior and medial thigh (Jungbluth *et al.*, 2004; Klein *et al.*, 2011).

Some patients with LOAM have also been found to carry variants in *RYR1*, some of which are also implicated in MH (Jungbluth *et al.*, 2009; Loseth *et al.*, 2013). In addition to variants in *RYR1*, LOAM has also been attributed to calpainopathy. Calpainopathy is a clinically heterogeneous, autosomal recessive, muscular dystrophy

caused by variants in calpain-3 (*CAPN3*). *CAPN3* is involved in sarcomere remodelling in skeletal muscle. Symptoms of this condition include; limb girdle weakness, exercise induced myalgia, rigid spine syndrome and asymptomatic hyperCKemia (Sáenz *et al.*, 2005; Burke *et al.*, 2010; Liewluck & Goodman, 2012).

1.3   *Mouse models of impaired calcium handling*

1.3.1   *Mouse models* of RYR1 *variants*

RyR1 knock out (KO) mice are not viable (Takekura *et al.*, 1995). However, knock in (KI) murine models of specific *RYR1* mutations implicated in MH, CCD and EHI have been developed. The variants that have been generated include: R163C (Yang *et al.*, 2006), Y522S (Chelu *et al.*, 2006), I4898T (Zvaritch *et al.*, 2007), T4826I (Yuen *et al.*, 2012). Details of these strains are summarised in Table 1.1.

Extreme exercise and heart failure are associated with leaky RyR1 channels. This can be due to phosphorylation of the channel at serine 2844 that leads to muscle weakness (Reiken *et al.*, 2003; Bellinger *et al.*, 2008). To investigate this, an S2844D KI mouse line was created (Andersson *et al.*, 2011). These mice express leaky RyR1 channels and at 6 months old display defective muscle function that is comparable to what is observed in 24 month old wild type mice (Andersson *et al.*, 2011). While this variant is not implicated in MH, it does share the feature of a leaky RyR1 with the R163C and Y522S mutations.

Table 1.1 Summary of Mouse models developed to investigate MH/CCD/EHI

Mouse model	Human condition implicated in	Strain details	Phenotype	Translational discoveries
R163C	MH (Robinson et al., 2006) CCD (Yang et al., 2006) EHI (Estève et al., 2010)	Heterozygotes viable Homozygous mice die shortly after birth/in utero	Halothane exposure: severe MH crises Exposure to 42°C (20 mins): MH-like crises	Myotubes have significantly higher resting Ca^{2+} l[...] = Ca^{2+} leakage from SR (Yang et al., 2006; Yan[...] al., 2007) Damaged mitochondrial function = increased [...] production (Giulivi et al., 2011) Low oxidative phosphorylation and glyco[...] (Giulivi et al., 2011)
Y522S	MH (Robinson et al., 2006) CCD (Chelu et al., 2006)		Presence of cores lacking mitochondria Halothane exposure: severe MH crises Exposure to 41°C (15 mins): MH-like crises	Development of cores worsens with increasing ag[...] (Boncompagni et al., 2009) Increased Ca^{2+} leak leads to increased ROS/RNS [...] production (Durham et al., 2008, Wei et al., 2011[...] AICAR inhibits Ca^{2+} leak (Lanner et al., 2012)
I4898T	MH (Robinson et al., 2006) CCD (Zvaritch et al., 2007)		Reduction in skeletal muscle force (Zvaritch et al., 2009, (Loy et al., 2011)	Attributed to decreased Ca^{2+} release (Zvaritch et al., 2009, (Loy et al., 2011)
T4826I	MH (Robinson et al., 2006)	Homozygous mice viable	Exposure to 37°C (20 mins): MH-like crises Halothane exposure: severe MH crises	Morpological variations in soleus muscle: Z[...] streaming, redistribution of mitochondira and reg[...] of contracture (Yuen et al., 2012)
		Heterozygous mice viable	Exposure to 37°C (20 mins): higher rectal temp Halothane exposure: variable MH reaction	Larger Ca^{2+} transients in mutant muscle (Barrientos et al., 2012)

1.3.2 *A* CACNA1S *variant model*

Impaired calcium handling is not only attributed to variants in RyR1. Variants in the α-1 subunit of the DHPR (Ca$_v$1.1), encoded by *CACNA1S*, have also been implicated in compromised calcium homeostasis in skeletal muscle and MH (Carpenter *et al.*, 2009a). Recently, a R174W mouse line has been created (Beqollari *et al.*, 2015). Homozygous mice are viable, move normally and have lifespans similar to wild-type. Exposure to isofluorane results in a hypermetabolic state and eventually death. Like a number of the RyR1 variant models, resting cytosolic calcium level in these mice is elevated. There was also evidence of mitochondrial displacement, variable calsequestrin content of the SR and some evidence of SR stacks (Beqollari *et al.*, 2015). FDB muscle fibres from homozygous R174W mice were lacking in L-type calcium current but intramembrane charge movement was similar to that recorded in wild type muscle, suggesting a mechanism for MH susceptibility that is related to calcium leak from the SR but EC coupling remains unaffected (Beqollari *et al.*, 2015).

1.3.3 *Calsequestrin null mice*

In addition to RyR1 and the α-1 subunit of the DHPR, calsequestrin 1 is also a key component of skeletal muscle calcium handling (Beard *et al.*, 2004). Unlike Ryr and Ca$_v$1.1 mouse models that use point mutation KI, calsequestrin 1 mouse studies have used a knock-out (KO) model (Paolini *et al.*, 2007). These mice are viable and fertile and show no significant behavioural alteration under normal housing conditions. Male Casq1-null mice were observed to have an increased rate of sudden death under usual stress conditions such as mating. They were also susceptible to a high mortality rate when exposed to halothane or high environmental temperatures (Dainese *et al.*, 2009).

Female Casq1-null mice had a higher survival rate than their male Casq1-null counterparts but lower than wild type mice. Contractile responses under normal conditions was compromised in fast muscles, but not slow, with increased twitch amplitude and time to peak and half-relaxation time prolonged (Dainese *et al.*, 2009; Paolini *et al.*, 2011). Casq1-null muscle was more resistant to low frequency fatigue than wild type, a feature that could be related to the increased mitochondrial density in Casq1-null muscle fibres (Scorzeto *et al.*, 2013). Altered mitochondrial density may be related to increase ROS production, and recent tests have shown that treatment of Casq1-null mice with anti-oxidants such as N-acetylcysteine can reduce damage to mitochondria, limit core formation, improve muscle function as well as attenuating the hypermetabolic response to halothane in these mice (Michelucci *et al.*, 2016).

In summary, mouse models have highlighted the effects of compromised calcium handling in skeletal muscle, how this has a detrimental impact on mitochondrial function and subsequently skeletal muscle energetics. Particular models, I4898T and Y522S, display alterations that are akin to premature muscle ageing, indicating the importance of calcium handling in sarcopenia and myopathic conditions.

1.4   Mitochondrial function and oxidative stress in ageing

Mitochondria produce ATP, which is, along with calcium, central to the energetic capacity of skeletal muscle. One of the best-known theories of aging is the free radical theory. This theory proposes a central role for the mitochondrion as the principle source of intracellular reactive oxygen species (ROS) which results in mitochondrial DNA mutations and progressive damage to mitochondria (Kraytsberg *et al.*, 2006). The production of ROS, reactive nitrogen species (RNS), and other types of free

radical by mitochondria contribute to oxidative stress which affects muscle function and adaptation (Zuo *et al.*, 2013). Cellular oxidative stress is a significant factor in skeletal muscle ageing (Liochev, 2013). Loss of mitochondria is a feature of skeletal muscle ageing, a phenomenon that is also a feature of *RYR1* myopathies (Zhou *et al.*, 2007; Payne & Chinnery, 2015; Pietrangelo *et al.*, 2015).

Sustained contractile activity, a feature of both exercise and an MH episode, can lead to inflammation and increased production of free radicals (Fittipaldi *et al.*, 2014). Nitric oxide (NO) is one of these reactive molecules that is vital for the mediation of signalling pathways during muscle contractions (Zuo & Pannell, 2015). NO has also been implicated in activation and inhibition of RyR1 (Hart & Dulhunty, 2000). NO release increases dramatically during active muscle contraction.

NO and ROS are both generated during skeletal muscle contraction leading to increased levels of peroxynitrite (Hayashi *et al.*, 2004). This can activate the adenosine monophosphate-activated protein kinase (AMPK) pathway to produce ATP (Xie *et al.*, 2006). The AMPK pathway is also involved in translocation of the glucose transporter type 4 (GLUT4) that leads to increased glucose uptake in myocytes (Figure 1.7).
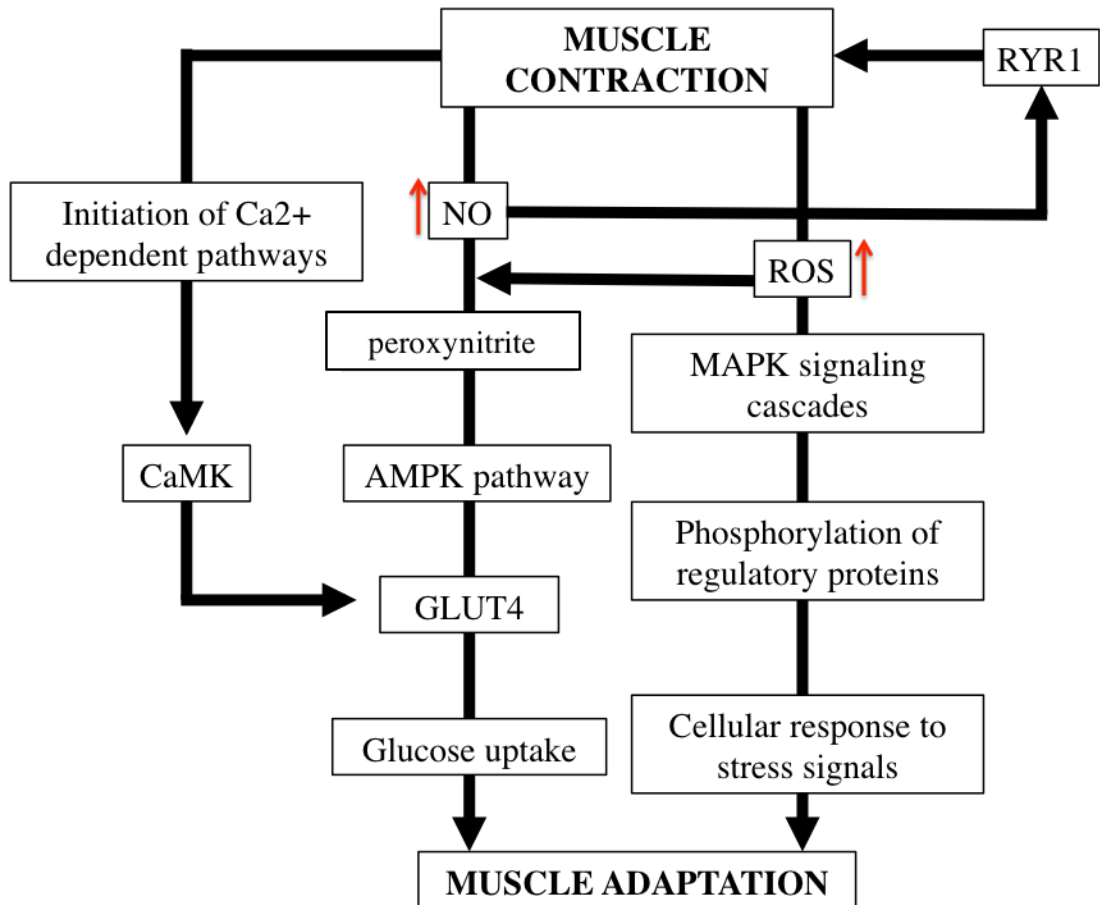
Figure 1.7 Schematic of the effects of ROS and NO in skeletal muscle, adapted from (Zuo & Pannell, 2015).

In addition to involvement in AMPK signalling, ROS is involved in initiating the mitogen-activated protein kinase (MAPK) signalling cascades (Figure 1.7). MAPK phosphorylates various regulatory proteins that either inhibit or activate other signalling pathways that induce a cellular response to stress signals and induce skeletal muscle adaptation (Powers *et al.*, 2010). Therefore, ROS are important for the adaptation of skeletal muscle under stress conditions, but when produced to excess can upset this process.

1.5   Project Aims and Objectives

This overall aim of this project was to investigate skeletal muscle energetics and ageing in the context of *RYR1* variants. Each results chapter begins with a chapter specific introduction in addition to the general introduction.

Chapter 2 aim: Investigate the potential for *Caenorhabditis elegans* models of *RYR1* myopathies to improve the understanding of skeletal muscle ageing.

Chapter 2 objectives:

- Utilise pre-existing and develop new *C. elegans* model strains of *RYR1* myopathies

    o Development of new strains will be achieved through recombineering specific *RYR1* variants in the *C. elegans* ryanodine receptor.

- Characterise the response of *C. elegans* model strains using phenotyping assays (employing caffeine and halothane)

- Develop additional *gfp*-myosin strains of all *RYR1* variant strains to enable assessment of skeletal muscle fibre organization

- Determine the effect of chosen *RYR1* variants on muscle ageing in the worm through assessment of skeletal muscle fibre organization

Chapter 3 aim: Expand the understanding of MH genetics through a whole genome approach with a view to highlighting alternative genes involved in MH and skeletal muscle ageing and ultimately develop a predictive risk score for MH susceptibility.

Chapter 3 objectives:

- Utilise existing whole-genome Affymetrix data derived from skeletal muscle and peripheral blood to determine the whole genome profile of MH in the different tissues
  - Pathway analysis will be used to highlight genes implicated in MH
  - LASSO regression analysis will be performed to determine predictive risk score for MH susceptibility
- Ultilise existing whole-genome Affymetrix data derived from skeletal muscle to determine genes of interest of relevance to muscle ageing and MH susceptibility
  - Follow up key genes with TaqMan® assays on a separate cohort of samples for validation.

Chapter 4 aim: Investigate the role of mitochondrial oxidative phosphorylation (OXPHOS) in MH susceptible and normal skeletal muscle in the context of ageing

Chapter 4 objectives:

- Carry out mitochondrial respirometry on patient muscle biopsies using the Oroboros system
  - Characterize different components of mitochondrial OXPHOS and estimate mitochondrial content and link alterations to MH status and age

Chapter 5 aim: Develop new equipment required to carry out heat measurements in isolated skeletal muscles that will enable calculation of skeletal muscle efficiency.

Chapter 5 objectives:

- Calibration and preliminary testing of new thermopile apparatus (using old and young mouse soleus muscle) to demonstrate functional capacity of the equipment

- Produce preliminary data on differences in skeletal muscle efficiency in old and young wild-type mice

2   A *Caenorhabditis elegans* model for studying *RYR1* variants and muscle ageing

2.1   Introduction

Caenorhabditis elegans is a free-living, transparent nematode. It has been used extensively used as a model organism for a large number of human conditions (Kaletta & Hengartner, 2006). These have included longevity models for the study of human ageing (Harrington & Harley, 1988; Tissenbaum & Guarente, 2002; Driscoll & Yu, 2011), vulval development models for cancer biology (Fisher *et al.*, 2005) and transgenic models to investigate neurological disorders such as Alzheimer's, Huntington's and Parkinson's disease (Link, 1995; Faber *et al.*, 1999; Link, 2001).

The adult worms measure approximately 1mm in length (Figure 2.1). In the wild, they live in soil, but in a laboratory setting they are housed on nematode growth medium in plates. These organisms are most commonly found as self-fertilising hermaphrodites (XX), but there are also male *C. elegans* occurring at a rate of ~0.1% (WormAtlas, 2006). It is possible to induce production of males by heat shocking at 30ºC and then housing the nematodes at temperatures of 25ºC (He, 2011). Wild-type *C. elegans* have a lifespan of 2-3 weeks, during which the self-fertilising hermaphrodites will produce large numbers of offspring (Stroustrup *et al.*, 2013).

Figure 2.1 Adult hermaphrodite *C. elegans*, left lateral side, scale bar 1mm. Adapted from (WormAtlas, 2006)

The body-wall structure of *C. elegans* exhibits longitudinal rows of obliquely striated muscle cells on the dorsal and ventral sides of the nematode (Wood, 1988). The striated nature of *C. elegans* body wall muscle has striking similarity to the striated appearance of human skeletal muscle. The primary difference is that the sarcomeres are not arranged in register (which is the case in mammalian muscle), but obliquely throughout the muscle (Figure 2.2).
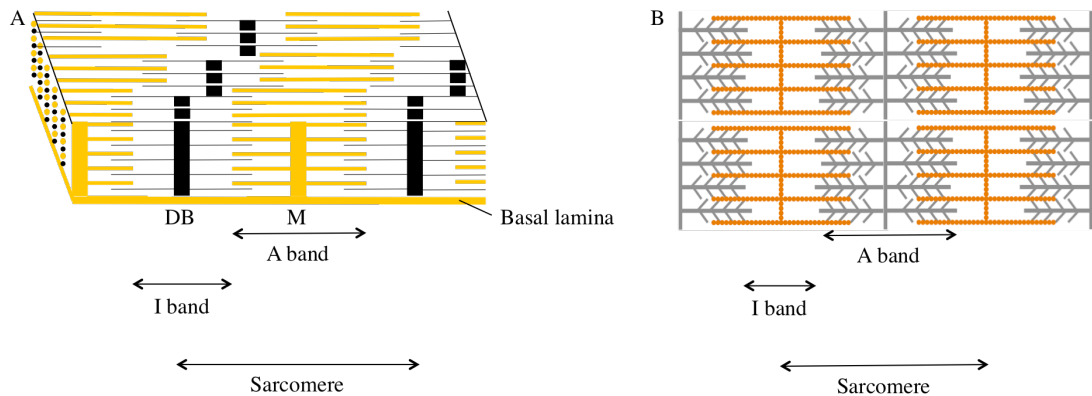
Figure 2.2 Schematic of somatic muscle sarcomere in *C. elegans* and humans. A: 3D rendering of myofilament lattice also showing sarcomere structure in *C elegans* somatic muscle, myosin fibres shown in yellow, actin shown in black, adapted from (Altun & Hall, 2009) B: 2D schematic of human sarcomere arrangement, myosin fibres shown in grey, actin shown in orange.

Movement is achieved through the co-ordinated contraction and relaxation of opposing dorsal and ventral muscle cells which results in a sinusoidal wave that is capable of propelling the worm forwards or backwards (Nicholas, 1984). Structural

changes in the sarcomere can be examined visually using GFP tagged myosin in the *C. elegans* body-wall muscle (Herndon *et al.*, 2002). These nematodes have a lifespan of just a few weeks, making it possible to easily examine ageing in *C. elegans* muscle and to do so in a high-throughput manner.

It has been documented that patients with some age-related muscle myopathies have *RYR1* mutations (Jungbluth *et al.*, 2009). Moreover, the myopathy associated with *RYR1* variants, which are also implicated in MH, imitates premature ageing in mice models (Boncompagni *et al.*, 2009; Boncompagni *et al.*, 2010). Examination of the structural changes in the muscle of worms containing single-point mutations in the worm ryanodine receptor will enable better understanding of how these variants affect the muscle ageing process.

The mammalian RyR1 protein is more than 5000 amino acid residues long. This makes manipulation of the mammalian gene difficult. The *C. elegans unc-68* gene is found to encode a ryanodine receptor ortholog that is expressed in body wall muscle cells and involved in regulating body-wall muscle contraction and maintaining normal tension in these nematodes (Maryon *et al.*, 1996). *C. elegans* has a compact genome, *unc-68* is about 30kb long and is entirely contained in the fosmid clone WRM069cA02 (Figure 2.3).

Figure 2.3 Fosmid clone WRM069cA02 (Hodgkin, 2015). It contains the entire *unc-68* gene with flanking intergenic regions. Scale is in base pairs.

Fosmids are a low-copy-number cosmid vector that is based on the *E. coli* F-factor replicon. Sequences that are cloned are more stable in fosmids than in multi-copy vectors such as cosmids (Kim *et al.*, 1992). Cosmids are plasmids that contain cos sequences enabling them to be packaged into lambda phage particles that allows for cloning of larger DNA fragments than standard plasmids (Kim *et al.*, 1992).

Unc-68(e540) (strain CB540) worms carry a point mutation near the centre of the gene, resulting in a premature stop codon that makes the worms genetically *unc-68* null mutants (Sakube *et al.*, 1997). Due to the relatively small size of the worm, they are still viable as diffusion of calcium into the myoplasm is sufficient to elicit a contraction, but the force of the contraction is reduced. In addition, the reduced force is associated with compromised coordination of the muscle contractions resulting in a slow, uncoordinated movement phenotype compared to wild-type worms. *Unc-68* has approximately 40% amino acid identity with the human *RYR1* gene (Sakube *et al.*, 1997). This homology is distributed along the length of the protein, suggesting that

the mammalian and nematode ryanodine receptor operate and are controlled in a similar manner.

Previous work involving exposure of *C. elegans unc-68* revertants has shown them to have altered responses to a number of reagents, including caffeine and ryanodine (Adachi & Kagawa, 2003). *Unc-68* null mutants are insensitive to the paralytic effect of ryanodine that is exhibited by the wild type (Maryon *et al.*, 1996). The pattern of behaviour in *C. elegans* in response to volatile anaesthetics is largely similar to what is observed in humans (Figure 2.4). In humans the concentration of anaesthetic required for surgical anaesthesia is termed "MAC" (minimal alveolar concentration), the concentration of gas at which 50% of patients will remain immobile during a surgical stimulus (Aranake *et al.*, 2013). To mimic this in *C. elegans,* reversible immobility is used as an endpoint to study control of anaesthetics in the behaviour of these worms (Morgan & Cascorbi, 1985).

Humans

Altered
mental
performance   Loss of smell
                 uncoordination   "Anaesthesia"   Lethality

0.05-0.1MAC   0.1-0.2MAC   1MAC   2-3MAC

C. elegans

                      Radial
Uncoordination   dispersion   Immobility   LC$_{50}$

         0.3%   3.2%   7%

Increasing concentration of halothane
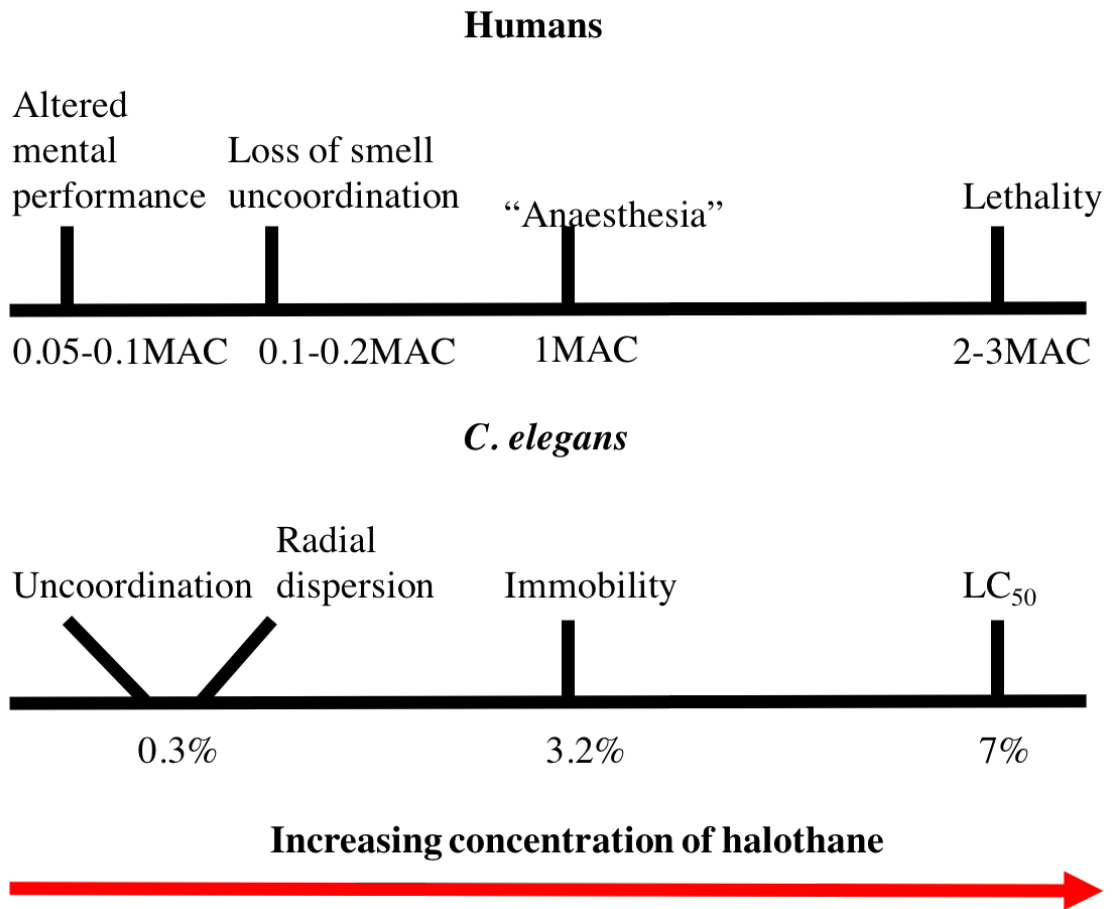
Figure 2.4 Concentrations of halothane required to reach several endpoints in humans and *C. elegans*. 1MAC=0.7% halothane. Radial dispersion: the ability of a worm to move radially from the centre of a plate towards a peripheral ring of food. Figure adapted from (Morgan *et al.*, 2007).

The concentration of halothane required to achieve the various endpoints are higher in *C. elegans* compared to humans (Figure 2.4). This is likely due to the mode of application of the anaesthetic, whereby in *C. elegans* the chemical must be absorbed through the thick cuticle of the worm whereas in humans it is inhaled through the respiratory tract. These endpoints serve as the typical criteria for assays that have been established to investigate anaesthetic sensitivity in a number of mutant *C. elegans* strains.

The majority of work involving volatile anaesthetics in *C. elegans* has examined the effects of these chemicals on the neural system of the worm and their effects on

neurotransmitter release (Crowder *et al.*, 1996; van Swinderen *et al.*, 1999). *C. elegans* strains found to exhbit hypersensitivity to volatile anaesthetics include those with 'fainter' phenotypes such as *unc-*79, *unc-80, nca-1* and *nca-*2. Fainting in *C. elegans* is defined as periods of inactivity lasting several seconds interspersing a period of normal locomotion. These animals are found to be immobile in 2% halothane while wild type animals display rapid movement at this concentration (Morgan *et al.*, 2007). The genes implicated in the aforementioned mutants are expressed in the neuronal tissue of the worm and affect expression of the protein stomatin. Stomatins co-localise in tissues such as the dorsal root ganglion (Fricke *et al.*, 2000), a vital component of the sensory pathway in mammals. A mouse knock-out for stomatin has been observed to have the same anaesthetic sensitivity as seen in the worm (Sedensky *et al.*, 2006).

Mitochondrial effects have also been investigated with respect to altered anaesthetic sensitivity in the worm. *Gas-1* (general anaesthetic sensitive) encodes a subunit of the *C. elegans* protein of complex I of the mitochondrial electron transport chain (Kayser *et al.*, 1999). The mitochondria of *gas*-1 mutants are defective in oxidative phosphorylation using complex I substrates with the rate of electron transfer through the chain reduced by over 90% (Kayser *et al.*, 2001). Other mutants such as *daf-2* display increased rates of complex I oxidative phosphorylation and are resistant to volatile anaesthetics (Morgan *et al.*, 2007). In both mammals and worms, complex I has been identified as most sensitive to inhibition by volatile anaesthetics (Kayser *et al.*, 2004). The data concerning volatile anaesthetics largely fails to reveal a single target that is responsible for the effects of these chemicals, indicating that there are different sites of anaesthetic action (Morgan *et al.*, 2007).

2.2   Materials and Methods

This chapter presents an investigation into the validity of *C. elegans* as a model organism for investigation of human skeletal muscle myopathies and ageing. Single point mutations in *unc-68* that correspond with point mutations in *RYR1* implicated in MH, CCD, EHI and LOAM were engineered by recombineering the fosmid clone containing *unc-68*. *Unc-68* null-mutants were then transformed using the altered fosmids to generate strains for each myopathy. Phenotyping assays, using caffeine and halothane, were performed to test whether the strains respond to these reagents in a similar manner to humans. Finally, ageing assays were carried out (using new strains generated from crossing myopathy models with *gfp* myosin worms) to investigate the potential impact of the variants on the process of age-related muscle structure decline.

2.2.1 Identification of variants

9 variants in *RYR1* were selected for investigation using *C. elegans* (Table 2.1).

Table 2.1 Amino acid alignment of all nine variants under investigation

HUMAN CONDITION	*RYR1* VARIANT	PROTEIN	ALIGNMENT
Malignant hyperthermia	p.G341R c.1021G>A	RyR1 UNC-68	KRDVEGMGPPEIKYGESLCFVQHVASGLW EKEEEGMGNATIRYGETNAFIQHVKTQLW
	p.R2163H c.6488G>A	RyR1 UNC-68	DTMSLLECLGQIRSLLIVQMGPQEENLMI DVTDFLVYLIQIRELLTVQFEHTEEAILK
	p.R2454H c.7361G>A	RyR1 UNC-68	CAPEMHLIQAGKGEALRIRAILRSLVPLE CAPDPMAIQAGKGDSLRARAILRSLISLD
	p.R2458H c.7373G>A	RyR1 UNC-68	IQAGKGEALRIRAILRSLVPLEDLVGIIS IQAGKGDSLRARAILRSLISLDDLGQILA
Exertional Heat Stroke and MH	p.R163C c.487C>T	RyR1 UNC-68	CWWTMHPASKQRSEGEKVRVGDDIILVSV CWWTIHPASKQRSEGEKVRVGDDVILVSV
Central Core Disease and MH	p.R4861H 14582G>A	RyR1 UNC-68	VVVYLYTVVAFNFFRKFY-NKSEDEDEPD VVVYLYTVIAFNFFRKFYVQEGEEGEEPD
	p.A4940T c.14820G>A	RyR1 UNC-68	FFFFVIVILLAIIQGLIIDAFGELRDQQE FFFFVIIILLAIMQGLIIDAFGELRDQQE
Late-onset axial myopathy	p.K3452Q c.10354A>C	RyR1 UNC-68	IFIYWSKSHNFKREEQNFVVQNEINNMSF IFRIWSQSQHFKREELNYVAQFEEDAAAT
	p.V4849I c.14545G>A	RyR1 UNC-68	KQLVMTVGLLAVVVYLYTVVAFNFFRKFY QQLILTIMMTLVVVYLYTVIAFNFFRKFY

Human variant residues and corresponding *C. elegans* residues are in red. Other amino acids identical in RyR1 and UNC-68 are in blue.

Selection of these specific variants was made according to whether the variant was conserved at the amino acid level and in the case of the MH variants, that they showed a strong MH phenotype (Carpenter *et al.*, 2009b). A strong MH phenotype is defined as a significantly more pronounced response to caffeine and halothane under the conditions of the IVCT when compared with the response of the most common RYR1 variant implicated in MH. This variant, G2434R, confers a relatively weak contracture response in the IVCT when compared to other rarer variants. These single point mutations were introduced into the *C. elegans* fosmid clone WRM069cA02 using a two-step counter-selection recombineering method. Those variants implicated in MH,

CCD and EHS, were recombineered by members of the Hope laboratory at the University of Leeds and all microinjection transformations to generate new strains were carried out by Professor Ian Hope. Recombineering and microinjection transformation of the two variants implicated in late-onset axial myopathy has been completed as part of this project. Microinjection transformation was only successful with one of the late-onset axial myopathy variants.

2.2.2 Strain maintenance

All strains used were maintained in culture at 20°C on 50mm NGM plates seeded with *E. coli* strain OP50. Desired transgenic worms were selected using a sterile worm pick and picked to fresh seeded plates on a regular basis.

2.2.3 Recombineering of RYR1 variants in unc-68

Modification of the target gene, *unc-68,* was achieved by a two-step counter-selection recombineering technique (Feng *et al.*, 2012). This is summarised in Figure 2.5.
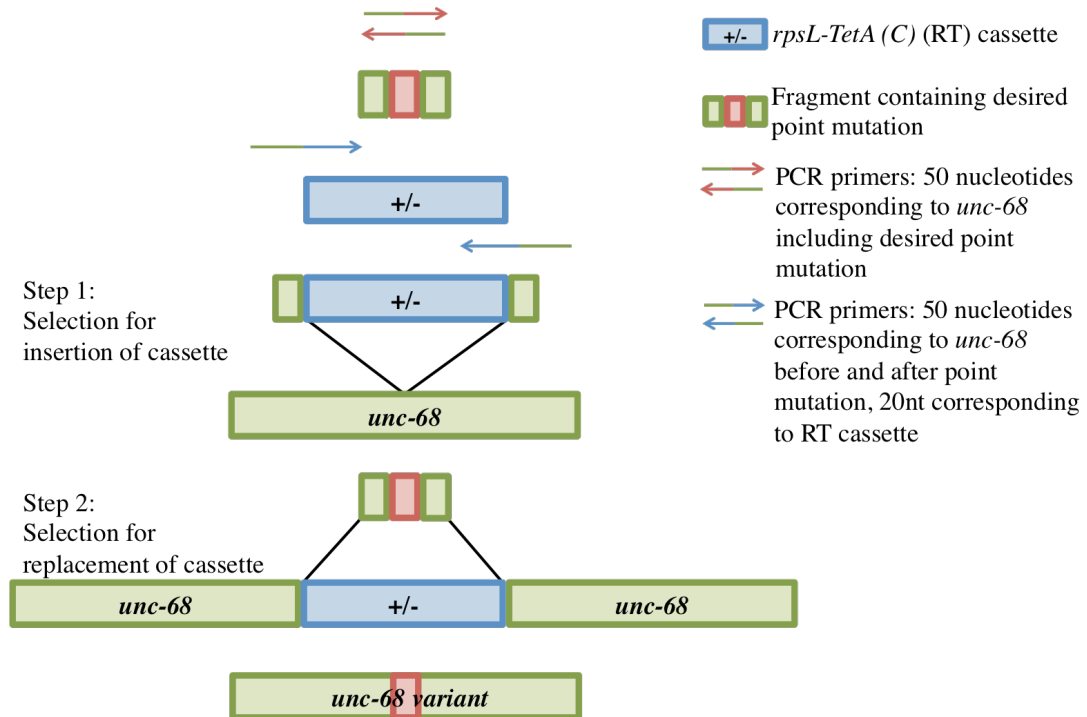
Figure 2.5 Schematic of the recombineering process. A PCR amplified variant and fosmid-specific counter-selection cassette is inserted into the target fosmid by bacterial transformation using positive selection for the cassette in step 1. The cassette is then replaced, with incorporation of the desired point mutation in the second step with a PCR product containing the desired point mutation.

Prior to recombineering, the following steps had to be completed. Fosmid clone DNA was electroporated into recombineering competent EL350 cells (Lee *et al.*, 2001). These cells have a defective lambda prophage incorporated chromosomally. This prophage conatins the *gam*, *bet* and *exo* genes arranged in their natural configuration and expressed from a native *PL* promoter that is stringently regulated by the temperature sensitive cI857 repressor (Yu *et al.*, 2000). The repressor is inactivated by a short-term temperature change to 42°C. This permits high-level co-ordinated expression of the Red genes that mediate homologous recombination between the recipient target gene and a double-stranded linear donor DNA. For this method, all incubations of EL350 cells were carried out at 32°C, and where shaking was used this was set at 200rpm in a waterbath, except for induction of Red functions where the temperature was raised to 42°C and shaking carried out at 150rpm.

2.2.3.1 PCR-amplification of the rpsL-tetA(C) recombineering cassettes

Amplification of the fosmid specific *rpsL-tetA(C)* cassette (RT cassette) DNA was achieved by PCR in 10x high fidelity buffer supplemented with 0.167mM dNTPs, 4mM MgSO$_4$, 1U platinum Taq DNA polymerase and 0.5µM of each primer (Table 2.2) for amplification of the cassette made up to a total reaction volume of 30ul using nuclease free H$_2$O.

Table 2.2 Primer details for amplification of variant specific cassettes

Primer details	Sequence 5'-3'
K3453Q Forward	atgaaaatgtagctgtcatcttccgtatttggagtcaaagtcaacatttcgat gataagctgtcaaacatgag
K3452Q Reverse	ggctgcagcatcctcttcaaattgagccacatagttcagctcttcacgtttcg ctgtcgagatatgacggtg
V4849I Forward	ttacacacaacttgcaacaactcattctcaccatcatgatgacacttgtagat gataagctgtcaaacatgag
V4849I Reverse	atagaatttacggaagaaattgaacgcgatgacagtgtagagatacacgatcg ctgtcgagatatgacggtg

An initial denaturation step lasting 2 minutes at 94°C preceded 30 cycles of 30 seconds at 94°C (denaturation), 45 seconds at 50°C (annealing) and 2.5 minutes at 68°C (extension). A final incubation at 68°C for 10 minutes ensured extension was complete. The PCR product was checked using agarose gel electrophoresis (0.7% gel in 1xTAE buffer) and the products purified from the gel using a Qiagen© PCR purification kit. The purified PCR product was then run on a gel (0.7% in 1xTAE) to quantify the concentration of DNA present.

2.2.3.2 Electroporation of fosmid DNA into electrocompetent cells

The following procedure was performed on ice. A 20µl aliquot of electrocompetent EL350 cells was thawed and mixed with 0.5µl of fosmid DNA. *E. coli* strain EL350 is recombineering-competent (Lee *et al.*, 2001). The mixture was then transferred to a chilled 0.1cm gap cuvette. Electroporation was then carried out under the following

parameters: 1.8kV, 200Ohms and 25μF. 1ml of room temperature LB (0.5% yeast extract, 1% tryptone, 171mM NaCl in H_2O, autoclaved) was then added to the cuvette and the resultant mixture transferred to a sterile 15ml culture tube. Cells were incubated for 3 hours at 32°C with shaking to allow the cells to recover. Following recovery the cells were plated out (using volumes of 1μl and 33μl) on LB agar plates (0.5% yeast extract, 1% tryptone, 171mM NaCl and 1.5% agar in H_2O, autoclaved) supplemented with chloramphenicol (12.5μg/ml) and grown for 24 hours at 32°C. From the resulting colonies, a single one was selected and streaked out and grown again for 24 hours at 32°C.

2.2.3.3 Preparation of competent EL350 cells

Pre-cultures were set up by inoculating 2ml LB containing either 12.5μg/ml chloramphenicol to select for fosmid containing EL350 cells (to be used in recombineering step 1) or 12.5μg/ml chloramphenicol and 5μg/ml tetracycline to select for fosmid+RT cassette containing EL350 cells (to be used in recombineering step 2) with a single colony of EL350 cells containing the fosmid or fosmid+RT cassette and then incubating at 32°C overnight with shaking at 200rpm. This was then used to inoculate 20ml of SOB medium (0.5% yeast extract, 2% tryptone, 10mM NaCl, 2.5mM KCl in ddH_2O and autoclaved) with appropriate antibiotic in a 50ml Falcon tube and incubated with shaking until OD600 (optical density ~0.6). The culture was then split equally between two 50ml Falcon tubes, one of which was kept on ice. This served as the non-induced control. The other tube was heat-shocked in a 42°C water bath with shaking for 20 minutes then immediately chilled on ice for 20 minutes. The cells were pelleted by centrifugation at 4°C, 3300g for ten minutes and the pellet re-suspended in 10ml ice-cold 10% glycerol. This process was repeated and

the pellet re-suspended in 5ml ice-cold 10% glycerol. The process was repeated a final time and the pellet re-suspended in ~100μl of supernatant. The cells were then used immediately for recombineering step 1 or 2.

2.2.3.4   Recombineering Step 1: Insertion of the RT-cassette

On ice, 150-250ng of purified PCR-generated variant-specific RT cassette was mixed with 100μl aliquots of induced electrocompetent or non-induced control EL350 cells as prepared in 2.2.3.3. The mixture was then transferred to a chilled 0.1cm gap cuvette and electroporated (using parameters described in 2.2.3.2). 1ml of SOB was then added to each cuvette and the resultant mixture transferred to a sterile 15ml culture tube which was incubated with shaking for 2-3 hours to allow cells to recover. 50μl of recovered cells was then plated onto LB plates supplemented with 12.5μg/ml chloramphenicol and 5μg/ml tetracycline and incubated for 36-48 hours. No colonies were present on plates containing non-induced cells. 6 positive colonies were streaked onto fresh LB agar plates supplemented with 12.5μg/ml chloramphenicol and 5μg/ml tetracycline and incubated for 24-48hours. Colony PCR was performed to confirm insertion of the cassette. PCR amplification of cells from a single colony (added using a sterile Gilson tip) was carried out in 10x high fidelity buffer supplemented with 0.167mM dNTPs, 4mM $MgSO_4$, 1U platinum Taq DNA polymerase and 0.5μM of each sequencing primer (Table 2.3), made up to a total reaction volume of 30μl using nuclease free H_2O.

Table 2.3 Primer details for sequencing primers

Primer Direction	Sequence 5'-3'
K3453Q Forward	ttgcatcgtgctcaatggct
K3452Q Reverse	tctttctctctgcaatcgcc
V4849I Forward	ttgacgtcgtgctctcattc
V4849I Reverse	gtgacactttcgatctggct

An initial denaturation step lasting 2.5 minutes at 94°C preceded 30 cycles of 30 seconds at 94°C (denaturation), 45 seconds at 50°C (annealing) and 2.5 minutes at 68°C (extension). A final incubation at 68°C for 10 minutes ensured extension was complete.

2.2.3.5 Generation of fragment containing mutation

The fragment containing the mutation for each variant being generated was produced by PCR in 10x high fidelity buffer supplemented with 0.167mM dNTPs, 4mM MgSO$_4$, 1U platinum Taq DNA polymerase and 0.5µM of each primer containing the desired variant (Table 2.4), made up to a total reaction volume of 30µl using nuclease free H$_2$O.

Table 2.4 Primer details for generation of DNA fragment containing desired variant (variant highlighted in red)

Primer details	Sequence 5'-3'
K3453Q Forward	atgaaaatgtagctgtcatcttccgtatttggagtcaaagtcaacattt ccaacgtgaagagctg
K3452Q Reverse	ggctgcagcatcctcttcaaattgagccacatagttcagctcttcacgt tggaaatgttgacttt
V4849I Forward	ttacacacaacttgcaacaactcattctcaccatcatgatgacacttgt aatcgtgtatctctac
V4849I Reverse	atagaatttacggaagaaattgaacgcgatgacagtgtagagatacacg actacaagtgtcatca

An initial denaturation step lasting 2 minutes at 94°C preceded 5 cycles of 30 seconds at 94°C (denaturation), 45 seconds at 50°C (annealing) and 30 seconds at 68°C (extension). A final incubation at 68°C for 10 minutes ensured extension was complete. The PCR product was checked using agarose gel electrophoresis (0.7% gel in 1xTAE buffer) and the producted purified from the gel using Qiagen© PCR purification kit.

2.2.3.6   Recombineering Step 2: Replacement of the RT cassette with mutation

100μl aliquots of electrocompetent EL350 cells containing the RT cassette were transformed by electroporation (using parameters detailed previously) with 10μl of the purified PCR product of the fragment containing the mutation. After cells had recovered 50μl was plated onto NSLB agar plates (1% Tryptone, 0.5% Yeast Extract and 1.5% Agar in ddH$_2$O, autoclaved) supplemented with 12.5μg/ml chloramphenicol, 500μg/ml streptomycin and incubated for 36-48 hours. 12 discrete colonies from the induced plates were streaked and incubated for 24-48 hours. Some background growth is expected on the plates containing non-induced controls due to streptomycin resistance. These colonies were screened by colony PCR (as described previously) for replacement of the RT cassette with the fragment containing the mutation. Following agarose gel electrophoresis the PCR products were extracted and purified using Qiagen© PCR purification kit. The purified PCR product was then sequenced to confirm that the mutation had been introduced and that no additional changes had been incorporated into the sequence.

2.2.3.7   Preparation of DNA for microinjection transformation

The recombineered fosmid DNA was isolated from the EL350 cells using a Qiagen© plasmid purification kit. The fosmid DNA was then transformed by electroporation into electrocompetent EPI300 cells. These cells were grown in culture containing 12.5μg/ml chloramphenicol and 0.01% arabinose for 24 hours. From these cells fosmid DNA was isolated following the standard protocol for a Qiagen© plasmid purification kit. The DNA obtained from this step was used for microinjection to transform the *unc-68* knock out (CB540) worm strains. EcoRI restriction enzyme digestion was carried out on DNA isolated from the final recombineered fosmid DNA,

the starting fosmid DNA and the fosmid+RT cassette DNA. This provided additional confirmation that the DNA was of the correct size following the recombineering process, and that no additional changes had been introduced. EcoRI digestion protocol used ~1μg/μl of DNA, 0.5μl EcoRI, 1X Buffer EcoRI in a total reaction volume of 10μl. The mixture was placed in a 0.5ml eppendorf tube and incubated at 37°C for 1 hour then 2μl of each sample run on a 0.7% agarose gel. DNA was also sequenced at the St James's university sequencing facility using Sanger sequencing to confirm that the correct point mutation had been introduced.

2.2.4   Microinjection transformation

Manipulated wild type *unc-68* fosmids were introduced into *unc-68(e540)* worms by microinjection. *Unc-68(e540)* carries a point mutation towards the centre of the gene and behaves genetically as a null (Sakube *et al.*, 1997). Microinjection needles were pulled from borosilicate glass capillaries with an internal filament (Harvard Apparatus, Kent, UK: GC100F-10, 1.0x0.58x100mm). DNA loading pipettes were created by softening standard glass capillaries (1.15x1.55x75mm micro haematocrit tubes) over a Bunsen flame. The capillary was subsequently removed from the flame and pulled manually to draw out the capillary to a diameter that will fit within the injection needle capillaries. It was then snapped in the centre to produce two loading pipettes. Agarose pads were made by dropping ~50μl 2% warm liquid agarose solution onto glass coverslips and covering with an additional coverslip to flatten. Once solidified, the top coverslip was removed and pads are left at room temperature overnight before use. Injections were carried out using an inverted DIC microscope (Zeiss Axiovert) for visualisation at 5x and 40x magnification and a micromanipulator

(Narashige MO-202) that provided fine mobility in 3 dimensions in conjunction with a pressurised injection system with needle holder.

Microinjections were executed by first filling the injection needles with the required DNA using the DNA loading pipettes. Then the loaded needle was placed in the needle holder controlled by the micromanipulator. A drop of liquid paraffin was placed on the agarose pad and under a dissection microscope 1-5 *unc-68(e540)* hermaphrodites were picked from a bacteria free region of a Nematode Growth Medium (1.7% Agar, 50mM NaCl, 0.25% Peptone in 1L H_2O autoclaved then cool and add 25ml 1M KH_2PO_4, 1ml 5mg/ml Cholesterol and 1ml of 1M $CaCl_2$) (NGM) plate and dropped into the paraffin. The animals fall through the paraffin and stick to the pad, holding them immobilised for injections. The pad is then placed on the stage of the inverted microscope. Using the 5x objective the worm was positioned with the needle at a 20° angle to the gonad arm. Then the objective was shifted to 40x and the needle top was brought against the cuticle and a slight tap of the microscope allowed the needle to pierce the cuticle. The air pressure in the injection system was then raised to push the DNA into the gonad until it was full. After all individual worms have been injected on the pad, 2-3 drops of M9 buffer (21.57mM KH_2PO_4, 42.27mM Na_2HPO_4, 85.6mM NaCl, 1mM $MgSO_4$) (Stiernagle, 2006) was then added to the paraffin to rehydrate the injected animals. Animals were then left to recover on the pad placed on a lid of an inverted NGM plate (to provide a humid environment to reduce evaporation). Once thrashing in the M9 they were picked onto fresh NGM agar plates and left to grow at 20°C.

Those worms bearing the extra-chromosomal array encoding a functional *unc-68* display a wild type phenotype of movement. Transgenic progeny of injected animals are picked to fresh NGM plates 3-4 days after injection. Two types of strain were established, one set using just a single fosmid and one set where a manipulated fosmid was injected alongside the wild type fosmid (Table 2.5). MH, CCD and EHI strains were generated by Professor Ian Hope, LOAM strains were generated by the author.

Table 2.5 Details of all transgenic strains generated by microinjection

Human condition	Model	Strain code (variant fosmid only)	Strain code (variant and wild type fosmid)
MH	G341R	UL4141	UL4167
	R2163H	UL4147	UL4153
	R2454H	UL4143	UL4165
	R2458H	UL4144	UL4158
CCD	R4861H	-	UL4152
	A4940T	UL4157	UL4156
EHI	R163C	UL4155	UL4160
LOAM	K3452Q	UL4168	UL4169

This provides models of the homozygous state (single fosmid rescue) and heterozygous state (dual fosmid rescue) for each variant studied. The fosmid expressing the variant equivalent to R4861H (implicated in CCD) was also injected in a mixture with pRF4, a plasmid bearing a defective *rol-6* gene that causes an obvious dominant roller phenotype. This was completed to determine why it was not possible to generate a single fosmid rescue strain using this altered fosmid.

The experimental control strain was developed under the same conditions, using only the wild type fosmid. The standard wild type (N2) was also maintained along with the CB540 strain necessary for microinjection transformation (Table 2.6).

Table 2.6 Details of additional strains used

Strain code	Details
N2	Wild type
UL4140	*Unc68(e540)* rescued with wild type fosmid
CB540	*Unc68(e540)*

2.2.5 Age synchronisation

Eggs were prepared by a bleaching protocol to synchronise worm populations for assay. Mixed stage populations of nematodes were washed from the NGM plates in 500μl M9 buffer. 150μl of Sainsbury's thin bleach and 100μl 4 M NaOH were added and the solution left at room temperature for 5 minutes. After microcentrifugation at 19100 rcf for 30 seconds the supernatant was removed and the pellet re-suspended in 1ml fresh M9 buffer. Centrifugation was repeated and the pellet re-suspended in ~50μl of residual supernatant for transfer to a freshly seeded NGM plate. This protocol kills all post-embryonic stages leaving the eggs that subsequently hatch and develop into adults, effectively ensuring that the worms used in the phenotyping assays will be of the same age.

2.2.6 Phenotyping assays

The transgenic strains were assayed to determine their sensitivity to caffeine and halothane. Individual adult worms, 4 days after age synchronisation, were selected from NGM plates using a sterile worm pick and placed in 1ml of 0, 1, 5, 10, 20, 40 or 80mM caffeine dissolved in S-medium (1L S Basal (5.85g NaCl, 1g K_2HPO_4, 6g KH_2PO_4, 1ml cholesterol (5mg/ml in ethanol), H_2O to 1L and autoclaved), 10ml 1 M potassium citrate pH6, 10ml trace metals solution (1L stock: 1.86g Na_2 EDTA, 0.69g $FeSO_4$ •7 H_2O, 0.2g $MnCl_2$•4 H_2O, 0.29g $ZnSO_4$ •7 H_2O, 0.025g $CuSO_4$ •5 H_2O, H_2O to 1L, autoclaved and stored in the dark), 3ml 1M $CaCl_2$, 3ml 1M $MgSO_4$) (Stiernagle, 2006). After 5 minutes the effect of the chemical was quantified by counting the number of body bends in 30 seconds by visualisation through a light microscope and using a clicker to record bends. Body bends were defined as the number of visible thrashes observed with the worm in liquid media. In liquid, the head of the worm

thrashes back and forth, with each thrash counting as a body bend. Halothane assays were carried out in a similar manner but using 1ml of 0, 0.5, 1, 1.5, 2 and 2.5mM halothane solution (prepared from a 25mM stock in DMSO and mixed into S-medium) and assaying after 1 minute exposure. Fifty worms were assayed for each strain at each concentration. All phenotyping assays were completed by the author.

2.2.7   Generation of GFP-myosin strains

GFP-myosin strains were developed by mating N2 males with *unc-68(e540)* hermaphrodites to generate hermaphrodite progeny heterozygous for *unc-68*. The males were selected and crossed with RW1596 (stEx30 (*myo-3:: gfp rol-6(su1006)*)) hermaphrodites. The RW1596 strain confers a rolling movement phenotype. The resulting hermaphrodite progeny were then allowed to self-generate uncoordinated rollers meaning they are homozygous for *unc-68(e540)* and express the extra chromosomal array for myo-gfp. These worms were then subjected to UV mutagenesis ($0.012J/cm^2$ for 30 seconds) (Mariol *et al.*, 2013) and screened for 100% uncoordinated rollers to ensure that the extra chromosomal array for myo-gfp had been successfully integrated. Hermaphrodites from this new strain were then mated with males each of the *unc-68* fosmid transgenic strains and offspring screened for worms with well-coordinated roller movement. This is due to the *unc-68* bearing extrachromosomal array and the chromosomally integrated *myo-3::gfp, rol-6(su1006)* transgenes. Self-fertilization and selection for well-coordinated rollers yielded *myo-3::gfp, rol-6(su1006)* homozygous strains bearing the *unc-68* transgenes. Strains were then catalogued, details of which can be found in Table 2.7. All GFP-myosin strains were generated by the author.

Table 2.7 Details of strains generated by genetic cross to create *myo-gfp* models of all variant strains

Human condition	Model	Strain code (variant fosmid only)	Strain code (variant and wild type fosmid)
MH	G341R	UL4193	UL4200
	R2454H	UL4195	UL4206
	R2458H	UL4201	UL4197
	R2163H	UL4194	UL4198
CCD	R4861H	-	UL4205
	A4940T	UL4203	UL4202
EHI	R163C	UL4191	UL4192
LOAM	K3452Q	UL4196	UL4199

2.2.8 Muscle ageing assays

The transgenic strains expressing the *myo-3::gfp* were age synchronised following the details in section 2.2.5 and then assayed on days 0, 2, 4, 6, 8, 10, 12 and 14 of adulthood. Day 0 was considered to be 3 days post-hatching. Only live worms were selected for analysis. 20 worms were assayed for each strain at each time point. The extent of muscle ageing was quantified by direct observation using an ageing scale from 1-5 (Figure 2.6) with half scores assigned where the appearance overlapped two stages.
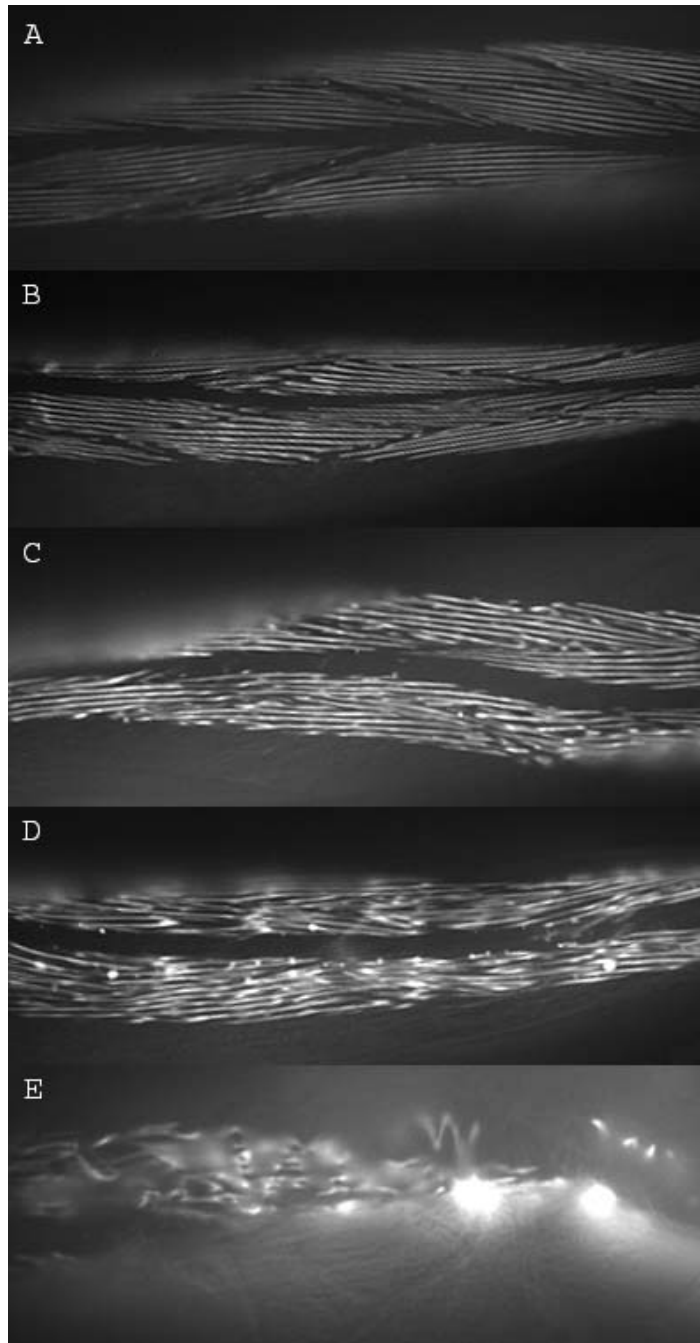
Figure 2.6 Examples illustrating the 5 grades in the muscle disorganization scoring scale. The myosin::gfp fusion protein is localized to the thick filaments and so distribution of the fluorescence reports on the regularity in the arrangement of the sarcomeres. Images captured by fluorescence microscopy. A: Typical structure of a grade 1 muscle score; myosin filaments are linear and well organised. B: Typical structure of a grade 2 muscle score; myosin filaments are starting to show more bends but the pattern is still well organised. C: Typical structure of a grade 3 muscle score; myosin filaments are more fragmented and there are apparently overlapping filaments. D: Typical structure of a grade 4 muscle score; myosin filaments are further fragmented and the regularity of pattern is no longer clear. E: Typical example of grade 5 muscle score; the pattern of myosin filaments is severely disorganized. Figure compiled by Matt Pipe.

A score of 1 indicates perfectly ordered myofilament structure, through to a score of 5 indicating total disorder, with half scores for worms that lay between the defining states. Visualisation and image capture was carried out using a Leica DMR fluorescence microscope and Improvision Openlab software. In preparation for microscopy animals were immobilised using 5mM levamisole and placed in individual wells of an 8 well microscope slide. Each individual was scored for extent of muscle ageing at the head, vulva and tail regions of the body at 20x magnification. These scores were combined to provide a whole body score.

Assessment of repeatability of this method was carried out by providing a cohort of 20 images from various regions of the worm's body to another observer. This was another member of the Hope laboratory trained in evaluating muscle structure using the scoring system described above. Each image was scored independently and the percentage agreement with the author measured.

2.2.9 Statistical Analysis

Results of phenotyping assays were analysed to establish any potential differences in the rate of body bends when the worms are subjected to halothane and caffeine. Each strain containing an altered fosmid was compared to the strain containing the unaltered fosmid at each discrete concentration of the reagent in question. Normal distribution of the data was established by plotting residuals in RStudio (version 3.2.2). A linear model was established describing body bends being dependent upon presence of the variant and statistical significance was measured by carrying out analysis of variance on the linear model. Post-hock Tukey tests were then performed to establish exactly

which strains showed a significant difference in body bends compared to wild type at each concentration.

Categorical muscle score data were analysed using ordered logistic regression with p values calculated by comparing the T-statistic to the standard normal distribution. Initial analysis tested for differences in the specific body regions scored and subsequent analysis incorporated the individual body region scores into a whole-body score. This enabled examination of any differences between the strains with modified *unc-68* and the strains rescued with the wild-type *unc-68*, evaluation of the effect of increasing age of the worm in days, and interactions between these two variables. Differences between the scores for the regions of the worm down the anterior-posterior axis were similarly carried out. All statistical analyses were completed using RStudio version 3.2.2 and figures compiled using Microsoft® Excel® for Mac 2011.

2.3   Results

2.3.1   Two-step counter-selection recombineering

This section presents the results of the two-step counter-selection recombineering carried out to introduce variants K3452Q and V8949I. Figure 2.7 displays the results of colony PCR following the first recombineering step. The bands at approximately 2kb indicate that the fosmid has taken on the RT cassette for each variant.
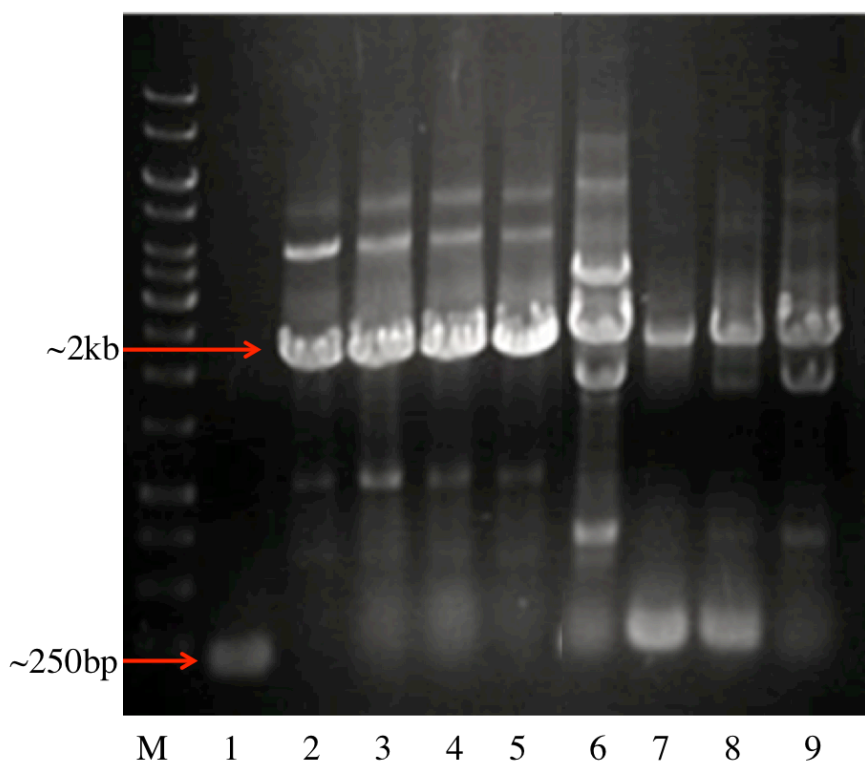
Figure 2.7 Colony PCR results of recombineering step 1. Lane 1 is PCR amplification of cells containing the unaltered fosmid, lanes 2-5 show PCR amplification of cells containing the fosmid +V4849I variant specific cassette, lanes 6-9 show PCR amplification of cells containing the fosmid +K3452Q variant specific cassette. Lane M is 1kb ladder.

Figure 2.8 shows the results of the colony PCR performed after completion of the second recombineering step along with alignment of the sequencing results for each variant. For all alignments the upper case sequence is the sequence of the original unchanged fosmid and the lower case sequence displays the results of sequencing analysis on the recombineered fosmid for each mutation.

60
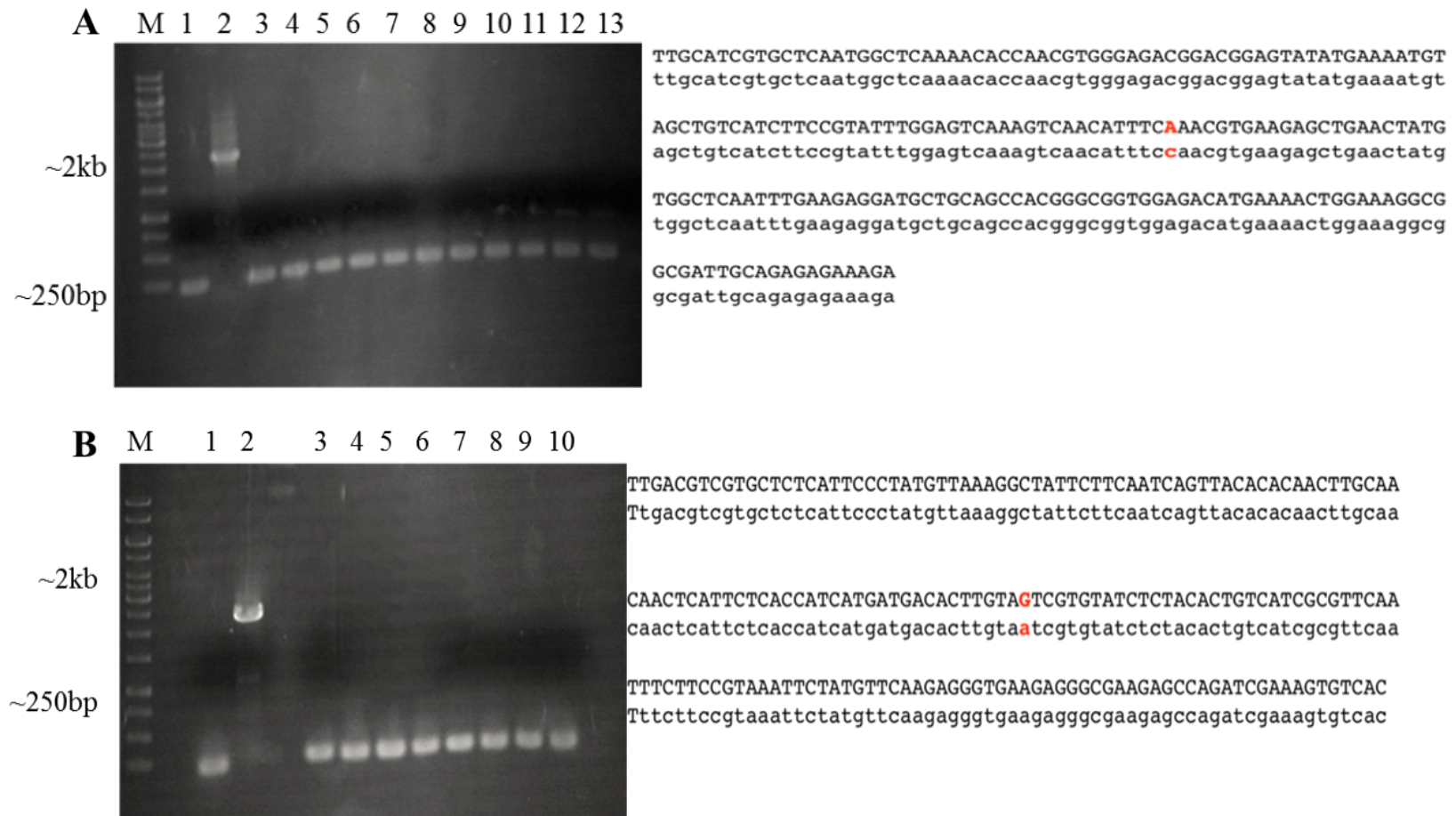
Figure 2.8 Colony PCR results of recombineering step 2 and alignment of sequencing results. The desired change for each variant is highlighted in **red**. A: K3452Q and alignment of sequencing results. Lane 1 shows PCR amplification of cells containing unaltered fosmid, lane 2 is PCR amplification of cells containing fosmid with the RT cassette and lanes 3-15 show PCR amplification of cells produced from recombineering step 2-fosmid DNA containing mutation. Lane M is 1kb ladder. B: V4849I and alignment of sequencing results. Lane 1 shows PCR amplification of cells containing unaltered fosmid, Lane 2 is PCR amplification of cells containing fosmid with the RT cassette. Lanes 3-10 shows PCR amplification of cells produced from recombineering step 2-fosmid DNA containing mutation. Lane M is 1kb ladder.

EcoR1 restriction digestion was carried out on the unaltered WRM069cA02 fosmid

DNA, WRM069cA02+RT cassette, and the final recombineered fosmid for each

variant. The results (Figure 2.9) show that the desired fragment sizes have been

obtained for the starting fosmid, the fosmid containing the RT cassette and for each

variant.
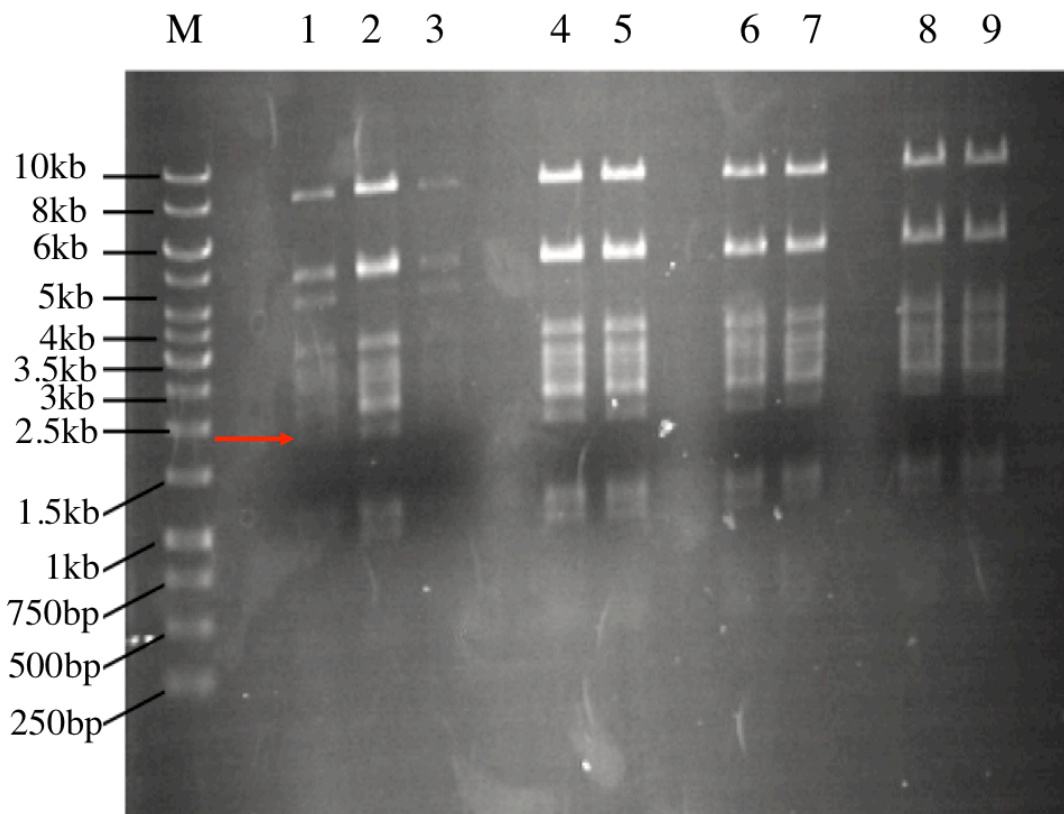
Figure 2.9 EcoR1 restriction digest. Lanes 1&3:WRM069cA02+RT cassette, lane 2: WRM069cA02-unaltered, lanes 4-6: WRM069cA02+K3452Q, lanes 7-9: WRM069cA02+V4849I. Red arrow indicates additional band at ~2000bp for fosmid containing cassette.

No additional cut sites were introduced by the recombineering, therefore the same

bands are expected for the recombineered fosmids as the original starting fosmid. An

additional band of approximately 2kb in size is evident for the digest carried out on

the fosmid+RT cassette DNA. This is consistent with successful introduction of the

RT cassette.

2.3.2   Rescue of unc-68(e540) by an unc-68 transgene

Microinjection of unaltered or manipulated WRM069cA02 into the gonad of *unc-68(e540)* hermaphrodites yielded progeny with apparently wild type locomotion suggesting WRM069cA02 does indeed contain the entire *unc-68* gene and all that is required for its expression. Transmission of the rescued phenotype to subsequent generations allowed establishment of transgenic strains and therefore the *unc-68* transgene on the extra chromosomal array provides appropriate levels of the ryanodine receptor in muscle cells. One of these strains, UL4140, with the highest extra chromosomal array transmission rate, was used as a baseline reference for comparison in subsequent experiments to examine ryanodine receptor variants. Not only was UL4140 fully rescued for locomotion but also the strain responded to increasing caffeine and halothane concentrations in the same manner as the standard wild type strain (N2) (Figure 2.10).

The wild type strain N2 and UL4140, rescued with the wild type fosmid, show an increasing frequency of body bends from 1mM to 10mM caffeine (Figure 2.10A). There is a progressive reduction in movement at 20mM, 40mM and 80mM (Figure 2.10A). Halothane inhibited *C. elegans* locomotion progressively with increasing concentrations of the anaesthetic, across all concentrations tested (Figure 2.10B). The similar behaviour of UL4140 and N2 strains suggests that UL4140 is a suitable experimental control with which to study the consequences of making *unc-68* changes equivalent to muscle myopathies.
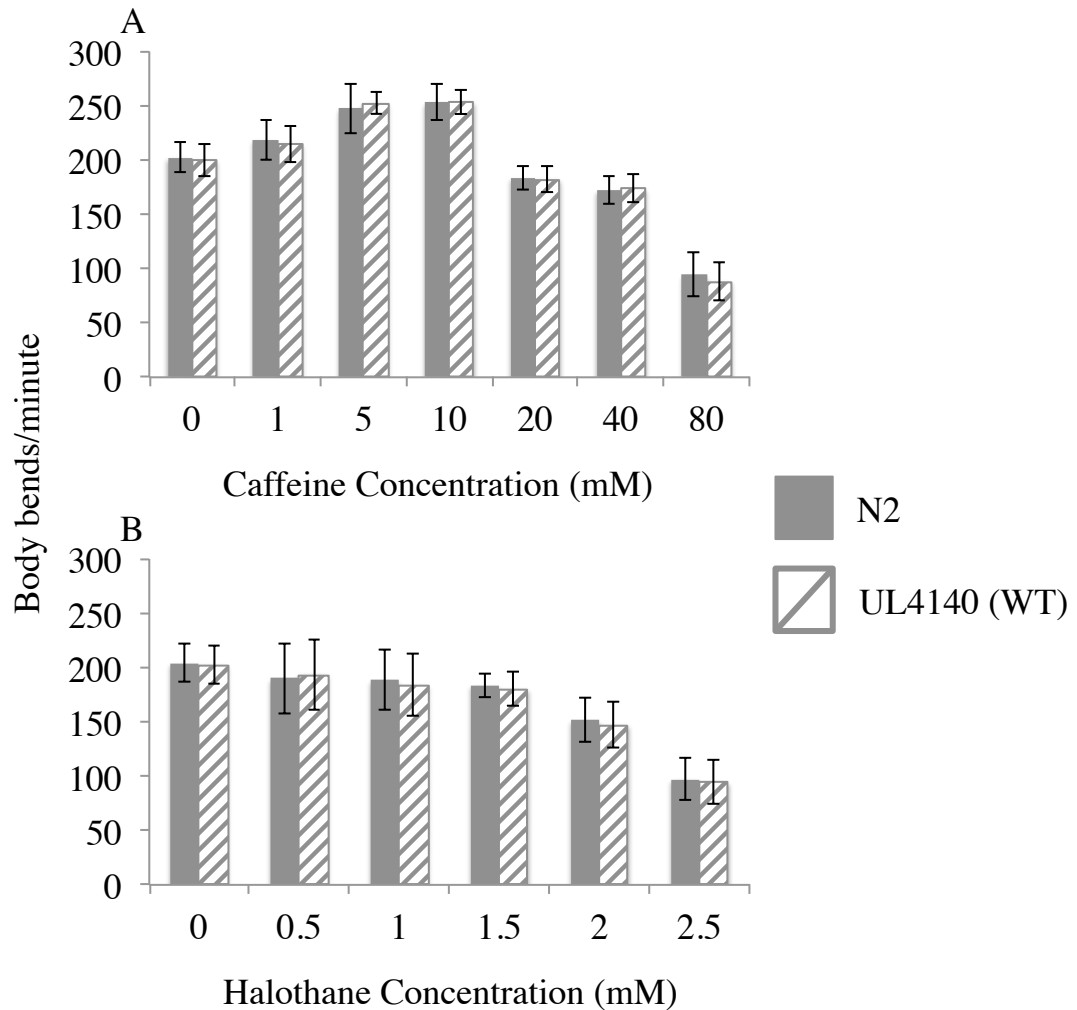
Figure 2.10 Comparison of the rate of locomotion of N2 and UL4140 *C. elegans* strains in increasing concentrations of caffeine or halothane. Mean body bends per minute in the presence of various concentrations of caffeine (A) or halothane (B) are presented. Error bars are standard deviation, n=50 for each strain at each concentration measured.

2.3.3 Establishing muscle myopathy strains

Nine variants in *RYR1* were identified for use in *C. elegans* (Table 2.1). All are conserved at the amino acid level. Four variants implicated in MH were chosen: G341R, R2163C, R2454H and R2458H. Patients carrying these variants are found to display a more severe MH phenotype when compared to the most common MH variant, G2434R (Carpenter *et al.*, 2009b). The G2434R variant is not conserved. The most common EHI variant (R163C, also implicated in MH) (Estève *et al.*, 2010) was selected along with the two CCD variants, R4861H which is implicated in CCD only

(Monnier *et al.*, 2001) and A4940T which is implicated in CCD and MH (Kraeva *et al.*, 2013), and K3452Q and V4849I variants implicated in LOAM.

Multiple strains were generated by microinjection with each DNA preparation, of which 15 with the strongest transgene transmission were utilised in this study. Transgenic strains were established for all variants through microinjection of modified fosmids alone and along with the wild type fosmid, except for one implicated in CCD, R4861H and one implicated in LOAM, V4849I. For variant R4861H, *unc-68* rescue was only possible upon microinjection in combination with the wild type fosmid. This suggested that the modification equivalent to R4861H had resulted in a non-functional *unc-68* protein. Co-injection of the R4861H fosmid alongside a pRF4 plasmid yielded transgenic worms with a slow rolling phenotype. pRF4 confers a rolling phenotype to the worm, and if expressed in combination with a functioning *unc-68* it would be stronger than what was observed here. This process, using the R4861H fosmid, failed to rescue *unc-68* to the wild type rate of locomotion. The extra chromosomal transgene array in these slow rolling transgenic worms would be expected to include the modified fosmid as well as pRF4, but the R4861H fosmid appeared incapable of providing wild type *unc-68* function. Co-injection of the V4849I fosmid alongside a pRF4 plasmid also yielded transgenic worms with a slow rolling phenotype. In addition, microinjection of the V4849I fosmid in combination with the wild type fosmid did not yield transgenic worms.

2.3.4   Malignant hyperthermia and central core disease

The strains established with the four modified *unc-68* fosmids equivalent to human *RYR1* variants G341R, R2454H, R2458H and R2163H implicated in MH were assayed for caffeine and halothane sensitivity (Figure 2.11).

The increase in body bends seen from 1 to 10 mM caffeine, in strains with wild type *unc-68,* is no longer evident. Strains equivalent to R2454H, R2458H and R2163H variants display a substantial decrease in locomotion rate between 1mM and 5mM caffeine (Figure 2.11A). There is a small progressive further decline from 10 to 40mM caffeine with almost complete cessation of movement occurring at 80mM, a concentration at which strains with unmodified *unc-68* still show considerable if somewhat reduced rate of movement. The models for the G341R variant behave in a distinct fashion. The rate of body bends remains fairly constant up to 40mM caffeine. This could be attributed to a failure to show the stimulated response of the strains with the wild type *unc-68* at 5 and 10mM caffeine. There is then a substantial decrease at 80mM caffeine for the G341R model strains. This level is significantly less than the strains with only wild type *unc-68* ($p < 0.01$), but not as reduced as the other MH model strains.

Strains for all four modelled MH variants behaved similarly in response to increased halothane concentrations (Figure 2.11B). Decreased body bends in comparison to the control strains were apparent even at 0.5mM halothane and were significantly less at all concentrations examined ($p < 0.01$).
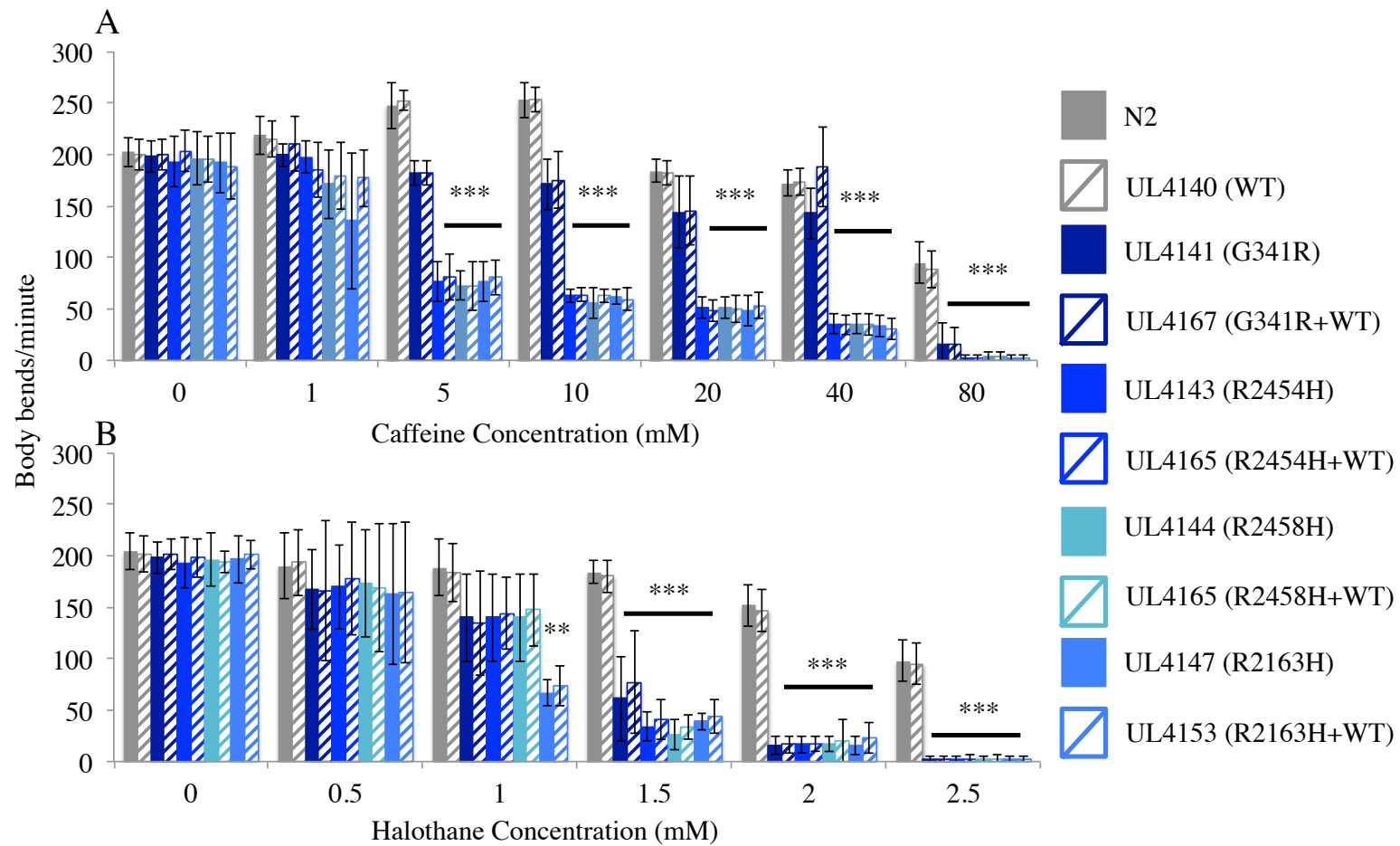
Figure 2.11 Comparison of the rate of locomotion of *unc-68* variant strains, implicated in malignant hyperthermia, and wild type *C elegans* in increasing concentrations of caffeine and halothane. A: Caffeine results, B: Halothane results. Error bars are standard deviation, n=50 for each strain at each concentration measured. **p<0.01 ***p<0.001 results from post-hoc Tukey test.

At 1.5mM halothane, a concentration at which strains with only wild type *unc-68* show no reduced rate of locomotion in the assay, the rate of movement in the MH model strains has reduced to 15% of that seen in the absence of halothane. The MH model strains show no movement by 2.5mM, while the strains with only wild type *unc-68* show a reduced but still substantial rate of movement at that concentration. There may be marginal increase in sensitivity to halothane in the R2163H strains, but this is only apparent in the more reduced locomotion at 1mM halothane.

As with caffeine, the G341R models may show slightly less sensitivity to halothane but only from the further reduction in the rate of movement observed at 1.5mM.

The CCD model strains for A4940T and R4861H variants behave in a similar manner to the R2454H, R2458H and R2163H MH model strains (Figure 2.12). The caffeine response appears identical for these CCD and MH models (Figure 2.12A).

In the halothane assays the models of the two CCD variants mirror subtle distinctions in response of the MH strains (Figure 2.12B). The A4940T CCD models appear to behave in the same way as the R2454H and R2458H MH models while the R4861H CCD model appears to behave in the same way as the R2163H MH model across the entire concentration range examined.
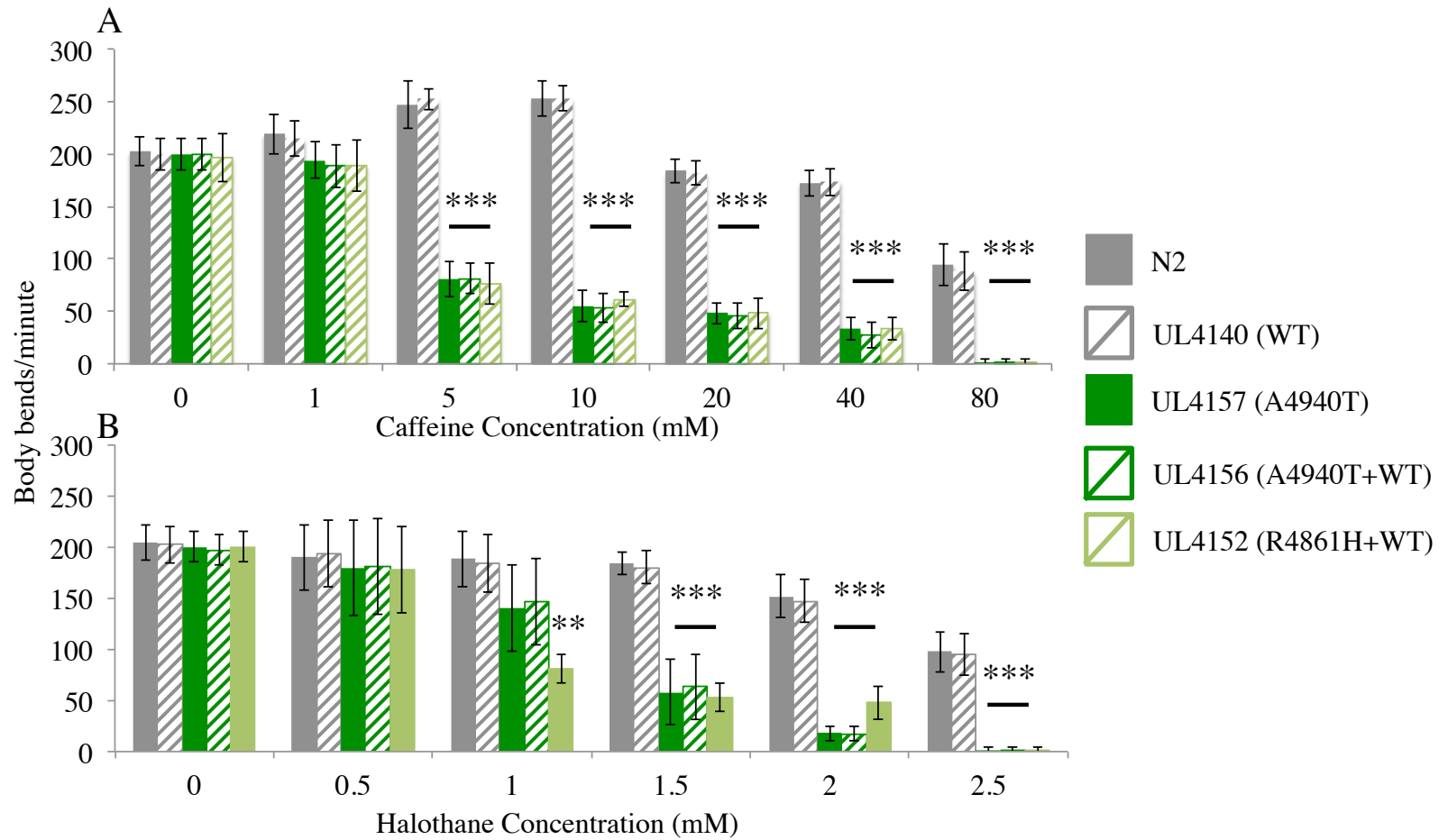
Figure 2.12 Comparison of the rate of locomotion of *unc-68* variant strains, implicated in central core disease, and wild type *C elegans* in increasing concentrations of caffeine and halothane. A: Caffiene results, B: Halothane results. Error bars are standard deviation, n=50 for each strain at each concentration measured. **p<0.01 ***p<0.001 results from post-hoc Tukey tes

2.3.5 Exertional heat illness and late onset axial myopathy

Only a single variant for EHI was recombineered in *unc-68*. The strains created with this fosmid behaved alike, in a way that was distinct from the response of the CCD and MH models (Figure 2.13). The response to caffeine is very similar to that of strains with only wild type *unc-68,* with the slight stimulation of locomotion at 5 and 10mM caffeine (Figure 2.13A).

At the highest concentration of caffeine assayed (80mM) both the EHI models appear virtually paralysed. In contrast to the minimal effect on caffeine sensitivity these variants did show a response to halothane similar to that seen in the CCD and MH model strains differing from wild type (Figure 2.13B). There is a slight reduction in locomotion at 0.5 and 1 mM halothane, with a considerable reduction to 1.5 mM, and almost complete paralysis at 2.5 mM.
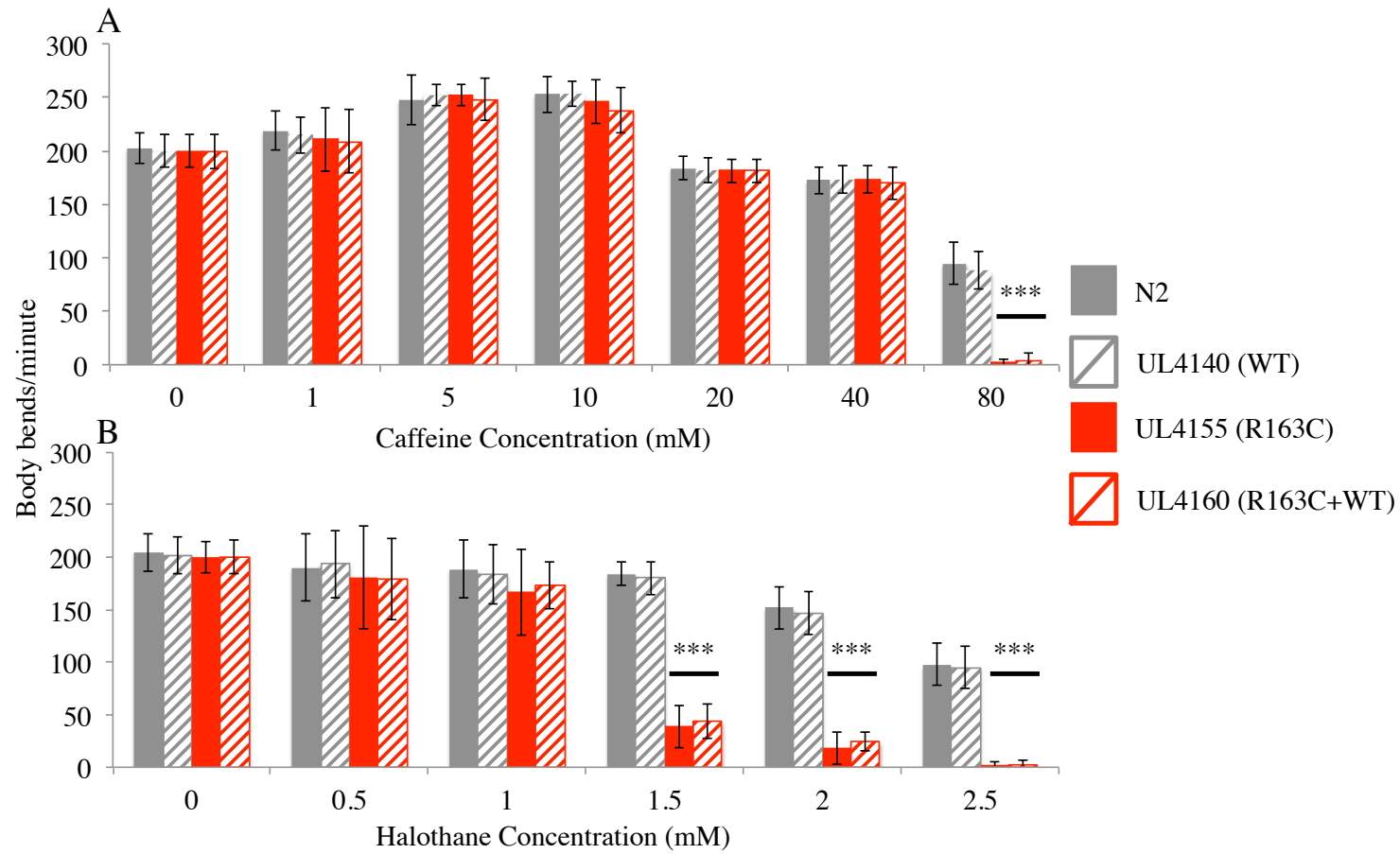
Figure 2.13 Comparison of the rate of locomotion of *unc-68* variant strains, implicated in exertional heat illness, and wild type *C elegans* in increasing concentrations of caffeine and halothane. A: Caffiene results, B: Halothane results. Error bars are standard deviation, n=50 for each strain at each concentration measured. ***p<0.001 results from post-hoc Tukey test.

Like the EHI models, only a single fosmid containing a variant implicated in LOAM was successfully engineered and strains generated by microinjection transformation. The response of these strains to caffeine was similar to that of the EHI model strains but there was no reduction in locomotion observed at 80mM caffeine when compared to UL4140 (Figure 2.14A).

The response to halothane in the LOAM model strains was consistent with the response of the MH, CCD and EHI models (Figure 2.14B), characterised by a progressive reduction in body bends with increasing halothane concentrations that is considerably more pronounced compared to the experimental control.
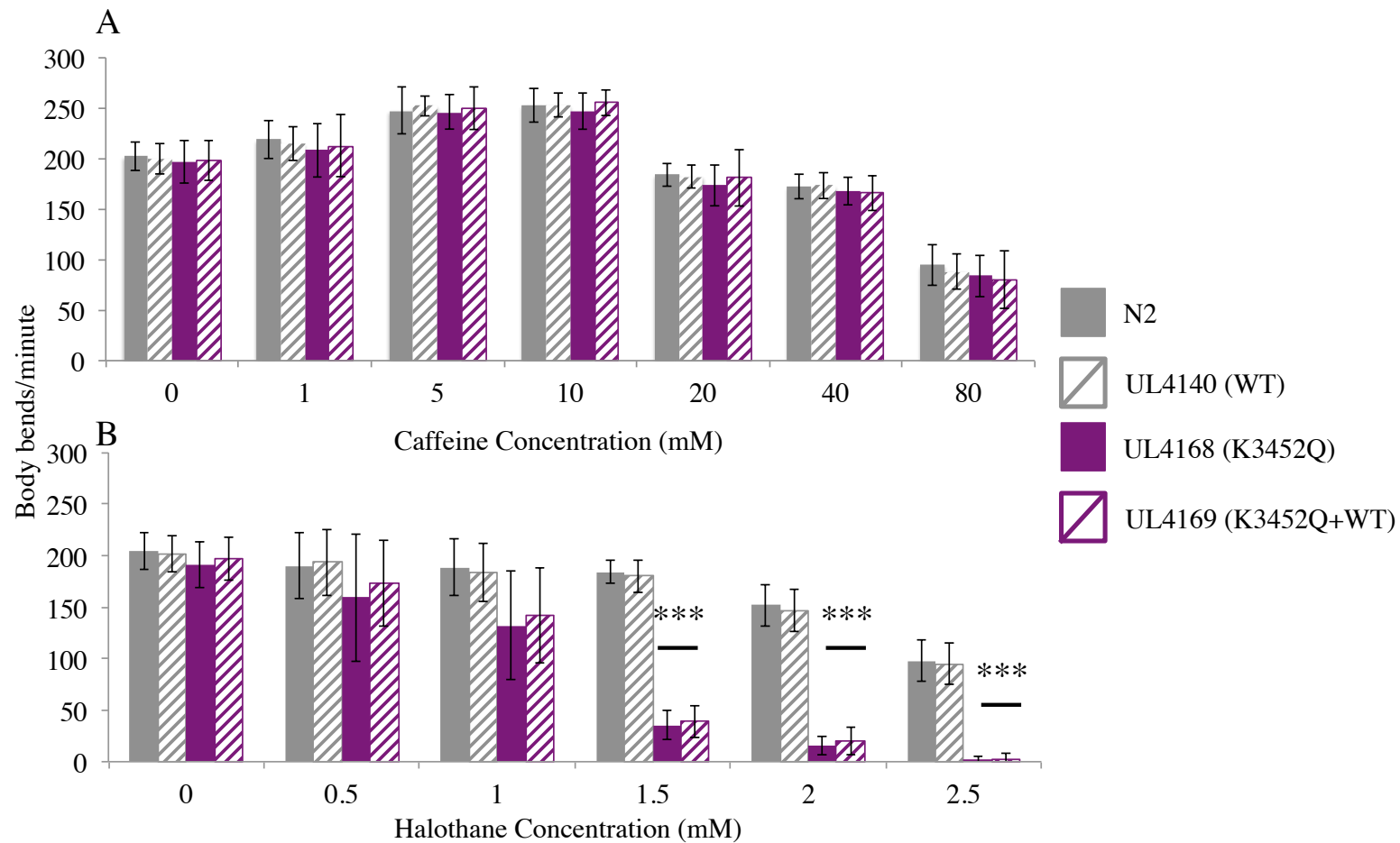
Figure 2.14 Comparison of the rate of locomotion of *unc-68* variant strains, implicated in late onset axial myopathy, and wild type *C elegans* in increasing concentrations of caffeine and halothane. A: Caffiene results, B: Halothane results. Error bars are standard deviation, n=50 for each strain at each concentration measured. ***$p < 0.001$ results from post-hoc Tukey test.

2.3.6 *Dominant sensitivity to halothane and caffeine*

Genetic dominance is a striking property of *RYR1* variants. Noticeably, there was no significant difference in the rate of body bends between a strain rescued with a variant *unc-68* and the corresponding strain rescued in combination with wild type *unc*-68, across the range of caffeine and halothane concentrations used. This is consistent with these amino acid changes in *unc-68* causing dominant effects in *C. elegans* as well. The one possible exception to this is the G431R variant (Figure 2.11B). A slightly elevated rate of body bends was seen at 40 mM caffeine and at 1.5mM halothane ($p<0.05$) for UL4141, rescued with only the modified *unc-68* fosmid, in comparison to UL4167, rescued in combination with the wild type *unc-68*.

2.3.7 *Differences in myosin disorganisation in different body regions*

As three distinct regions of the worm's body (head, vulva and tail) were scored for analysis it was possible to evaluate differences between these three regions, prior to establishing the whole body score. In the wild type model strain (UL4190) it is shown that while there is some overlap in the median muscle age scores assigned to the head and vulva regions, the tail region is scored higher across the range of days. (Figure 2.15).
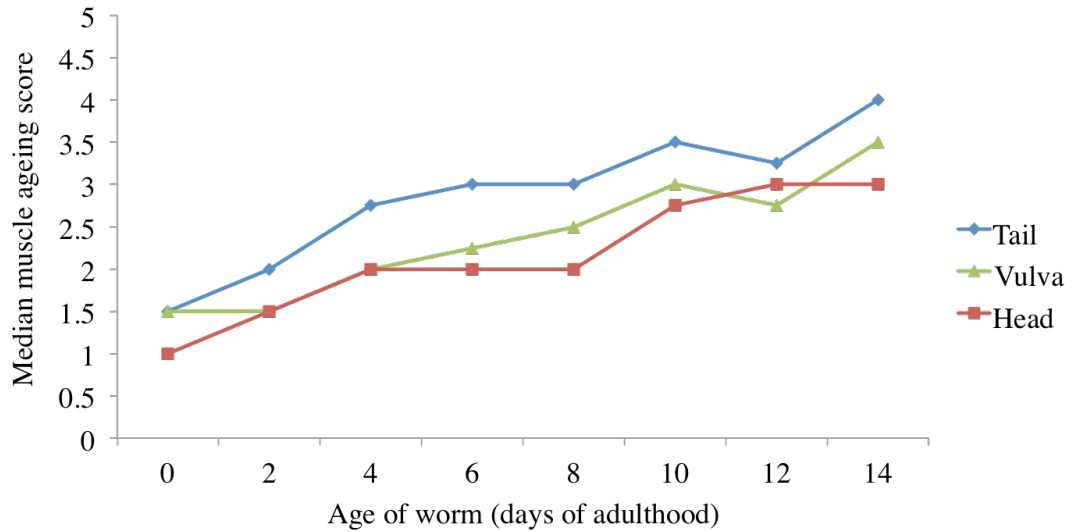
Figure 2.15 Line graph of the progressive ageing pattern observed in the head, vulva and tail regions of the wild type worm (UL4190).

Overall, across the range of days observed, the median score for the vulva is significantly higher than the head, p=0.04 and the tail is scored very significantly higher   than the head, p=0.0002. This same pattern of increased myosin disorganisation in the tail and vulva compared with the head is evident in the MH model strains (Figure 2.16A-D).

It is important to note that no significant difference was observed when comparing the progressive decline of muscle structure between the different types of rescue, so scores for the respective variants for each rescue type were combined for analysis. In addition to the MH model strains, the same pattern of exaggerated muscle structure decline in the tail and vulva regions was observed in the CCD, EHI and LOAM model strains (Figure 2.17A-D).
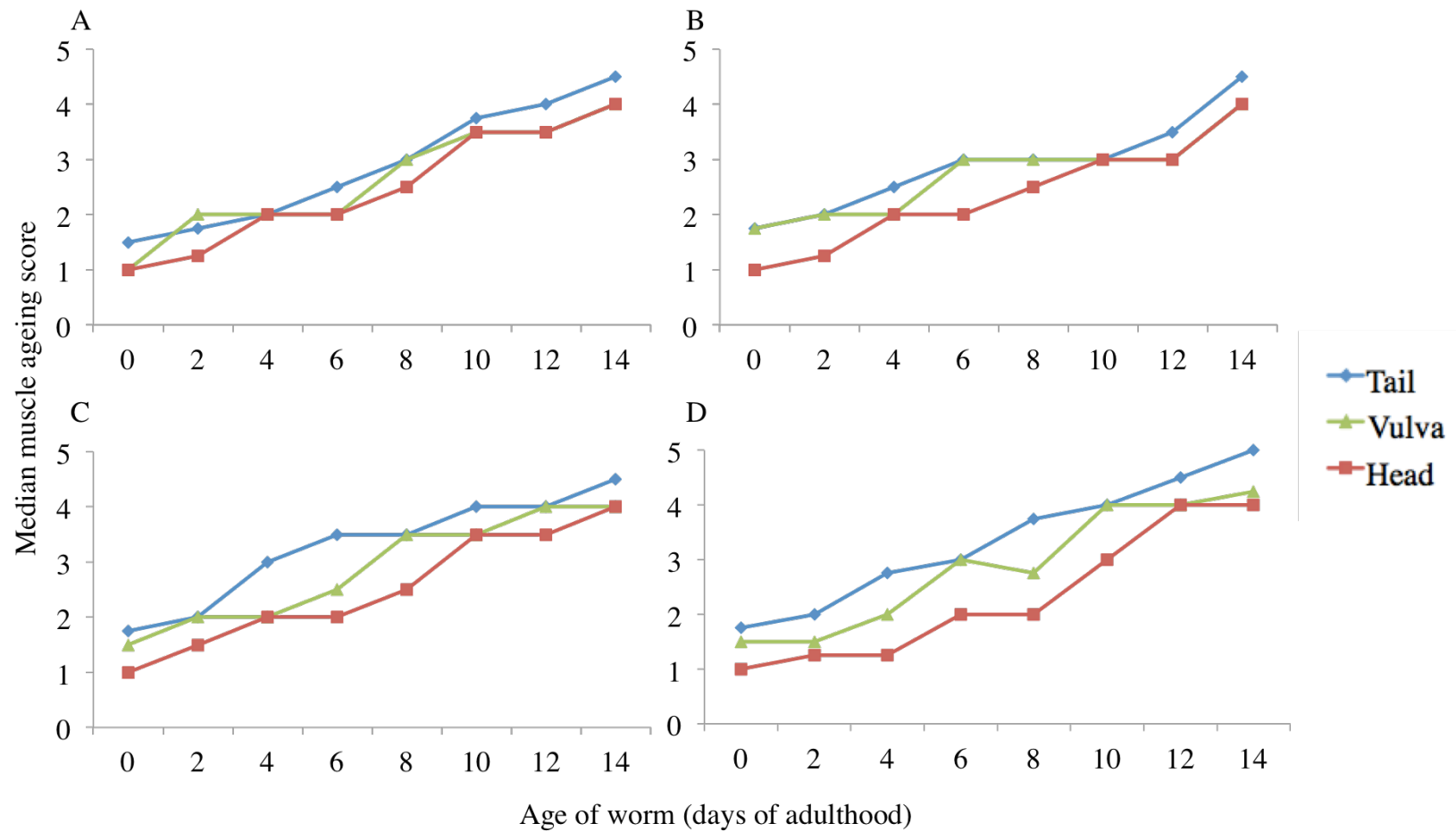
Figure 2.16 Line graphs of muscle ageing scores in MH strains. A: G341R model strains (scores for UL4190 and UL4200 combined), B: R2454H model strains (scores for UL4195 and UL4206 combined), C: R2458H model strains (scores for UL4201 and UL4197 combined), D: R2163H model strains (scores for UL4193 and UL4198 combined).
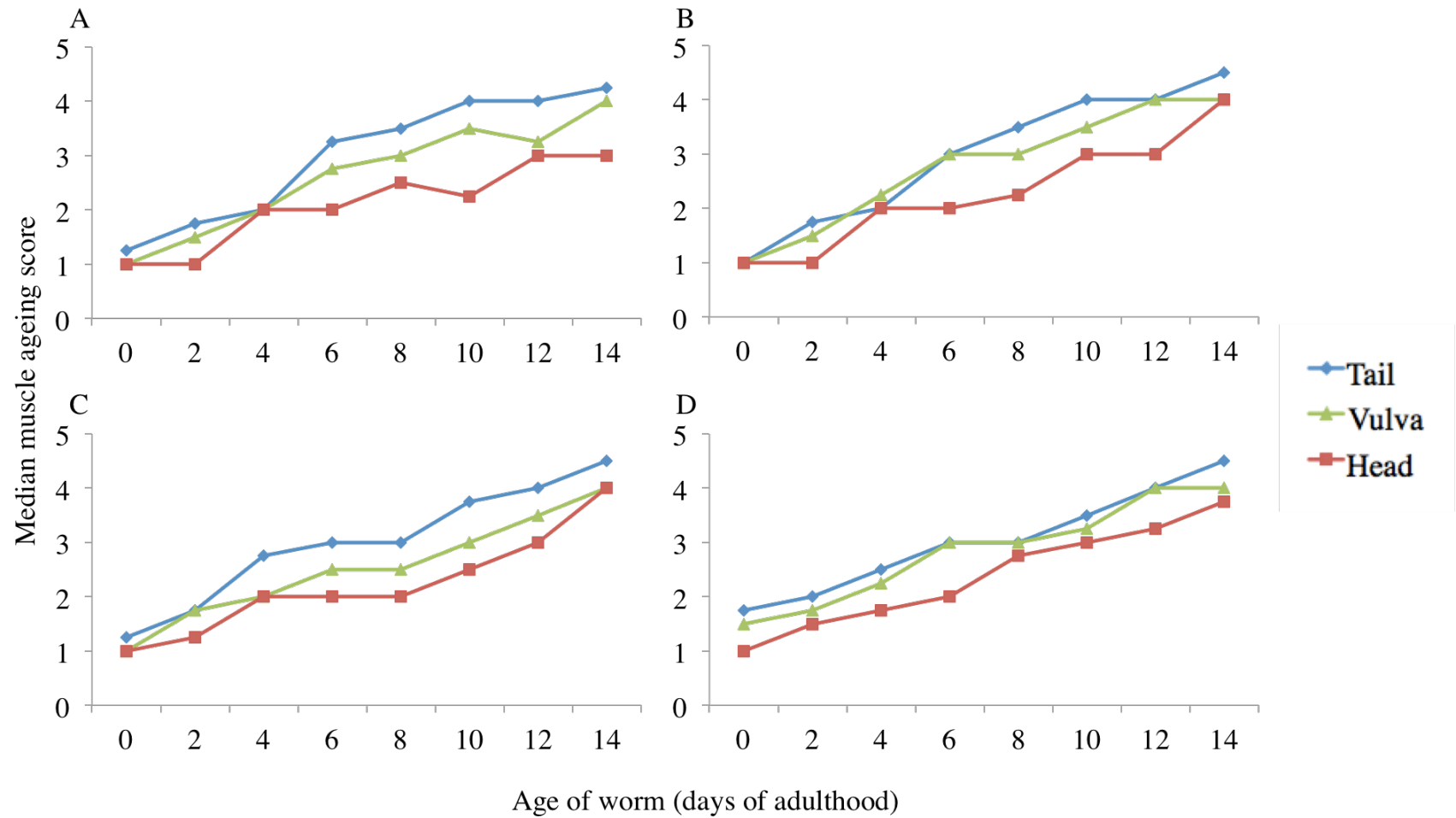
Figure 2.17 Line graphs of muscle ageing scores in CCD (A and B), EHI (C) and LOAM (D) strains. A: A4940T model strains (scores for UL4203 and UL4202 combined), B: R4861H model strain, C: R163C model strains (scores for UL4191 and UL4192 combined), D: K3452Q model strains (scores for UL4196 and UL4199 combined).

As the same pattern of progressive myosin disorganisation was observed across all of the strains tested it was then decided that the individual region scores could be combined to make a 'whole body score' that would be used in subsequent analyses to investigate any potential differences in the pattern of muscle ageing relative to the variants in question.

2.3.8 Progressive decline in muscle structure with age

The whole body score devised following analysis of the independent body regions was analysed to determine the differences in the progressive decline in muscle structure with age across all the strains examined. In order to characterise the reproducibility of the scoring method for assessing age-related muscle fibre disorganisation, a test cohort of 20 images was assessed by an additional researcher from the Hope laboratory. This individual was considered to have equivalent experience with the microscopy techniques used by the author. 19 out of 20 images scored were given the same score between both examiners. The one image where the scores disagreed, it was classified as a 2.5 by one examiner and a 2 by the other.

The wild type rescue model served as the basis for comparison in all statistical tests. It demonstrates a clear increase in the median whole body score assigned to the myosin structure with increasing age of the worm (Figure 2.18). In the wild type model strain, the age profile begins with a median whole body score of 4 on day 0, increasing to 5 by day 2 and culminating in a median whole body score of 11 on day 14. No significant difference in body score was found in any of the variant strains when compared to wild-type on day 0 or day 2.

Figure 2.18 Increasing myofilament disorganisation with age in wild type model strain (UL4190) n=20, boxplots show median, IQR and min and max score.

No significant difference was found between a strain rescued with a variant *unc-68* and the corresponding strain rescued in combination with wild type *unc*-68 for any of the variants studied across the time period examined. This further supports the finding in relation to the phenotyping assays where no differences were found in the response to caffeine and halothane between the two types of rescue. As a result the information gathered on the two rescue types was combined and so the data represent 2 strains for each variant, with the exception of the R4861H variant, which only has one strain. Overall, variant as a predictor variable was found to significantly affect the dependent variable (whole body score), p<0.001. When examining the MH strains, the overall picture of muscle degradation appears similar to the wild type, whereby there is a progressive decline of muscle structure across the range of ages examined (Figure 2.19A-D, Figure 2.20).
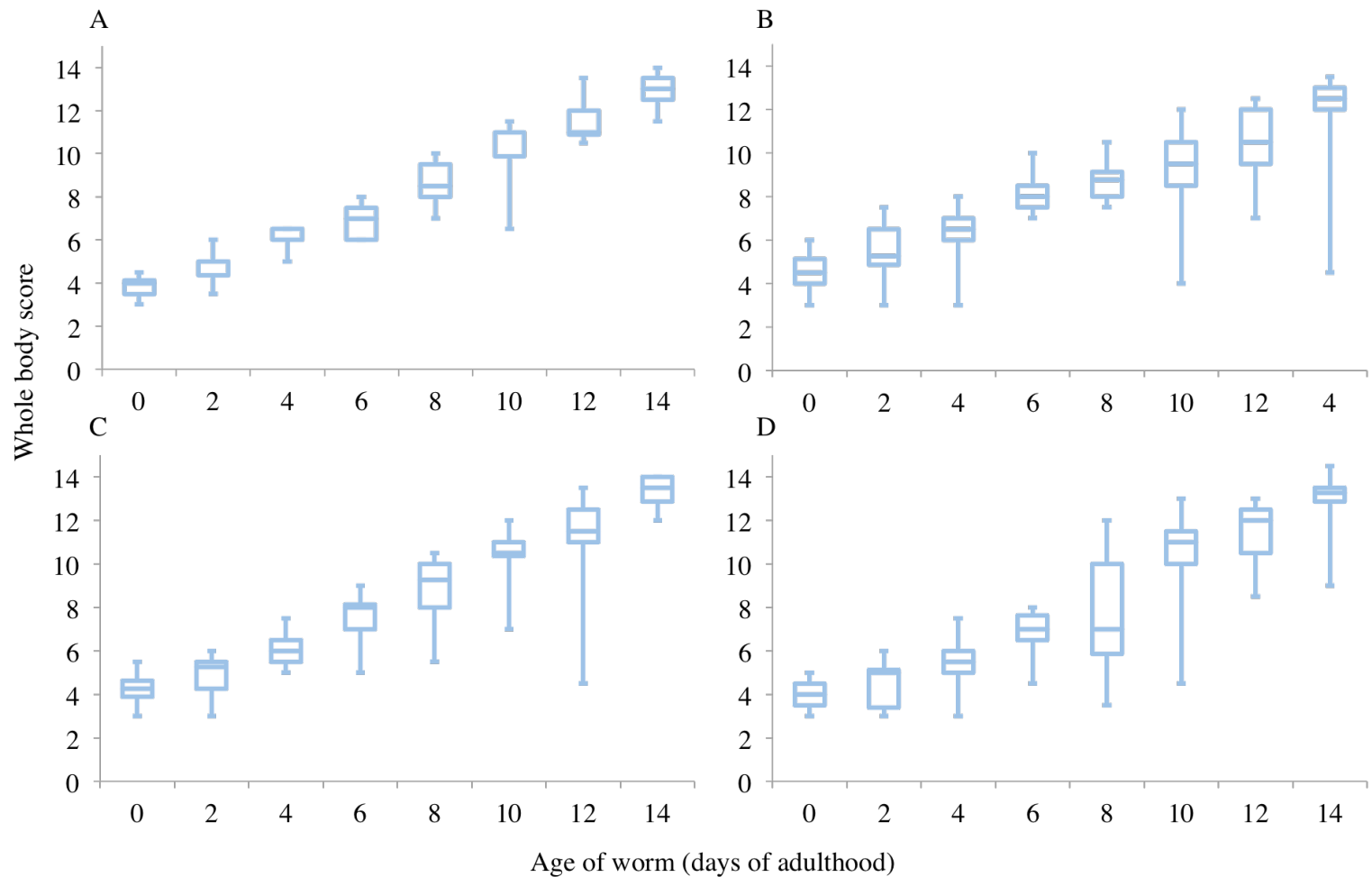
Figure 2.19 Whole body scores for increasing myofilament disorganisation from 0 to 14 days of adulthood in MH (G341R (A) (n=40), R2454H (B) (n=40), R2458H (C) (n=40) and R2163H (D) (n=40)), boxplots show median, IQR and min and max score.
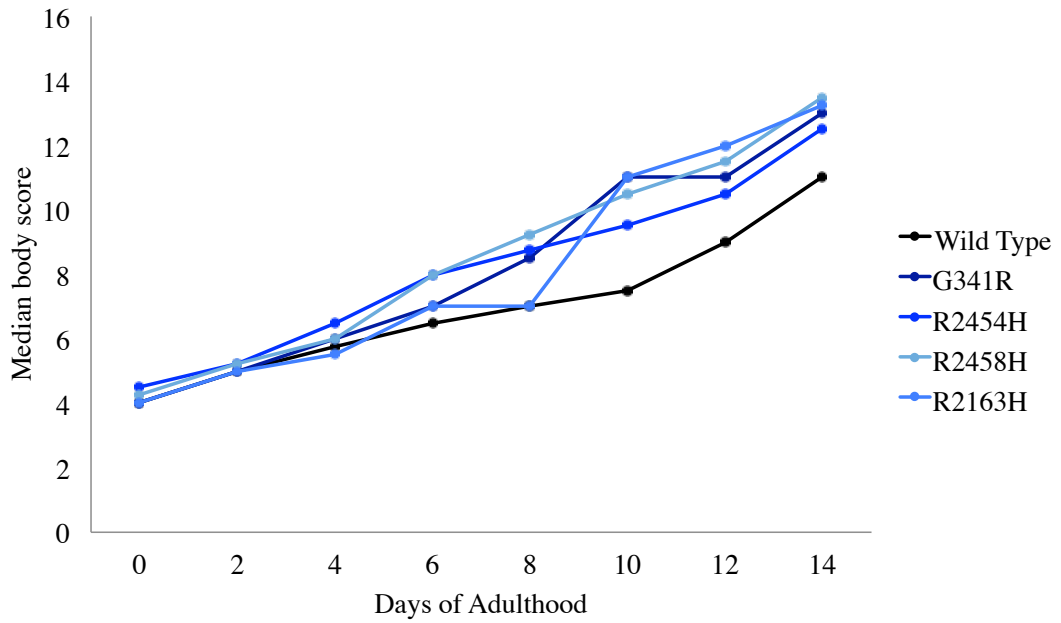
Figure 2.20 Summary of median scores from all MH strains (n=40 for all variants) compared to wild type (n=20)

By day 8, strains expressing the G341R variant displayed a significant difference (P=0.0001) from wild type in whole body score, exemplified by a marked increase in score assigned to the muscle (Table 2.8). In the R2454H and R2458H strains, this difference was evident by day 6 and in the R2163H strains by day 10 (Table 2.8).

The two CCD variants displayed slightly different profiles of increased ageing when compared to the wild type (Figure 2.21A&B, Figure 2.22). The A4940T model displayed markedly higher whole body scores as early as day 4 of adulthood (Figure 2.21A, Figure 2.22) and this pattern remains significantly higher across the rest of the days examined. In contrast the R4861H strain only demonstrates a significant difference in whole body score on days 10 and 12 (Table 2.8).

Table 2.8 Comparison of strains transgenic for variant and wild type *unc-68*, in terms of the combined effects of variant and worm age on whole body score of muscle organization.

		DAY of ADULTHOOD						
		2	4	6	8	10	12	14
V	G341R	-0.71 (0.48)	1.23 (0.22)	1.48 (0.14)	3.72 (0.0001)	5.33 (<0.0001)	4.83 (<0.0001)	4.53 (<0.0001)
A	R2454H	-0.66 (0.51)	0.55 (0.58)	2.35 (0.018)	2.45 (0.014)	1.86 (0.063)	1.64 (0.0101)	2.07 (0.038)
R	R2458H	-0.96 (0.34)	0.61 (0.54)	2.15 (0.018)	3.39 (<0.0001)	4.77 (<0.0001)	4.47 (<0.0001)	4.79 (<0.0001)
I	R2163H	-1.65 (0.099)	-0.65 (0.515)	1.27 (0.204)	0.71 (0.478)	5.05 (<0.0001)	4.97 (<0.0001)	4.72 (<0.0001)
A	R163C	-0.24 (0.81)	2.01 (0.04)	2.73 (0.006)	2.31 (0.02)	3.75 (0.0002)	2.75 (0.006)	2.75 (0.006)
N	A4940T	-0.77 (0.85)	2.69 (0.007)	3.13 (0.002)	3.65 (<0.0001)	3.36 (<0.0001)	4.38 (<0.0001)	2.91 (0.0036)
T	R4861H	0.19 (0.44)	0.27 (0.78)	0.67 (0.501)	1.19 (0.234)	2.61 (0.009)	2.71 (0.007)	1.38 (0.168)
	K3452Q	0.70 (0.48)	1.91 (0.055)	2.09 (0.036)	2.99 (0.003)	2.87 (0.004)	3.23 (0.001)	2.45 (0.01)

T-statistic is displayed correct to 2 decimal places with associated p-value in brackets. Day 2 represents 5 days after hatching.
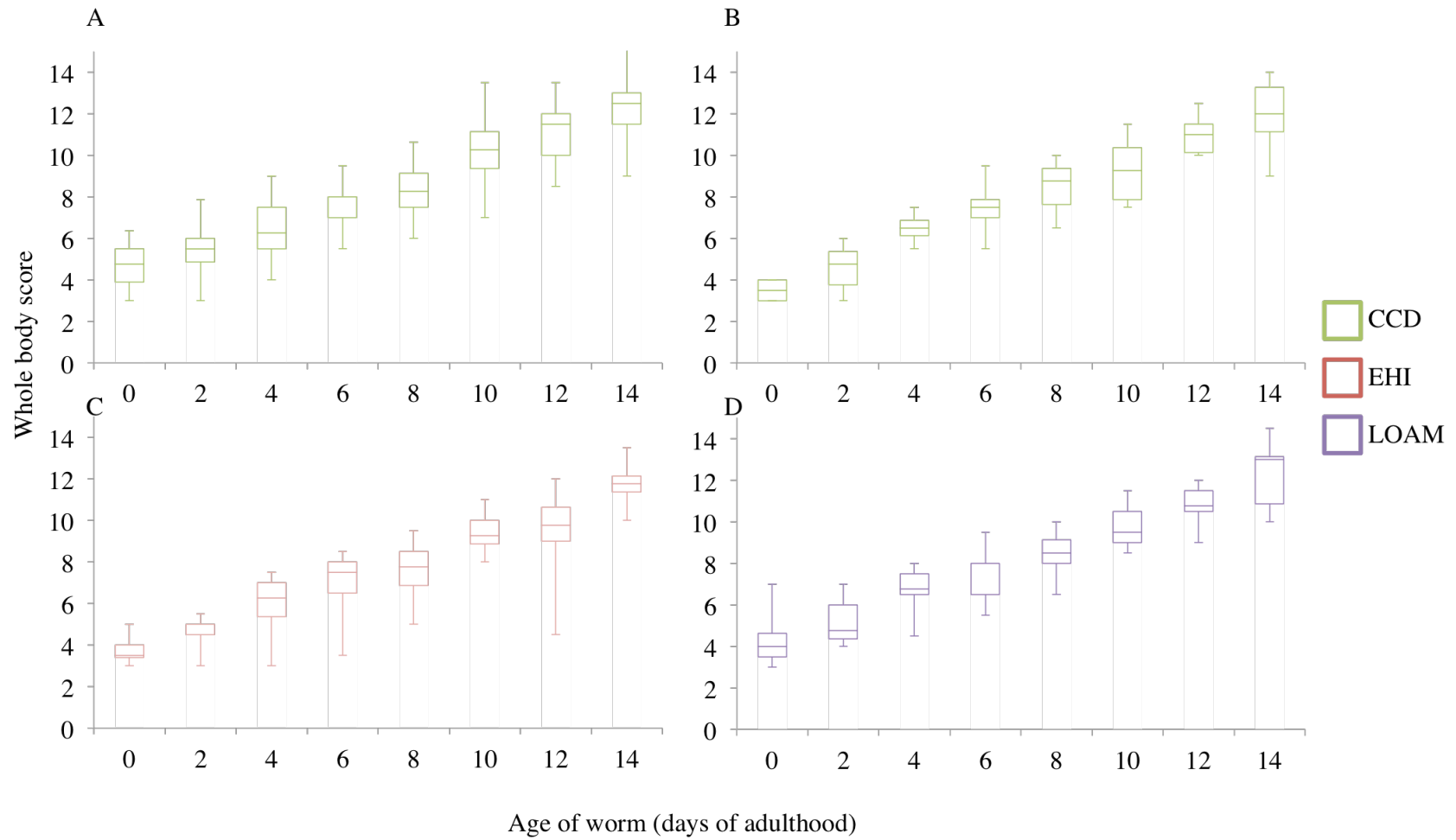
Figure 2.21 Whole body scores for increasing myofilament disorganisation from 0 to 14 days of adulthood in CCD (A4940T (A) (n=40), R4861H (B)(n=20)), EHI (R163C (C) (n=40)) and LOAM (K3452Q (D) (n=40)), boxplots show median, IQR and min and max score.
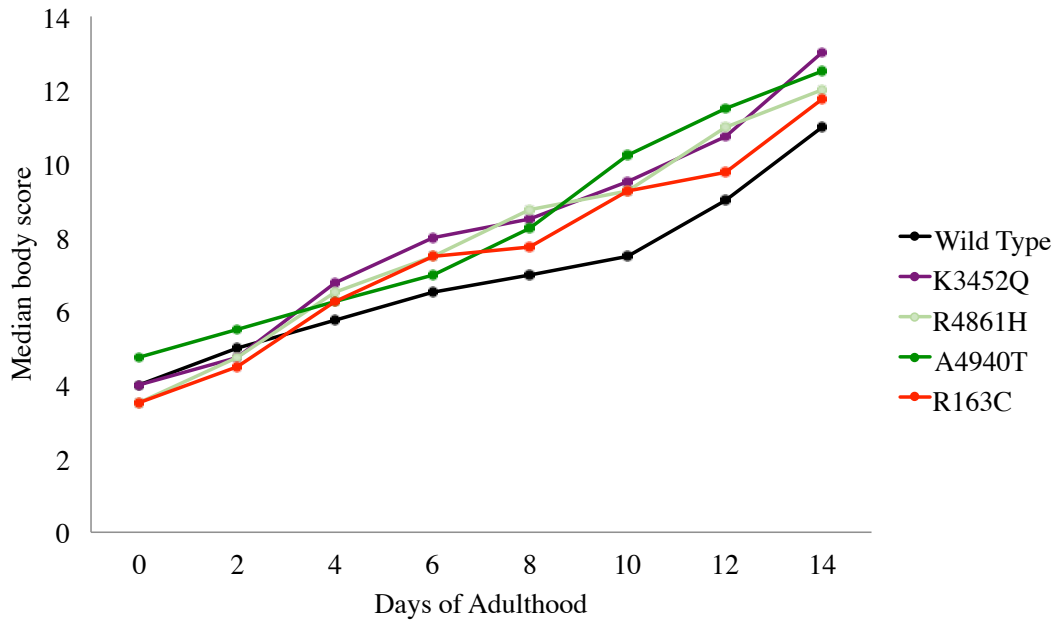
Figure 2.22 Summary of median scores from EHI (n=40), CCD (n=40 A4940T variant, n=20 R4861H variant), LOAM (n=40) compared to wild type (n=20) strains

The pattern exhibited by the A4940T strains was also evident in the strains expressing *RYR1* variants R163C (Figure 2.21C, Figure 2.22) and K3452Q (Figure 2.21D, Figure 2.22) implicated in EHI and LOAM respectively.

2.4 Discussion

This chapter aimed firstly to evaluate the suitability of *C. elegans* as a model for MH and other myopathies and secondly to investigate the potential effect of these variants on ageing in the muscle of the worm.

Microinjection of fosmid clone WRM069cA02 independently and alongside versions altered by recombineering into the distal gonad of *unc-68(e540)* mutants produced worms rescued for wild type movement under normal environmental conditions. All strains display a rate of movement indistinguishable from each other in liquid in the absence of caffeine or halothane. Therefore, WRM069cA02 and its altered versions appear to include a fully functional copy of *unc-68* and arrays generated by microinjection provide appropriate expression of the *unc-68* transgene.

UL4140 was established as the control strain, due to its locomotory pattern being indistinguishable from the wild type in response to halothane and caffeine and contains only the wild type version of the fosmid clone. It served as a baseline for comparison when examining the ryanodine receptor variants. The fosmid is expressed as an extra-chromosomal array, meaning that the functional copy of *unc-68* is not chromosomally integrated. In this strain the array was expressed at a high rate and the majority of offspring were transgenic, however to avoid the possibility of low transmission rates it would be better for future work to focus on using CRISPR as a method for direct genome editing (Jinek *et al.*, 2012). UL4140 is also the only strain serving as a control for these experiments, meaning that any problems with this strain, arising from poor maintenance or possible loss of the extra chromosomal array could

result in error in interpreting the data. Extra care was taken to ensure correct maintenance during these experiments to avoid these issues.

Selection of the variants for investigation was made based on conservation at the amino acid level. There are currently 35 mutations in *RYR1* that are considered to be causative of MH and many other variants of unknown pathogenicity (EMHG, 2016) The majority of MH patients have variant G2434R, and this is considered to confer a weak MH phenotype in the IVCT (Carpenter *et al.*, 2009b). This variant is not conserved between *C. elegans* and humans, unlike some of the variants conferring more severe IVCT phenotypes used in this study.

The fosmid containing the equivalent R4861H variant, implicated in central core disease, did not successfully rescue the mutant strain on its own. It was possible to generate a strain by co-injection of this fosmid with the wild type version. This was also tested by co-injection of the R4861H fosmid with pRF4 that resulted in uncoordinated rollers. If the *unc-68* gene was being successfully expressed the rolling phenotype conferred by the pRF4 plasmid should be wild type (strong rolling movement). As such this indicated that the R4861H fosmid was not functional. As for most *RYR1* variants, all CCD patients with the R4861H variant have this variant in the heterozygous state (Zhou *et al.*, 2007). The V4849I fosmid did not successfully produce transgenic strains by the process of microinjection either independently or with co-injection with the wild-type fosmid or pRF4 plasmid. It is possible that this variant results in a lethal phenotype that resulted in unviable offspring. Alternatively, the micro injection process may have been unsuccessful at introducing the DNA in the worm's gonad and therefore the DNA was not expressed as a result.

The variant strains were subjected to conditions known to result in dysfunctional activity of the RyR1 calcium channel in humans. MH is most commonly triggered by volatile anaesthetics such as halothane and this reaction is utilised in clinical diagnostic tests for MH (IVCT) (Ording *et al.*, 1997). In addition to halothane, caffeine is also used as a trigger agent in the IVCT as it confers increased calcium sensitivity at high concentrations on a normal ryanodine receptor. In individuals considered to be sensitive to MH this increased calcium sensitivity is observed at lower concentrations of caffeine. Hence the method of testing the worms was based on the clinical diagnostic test.

Caffeine is considered to be a valuable tool for the purposes of muscle function research, though the mechanism of action is complicated (Stephenson, 2008). Caffeine is considered to have a low binding affinity to RyR1 and induces conformational changes in the channel when present in high concentrations making it more sensitive to activation by calcium and voltage (Sitsapesan & Williams, 1990). This finding was confirmed by studies using frog muscle (Olorunshola & Achie, 2011) and mouse muscle (Rossi *et al.*, 2001; James *et al.*, 2004). The pattern of movement displayed by the strains containing only wild type *unc-68* is characterised by an increase in activity from 0 to 10 mM and then a gradual decrease from 10 to 40 mM with a final drop off from 40 to 80 mM. This initial excitation followed by a subsequent inhibition of activity suggests that caffeine may be acting by two mechanisms in the worm or perhaps a single biphasic mechanism. The differential response to changing caffeine concentration could reflect different targets of caffeine at different concentrations. The MH and CCD model strains display no excitatory response to caffeine and a greater decrease in movement at the higher concentrations of the chemical. Here there is only

one mechanism of action as the excitatory response is lost. This indicates that the presence of the variants investigated for these conditions may be altering the way in which the ryanodine receptor is responding to caffeine across the range of concentrations tested.

While caffeine has been shown to sensitise RyR1 to calcium activation, the actual binding site for caffeine is unknown (MacLennan & Wayne Chen, 2010). It is thought that caffeine and halothane act by increasing the affinity of the A-site on the ryanodine receptor for calcium making the receptor more open and subsequently decreasing the affinity of the I-site in mutant proteins (Balog *et al.*, 2001; Yang T. *et al.*, 2003). RyRs consists of four identical protomers folded into a cytoplasmic and transmembrane regions, and the cytoplasmic region is responsible for sensing interactions with ions such as calcium (Meissner, 1994; Lanner *et al.*, 2010). Therefore, the A and I-sites are likely in this cytoplasmic region. In 2015, three papers were published in Nature that mark a significant step forward in understanding the structure of the ryanodine receptor (Zalk *et al.*, 2015; Yan *et al.*, 2015; Efremov *et al.*, 2015). The G341R and R163C variants are located in the N-terminal domain (NTD), variants R2163H, R2454H, R2458H and K3452Q found within the handle and helical domains and R4861H and A4940T are found somewhere within the transmembrane regions S1-S6 (Figure 2.23).
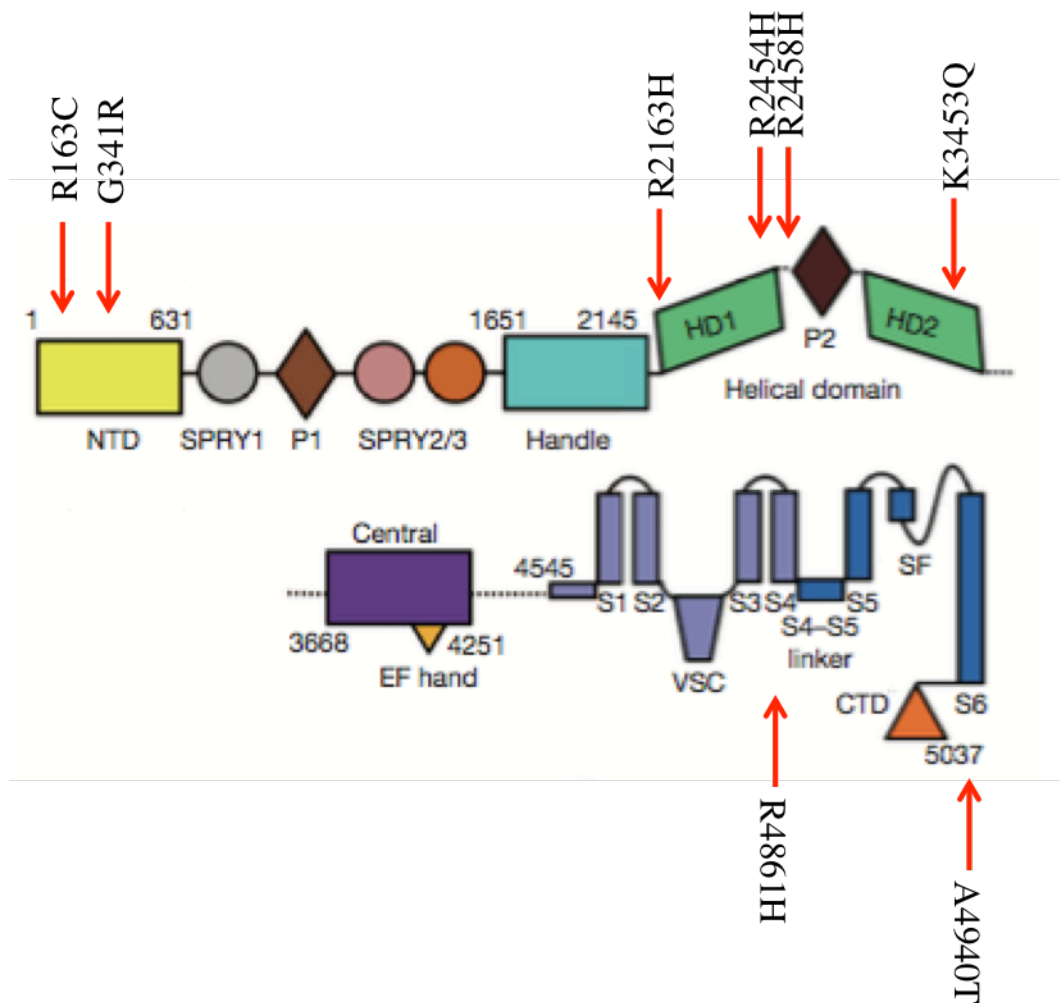
Figure 2.23 Schematic of RyR1 domain organisation with putative locations of *RYR1* variants indicated by red arrows. Original image from (Yan *et al.*, 2015)

The NTD, handle and helical domains are all found in the cytoplasmic region of the protein (Yan *et al.*, 2015). According to the proposed mechanism of calcium-induced calcium release proposed by Efremov and colleagues, calcium binds to the EF-hand domain and induces conformational changes in the protein making it more open (Efremov *et al.*, 2015). None of the *RYR1* variants studied here were found in the EF-hand domain. It is possible that the effect of these variants causes alterations in the way in which the rest of the ryanodine receptor changes conformation in response to calcium.

In mammals, RyR1 is considered primarily a skeletal muscle calcium channel with other isoforms expressed in other cell types. In *C. elegans* there is only a single isoform of the ryanodine receptor, UNC-68, and this is likely to be a key intracellular calcium channel in all cells and critically excitable cells. Caffeine resistant mutations have been localised on two *C. elegans* genes, *osm-3* and *che-3* which are required for chemosensory nerve function (Hartman, 1987; Hartman *et al.*, 2001). Work carried out after completion of this chapter has examined the role of these genes in the differential response to caffeine exhibited by the *unc-68* variants using RNAi knockdown of *che-3* and *osm-3*. Findings showed that for all strains examined (one for each myopathy and the two wild type strains) the locomotor response to increasing caffeine concentrations was eliminated or markedly reduced. These results could indicate that the focus of influence of the UNC-68 amino acid changes upon caffeine response is actually in these chemosensory nerve cells. These findings are also consistent with the primary site of action of caffeine being in the chemosensory nerve cells with downstream consequences dependent on UNC-68 in other cells, including or specifically muscle cells (Ferreira, Shaw and Hope, unpublished findings).

The effect of volatile anaesthetics, such as halothane, on *C. elegans* has been investigated largely in the context of its effect on the nervous system, often focusing on the differing effects of different types of volatile anaesthetic (Morgan & Carscobi, 1985; Crowder *et al.*, 1996). Genetic studies strongly suggest a number of potential targets of volatile anaesthetics in *C. elegans*, such as the SNARE complex (Nonet *et al.*, 1998), mitochondria (Hartman *et al.*, 2001; Kayser *et al.*, 2003; Falk *et al.*, 2006); G-protein coupled receptors and calcium/cation channels (Morgan *et al.*, 2007). While numerous other 'unc' strains have been investigated in relation to their specific

anaesthetic phenotype, e.g. *unc-79* and *unc-80,* both of which are hyper-sensitive to halothane, no previous research has investigated the role of *unc-68* in volatile anaesthetic sensitivity (Morgan *et al.*, 2007). The findings presented in this chapter show that variants in *unc-68*, that are homologous to variants in the human ryanodine receptor, confer increased sensitivity to halothane in strains expressing these variants. However, it does not conclusively prove that this altered response to halothane is due to the interaction of halothane with the worm's ryanodine receptor. Better understanding of the way in which these chemicals are interacting with the ryanodine receptor will be supported by increased understanding of the structure of this protein on which progress has recently been made (Zalk *et al.*, 2015; Yan *et al.*, 2015; Efremov *et al.*, 2015).

The method of halothane application used in these experiments was designed to allow for quantification of behavioural adaptation in a similar manner to exposure to caffeine. Caffeine is easily dissolved in an aqueous solution up to concentrations of 80mM at room temperature. However, halothane is lipid soluble and therefore requires dilution in DMSO prior to dissolving into the S-medium used as the buffer for all phenotyping assays. The method devised here used a single stock concentration of 25mM halothane in DMSO. This naturally meant that the resulting concentration of DMSO in S-medium for the different halothane concentrations also varied. It was established that the concentration of DMSO in the strongest working solution of halothane (2.5mM) was 1% as it is acknowledged that the only known possible impact of immersing *C. elegans* in DMSO is that it extends the lifespan of the worm at concentrations of greater than 1% (Boyd *et al.*, 2011). As lifespan was not being examined using the halothane assays any possible effect it may have had on lifespan

was considered negligible. Indeed, *C. elegans* have been observed to tolerate DMSO concentrations of up to 2% without displaying an effect on locomotion (Katiki *et al.*, 2011). It would be pertinent to consider, when repeating these assays, to establish stock solutions of halothane that permit for the same concentration of DMSO in each working solution used in order to determine any potential consequences of the DMSO affecting worm locomotion.

Each of the variants selected for investigation displays a dominant phenotype in the human conditions in which they are implicated. This was investigated using the nematode models through examining the differences between the models of the heterozygous and homozygous states. No observable difference was found when comparing the majority of the homozygous and heterozygous models for each variant across the range of caffeine and halothane concentrations. This suggests that the phenotype conferred by the variant fosmid is dominant over the wild type and so mirroring the situation in each of the human conditions. The exception to this was the strains expressing the G341R variant fosmids. There is an increased rate of body bends in the strain rescued with the variant and the wild type fosmid at 1 mM caffeine compared to the strain rescued only with the variant fosmid. However, this difference is not evident at any other concentration of caffeine. Additionally, the general pattern of behavior over the range of caffeine and halothane concentrations in the G341R strains appears consistent with the other MH models. In future, it may be of use to repeat the process of generating strains containing this variant to test if this anomaly is significant.

Additional work completed in the Hope Laboratory, after the data presented in this chapter was obtained, examined the possibility for age-related change in caffeine response for these myopathy model strains. A subset of the strains was used for this experiment: UL4147, UL4141 (MH), UL4157 (CCD), UL55 (EHI) and UL4168 (LOAM), UL4140 (wild type control) and N2 (wild type). It was found that in N2 and UL4140 young adults (of equivalent age to those used in the phenotyping assays for this chapter) the locomotory response was consistent with the findings in shown in Figure 2.10, providing independent verification of this finding. Additionally the results for young adults of all the myopathy strains used here was also consistent with the findings in this chapter (Figure 2.11-2.12). However, in older worms expressing the variant implicated in LOAM (strain UL4168), the locomotory response was altered. With increasing concentrations of caffeine there was an increased rate of locomotion compared with younger worms at the same doses of caffeine. This could be evidence of a strong link between the age-related symptoms that are characteristic of LOAM. All other strains showed the progressive dampening in rate of locomotion in response to increasing caffeine concentrations with age, but the same general pattern of response persisted (Ferreira, Shaw and Hope, unpublished findings).

Subsequent work by the Hope Laboratory also examined the lifespan of all strains used in this study. Overall, the presence of an *unc-68* variant was found to decrease median lifespan. The wild type control strain UL4140 and the standard wild type strain N2 can live up to 25 days, whereas the lifespan of strains containing any and only the *unc-68* variant only live for a maximum of 16 days. It is clear therefore that while these altered versions of *unc-68* confer a functional ryanodine receptor, these single amino acid changes also result in a shorter lifespan in the worm. This altered lifespan

may have an impact on the extent of muscle degeneration observed in ageing assays carried out in this chapter. The ageing assays were carried out on only live worms (essential in order to visualise the muscle with gfp) and if the variant worms have a shorter lifespan than the wild type this will have a bearing on the extent of muscle ageing.

C. elegans models for muscle ageing have highlighted the way in which the muscle displays increasing levels of disorder (Herndon *et al.*, 2002; Glenn *et al.*, 2004). The results of ageing assays to quantify the extent of muscle ageing indicate that muscle appearance and the deterioration of that appearance is dependent on age. Previously, the head region has been used in isolation as a measure of muscle degradation (Garigan *et al.*, 2002). The method employed here assessed muscle degradation across 3 regions of the worm: head, vulva and tail. This enabled assessment of the potential differences in the extent of myosin disorganisation in the different regions of the worm's body. When examining the scores for the different regions independently it was found that the tail region was consistently scored at a higher level than the head and vulva and the vulva was scored consistently higher than the head region. This indicates a progressive pattern of muscle ageing throughout the length of the worm, characterized by a progressive decline in myosin fibre organisation from the head to the tail. Thus the tail region of the worm is subject to increased age-related structural decline perhaps due to the increased movement in this region of the worm's body.

The scoring method employed here is reliant on human observation to evaluate the extent of myosin disorganisation in the worm muscle. This has the potential to be subjective as it is based on individual interpretation of appearance. However, with

training the execution of the technique becomes more effective and consistent. A separate observer scored a subset of images blindly and the only incidence of disagreement was for one image that was scored as a 2 by one observer and as a 2.5 by the other. In addition, due to the reliance on scoring live worms (dead worms do not express GFP and thus it is not possible to evaluate the disorganisation in the muscle of dead worms), the results presented here are a conservative assessment of the age-related structural decline that occurs in the worm's muscle. Those worms that die early, and are excluded from the analysis, may display more disordered myosin fibre arrangements.

In humans, disorganisation of myosin fibres, lowered cross-bridge stability (Lowe *et al.*, 2001) and defective EC coupling (Payne & Delbono, 2004) are all processes that have been proposed as explanations for the contractile dysfunction that occurs with age. Mouse models for muscle ageing in relation to *RYR1* variants show evidence of variants having an effect on age-related changes in skeletal muscle. $RYR1^{Y522S/+}$ mice have been found to develop metabolically inactive cores as they age, a feature which is in accordance with the CCD phenotype associated with Y522S mutation in humans (Boncompagni *et al.*, 2009). $RYR1^{I4898T/+}$ (variant implicated in MH, CCD and LOAM) mice exhibit a slowly progressive myopathy with skeletal muscle weakness and age-dependent formation of cores in their muscle fibres (Zvaritch *et al.*, 2009; Boncompagni *et al.*, 2010).

Patients with late-onset axial myopathy exhibit age-related changes in muscle function through a variety of symptoms such as camptocormia and other pathologies of the axial musculature (Loseth *et al.*, 2013). In the nematode model for this condition

(strains expressing K3452Q variant fosmids) the extent of muscle ageing, assessed using a method for scoring the degree of disorganisation of the myosin filaments, found the pattern of ageing in these model strains to differ significantly from that of the wild type. There was still the same progressive increase in disorder of the muscle structure, but the extent of muscle disorder was increased as early as day 4 of adulthood and this increased disorder persisted over the observed time period. The increased disorganisation of the myosin filaments was also exhibited by strains expressing variants implicated in MH, CCD and EHI, indicating that the presence of these variants is having a significant effect on the process of muscle ageing in these model strains. Notably, the MH and EHI variants that were engineered in this study are all associated with a relatively severe IVCT phenotype when compared to the most common MH variant (Carpenter *et al.*, 2009b).

These nematode models have provided considerable insight into the ways in which *unc-68* variants alter behavior in response to caffeine and halothane and support the use of these models in investigations into muscle ageing. There are parallels between these models and the human conditions that they represent. This raises interesting questions regarding the potential mechanisms for the way in which caffeine and halothane interact with normal and altered ryanodine receptors. This study has provided a novel insight into the altered process of muscle ageing that is evident in these myopathies.

3   Differential mRNA expression in MH patients and muscle ageing

3.1   Introduction

This chapter will explore differential mRNA expression in skeletal muscle and blood samples from MH patients. This information will help to address the genetic complexity of malignant hyperthermia as well as many of the unexplored areas of skeletal muscle ageing, namely changes in expression of key genes involved in skeletal muscle function. It will also evaluate the potential for a predictive risk score of MH susceptibility to replace the invasive IVCT used to diagnose MH.

3.1.1   Diagnosis of MH susceptibility: status quo

The diagnosis of susceptibility to MH has been possible since 1972 using the IVCT (Ellis *et al.*, 1972). However, this requires a formal operative procedure through a 5-8cm incision. As a result, it is relatively expensive, causes 1-2 weeks of discomfort and absence from work and leaves a permanent scar on the leg. Due to these factors, the test is only used to confirm the diagnosis in individuals that have survived a suspected MH reaction and in relatives of individuals shown to have a positive IVCT test. It is not applicable to children under the age of 10 or patients on long-term steroid therapy due to doubts concerning the sensitivity of the test in these groups (Hopkins, 2000). Patients unable to travel to Leeds, for medical or social reasons, for the procedure also cannot be tested.

There has been some progress made to develop guidelines for the introduction of limited DNA-based screening (Robinson & Hopkins, 2001; Urwyler *et al.*, 2001) but,

for the most part this was problematic due to the complex genetic basis of MH. Up to 40 % of MH susceptible families have no known mutations in either *RYR1* or *CACNA1S* (Robinson *et al.*, 2006). Discordance between IVCT phenotype and *RYR1* genotype is also a feature in some MH families, exemplified by the incidence of MHS mutation negative and MHN mutation positive patients. 2.5% of individuals without the familial *RYR1* variant test MH susceptible (Robinson *et al.*, 2003b). This discordancy indicates that MH may not be a single gene disorder and there is evidence to suggest the existence of modifier loci that may be causative of MH (Robinson *et al.*, 2000; Robinson *et al.*, 2003a).

Transmission disequilibrium testing has demonstrated independently in UK families and collectively in European pedigrees that MH status might be related to multiple interacting gene products (Robinson *et al.*, 2000; Robinson *et al.*, 2003a). This information suggests that variability in genes other than *RYR1* could contribute to for MH susceptibility in some cases. In addition to the 35 functionally characterised *RYR1* variants implicated in MH, there are also three functionally characterised variants in *CACNA1S* (encoding the α-1 subunit of the DHPR) that are accepted as diagnostic mutations by the EMHG (Weiss *et al.*, 2004; Eltit *et al.*, 2012; EMHG, 2016).

At present, DNA-based screening for MH susceptibility is limited to characterising MH risk in patients known to have had MH reactions and their relatives. If they test negative in the IVCT there is no further testing, either genetic or functional for any family members. If they test positive, they are screened for known MH variants. Where no mutation is identified their family members are offered the option of an IVCT for diagnosis. Where a mutation is identified family members are subsequently

invited for mutation screening and if the same variant is detected they are automatically considered to be MHS without an IVCT. If the variant is not detected they are offered IVCT. This process clearly ignores a number of potentially confounding genetic factors that may contribute to MH. Expanding the genetic screen to target the wider population requires consideration of additional genetic information to better understand the genetic complexity of this condition.

3.1.2   Whole genome approach to disease profiling

The current version of GeneChip® Human Genome U13 Plus 2.0 Array from Affymetrix © is the most comprehensive whole human genome array (Affymetrix, 2015). It allows evaluation of over 53,000 transcripts, representing all genes in the human genome. This can provide information on the regulation of individual genes and patterns of genes whose expression is co-ordinately regulated. For example, arrays have been used to evaluate expression profiles in microarray analysis of myocardium from healthy and heart failure patients (Dos Remedios *et al.*, 2003). This approach has also been used to establish two unique forms of diffuse large B-cell lymphoma (Alizadeh *et al.*, 2000) and to accurately predict survival probability in cases of leukaemia (Valk *et al.*, 2004).

In addition, it has been shown that it is not necessary to perform the transcriptional analysis on the tissue that is the primary focus for the disease process. Transcriptional profiling of peripheral blood has demonstrated, in patients with coronary artery disease, over 100 genes that are differentially expressed, compared to controls. Subsequent functional characterisation of these genes indicated that the changes occur in response to the presence of coronary artery disease (Ma & Liew, 2003).

Schizophrenia patients have been found to exhibit co-ordinately altered expression of *SELENBP1* in both brain and blood as well as a further two genes that showed altered expression levels in both blood and brain tissue (Glatt *et al.*, 2005). Microarray analysis has also been used to show the presence of unique genetic signatures of schizophrenia and bipolar disorder, with distinct clustering of the specific diseases compared with controls (Lewis *et al.*, 2003). This method of transcriptional profiling in blood samples has been further expanded to study additional neurological diseases such as neurofibromatosis type 1, epilepsy and Tourette syndrome (Tang *et al.*, 2005).

To date this approach has not been applied to specific skeletal muscle disorders, and so it is proposed that despite the heterogeneity of the underlying DNA defect in MH, there is a sufficiently homogenous transcriptional response in skeletal muscle, which may be reflected in blood in order to distinguish those individuals susceptible to MH. The transcriptional profile in blood may not necessarily show the same genes of interest as found in skeletal muscle but may provide a unique profile of MH specific to that tissue. Using Human Genome U13 Plus 2.0 Arrays should provide a wealth of information, and as such it may also be possible to interrogate for genes implicated in MH and muscle ageing.

3.1.3   *Genetics of skeletal muscle ageing*

Ageing in skeletal muscle is poorly understood. Loss of muscle mass does not entirely explain the compromised functional capacity of the muscle. A noted limitation to previous gene expression research is the focus on genes already characterised in muscle or having importance in muscle structure and function (Jozsi *et al.*, 2000; Welle *et al.*, 2000; Welle *et al.*, 2001; Welle *et al.*, 2004). More recent work has

established 'exploratory' gene approaches as a means to identifying genes not previously shown to have an important role in muscle function (Roth *et al.*, 2002). This exploratory gene approaches have also utilised whole-genome arrays to profile the phenomenon of muscle ageing.

Roth and colleagues investigated the influence of age, sex and strength training (ST) on gene expression using microarrays (Roth *et al.*, 2002). Their study utilised 2 age groups comprising 5 individuals in each, consisting of both men and women, isolated total RNA from muscle biopsy samples and subjected them to GF211 microarrays. These arrays contain probe spots for ~4000 human genes. Their results highlighted significant sex differences, with >1.7-fold differential expression for ~200 genes and ~50 genes showed differential expression for age. However, there are clear limitations to their approach, namely the small sample size and subsequent bias this has on the data. Statistical analysis only comprised pairwise comparisons and 1-way ANOVA, meaning that no consideration was made for potential interactions with age and sex. The analysis is also over simplified by the categorisation of age into two distinct groups. While young versus old may be applicable to mouse models, or other organisms with a much shorter life span, it is clear that age in humans is continuous and there may be distinct expression differences throughout the course of human life. This segregation into specific age groups is a common feature of microarray profiling in human studies (Jozsi *et al.*, 2000; Welle *et al.*, 2000; Welle *et al.*, 2003; Welle *et al.*, 2004).

Work by Lee and colleagues, using a mouse model for muscle ageing, characterised over 6,000 genes expressed in the soleus muscle that displayed a greater than 2-fold

decrease in expression when comparing old to young adult mice. In addition they found that this could be offset by calorific restriction, suggesting that changes in gene expression may contribute to deterioration in muscle (Lee *et al.*, 1999). This study was followed up by research using Rhesus monkeys, comparing aged to young animals, that indicated a selective up-regulation of transcripts involved in inflammation and oxidative stress, and a down-regulation of genes involved in mitochondrial electron transport and oxidative phosphorylation (Kayo *et al.*, 2001). Human studies, also using microarray methods, have shown similar results though have indicated smaller numbers of genes to be important, particularly those responsible for encoding metabolic enzymes (Welle *et al.*, 2000) and stress-related genes (Jozsi *et al.*, 2000). Studies examining age-associated gene expression in human skeletal muscle have highlighted the involvement of mitochondrial oxidative phosphorylation (Zahn *et al.*, 2006) in skeletal muscle ageing as well as reduced expression of genes associated with energy metabolism (de Magalhães *et al.*, 2009). Recent evidence has suggested that changes in gene expression with increased age may contribute to muscle ageing (Su *et al.*, 2015). Alterations in gene expression in response to acute resistance exercise were characterised, with indication that maintaining a high physical capacity being beneficial in preventing age-related sarcopenia (Su *et al.*, 2015).

The National Institutes of Health (NIH) launched the Genotype-Tissue Expression (GTEx) project in 2010 (NIH News, 2010). It aims to increase understanding of how changes in our genes contribute to common human diseases by establishing a database and tissue bank to investigate these conditions (NIH, 2016). This project has generated RNA sequence data that has detected 1993 genes that change expression with age

(Melé *et al.*, 2015). Those genes that decrease expression are enriched in pathways involved in neurodegenerative disorders. At present the data with regards to ageing in skeletal muscle has not been reported.

Evaluating differential mRNA expression in MH skeletal muscle therefore has many avenues for exploration. This chapter presents analysis of whole human genome microarray data with a view to understanding the gene expression profile of MH in both muscle and blood tissue. Similarities in expression profiles between blood and muscle were explored as well as investigation of key pathways highlighting new areas that may aid understanding of the genetic complexity of MH. Predictive risk scores of MH susceptibility were devised using the whole genome data to establish the potential for a simple blood test as a diagnostic parameter that may in future replace the invasive IVCT.

In addition to these aspects of the investigation, the microarray data was also interrogated to establish a list of genes of interest (GOI), alongside other genes involved in skeletal muscle calcium handling, mitochondrial function and EC coupling that were validated using TaqMan® gene expression assays on a different cohort of muscle samples from the array data. This ultimately provides a greater insight into the genetics of skeletal muscle ageing.

3.2 Materials and Methods

3.2.1 Sample Information

RNA samples are routinely extracted from the muscle biopsies received at the Leeds MH unit for IVCT diagnostics as well as from patient blood samples. Two sets of samples are used in this chapter, one comprising blood and muscle samples that were used for Affymetrix arrays and one comprising additional muscle samples used for Taqman® assays (Table 3.1).

Table 3.1 Samples information for Affymetrix and TaqMan® experiments

Experiment	Affymetrix Array				TaqMan® assays	
Tissue	Blood (n=94)		Muscle (n=59)		Muscle (n=108)	
Sex	Male	Female	Male	Female	Male	Female
MHN	18 (10-71)	21 (10-78)	11 (10-61)	8 (10-47)	21 (10-74)	22 (10-87)
MHS+	19 (11-70)	15 (11-69)	10 (11-71)	8 (15-45)	20 (10-71)	22 (11-69)
MHS-	12 (19-49)	9 (10-74)	18 (9-66)	4 (11-40)	11 (10-55)	12 (11-66)
Total	49	45	39	20	52	56

Age ranges (in years) are displayed in brackets, MHN Malignant Hyperthermia Normal, MHS+ Malignant Hyperthermia Susceptible with identified causative *RYR1* mutation, MHS- Malignant Hyperthermia Susceptible with no causative *RYR1* mutation

3.2.2 Total RNA extraction and quantification

RNA extraction for Affymetrix Arrays was completed by Dorota Miller. RNA extraction for TaqMan® assays was completed by Katie Nicoll Baines. RNA was extracted usng the chloroform/isopropanol method, followed by clean-up using RNeasy™ columns (Qiagen). For muscle samples, small sections of tissue (~50mm length) were taken from long-term liquid N_2 storage and incubated in 500ml RNAlater Ice overnight at -80°C. Tissue was then transferred to 1ml TRIzol© prior to rapid homogenisation using a rotor stator homogeniser. Following homogenisation, samples were thoroughly mixed with 200μl chloroform and centrifuged for 10 minutes. The upper aqueous phase was removed and transferred to a fresh 1.5ml tube containing

600µl isopropanol (approximately 1:1 ratio of isopropanol:aqueous phase) and mixed by inverting the tube. Samples were then stored overnight at -80°C to precipitate RNA. RNA was then pelleted by centrifugation at 19,000 rcf in a microfuge for 30 minutes at 4°C. The supernatant was discarded and the pellet was then washed in 500µl 75% ethanol and spun for 10 minutes. This step was repeated and (after discarding supernatant from the first wash) then the final supernatant discarded and the pellet left to air dried and then dissolved in 100µl RNase-free water.

A clean-up step was then performed using RNeasy™ mini-columns (Qiagen), according to manufacturer's instructions. Briefly, 350µl Buffer RLT was added to the sample and mixed well. Then, 250µl of 100% ethanol was added to the diluted RNA mixed by pipetting. The mixture was then transferred to an RNeasy™ spin column placed in a 2ml collection tube and spun for 15 seconds at 17,000 rcf in a microfuge. The column was then transferred to a fresh collection tube, and 500µl of Buffer RPE added to the top of the column to wash the RNA. The column was centrifuged for 15 seconds at 17,000 rcf in a microfuge and flow-through discarded, followed by addition of a further 500µl of Buffer RPE and 2 minutes' centrifugation at 17,000 rcf in a microfuge. The column was again transferred to a fresh collection tube and centrifuged for 1 minute at 17,000 rcf to ensure all ethanol was removed.

Finally, RNA was eluted from the column in 30µl RNase-free water. RNA purity and quantity was determined using a NanoDrop spectrophotometer (Thermoscientific) and BioAnalyser (Agilent 2100). The Agilent 2100 Bioanalyser system evaluates both RNA concentration and RNA integrity, assigning an 'RNA integrity number' (RIN).

It was ensured that all samples used in subsequent analysis had a RIN of 8.0 or greater to ensure suitable quality control of the experiment.

3.2.3   *Affymetrix Arrays*

Affymetrix HG_U133Plus 2.0 arrays were used to examine gene expression in muscle and blood samples (Table 3.1). RNA labelling, hybridization and image acquisition were done according to the standard Affymetrix protocol in the Microarray and DNA Analysis Section, Faculty of Biomedical and Life Sciences, University of Glasgow.

3.2.4   *Affymetrix Data: Data Handling and Statistical Modelling*

3.2.4.1   *Pre-processing and quality control*

The samples processed using whole genome Affymetrix arrays yielded a total of 143 CEL files (59 muscle samples, 94 blood samples). The CEL files were pre-processed and sample IDs and corresponding biological information were assigned using RStudio 3.0.2. Then the package 'Affy' was employed to carry out quality control of the data set. This package enables the user to draw images of each individual chip, plot RNA degradation and carry our robust multichip analysis (RMA) whereby the data is normalised for between and within chip variation. The chip image can be examined in 3 different ways (Figure 3.1).
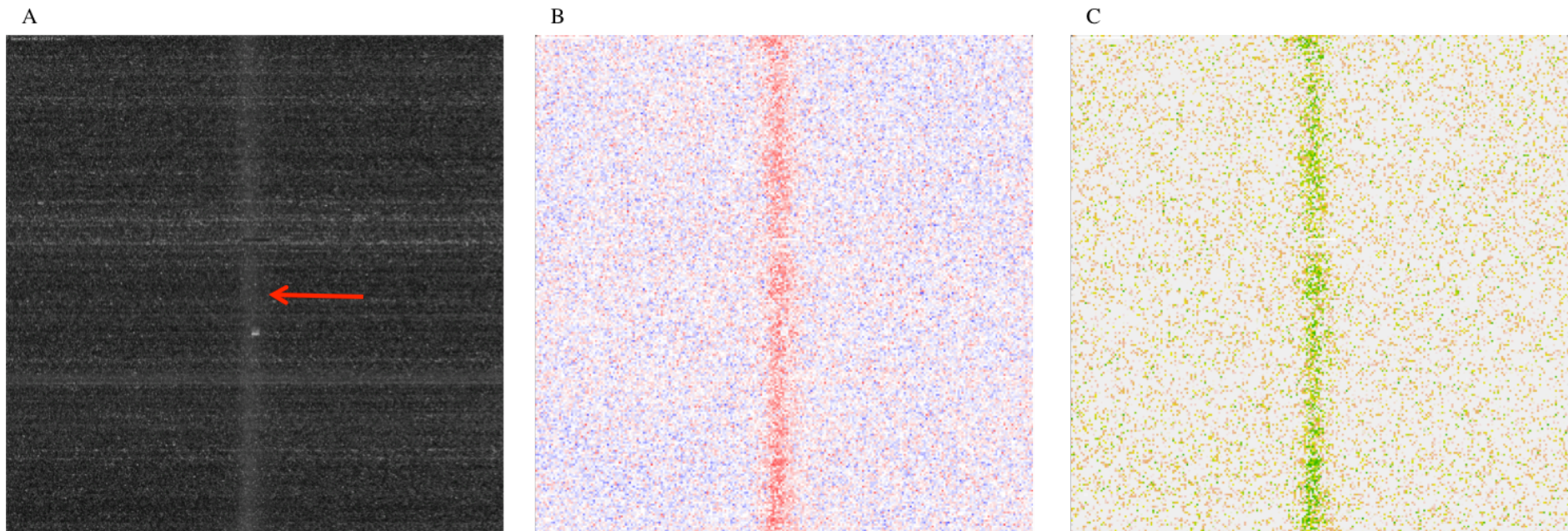
Figure 3.1 Chip images derrived from using package 'Affy' in R. A: raw chip image. B: Image of chip defined by residual variance in the chip data, generated using a probe level model. C: Image of chip defined by weights of the residual variance in the chip data.

The raw chip image is visualised in black and white pixels (Figure 3.1A) and in this example there is evidence of a possible smear running down the centre of the chip (indicated by the red arrow). These anomalies are dealt with in the 'Affy' package using a construct called the 'probe level model' that determines the residual variance between the probe sets relative to the defined norm. This visualised by blue and red pixels (Figure 3.1B), those probes assigned a red pixel have greater residual variance than the blue. Then, the probe level model assigns weights to these residuals, with probes highlighted in green down weighted relative to those probes highlighted in orange (Figure 3.1C). Finally, the correct annotations (Gene ID, Affymetrix ID) for the probe data were assigned.

3.2.4.2 Statistical Analysis

The normalised expression data for all chips was analysed using the loop function in RStudio 3.0.2, to assign the following different nested linear models to the data:

- Linear model 1 factored in age, sex and MH phenotype and all possible interactions
- Linear model 2 factored in sex and MH phenotype and the pairwise interaction
- Linear model 3 factored in age and sex and the pairwise interaction
- Linear model 4 was effectively the same as model 1 but left out the age-phenotype interaction term.

After constructing these models Akaike Information Criterion (AIC) values were calculated using the formula: AIC = 2K-2log(L), where K is the number of predictors

and L is the maximised likelihood value. Therefore, the '2K' part of the equation is effectively a penalty for including extra predictors in the model and the '-2log(L)' part rewards the fit between the model and the data. As such, the lower the AIC value assigned to a model, the better that model fits the data and is the preferred model of choice. A difference is AIC values of -2 is considered to be the minimum threshold for choosing an appropriate model, with a difference of -10 retaining only a 0.9% chance of retaining the incorrect model (Richards, 2005). This effectively ensures against falsely discovering genes that show expression differences according to the features of the model chosen. This provided the means to compare between models to determine those probe sets where age, phenotype and specifically, the age-phenotype interaction were important prediction variables.

Firstly, the data from muscle samples was analysed to evaluate the genetic signature for MH susceptibility (comparing linear models 1 and 3). Susceptibility was initially defined as simply MHS (positive IVCT result) and MHN (negative IVCT result). The data was then re-analysed to factor in potential differences between MHS$^+$ (positive IVCT with presence of diagnostic *RYR1* variant), MHS$^-$ (positive IVCT with no diagnostic *RYR1* variant) and MHN. This process was then repeated using the data derived from patient blood samples, specifically re-examining those pathways shown to be interesting in skeletal muscle and determining if similar gene expression differences could be identified in patient blood samples. The Affymetrix data was then analysed to investigate those genes where age (comparing linear models 1 and 2), and the age-phenotype interaction (comparing linear models 1 and 4) was a significant predictor variable. This analysis was performed using the three levels of MH

phenotype (MHS$^+$, MHS$^-$ and MHN). This yielded lists of possible genes of interest that could then be further interrogated by completing pathway analysis in MetaCore™from Thomson Reuters.

MetaCore™ is a comprehensive biological analysis package that can be used to perform pathway enrichment, biomarker identification, sample comparison and variant analysis. It is compiled based on peer-reviewed literature and provides well-designed pathway maps for interpretation of experimental results. Briefly, a list of probes of interest, coded as Affymetrix IDs, is uploaded from a source file (.txt format) into the MetaCore^{TM} online package (the package is designed to recognise Affymetrix IDs and the appropriate annotation, provided the user selects the correct species). The 'Which pathways are the most significant in my data?' question was then selected from the 'Most Popular Questions' tab. This then provides a list of pathways that have been detected based on the list of Affymetrix IDs supplied. In addition to MetaCore™, gene functional classification was carried out using the Database for Annotation, Visualization and Integrated Discovery (DAVID) version 6.7. DAVID is an integrated package that provides the means to extract biological meaning from large gene or protein lists derived from high-throughput experiments (Huang *et al.*, 2008). The gene functional classification tool in DAVID was used to classify the list of genes identified as being important in relation to the interaction between MH phenotype and age into functional related gene groups. This makes it possible to summarise the major biology of the groups identified. The genes defined as interesting following the process of model comparison and pathway analysis/functional classification were then subjected to ANOVA to determine exactly what the differences were between normal and

susceptible in those genes, while also examining effects of age and sex. From the results of this analysis a set of candidate genes for further investigation on a different cohort of muscle samples using TaqMan® assays was established.

3.2.4.3   Determination of predictive model of MH susceptibility in muscle and blood

Muscle and blood samples were assessed independently using Least Absolute Shrinkage and Selection Operator (LASSO) penalised regression analysis to predictive susceptibility to MH. LASSO has the ability to select variables based on their contribution to susceptibility while also taking into consideration the other variables in the model (Tibshirani, 1996). LASSO was carried out in R software with the Penalized package (Goeman, 2010). Firstly, an appropriate penalization parameter was determined using the OptL1 function (part of the Penalized package in R), LASSO regression was then carried out using the Penalized function. The list of probes derived from the model comparison, ΔAIC-10, were used in order to start with the most refined list of probes. From this list a refined number of probes were identified, based on the LASSO regress as having the greatest predictive power for determining susceptibility. Using these probes and their coefficients it was possible to derive a risk that predicts susceptibility and subsequently determine a score from this equation that is definitive of MHN and a score that defines MHS individuals. Score plots were created using R Studio. The optimal cut off for determine whetere a sample is MHS or MHN was established using the Youden's J statistic in conjunction with receiver operating characteristic (ROC) analysis. The probes in the equation were also annotated to determine which genes they correspond to and were investigated to determine the biological relevance of those genes in relation to MH susceptibility.

3.2.5   Preparation of cDNA by reverse transcription

Reverse transcription on the skeletal muscle RNA samples (n=108, Table 3.1) was carried out using a TaqMan® high capacity cDNA reverse transcription kit. 10µl of 200ng total RNA was added to 10µl reverse transcription master mix (1X reverse transcription buffer, 1X RT random primers, multiscribe reverse transcriptase, 1U/µl RNase inhibitor, 1X dNTP in nuclease-free H_2O). Annealing of random primers was achieved by incubation for 10 minutes at 25°C, followed by 2 hours at 37°C to complete reverse transcription and subsequent deactivation of reverse transcriptase at 85°C for 5 seconds with a final hold at 4°C.

3.2.6   TaqMan® assays

A complete list of the genes of interest selected for investigation using TaqMan® can be found in (Table 3.2).

Selection of these GOIs was based on a number of criteria:

- implicated by the Affymetrix data analysis with respect to age and MH susceptibility

- involved in calcium handling in skeletal muscle that may be involved in skeletal muscle ageing

- involved in skeletal muscle mitochondrial function and ageing

- involved in EC coupling and ageing

- undergoing next generation sequencing by the Leeds MH unit due to their potential involvement in MH susceptibility

Table 3.2. Summary of all genes used in Taqman® assays

GENE	PROTEIN	SELECTION REASONS
B2M	Beta-2 microglobulin	Reference Gene (Vandesompele *et al.*, 2002)
GAPDH	Glyceraldehyde 3-phosphate dehydrogenase	
RPLP0	Ribosomal protein, large, P0	
HPRT1	Hypoxanthine-guanine phosphoribosyltransferase	
TBP	TATA-binding protein	
UNC13C	UNC13C	Involved in skeletal neuro-muscular disorder ALS (Kwee *et al.*, 2012) Affymetrix data analysis
JUN	c-Jun	Affymetrix data analysis
CAV1	Caveolin 1	
DTNA	Dystrobrevin alpha	
SNTB1	Beta-1-syntrophin	
CAPN3	Calpain 3	
KCNA1	Potassium voltage-gated channel	
CHERP	Calcium homeostasis endoplasmic reticulum protein	Modulates caffeine-mediated Ca^{2+} release, potential regulator of RyR1 (Ryan *et al.*, 2011) Potential role in ageing (Puzianowska-Kuznicka & Kuznicki, 2009)
CALM1	Calmodulin 1	Involved in regulation of L-type Ca^{2+} channels (Mori *et al.*, 2004)
CASQ1	Calsequestrin 1	Involved in Ca^{2+} storage in SR and EC-coupling (Beard *et al.*, 2004)
ORAI1	ORAi 1	Involved in SOCE in skeletal muscle, SOCE affected by age (Lyfenko & Dirksen, 2008)
STIM1	Stromal interactin molecule 1	Involved in SOCE in skeletal muscle, SOCE affected by age (Lyfenko & Dirksen, 2008)
TRPC3	Transient receptor protein 3	Involved in ROCE in skeletal muscle, interacts with STIM1 (Horinouchi *et al.*, 2012)
TRPC6	Transient receptor protein 6	Involved in ROCE in skeletal muscle, interacts with STIM1 (Horinouchi *et al.*, 2012)
PDE1A	Phosphodiesterase 1A, calmodulin-dependent	Activated by Calmodulin(NCBI, 2016)
HSPA4	Heat-shock protein 4	Potential role in ageing in skeletal muscle (Broome *et al.*, 2006)
NFKB1	Nuclear factor K	Potential relevance to human ageing process (GenAge, 2013)
MICU1	Mitochondrial induced calcium uptake protein 1	Involved in Ca^{2+} handling in mitochondria, implicated in muscle ageing (Csordas *et al.*, 2013; Gene Cards, 2013)M
MCU	Mitochondrial Calcium Uniporter	Mediates Ca^{2+} uptake into mitochondria, interacts with MICU1, implicated in muscle ageing (Pietrangelo *et al.*, 2015)
SLC25A37	Solute carrier family 25, member 37	Translocated to the inner mitochondrial membrane during oxidative phosphorylation.
RAD	Ras-related associated with Diabetes	Expression enhanced in response to oxidative stress (Sumner *et al.*, 2013)
REM2	Ras-like GTP binding protein	Over-expression mimics EC coupling (Sumner *et al.*, 2013)

TaqMan® gene expression assays were designed (following the guidelines in the TaqMan® protocol) for each gene of interest and the 5 reference genes. These references genes were utilised as they had been previously established to be consistently expressed in human skeletal muscle (Vandesompele *et al.*, 2002).

Assays were carried out according to the protocols outlined for TaqMan® gene Expression Assays. Briefly, amplification of ~100ng cDNA was carried out in 1X gene expression master mix supplemented with 0.5x gene specific assay made up to a total reaction volume of 10µl with nuclease-free H_2O. Amplification of samples was on an Applied Biosystems 7900HT Real-Time PCR system: STAGE 1: 50°C for 2 minutes, STAGE 2: 95°C for 10 minutes and STAGE 3: 95°C for 15 seconds then 60°C for 1 minute (40 cycles).

3.2.7   *Normalisation of TaqMan® expression data*

The process of normalisation controls for variation in extraction and reverse transcription yield as well as efficiency of amplification (Rome *et al.*, 1988). The use of reference genes is commonly accepted as the most applicable strategy for normalisation (James *et al.*, 1995b). The expression data obtained from qPCR was normalised using Microsoft® Excel® geNorm freeware. This procedure normalises the expression levels of the GOI based on the reference genes utilised in these assays. It ranks the reference genes based on stepwise elimination of the least stable gene and defines expression stability as average pairwise variation (standard deviation of log transformed ratios) of a given gene with all other candidate reference genes (Vandesompele *et al.*, 2002).

3.2.8 *Statistical Analysis of TaqMan® expression data*

Statistical analysis was carried out using freeware statistical package RStudio 3.0.2. Linear models were fitted to the normalised, observed expression levels that incorporated all possible interactions with the independent variables, in this case; age, sex and MH status. Residuals were plotted to confirm normal distribution. ANOVA was then carried out on these fitted models to establish whether expression levels were significantly different according to these three variables or any interaction between them. Akaike Information Criterion (AIC) was used to establish the best-fit model for the observed expression levels and ANOVA carried out on the simplified model. Tukey tests were used to investigate further where there were significant p values for MH phenotype. Graphical illustration of results was completed in Microsoft® Excel® for Mac 2011.

3.3 Results and Discussion

3.3.1 Genome wide profile of MH susceptibility in skeletal muscle and blood

Linear model comparison using AIC scores was carried out on the following models:

- probe ~ age + sex + status + age:sex + sex:status + age:status + age:sex:status (model 1)

- probe ~ age + sex + age:sex (model 3)

It was possible to derive lists of probesets from the whole genome data. A minimum cut off from the AIC model comparison of -2 was established to include all those probes relevant to differences in MH susceptibility (summarised in Table 3.3).

Table 3.3 Results of linear model comparison on Affymetrix expression data derived from patient muscle and blood samples

ΔAIC	Muscle (n=59)		Blood (n=94)	
	Probes	Genes	Probes	Genes
-2	4561	3506	2347	1687
-5	1671	1401	712	532
-10	281	249	79	74

Additional cut offs were established at -5 and -10 ΔAIC to derive lists with the most differentially expressed genes with respect to MH susceptibility. These results highlight the distinctly lower number of probe sets implicated in MH susceptibility detected across the whole genome in blood compared to muscle. As the manifestation of this condition is primarily concerned with compromised regulation of skeletal muscle function, then this result is not surprising. What is clear is that it is possible to establish a profile of MH susceptibility purely using peripheral blood when expression across the whole genome is analysed. When plotted graphically the proportion of probes of interest in relation to MH phenotype relative to the entire collection of human genome probes can be visualised (Figure 3.2 and Figure 3.3).

116
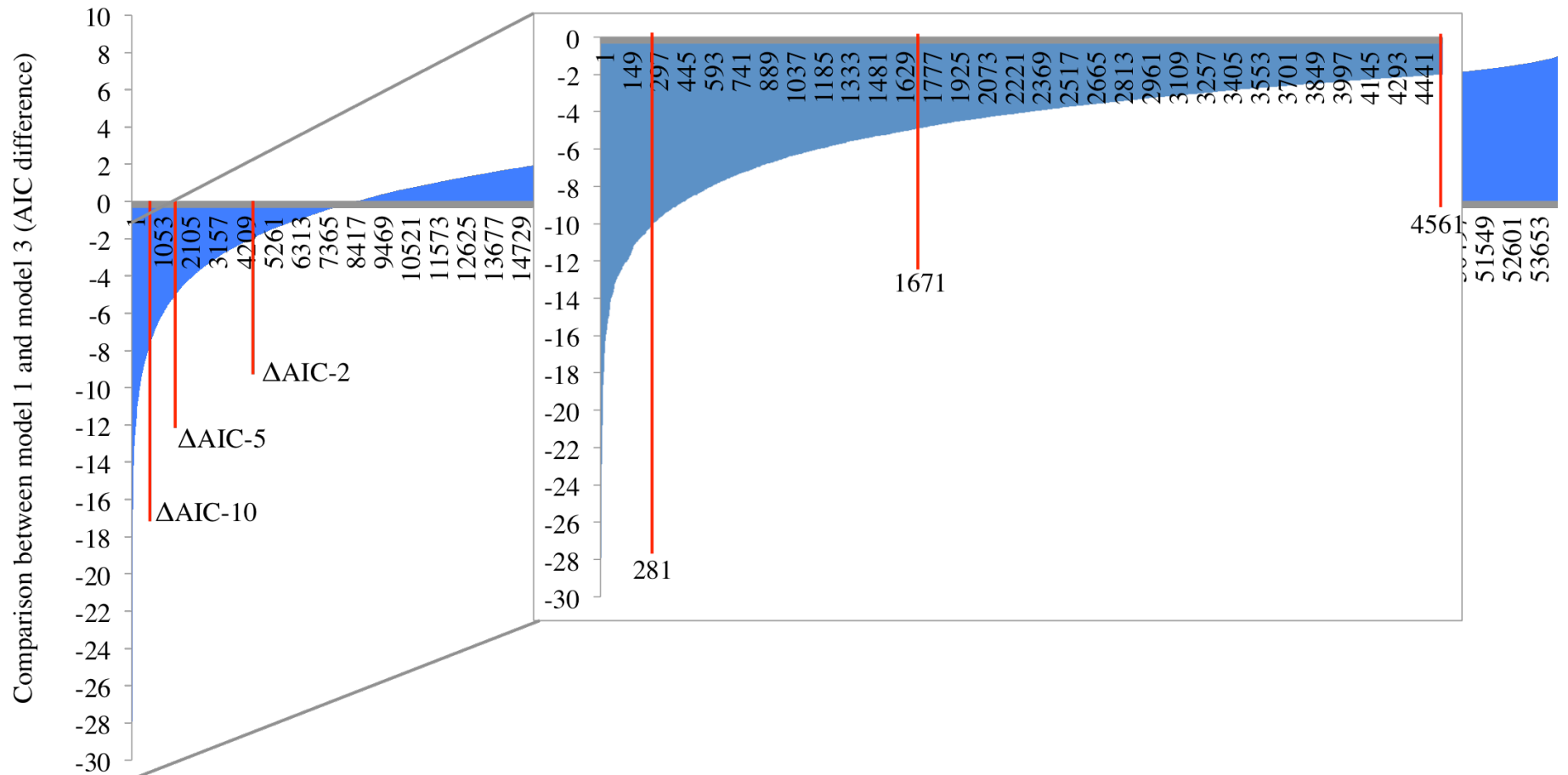
Figure 3.2 Bar plot of AIC differences when comparing linear models 1 and 3 for analysis of patient muscle samples. Red lines indicate the -10, -5 and -2 cut offs with -10 being nearest to the y axis and -2 being further away. Enlarged plot shows the selection of probes from delta AIC -2 (4561 probes) to the delta AIC -10 (281), it overlies the large selection of probes where MH susceptibility is not an important factor in the model.
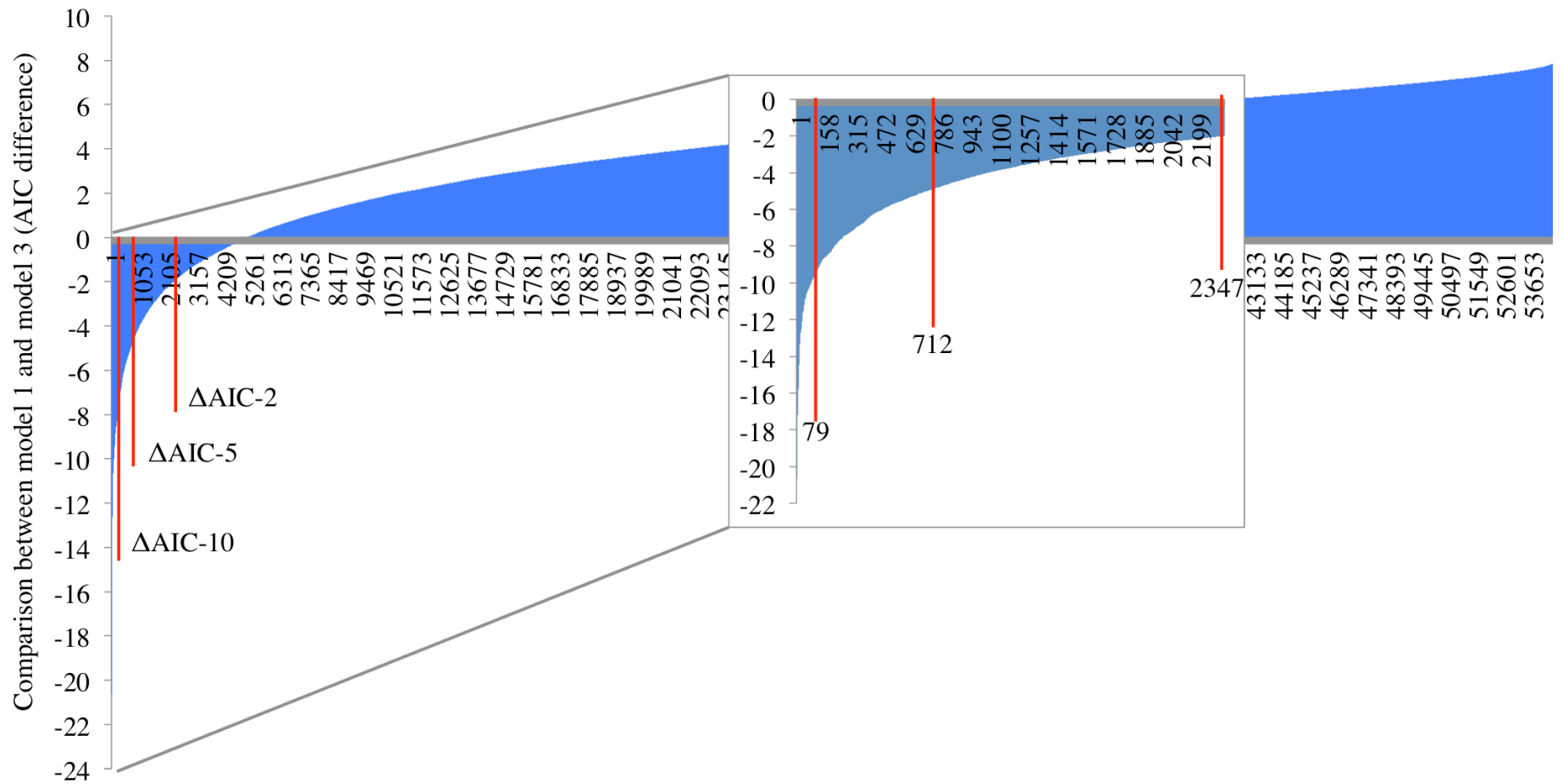
Figure 3.3 Bar plot of AIC differences when comparing linear models 1 and 3 for analysis of patient blood samples. Red lines indicate the -10, -5 and -2 cut offs with -10 being nearest to the y axis and -2 being further away. Enlarged plot shows the selection of probes from delta AIC -2 (2347 probes) to the delta AIC -10 (79), it overlies the large selection of probes where MH susceptibility is not an important factor in the model.

3.3.2 Pathway analysis to determine genetic signature for MH susceptibility in skeletal muscle and peripheral blood

Using the data derived from microarray experiments using patient muscle and blood samples, it was possible to investigate potential pathways of interest in relation to MH phenotype. Potential pathways were first evaluated in the muscle sample cohort, as this is the tissue directly affected by an MH episode. The blood sample cohort was then interrogated for the same pathways of interest to ascertain whether it was possible to detect first, the same pathway and second, any of the same genes implicated in that pathway.

A total of 880 pathways were detected based on the probes fed into the MetaCore™ pathway analysis software. Through further manual interrogation, searching for pathways with particular relevance to skeletal muscle this number was refined to two pathways that were followed up by direct examination of the genes involved in those pathways.

3.3.2.1 The development role of HDAC and calcium/calmodulin-dependent kinase in control of skeletal myogenesis

The first pathway identified through this process, was the 'development role of HDAC and calcium/calmodulin-dependent kinase (CaMK) in control of skeletal myogenesis'. Fifty-four genes are featured in this pathway, with 12 of them identified by the model comparison process as being of interest in relation to MH phenotype in patient muscle samples. A schematic of this pathway with those 12 genes highlighted can be found in Figure 3.4. Expression levels of these 12 genes was then analysed using 3-way

ANOVA (testing for effects of age, sex and MH phenotype and all possible pairwise and 3-way interactions) to determine the specific differences in gene expression occurring in this pathway in relation to MH phenotype.
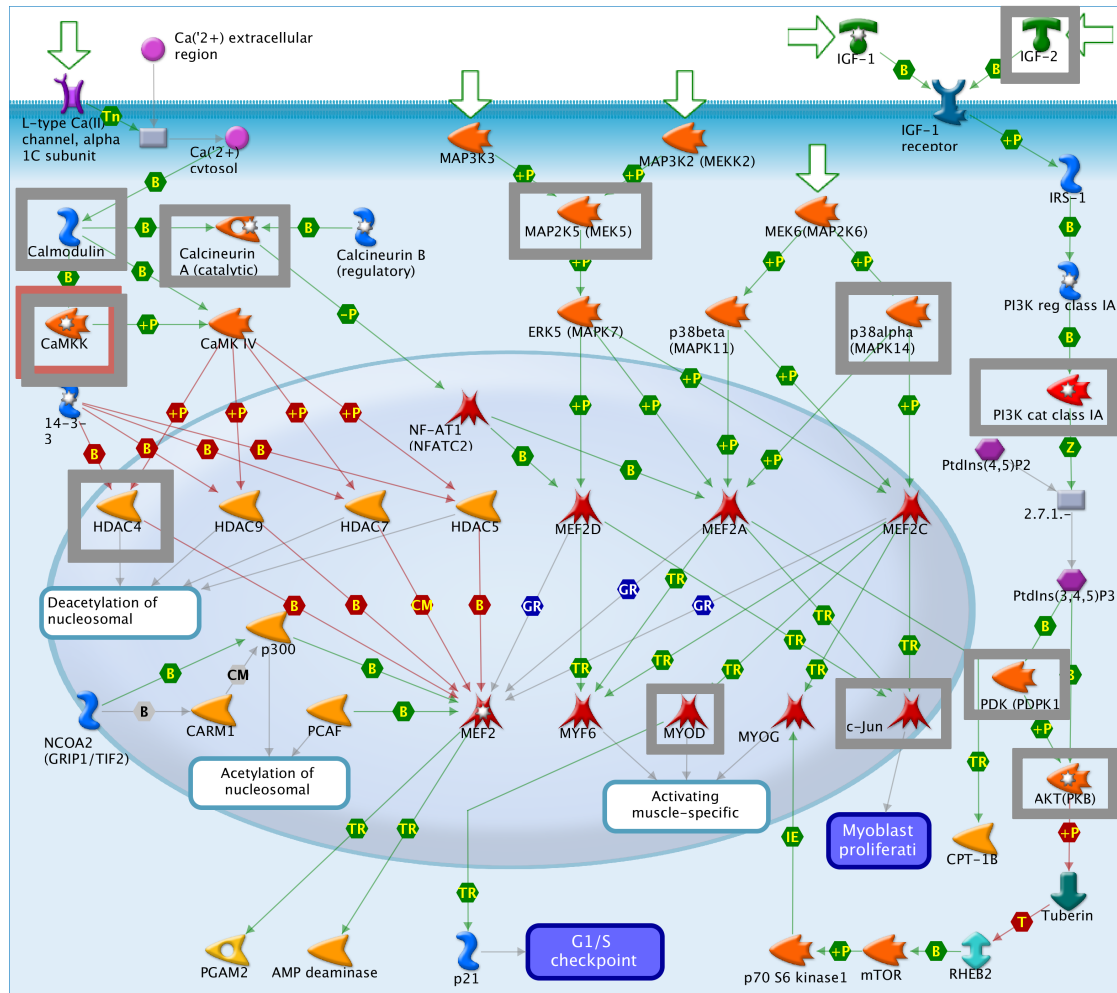
Figure 3.4 Pathway schematic showing the development role of HDAC and calcium/calmodulin-dependent kinase (CaMK) in control of skeletal myogenesis. Grey boxes mark those genes shown to be of interest in MH phenotype from skeletal muscle, red boxes mark those genes shown to be of interest in relation to MH phenotype in peripheral blood.

Calcineurin A is encoded by the *PPP3CC* gene. Expression of this gene was found to be significantly different according to the age, sex and MH status 3-way interaction, p=0.038 (F=4.54, df=1, 51). There was no significant difference when considering MH status independently. Calcineurin A is activated by calmodulin (encoded by *CALM1*), expression of which was found to be significantly lower in MHS samples

compared to MHN, p=0.0013 (F value= 11.56, df=1, 51). There was also found to be a significant effect of the sex-MH phenotype interaction on expression of this gene, p=0.0013 (F=11.48, df=1, 51).Using a post-hoc Tukey test it was established that, there was significantly higher expression of this gene in male MHN samples compared to female MHN (p=0.008) and male MHS (p<0.001).

Therefore, the significant difference between all MHN individuals compared to the MHS group could be influenced by the significant difference in expression of *CALM1* that is specific to male MHNs. Female MHNs show no significant difference in expression of this gene compared to male or female MHSs.

There is a significant difference in expression of *IGF-2* in relation to the sex-phenotype interaction, p=0.031 (F=4.92, df=1, 51). *IGF-2* encodes for insulin-like growth factor 2, which is involved in stimulation of myogenesis. The specific differences in expression are reflected as a reduction in expression in male MHS compared to male MHN, p=0.031 (Tukey test).

This could indicate an altered muscle development profile in males with susceptibility to MH compared to males that are not susceptible. IGF-2 binding to the IGF receptor which initiates a signalling cascade that involves a number of molecules that eventually activates the transcription factor myogenin (MYOG) that is ultimately responsible for activating muscle-specific genes (Figure 3.4) (Xu & Wu, 2000). Other aspects of this signalling cascade were highlighted by the pathway analysis looking at the Affymetrix probes in relation to MH susceptibility. *PIK3CB* that codes for PI3K category class IA showed a significant effect of the sex-MH phenotype interaction on

expression, p=0.006 (F=8.08, df=1, 51). By applying a post hoc Tukey test to the expression data it was revealed that the expression difference was a significant decrease in expression in male MHS patients compared with male MHNs, p=0.04.

Expression of *PDPK1* that encodes for PDK showed a significantly higher level of expression in MHS individuals compared to MHN, p=0.008 (F=7.59, df=1, 51). There was also found to be a significant effect of the sex-MH phenotype interaction on expression of this gene, p=0.014 that was specifically evident when observing the significantly higher expression in male MHS individuals to male MHNs, p=0.006.

Expression of *c-JUN* also differed in relation to the sex-MH phenotype interaction, p=0.005 (F= 8.63, df=1, 51). Specifically, there was decreased expression of this gene in male MHN samples compared to female MHN (p=0.009, Tukey test) and increased expression in male MHS samples compared to male MHNs (p=0.034, Tukey test). *c-JUN* is a transcription factor oncogene involved in the control of duration of myoblast differentiation (Daury *et al.*, 2001). These expression differences could indicate alterations in the profile of myoblast differentiation in male patients with MH.

Mammalian skeletal muscle differentiation is coupled to withdrawal from the cell cycle and associated with transcriptional activation of an array of muscle-specific genes (Lu *et al.*, 2000). Two families of transcription factors play important roles during this process. One includes MyoD family proteins which is sometimes referred to as myogenic regulatory factors (MRFs) which contains four members: Myf5, Myogenic differentiation 1 (MYOD1), Myogenin (MYOG), and Myogenic factor 6 (MYF6) that are exclusively expressed in skeletal muscle. Of the genes involved in

122

this aspect of the pathway, only *MYOD1*, shown as MYOD in Figure 3.4, expression was found to differ significantly according to MH phenotype (p=0.017, F=6.02, df=1, 51), evidenced by a significant reduction in expression in MHS individuals compared to MHN.

Sustained expression of MYOD1 is essential for retaining the expression of muscle-related genes (Fong & Tapscott, 2013). Further investigation of this gene is required, perhaps at the functional or protein level to better understand the consequences of this reduction in expression. As it is such a crucial factor in myogenic regulation this gene could play a role in the pathogenicity of MH.

The other group consists of Myocyte enhancer factors 2 (MEF2): MEF2A, MEF2B, MEF2C, and MEF2D. The latter can form homo- and heterodimers that constitutively bind to the promoters or enhancers of the majority of the muscle-specific genes. Additionally, MRF and MEF2 members can physically interact with each other to synergistically activate many muscle-specific genes (Xu & Wu, 2000; McKinsey *et al.*, 2002). As is shown in Figure 3.4, MEF2 is associated with a number of regulating proteins, including four and as a result regulation of its activity is complex.

HDAC4 was found to differ significantly according to the sex-phenotype interaction, p=0.002 (F=10.31, df=1, 51). Through investigation using a post-hoc Tukey test this significance can be attributed to the decreased expression of this gene in male MHN samples compared to female samples of the same phenotype, p=0.0008.

HDAC4 acts to block conversion of fibroblasts into myotubes during myoblast proliferation by inhibiting MEF2-dependent transcription (Lu *et al.*, 2000). Upon differentiation it is translocated to the cytoplasm and as a result no longer inhibits MEF2 and myoblast differentiation can occur (Moresi *et al.*, 2015). HDAC4 expression has been shown to be up-regulated in the muscle of amyotrophic lateral sclerosis (ALS) patients and is inversely correlated with disease severity. Indeed it has been shown that treating ALS mice with HDAC inhibitors has beneficial effects on survival and muscle maintenance (Yoo & Ko, 2011). As the expression differences in this cohort appear to be between males and females in the MHN group this gene may not be of interest in relation to MH susceptibility.

CaMK IV is essential in the process of translocating HDACs to the cytoplasm to allow for initiation of myoblast differentiation. CaMK IV is phosphorylated by CAMKK (encoded by *CAMKK2,* calcium/calmodulin-dependent protein kinase 2) and therefore plays an essential role in the signalling cascade involved in skeletal muscle development. Expression of *CAMKK2* was found to be significantly lower in MHS samples compared to MHN, p=0.02 (F=5.4, df=1, 51).

The lists of probes derived from Affymetrix arrays on patient blood samples were also subjected to the same process of pathway analysis in MetaCore as the patient muscle samples. The resulting list of 536 pathways was manually interrogated establish whether the same pathways were evident in the blood data as were found in the muscle data. As highlighted by the red box in Figure 3.4, *CAMKK2* was also detected as having significantly lower expression in the blood samples from MHS patients,

compared to expression levels in blood from MHN patients, p<0.001 (F=15.67, df=1, 51).

The expression profile for this gene detected in peripheral blood samples complements the expression profile of the same gene in skeletal muscle biopsies. Additional work would be necessary on a larger population, including more susceptible individuals and a larger control group from the general population to better understand how definitive this expression pattern is in relation to the MH phenotype.

3.3.2.2 nNOS signalling in skeletal muscle

Nitric oxide (NO) is a gaseous free radical that has been established as an important endogenous regulator of skeletal muscle physiology at both the tissue and cellular level (Reid, 1998). Storage of NO is not possible, therefore control of signalling specificity is controlled at the level of synthesis (Bredt, 2003).

There are three major isoforms of nitric oxide synthase (NOS) enzymes that act to generate NO from L-Arginine, molecular oxygen and NADPH.

- Type I NOS, also referred to as neuronal NOS or nNOS, is localised to the sarcolemma of the myocyte.

- Type II NOS, also known as inducible NOS or iNOS is localised to the cytosol.

- Type III NOS or endothelial NOS (eNOS) is localised to the mitochondria (Reid, 1998).

The nNOS signalling pathway in skeletal muscle was identified using MetaCore pathway analysis on the list of genes derived from the AIC comparison (ΔAIC-2) for

those probes (4561) that show significantly different expression in relation to MH phenotype (Figure 3.5).
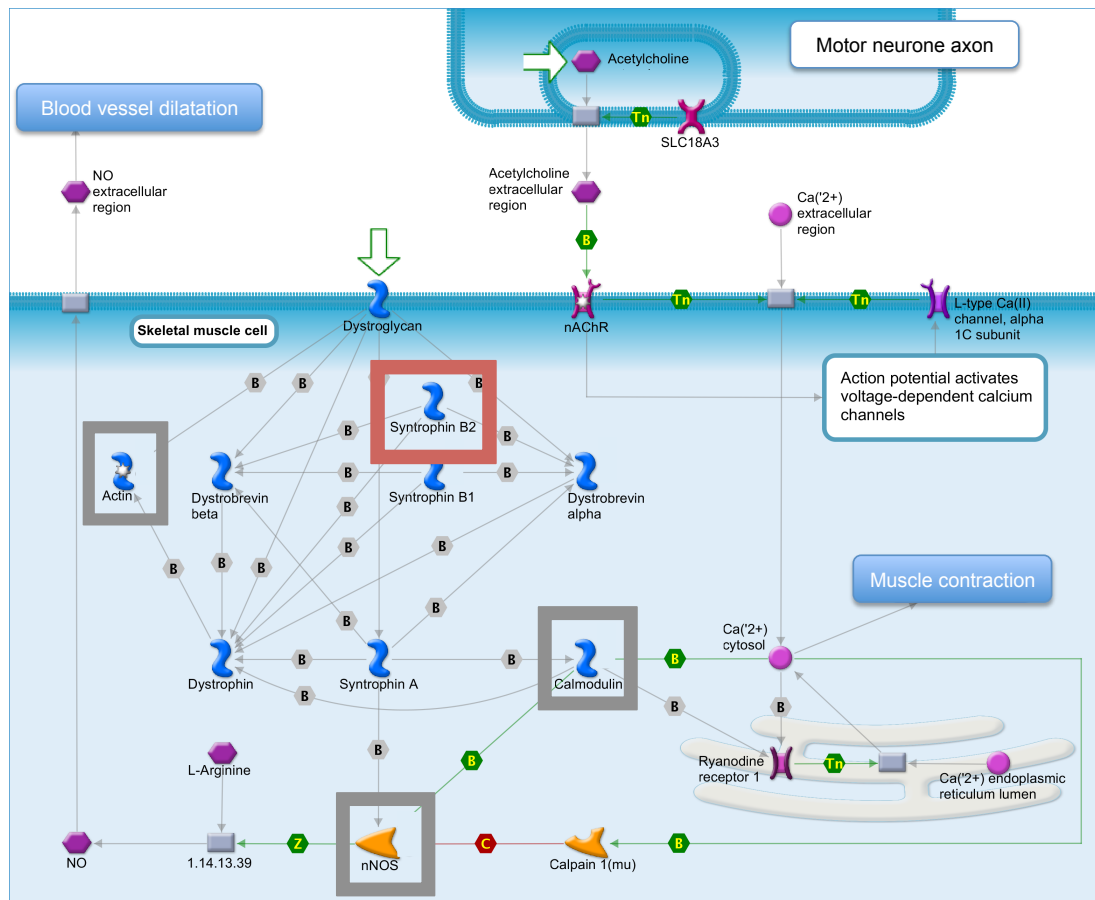
Figure 3.5 Pathway schematic showing nNOS signalling in skeletal muscle. Proteins outlined in boxes (**grey**=from in muscle samples, **red**=from in blood samples) were shown to be of interest in relation to MH phenotype based on AIC model comparison (ΔAIC-2).

Nitric oxide synthases are of considerable importance in maintaining sarcolemmal integrity due to their direct interaction with the Actin (encoded by *ACTB*) cytoskeleton (Chen *et al.*, 2003; Rybakova *et al.*, 2006). Expression of *ACTB* was found to differ significantly according to phenotype (p=0.0005, F=15.79, df=1, 51) in the skeletal muscle cohort, with significantly lower expression levels detected in the MHS cohort compared to MHN muscle.

The arrangement of the actin cytoskeleton with dystrophin and dystroglycan associated nNOS with the sarcolemma. Here it can generate NO and this skeletal

muscle derived NO then diffuses to adjacent blood vessels to increase perfusion of contracting muscle (Stamler & Meissner, 2001). It was found that in MHS patients, expression of nNOS was significantly reduced compared to the level detected in MHN samples by microarray analysis ($p=0.04$, $F=4.19$, $df=1$, 51).

nNOS is dependent on calcium/calmodulin binding in order to carry out NO production, whereby calmodulin functions to allow electron transport from the reductase domain of the haem group of nNOS (Su *et al.*, 1995). Unlike iNOS, nNOS and eNOS are inactive at resting intracellular calcium levels. They are activated when calcium concentrations are elevated to maintain calmodulin binding (Kone, 2000; Shirran *et al.*, 2005). Calmodulin 1, as encoded by *CALM1*, expression which was found to be significantly reduced in individuals susceptible to MH compared with those not susceptible ($p=0.001$, $F= 11.56$, $df=1$, 51). *CALM1* was also a feature of the HDAC and CaMK pathway discussed in section 3.3.2.1.

Interestingly, none of the genes identified in the skeletal muscle cohort from this pathway were highlighted as being significant in the blood samples. None the less, this pathway was still identified as one of interest in the pathway analysis on the blood samples because a different gene, *SNTB2* was highlighted as being of interest in relation to MH phenotype. Expression was found to differ significantly according to the sex-phenotype interaction ($p=0.002$, $F=9.08$, $df=1$, 51). Specifically, it was significantly higher in male MHS samples compared to male MHN and significantly lower in female MHS samples compared to female MHN.

While none of the genes in this pathway that were detected in the muscle samples were correspondingly detected in blood, it is of potential use that another gene involved in nNOS signalling was detected. It could provide an avenue for investigation towards developing a blood test for MH susceptibility, perhaps in combination with *CAMKK2* detected in the skeletal myogenesis pathway.

3.3.3   Determination of a predictive model for MH susceptibility

3.3.3.1   Predictive model based on Affymetrix array data from skeletal muscle

In order to identify genes from the Affymetrix array that are associated with MH susceptibility (either MHS or MHN), LASSO regression was performed using the ΔAIC-10 refined list of 281 probes implicated in MH susceptibility from patient skeletal muscle samples. This method performs a sub-selection of probes involved in MH by shrinkage of the regression coefficient through imposing a penalty proportional to their size. This results in most predictors being shrunk to zero, leaving only a small number with a weight of non-zero.

Using this method, 17 probes were identified with non-zero regression coefficients (Table 3.4). In order to make subsequent equation definition more manageable, Affymetrix probe IDs were simplified using the format 'm000'. The penalised regression coefficients were used to define the parameters for generating the risk score for MH susceptibility. Probes assigned a negative LASSO coefficient are positive predictors of MH susceptibility and those with a positive LASSO coefficient are negative predictors of MH susceptibility.

Three of the probes identified are unannotated and one probe targets two genes.

Therefore, 15 genes are implicated in this predictive model for MH susceptibility.

Table 3.4 Probes associated with susceptibility to MH using the LASSO regression test (muscle samples)

Probe ID	Probe Code	Gene	LASSO penalised coefficient for risk score (log2)
218806_s_at	m026	VAV3	-3.8965086
239370_at	m272	LINC01133	-3.2144525
1556763_at	m178	unannotated	-2.8517881
227404_s_at	m217	EGR1	-1.1678859
210139_s_at	m095	PMP22	-0.7981979
208917_x_at	m084	NADK	-0.5811914
217259_at	m165	unannotated	-0.5413827
212525_s_at	m004	H2AFX	-0.4614276
213931_at	m182	ID2	-0.3866819
220359_s_at	m160	ARPP21	-0.3670338
231926_at	m259	EPS15L1	-0.3637492
202426_s_at	m046	RXRA	-0.0920112
233637_at	m252	DCAF8	0.2519220
1555272_at	m120	RSPH10B2	0.5552463
221960_s_at	m244	RAB2A	0.9616943
214290_s_at	m172	HIST2H2AA3; HIST2H2AA4	1.2790261
231042_s_at	m031	unannotated	2.0465129

A risk score was generated using the sum of the probe expression values weighted by the coefficients from the LASSO regression:

$$(-3.896509*m026) + (-3.214453*m272) + (-2.851788*m178) + (-1.167886*m217) +$$

$$(-0.798198*m095) + (-0.581191*m084) + (-0.541383*m165) + (-0.461428*m004) +$$

$$(-0.386682*m182) + (-0.367034*m160) + (-0.363749*m259) + (-0.092011*m046) +$$

$$(0.251922*m252) + (0.555246*m120) + (0.961694*m244) + (1.279026*m172) +$$

$$(2.046513*m031)$$

The risk score was applied to all muscle samples in the dataset. This identified a clear distinction between normal and susceptible samples using this predictive model,

where samples with a median score of <0 being MHN and those with a median score >0 are MHS (Figure 3.6).
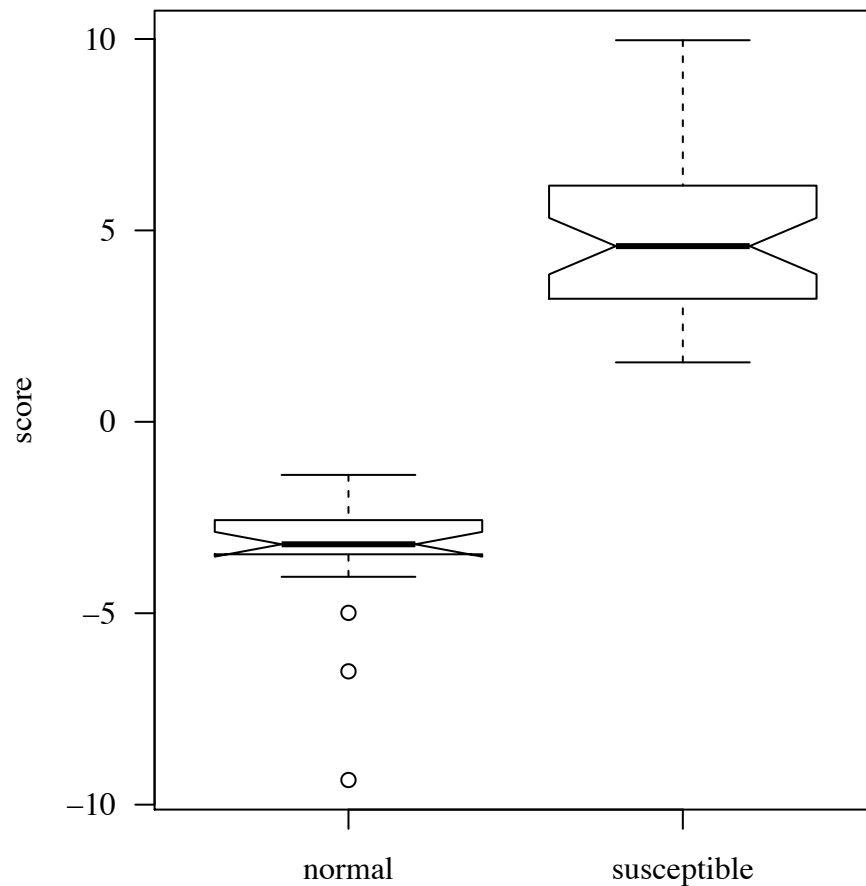
Figure 3.6 Comparison of median scores for normal and susceptible samples derived from muscle risk score.

The notches on the boxplots roughly represent the 95% confidence interval for the difference in the two medians (Chambers *et al.*, 1983). This indicates that this prediction very clearly distinguishes between MHS and MHN in this dataset, as the notches do not overlap (Figure 3.6).

3.3.3.2 *Predictive model based on Affymetrix array data from peripheral blood*

LASSO regression was performed using the ΔAIC-10 refined list of 78 probes implicated in MH susceptibility from patient peripheral blood samples. Using this

method, 18 probes were identified with non-zero regression coefficients (Table 3.5). In order to make subsequent equation definition more manageable, Affymetrix probe IDs were simplified using the format 'b00'. One of the probes identified is unannotated and one probe targets two genes. Therefore, 18 genes are implicated in this predictive model for MH susceptibility.

Table 3.5 Probes associated with susceptibility to MH using the LASSO regression test (blood samples)

Probe ID	Probe Code	Gene	LASSO penalised coefficient for risk score (log2)
215505_s_at	b45	STRN3	-1.140474
215013_s_at	b25	USP34	-0.837732
227393_s_at	b29	TRA2A	-0.581304
218433_at	b61	PANK3	-0.567443
222930_s_at	b39	AGMAT	-0.123679
222919_at	b27	TRDN	0.012401
222134_at	b75	DDO	0.239126
220436_at	b04	unannotated	0.244762
206740_x_at	b14	SYCP1	0.251144
216876_s_at	b71	IL17A	0.455281
244839_at	b16	LINC00518	0.603584
213455_at	b51	FAM114A1	0.894760
204926_at	b09	INHBA	1.289086
231943_at	b49	ZFP28	1.355012
1569110_x_at	b15	LOC728613	1.385875
241713_s_at	b17	DYXC1;DYXC1-CCPG1	1.413366
220551_at	b38	SLC17A6	1.574433
205838_at	b20	GYPA	2.099101

The penalised regression coefficients were used to define the parameters for generating the risk score for MH susceptibility. Probes assigned a negative LASSO coefficient are positive predictors of MH susceptibility and those with a positive LASSO coefficient are negative predictors of MH susceptibility. A risk score was generated using the sum of the probe expression values weighted by the coefficients from the LASSO regression:

(-1.140474*b45) + (-0.837732*b25) + (-0.581304*b29) + (-0.567443*b61) +

(-0.123679*b39) + (0.012401*b27) + (0.239126*b75) + (0.244762*b04) +

(0.251144*b14) + (0.455281*b71) + (0.603584*b16) + (0.894760*b51) +

(1.289086*b09) + (1.355012*b49) + (1.385875*b15) + (1.413366*b17) +

(1.574433*b38) + (2.099101*b20)

The risk score was applied to all blood samples in the dataset with incorporation of the intercept (-30.996903) to set the baseline to zero. This identified an overlap between normal and susceptible samples using this predictive model (Figure 3.7).
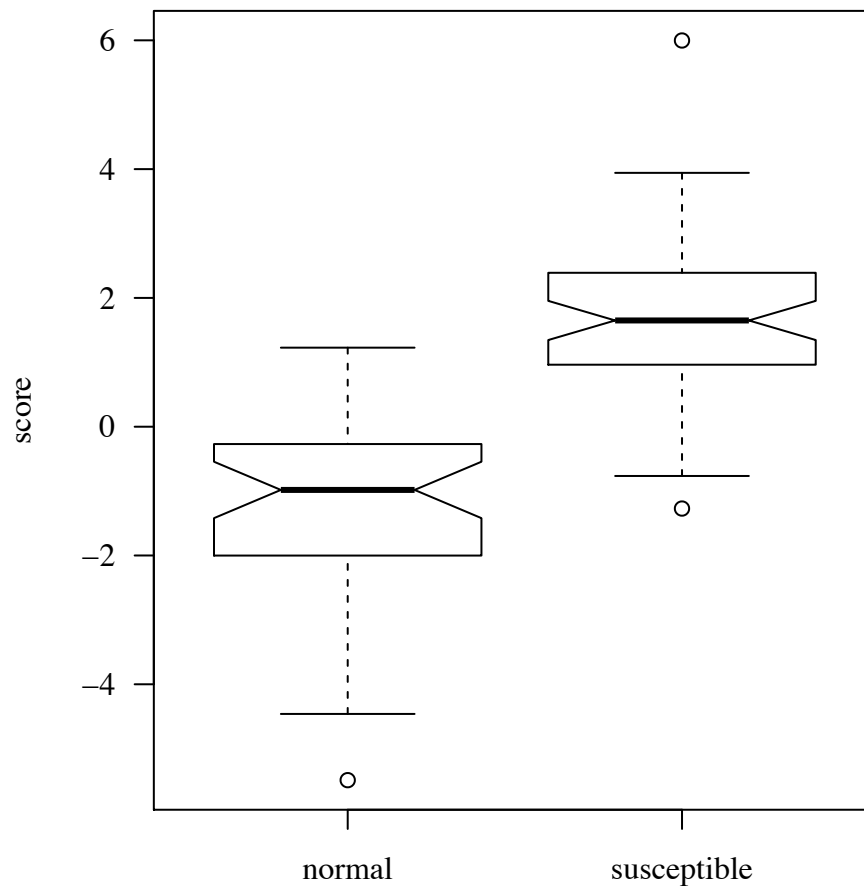
Figure 3.7 Comparison of median scores for normal and susceptible samples derived from blood risk score.

The optimal cut off for the risk score difference between normal and susceptible patients using blood was not as clear as in the muscle data. Therefore, an optimal cut off was established using the Youden's J statistic in conjunction with receiver operating characteristic (ROC) analysis (Figure 3.8). Using the Youden method it was established that the optimal cut off for discriminating between normal and susceptible individuals using blood samples is 0.52 with a sensitivity of 0.87 and specificity of 0.97 where the area under the curve at that cut off is 0.92.
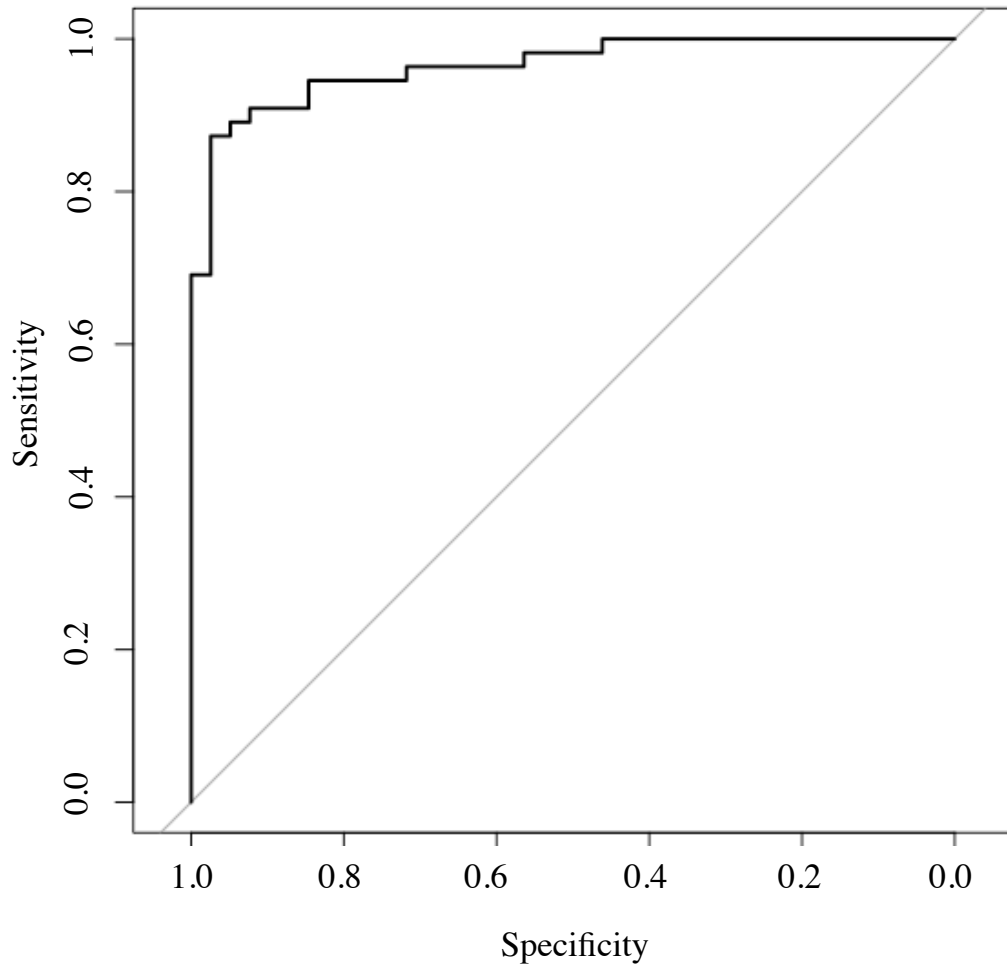
Figure 3.8 ROC curve for risk scores from blood

3.3.3.3   Risk score validation

The risk scores defined in sections 3.3.3.1 and 3.3.3.2 have been generated and tested on the same data set. This is possible because LASSO employs leave-one-out cross validation, where the model is rerun iteratively, each time leaving a sample out (Goeman, 2010). This reduces over fitting of the model to the dataset. Ideally, validation should be performed on an independent dataset from a different population or with a different technique. However, this data is not available. Further work could be carried out to validate the predictive models generated here through the use of qPCR on a separate cohort of muscle and blood samples to quantify the sensitivity and specificity of this test as a means of determining susceptibility to MH.

3.3.4   *Targeted analysis of genes implicated in MH and ageing in skeletal muscle*

The aim of this process was to define potential genes of interest that could be analysed using TaqMan® assays on a separate cohort of skeletal muscle samples to perform a more detailed analysis of genes implicated in MH susceptibility and skeletal muscle ageing. In order to account for all potential genetic complexities, the data was re-analysed using 3 levels of MH phenotype:

- MHN: Malignant Hyperthermia normal

- MHS+: susceptible to MH with a causative mutation in *RYR1*

- MHS-: susceptible to MH with no causative mutation in *RYR1*

The two pathways highlighted in the previous section that were of relevance to MH susceptibility (just comparing MHS and MHN) also indicated a number of potential genes of interest in relation to MH susceptibility considering the 3 levels of MH phenotype and ageing. The -10 delta AIC difference should be used as a cut off for

deciding which probes should be followed up using TaqMan®. Summarised in Figure 3.9 is the distribution of probes that showed to be of interest in relation to MH susceptibility. Compared to the first analysis that used two levels of MH phenotype and established 281 probes at the -10 delta AIC cut off, this analysis using three levels of MH phenotype highlighted 302 probes at the same cut off (Figure 3.9).
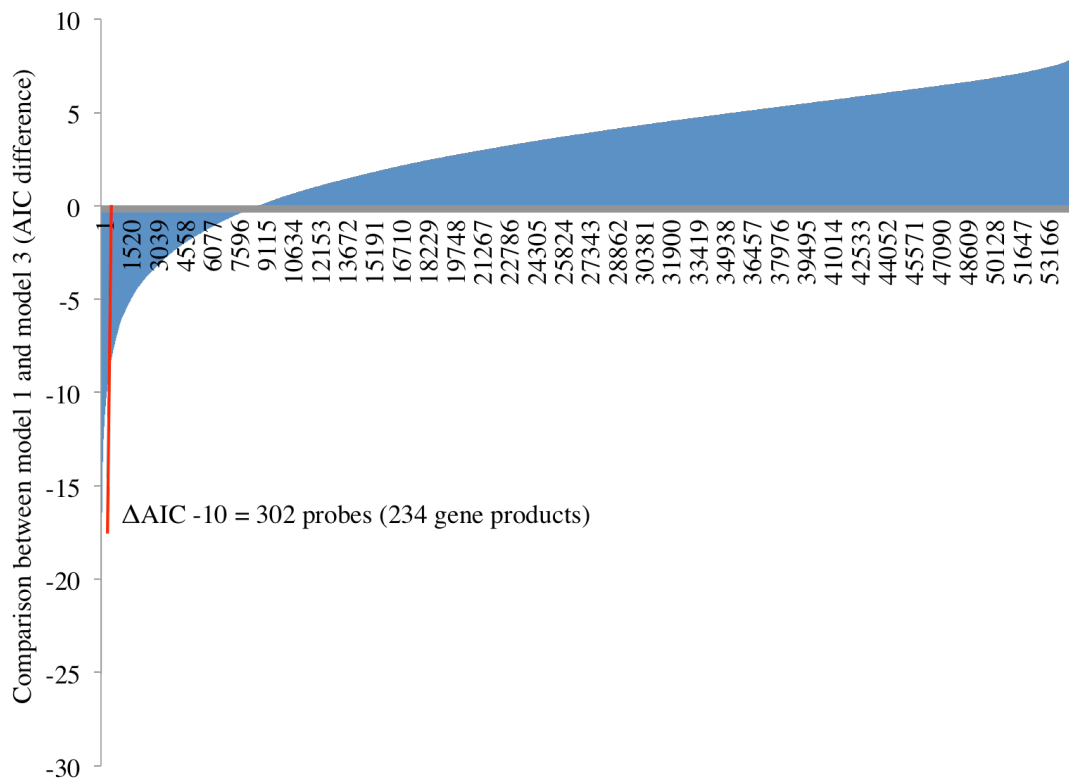
Figure 3.9 Bar plot of AIC score differences for comparison of models 1 and 3, demonstrating those probes that show significant differences in gene expression where MH status is an important predictor variable. ΔAIC-10 is marked by red line.

This indicates that at the whole genome level there are differences in the expression profile when considering whether or not a susceptible individual carries a causative *RYR1* mutation.

A model comparison to determine those probe sets of interest in relation to age was also carried out in order to establish possible genes of interest in relation to skeletal muscle ageing. The -10 delta AIC was used in this process to refine the list of genes. It resulted in 1607 probes with a delta AIC equal to or less than -10 that equates to 1411 gene products (Figure 3.10).
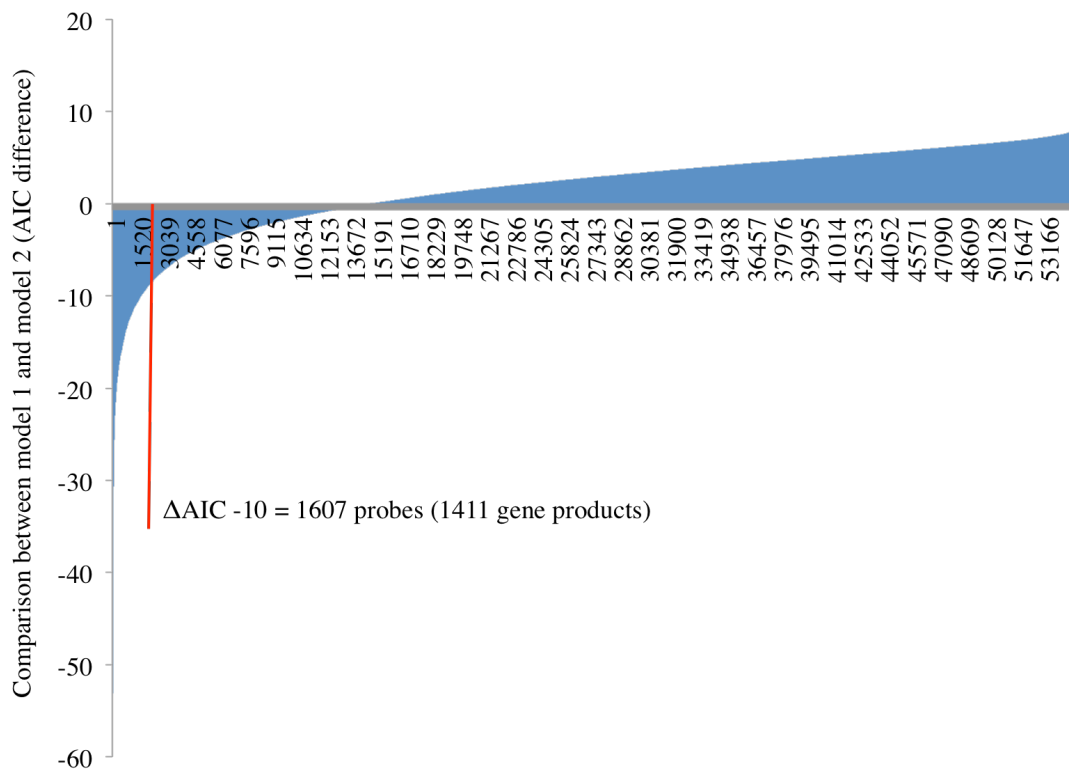
Figure 3.10 Bar plot of AIC score differences for comparison of models 1 and 2, demonstrating those probes that show significant differences in gene expression where age is an important predictor variable. ΔAIC-10 is marked by red line.

A final comparison was made between models 1 and 4 to establish a refined list of genes where the age-MH phenotype interaction is an important predictor variable. This resulted in 85 probes representing 69 specific gene products. These lists of probes were then interrogated based on the pathways that had been previously established (in

sections 3.3.2.1 and 3.3.2.2) as well as using gene functional characterisation using DAVID to determine genes that may be worthy of follow up using TaqMan®.

When examining the list of probes determined in relation to age, MH phenotype and the age-phenotype interaction, the CaMK pathway exhibited a different selection of genes of interest compared to the previous analysis Figure 3.11.
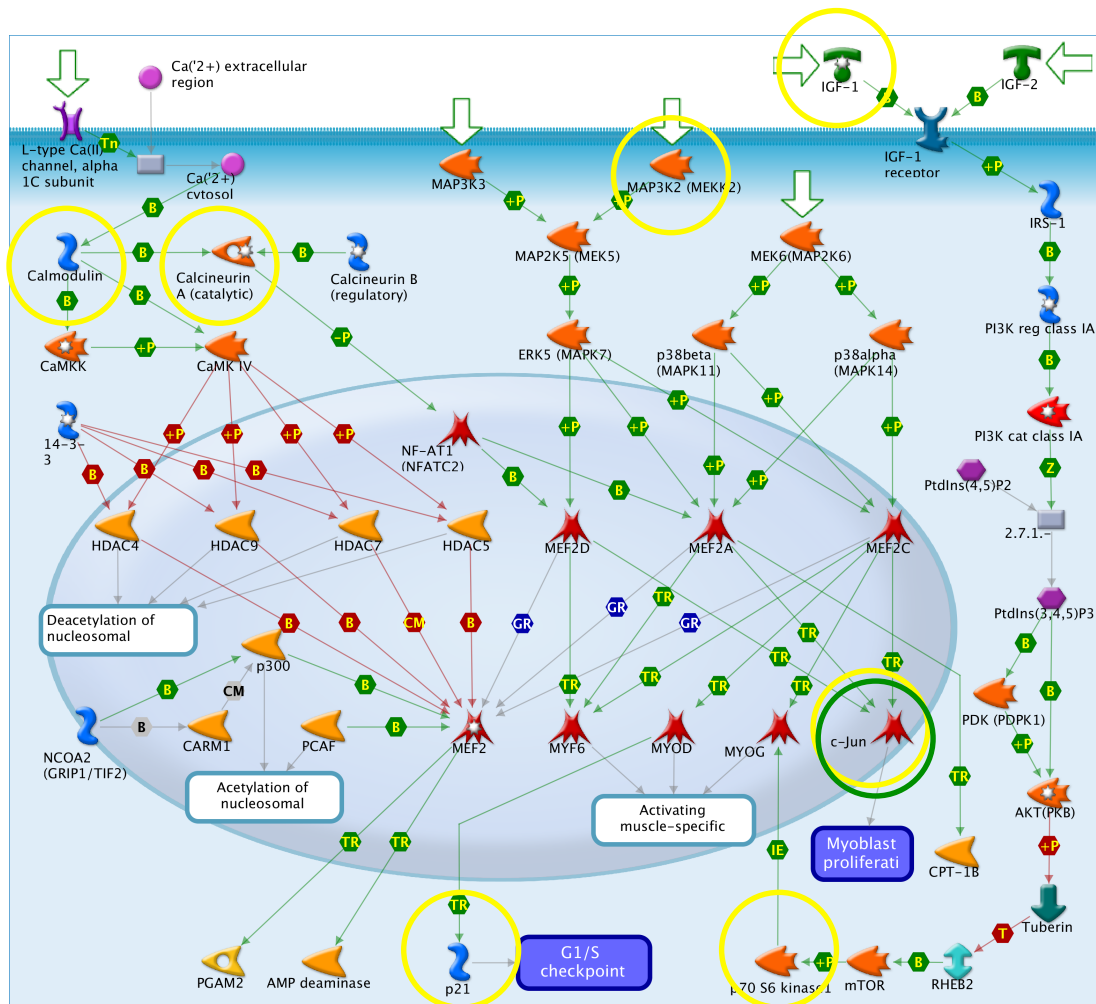
Figure 3.11 Pathway schematic showing the development role of HDAC and calcium/calmodulin-dependent kinase (CaMK) in control of skeletal myogenesis. Proteins circled in green showed a significant difference for MH phenotype, proteins circled in yellow showed a significant difference for age and presence of both coloured circles denotes an interaction between age and phenotype.

This analysis only included those probes with a delta AIC of -10 or lower and so it is not surprising that many of the aspects of the pathway identified previously are no longer highlighted. This process was devised in order to better refine the list of genes to be followed up by TaqMan®.

Only one feature of this pathway, c-Jun (encoded by *JUN*), was found to have an altered expression profile in response to MH phenotype and age. Expression of *JUN* was significantly higher in MHN samples compared to MHS+, p=0.04 (F=3.48, df=2, 47). Expression of *JUN* was found to decrease significantly with increasing age, p=0.00004 (F=20.03, df=1, 47) and the interaction of age and MH status also showed a significant effect on expression of *JUN*, p=0.02 (F=3.51, df=1, 47). Increasing age in the MHS- samples did not show decreased expression of *JUN* unlike the MHS+ and MHN samples which both showed decreased expression with increased age.

In combination with c-Fos, c-Jun forms the AP-1 early response transcription factor and in skeletal muscle it is involved in controlling the duration of myoblast proliferation (Bergstrom & Tapscott, 2001). c-Jun activity is found to be regulated by c-Jun amino N-terminal kinases (JNKs) (Cargnello & Roux, 2011). Activation of JNKs in skeletal muscle is associated with age, however using a mouse model, this activation can be suppressed by application of testosterone showing that sarcopenia can be reduced in aged mice through testosterone suppression of age-related oxidative stress that is mediated by JNKs (Kovacheva *et al.*, 2010). Alteration of elements in this skeletal myogenesis pathway have been shown to be age related, suggesting that the process of muscle development is altered with age and that genes such as *JUN* may be worthy of additional investigation in the context of MH and ageing.
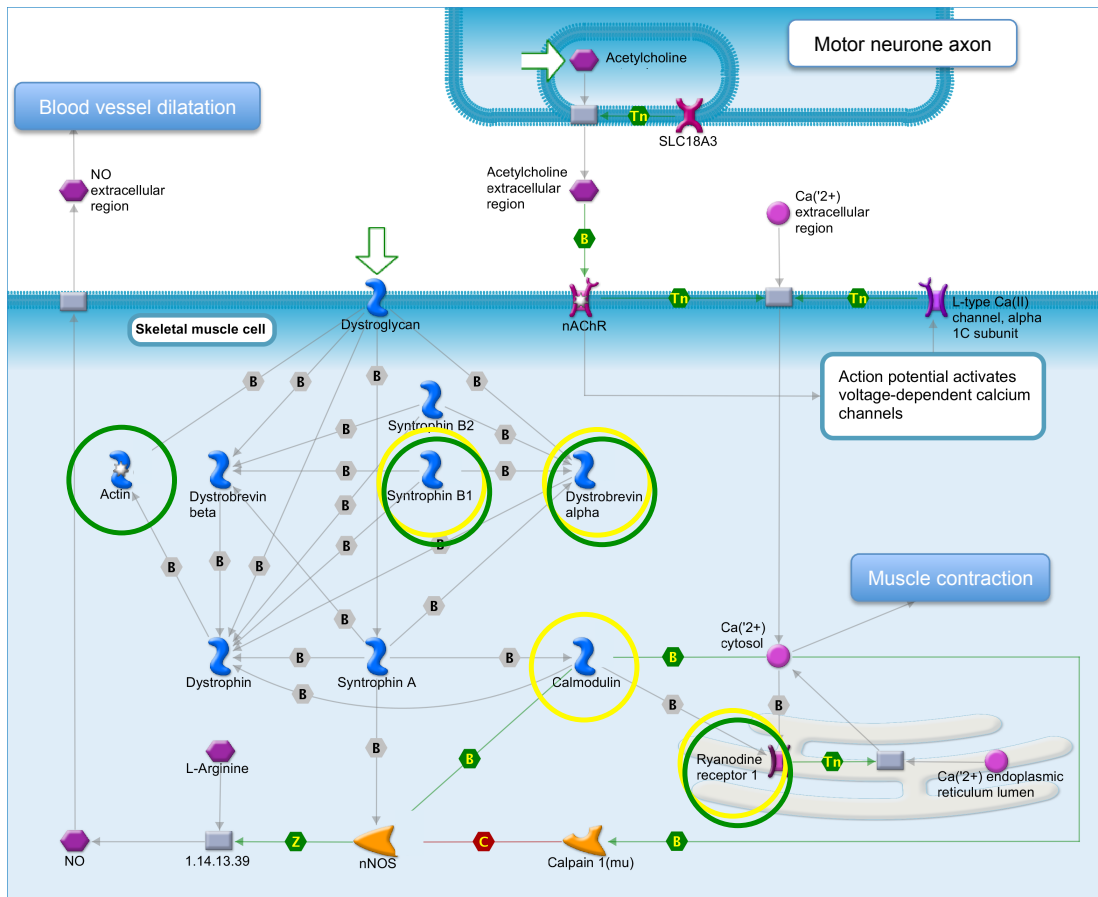
Figure 3.12 Pathway schematic showing nNOS signalling in skeletal muscle, results of pathway analysis on Affymetrix data investigating importance of age-phenotype interaction. Proteins circled in green showed a significant difference for MH phenotype, proteins circled in yellow showed a significant difference for age and presence of both coloured circles denotes an interaction between age and phenotype

When re-examining the nNOS signalling pathway using the lists of genes derived from the model comparison to determine genes of interest in relation to MH susceptibility and ageing and the interaction between these factors, five genes were identified (Figure 3.12). The gene coding for Actin was found to have significantly different expression between MH phenotype groups and the gene coding for Calmodulin was found to have significantly different expression with respect to increasing age. Genes coding for the skeletal muscle Ryanodine Receptor (RyR1), Syntrophin B1 and Dystrobrevin alpha were found to show differences in gene expression relating to both age and MH phenotype.

Expression of *CALM1* was shown to differ significantly with age (p=0.01, F=10.12, df=1, 47), with expression increasing with increasing age.

In the previous analysis, *CALM1* expression differed significantly according to MH phenotype and the sex-MH phenotype interaction, where expression was higher in MHNs, specifically male MHNs. However, when the MHS category is subdivided into MHS+ and MHS-, this significance is no longer evident. Altered expression of *CALM1* could have an impact on calcium handling in skeletal muscle as these molecules have been shown to interact with calcium channels (Tripathy *et al.*, 1995; Mori *et al.*, 2004). There is no information relating to changes in expression of this gene being related to ageing in human skeletal muscle, however its involvement in calcium handling could indicate its relevance considering that there is evidence of other aspects of calcium handling in skeletal muscle being disrupted with age (Weisleder *et al.*, 2006).

Expression of *ACTB* was found to differ significantly between MHN samples and both distinct groups of MHS samples (p<0.001, F=4.37, df=2, 47), with expression levels in MHS+ and MHS- groups being of a similar level. This is consistent with the finding in the previous analysis and suggests that with respect to expression of this gene in the MHS groups, is unlikely to be of value in explaining the evident genetic differences in conjunction with similar IVCT phenotype.

RYR1 was not identified using the model comparison between MHS and MHNs. However, when the MHS category was subdivided according to whether the sample has a causative *RYR1* mutation, and the data re-analysed using a model comparison to

highlight genes of interest in relation to age and MH phenotype *RYR1* was found to be important.

There was a significantly higher level of *RYR1* expression was detected in males compared to females, p=0.002 (F=8.3, df=1, 47). There was also a significant increase in *RYR1* expression with increasing age, p=0.0007 (F=10.12, df=1, 47) and as a result a significant effect on expression when factoring in age and sex, p=0.02 (F=3.41, df=1, 47), with a marked increase in expression with age in males compared to females.

It could be argued that this significantly higher level of expression in males could actually be due to the increased number of older males in this sample (n=39 males, n=20 females). The oldest female participants are in their late 40s, whereas the male cohort includes individuals spanning a much wider age range (Table 3.1). Indeed, there is still an observed increase in expression with age in the female cohort. *RYR1* expression clearly increases with age and this result is consistent with other research concerning expression of this gene though the tissue type in question for this study was skin (Glass *et al.*, 2013).

The sarcolemmal localisation of nNOS in skeletal muscle is related to the way it interacts with the dystrophin glycoprotein complex, which influences the activity and distribution of this enzyme in skeletal muscle (Kone, 2000). *DTNA1* encodes for Dystrobrevin alpha, a component of the dystrophin glycoprotein complex. *DTNA* expression in skeletal muscle was also shown to be of interest in relation to MH phenotype and age. There was significantly higher expression in MHS+ muscle

compared to MHS-, p=0.04 (F=3.18, df=2, 47). There was also a significant increase in expression with increasing age, p=0.0003 (F=12.7, df=1, 47) and a significant interaction between the two factors, p=0.03 (F =3.9, df=2, 47).

Dystrobrevin alpha binds to Syntrophin B1 (coded by *SNTB1*), another molecule in this complex. *SNTB1* expression also increased with increasing age, p<0.001 (F=13.02, df=1, 47) and the age-phenotype interaction (p=0.04, F=4.54, df=1, 47). There is an increase in expression relative to age in the MHS+ group compared to the MHS- group and the increase with age in the MHN group is most consistent with the MHS+ group.

The pathways defined by MetaCore are extensive but no means exhaustive, and as a result it was considered necessary to test for potential GOIs by other means. In addition to carrying out pathway analysis in MetaCore, lists of probesets defined by the AIC model comparison process (ΔAIC-10) as being of potential interest in relation to the interaction between MH phenotype and age were also subjected to gene functional classification using DAVID. Nineteen probe sets were present in this list that belonged to the 'muscle contraction' functional group defined by this software (Table 3.6).

Table 3.6 Probe sets implicated in muscle contraction according to DAVID gene ontogeny

Affy Probe ID	Gene Name
224528_s_at	Kv channel interacting protein 2
221232_s_at	ankyrin repeat domain 2 (stretch responsive muscle)
226277_at	collagen, type IV, alpha 3 (Goodpasture antigen) binding protein
208430_s_at	dystrobrevin, alpha
217154_s_at	endothelin 3
216235_s_at	endothelin receptor type A
204271_s_at, 204273_at	endothelin receptor type B
228563_at	gap junction protein, gamma 1, 45kDa
230090_at	glial cell derived neurotrophic factor
204763_s_at	guanine nucleotide binding protein (G protein), alpha activating activity polypeptide O
209342_s_at	inhibitor of kappa light polypeptide gene enhancer in B-cells, kinase beta
205826_at	myomesin (M-protein) 2, 165kDa
232871_at	myomesin 1, 185kDa
206394_at	myosin binding protein C, fast type
34471_at	myosin, heavy chain 8, skeletal muscle, perinatal
228414_at	potassium large conductance calcium-activated channel, subfamily M, alpha member 1
226660_at	ribosomal protein S6 kinase, 70kDa, polypeptide 1
205485_at	ryanodine receptor 1 (skeletal)
215431_at	syntrophin, beta 1 (dystrophin-associated protein A1, 59kDa, basic component 1)

Nine probe sets were identified as of interest in the 'response to calcium ion' functional group (Table 3.7).

Table 3.7 Probe sets implicated in response to calcium ion according to DAVID gene ontogeny

Affy Probe ID	Gene Name
224528_s_at	Kv channel interacting protein 2
AFFX-HSAC07/X00351_3_at	actin, beta
212363_x_at	actin, gamma 1
243922_at	calcium-sensing receptor
211985_s_at	calmodulin 3 (phosphorylase kinase, delta)
214475_x_at	calpain 3, (p94)
212097_at	caveolin 1, caveolae protein, 22kDa
202389_s_at	huntingtin
228414_at	potassium large conductance calcium-activated channel, subfamily M, alpha member 1

It is clear from examining these tables that a number of the genes detected in the pathways shown by pathways shown by the MetaCore analysis have come up again such as actin, calmodulin (Nine probe sets were identified as of interest in the 'response to calcium ion' functional group (Table 3.7).

Table 3.7) dystrobrevin alpha, syntrophin beta 1 and the ryanodine receptor (Table 3.6). This indicates that these genes may be worth following up with additional gene expression experiments to investigate genes related to MH phenotype and muscle ageing. Other genes were also highlighted, including calpain 3 (*CAPN3*). This gene has been established as coding for a major intracellular protease, though its function has not been well established. Calpain 3 has been shown to interact with titin and is implicated in limb girdle muscular dystrophy type 2A (Yasuko *et al.*, 1998).

In the array data, *CAPN3* expression was significantly reduced in MHS- individuals compared to MHN, p=0.02 (F=4.42, df=2, 47). With age, expression of this gene is shown to increase significantly, p=0.0001 (F=11.98, df=1, 47). The combined effect of age and phenotype on expression of *CAPN3* was very highly significant, p=0.0008 (F=11.87, df=2, 47) whereby there is a clear increase in expression with age in MHN and MHS+ individuals but no increase in expression with age in MHS- individuals.

The pattern in the data here could explain the altered expression level evident in the MHS- group as this cohort is not shown to have increased expression of *CAPN3* with age, compared to both the MHS+ and MHN groups. Further analysis of this gene using TaqMan® assays on a larger sample set, will help to investigate this interaction and the potential role of this gene in MH susceptibility and ageing.

CAV1 encoding for Caveolin 1 was also identified by the DAVID gene ontogeny (Table 3.7). It showed significantly decreased expression with increasing age, p<0.001 (F=10.89, df=1, 47). Caveolin is the main constituent of caveolae which are responsible for a number of cellular functions such as vesicular transport and

cholesterol and calcium homeostasis (Mougeolle *et al.*, 2015). These structures also constitute a plasma membrane reservoir that is activated under conditions of mechanical stress (Sinha *et al.*, 2011). In skeletal muscle, they are specifically involved in maintaining the contractile unit of differentiated muscle and also the differentiation of myogenic regenerative cells. High oxidative stress results in rapid degradation of Caveolin 1 in proliferative mouse myoblasts, leading to impairment of endocytosis and a reduction in the ability to adapt to mechanical stress (Mougeolle *et al.*, 2015). The reduction in expression of *CAV1* with increasing age could be a reflection of increased oxidative stress in skeletal muscle that has been indicated in impaired caveolae function. However additional experiments such as western blot analysis of Caveolin 1 content of skeletal muscle in addition to measurement of oxidative stress in older versus younger muscle would be required to support this result.

Another gene implicated in the DAVID analysis was *KCNA1*, which codes for a potassium voltage-gated channel. This gene is involved in the regulation of muscle contraction at the neurological level and is implicated in episodic ataxia and myokymia (D'Adamo *et al.*, 1999). In the muscle samples examined using Affymetrix whole genome arrays, expression of *KCNA1* was found to differ significantly according to the age-phenotype interaction, $p < 0.01$ (F=8.91, df=2, 47). Specifically, it decreased with increasing age in the MHN and MHS+ groups but increased with increasing age in the MHS- group. This age-phenotype effect on expression suggests that it may be a potential GOI in relation to MH phenotype and muscle ageing and worthy of follow-up using TaqMan® gene expression assays.

3.3.5 TaqMan® assay results

A total of 22 genes were selected for TaqMan® assay validation, the results of which

are summarized in table 3.8.

Table 3.8 Summary of results from TaqMan® assays on selected GOIs

Gene	Sex effect	Phenotype effect*	Age effect	Interactions
UNC13	⇑in males	None	⇑with ⇑ age	Age+Sex Greater ⇑males with ⇑age
JUN	None	None	None	Age+Sex ⇑females with ⇑age ⇓males with ⇑age
CAV1	None	⇓in MHS-	None	None
DTNA	None	⇓in MHS-[#]	None	None
SNTB1	None	None	None	Age+Sex ⇑females with ⇑age ⇓males with ⇑age Age+Phenotype ⇑MHS+ with ⇑age ⇓MHS- with ⇑age
CAPN3	None	⇑in MHS+	⇑with ⇑ age	None
ACTB	None	None	None	None
KCNA1	None	None	None	None
CHERP	None	None	None	None
CALM1	None	None	None	None
CASQ1	⇑in males	None	⇓with ⇑ age	Sex+Phenotype ⇓female MHN
ORAI1	None	None	⇓with ⇑ age	None
STIM1	None	⇑in MHS-	None	Age+Sex ⇑females with ⇑age ⇓males with ⇑age
TRPC3	⇑females	⇓in MHS	None	None
TRPC6	⇑females	⇓in MHS	None	None
PDE1A	None	⇓in MHS-	None	None
HSPA4	None	None	None	Age+Sex ⇑females with ⇑age ⇓males with ⇑age
NFKB1	None	None	None	None
MCU	None	None	⇓with ⇑ age	None
MICU1	None	None	⇑with ⇑ age	None
SLC25A37	None	⇓in MHS-	None	None
RAD	None	None	⇓with ⇑ age	None
REM2	None	None	None	None

*Defined as comparison with MHN unless specified otherwise

UNC13C, while not involved in calcium handling, or even directly involved in skeletal

muscle function, was identified as the highest ranked gene in the list of important

probesets in relation to age and MH phenotype in the Affymetrix data (according to

AIC model comparison). This gene plays a role in neurotransmitter release by acting in synaptic vesicle priming prior to vesicle fusion as well as engaging in the activity-depending refilling of readily releasable vesicle pool. In addition, it has been implicated in Amyotrophic Lateral Sclerosis (ALS), a fatal disease characterised by age-related motor neurone degeneration and muscle wasting (Kwee *et al.*, 2012). It therefore represents a key component of the neurological control element of skeletal muscle function.

There was found to be a significant difference between males and females for expression of this gene (p=0.003, F=9.55, df=1, 89), with significantly higher levels shown in males. Expression of *UNC13C* was found to differ significantly with age (p<0.001, F=34.63, df=1, 89). Specifically, expression of *UNC13C* increased with increasing age. In addition, when considering the interaction between age and sex, it was clear that there was a significant difference between males and females with respect to age for expression of UNC13C (p=0.04, F=4.18, df=1, 89).

Alterations in the *C. elegans* version of this gene (*unc-13)* have been shown to alter lifespan of worms, indicating the importance of synaptic transmission in the control of the animal's lifespan machinery (Shen *et al.*, 2007). Alterations in expression of this gene in human ageing could have an impact on the efficacy of synaptic transmission, and provide a potential insight into the underlying mechanisms of muscle ageing in humans.

Expression of *JUN* in the TaqMan® muscle samples was found to differ significantly according to the interaction between sex and age, p=0.05 (F value=2.87, df=1, 98).

Across the span of ages, the overall expression of this gene in male samples decreases, whereas in female samples expression increases. This result is evidently different from the expression profile outlined in the Affymetrix data that previously highlighted this gene as being of interest in relation the MH phenotype and age (Figure 3.4 and Figure 3.9). There is still an age effect but in this cohort of samples it appears to also be related to gender differences in expression. These gender differences are only evident in conjunction with age, suggesting age-related, sex-specific changes in expression of *JUN* in skeletal muscle. It could be of importance in explaining the alteration in skeletal muscle that appears to be more related to gender differences compared to overall structural and functional compromises.

CAV1 expression was significantly lower in the MHS- samples compared to the MHS+ in the TaqMan® assays, p=0.05 (Tukey test). The level of expression in MHS samples when the MHS+ and MHS- groups are combine is not shown to be significantly different from MHN samples. There is also no significant difference in expression between MHN and either of the MHS groupings when they are considered separately. However, the evidence of significantly lower expression in the MHS- group compared to MHS+ samples, suggests that expression of this gene could be related to manifestation of MH episodes in the absence of causative *RYR1* variants. This claim would have to be followed up with functional analysis and determination of the altered gene expression consequences at the protein level.

In the Affymetrix array data, expression of this gene was found to decrease with increasing age, however this was not supported in the samples tested using TaqMan® assays for the same gene. Expression of *DTNA* was also significantly reduced in MHS-

samples compared to MHS+ samples, p=0.002 (Tukey test). This expression pattern is similar to that of *CAV1*, though *DTNA* is expressed at a lower level. This reduction in expression in the MHS- group was also observed in the Affymetrix cohort. However, the additional reduction in expression with age shown in the Affymetrix data set was not seen in the TaqMan® assays. This could be attributed to the increased sample size in the TaqMan® cohort, with the greater range of ages actually reducing the age effect that was observed previously. This gene has been shown to have a role in other muscular dystrophies. The results here indicate a potential role for *DTNA* in the manifestation of the MHS phenotype in individuals lacking a causative mutation in *RYR1*.

Expression of *STNB1* was found to differ significantly according to the age-sex, p=0.02 (F=3.67, df=1, 98) and age-MH phenotype interaction, p=0.009 (F=8.51, df=2, 98). Overall expression of this gene was detected at a low level, especially compared to the levels identified in the Affymetrix arrays. This could be related to the sensitivity of the TaqMan® assay compared to the Affymetrix array being reduced.

SNTB1, along with *DNTA*, is an important component of the dystrobrevin glycoprotein complex. Alteration of this complex is implicated in Duchenne Muscular Dystrophy (DMD). It appears from the results of this analysis that *STNB1* may also have a role in ageing and MH.

Expression of *CAPN3* was significantly elevated in MHS+ samples compared to MHN, p=0.018 (F=2.98, df=2, 98). There was also shown to be a significant increase in expression with age, p=0.011 (F=4.31, df=1, 98).

This gene has been implicated in the neuromuscular disorder calpainopathy, which is autosomal recessive (Yasuko *et al.*, 1998; Burke *et al.*, 2010; Liewluck & Goodman, 2012). Patients with calpainopathy typically exhibit the first symptoms during childhood and are wheelchair bound by their early 40s (Burke *et al.*, 2010). It is apparent from these results that expression differences of this gene may be implicated in the manifestation of MH and distinctly in the process of skeletal muscle ageing.

ACTB expression was also investigated using TaqMan® assays on the 108 skeletal muscle cDNA samples identified for this process. In the Affymetrix data, this gene was found to have decreased expression in both MHS+ and MHS- groups, however in this data there was no significant difference found in expression of this gene between the different MH phenotype groups, nor for sex, age or any combination of the factors.

Expression of *KCNA1* determined using TaqMan® was not found to differ significantly according to any of the variables examined. This is in contrast to the result from the Affymetrix data where a significant effect of age-MH phenotype was found.

Additional cohorts of genes were investigated using TaqMan® assays. Impaired calcium handling in skeletal muscle is of relevance to muscle ageing (Weisleder *et al.*, 2006; Zhao *et al.*, 2008) as well as the pathophysiology of MH (Duke *et al.*, 2010) and other myopathies related to *RYR1* mutations (Dirksen & Avila, 2004).

CHERP encodes the calcium homeostasis endoplasmic reticulum protein and is identified as a potential gene of interest based on its interaction with *RYR1* (Ryan *et al.*, 2011). It has also been indicated to play a role in ageing (Puzianowska-Kuznicka

151

& Kuznicki, 2009) therefore it was considered to be of potential interest in relation to skeletal muscle ageing and MH. *CALM1* encodes the protein calmodulin that has a high affinity for calcium and is involved in signal transduction and the synthesis and release of neurotransmitters. It was also highlighted in the Affymetrix data analysis as having significantly increased expression with age and significantly lower expression in MHS patient muscle samples compared to MHNs. However, in the cohort analysed using TaqMan® gene expression assays no significant difference was found in expression of either *CHERP* or *CALM1* for age or MH status or the combined effect of these variables. This could be due to the use of a different cohort of samples. The TaqMan® assays were performed on a much larger sample set (n=108), almost double that used in the Affymetrix arrays on skeletal muscle (n=59).

CASQ1 is a gene of interest identified by the Leeds MH unit. It encodes calsequestrin which is involved in the process of excitation-contraction coupling in skeletal muscle (see 1.1.2 for full details) (Beard *et al.*, 2004). Differences in expression levels of this gene with age could provide some insight into the mechanisms affecting EC-coupling in ageing. Expression levels of *CASQ1* was found to differ significantly between males and females, $p=0.003$ ($F=9.06$, $df=1, 95$).

No significant difference was found between the mean expression levels in each group of MH phenotype however, following simplification of the linear model (simplified model: Expression~Age+Sex+Status+Sex:Status) and ANOVA on the simplified model, there was found to be a significant difference in expression levels of *CASQ1* when considering interaction between sex and MH status, $p=0.043$ ($F=3.24$, $df=2$,

100). This gene was found to differ significantly according to age (p=0.01, F=6.28, df=1, 100) with expression levels decreasing with increasing age.

Calsequestrin is responsible for binding to calcium in the SR and therefore is inherently related to the level of calcium available for muscle contraction. Earlier work using mouse models for muscle ageing did not identify altered expression levels of *CASQ1* in relation to age (Narayanan *et al.*, 1996). However, more recent proteomic analysis of mouse muscle has shown differential expression of calsequestrin in aged mice, suggesting a potential role in muscle ageing (Hwang *et al.*, 2014). This indicates that there is a clear conflict in the literature regarding the role of this gene in muscle ageing and this result could form the foundation for more investigation into its part in this process.

STIM1 encodes stromal interactin molecule 1 (Jungbluth *et al.*, 2004). It acts as a calcium sensor in the SR, upon detecting a decrease in calcium concentration is activates Orai1 calcium channels in the plasma membrane, to increase intracellular calcium concentration. This process is termed 'store-operated calcium entry' (SOCE) and is described in detail in section 1.1.4. It has been suggested that SOCE limits fatigue in aged skeletal muscle fibres and in addition, increased SOCE has been proposed as contributing towards Ca^{2+} dysregulation in MH (Lyfenko & Dirksen, 2008). Based on its involvement in SOCE *ORAI1* (encoding for Orai1 calcium channels) was also identified as a potential gene of interest. *TRPC3* and *TRPC6* encode transient receptor potential cation channel subfamily 3 and 6 respectively. They also play a role in calcium handling in skeletal muscle. They are involved in 'receptor-

operated calcium entry' (ROCE) and have been found to interact with STIM1 (Horinouchi *et al.*, 2012).

ORAI1 expression levels were also found to differ significantly with Age (p<0.001, F=16.02, df=1, 100). As age increases, expression levels of this gene are shown to decrease. There was no significant difference in expression levels between males and females, or between individuals with different MH phenotypes.

STIM1 expression was found to differ significantly between individuals of different MH Status, p=0.049 (F=4.39, df=2, 100). There is increased expression of this gene in the MHS- group compared with MHN. This suggested the potential role for this gene in the manifestation of MH, particularly in individuals that do not exhibit a variant in *RYR1* that is causative of the condition. Expression of *STIM1* also differed according to the age-MH status interaction, p=0.018 (F=4.79, df=2, 100), with evidence of a slight increase in expression with age in MHN samples, compared to a clear decrease in expression in both MHS+ and MHS- samples.

Expression of *TRPC3* was found to differ significantly between males and females (p=0.029, F=4.38, df=1, 100), with increased expression in females. There was no significant difference found in expression level of *TRPC3* according to age of the patients tested. *TRPC3* expression was found to differ significantly according to MH status, p=<0.001(F=9.87, df=2, 100).

There is greater expression of this gene in the MHN group, compared with MHScombined and MHS- groups. The lowest mean expression levels are

demonstrated in the MHS- group and were significantly lower than the level found in the MHS+ group. This indicates the potential value of this gene as being involved in MH, particularly in individuals lacking a causative variant in *RYR1*. Additional work to investigate the potential consequences of this altered expression profile would be required to support this. Expression levels of *TRPC6* were found to differ significantly according to sex, $p=0.043$ ($F=4.31$, $df=1, 100$).

PDE1A expression in MHS- skeletal muscle was significantly lower than expression in MHN muscle, $p=0.03$ ($F=3.89$, $df=2, 95$) but no difference in expression in MHS+ muscle. A similar pattern of expression of this gene was observed in the Affymetrix samples, though the results showed greater significance. There is potential for this gene to be involved in the pathophysiology of MH, specifically with regards to those individuals that test positive in the IVCT but do not carry a causative *RYR1* variant.

HSPA4 (also named HSP70) encodes heat shock 70kDa protein 4. The ability of cells to induce heat shock proteins is found to be reduced in aged individuals (Boncompagni *et al.*, 2009). This heat shock protein belongs to heat shock protein (HSP) family A, a family that has been identified as having a possible role in ageing of skeletal muscle (Broome *et al.*, 2006). This study specifically focused on the reduced capacity for aged mice to produce HSPs in response to stress. It was also indicated that old wild type mice became unable to activate nuclear factor kappa B (NF-κB encoded by *NFKB1*) after contractions, compared to adult wild type mice (Broome *et al.*, 2006). In humans, one study has shown that protein concentrations of NF-κB is fourfold higher in elderly muscle compared to young muscle (Cuthbertson *et al.*, 2005). Despite this observation

155

there has been no investigation of the exact mechanism of how NF-κB might be involved in ageing muscle (Mourkioti & Rosenthal, 2008).

Expression of *NFKB1* was not found to differ significantly according to age, sex, MH phenotype or any interaction between these factors. Expression of *HSPA4* was found to differ significantly according to an interaction between age and sex, $p<0.05$ (F=3.57, df=1, 95).

In males, expression of this gene decreases with age, whereas in female samples expression appears to slightly increase. No alteration in expression was detected between MHN and MHS groups. Up regulation of *HSPA4* is part of a highly coordinated stress response that limits the stress induced rate of cellular degeneration and as a result prevents muscular atrophy (Chung & Ng, 2006). Impairment of this response it thought to be involved in age-related contractile deficits (McArdle *et al.*, 2004). Indeed, mice that overexpress *HSPA4* are partly protected from fibre degeneration (Broome *et al.*, 2006). The pattern observed in the male samples indicates that decreased expression of *HSPA4* is evident in individuals of increased age, suggesting that in older muscle there is impairment of the stress response that mediates muscle atrophy. However, this profile is not observed in the female samples indicating there may be sex specific differences in muscle ageing relative to the stress response.

EC coupling at calcium release units (CRUs) is essential for skeletal muscle function. Impaired EC coupling in aged skeletal muscle leads to a reduced supply of calcium ions available for the contractile elements and results in reduced specific force during

contraction (Delbono *et al.*, 1995). Alteration in mitochondrial structure, function and number are implicated in muscle ageing (Trounce *et al.*, 1989; Shigenaga *et al.*, 1994; Balaban *et al.*, 2005; Peterson *et al.*, 2012). These types of deficits are also observed in murine models of MH, with Y522S mice exhibiting swollen and misshapen mitochondria (Durham *et al.*, 2008) and evidence of compromised oxidative phosphorylation in R163C mice mitochondria (Giulivi *et al.*, 2011).

CRUs and mitochondria are functionally linked *via* Ca^{2+} and reactive oxygen species (ROS) (Rossi *et al.*, 2009; Eisner *et al.*, 2013). This is demonstrated by the uptake of a small fraction of Ca^{2+} ions, released during EC coupling, into the mitochondrial matrix (Baughman *et al.*, 2011). Three genes, two involved in mitochondrial calcium handling (*MCU* and *MICU1*) and one (*SLC25A37*) involved in oxidative phosphorylation were identified for investigation using TaqMan® assays.

MCU encodes the mitochondrial calcium uniporter. *MICU1* encodes mitochondrial calcium uptake protein 1. It is a key regulator of the mitochondrial calcium uniporter which acts to inhibit calcium uptake when the concentration of calcium in the cytoplasm is low (Csordas *et al.*, 2013). It has been identified as a potential gene of interest bases on its role in the mitochondria and how this may be affected with age (Pietrangelo *et al.*, 2015). Mutations in *MICU1* are implicated in a muscle disorder lined to impaired mitochondrial calcium signalling (Logan *et al.*, 2014). Expression of *MCU* was found to significantly increase with increasing age, $p < 0.001$ (F=11.87, df=1, 95).

Expression levels of *MICU1* were found to differ significantly according to age (p=0.001, F value=9.56, df=1, 100). As age increases there is a decrease in expression of this gene. There was no significant difference detected between individuals of different MH status or between males and females for either *MCU* or *MICU1* expression.

Handling of calcium by mitochondria is crucial to effective mitochondrial function. It has been shown that excessive calcium levels can be damaging to mitochondria and lead to mitochondrial fragmentation (Finkel *et al.*, 2015). Overexpression of *MCU* has recently been shown to protect against denervation-induced muscle atrophy, indicating that modulation of mitochondrial calcium uptake may be a means to preventing loss of muscle mass (Mammucari *et al.*, 2015). The increased expression of this gene found here could be the result of an increased age-related demand, coupled with the decreased expression of *MICU1* and may show that regulation of this complex is deteriorating with age despite increased expression of the gene itself. A better understanding of the exact mechanism would require more experiments at the protein level to determine if the increased gene expression translates to increased protein expression, to ascertain the impact of this altered gene expression on muscle ageing.

Expression of SLC25A37 was significantly lower in MHS- individuals compared to MHN and MHS+ (p<0.01, F=8.71, df=2, 95). When the MHS cohort was combined, no significant difference is observed.

Impaired EC coupling has been associated with the age related reduction in the number of L-type channels in the muscle cell plasma membrane (Wang *et al.*, 2000). A

potential link between compromised EC coupling and oxidative stress (an age-dependent cellular signal) is the RGK family of G proteins, including Rad and Rem2, because Rad expression is increased in response to oxidative stress in skeletal muscle and over-expression of Rem imitates excitation contraction uncoupling (Sumner *et al.*, 2013). More recent work has identified that members of the RGK family inhibit L-type calcium channels, with Rad doing so *via* voltage-sensor limitation and Rem supporting inhibition through a mechanism that allows for translocation of $Ca_v1.1$'s voltage sensors (Beqollari *et al.*, 2014). *RAD* and *REM2*, two of the genes from the RGK family were chosen for investigation using TaqMan®. Expression levels of *RAD* were found to differ significantly according to MH status, $p=0.007$ ($F=6.98$, $df=2, 95$). Expression of *RAD* was also found to differ significantly with age, $p=0.004$ ($F=4.86$, $df=1, 95$), with an apparent decrease in expression of the gene with increasing age. Expression of *REM2* in this cohort was not found to be significantly different for any of the factors considered in the analysis.

These results highlight that the significant difference is found when comparing the MHS- group to the MHN and MHS+ groups, $p<0.05$ for both comparisons. This result is indicative of the genetic complexity associated with MH. For expression levels of this gene to differ so significantly between the MHS+ and MHS- groups, suggests that there might be other genetic factors involved in the manifestation of the condition.

Expression of *RAD* is significantly reduced in the MHS- cohort. As increased expression of this gene is shown to be related to oxidative stress, it could be the case that oxidative stress is less of a feature in individuals susceptible to MH but with no mutation in RyR1.

159

3.3.6 Summary discussion of gene expression in skeletal muscle in the context of ageing and MH phenotype

Affymetrix data was analysed to devise a list of genes of interest in relation to MH status and age in skeletal muscle. These genes were also analysed using TaqMan® assays in order to validate the result from the array data (Table 3.9).

Table 3.9 Summary of results from Affymetrix array data on GOIs

Gene	Sex effect	Phenotype effect*	Age effect	Interactions
UNC13	⇑ in males	None	⇓ with ⇑ age	None
JUN	None	⇓in MHS+	⇓ with ⇑ age	Age:Phenotype No ⇓ with ⇑ age in MHS-
CALM1	None	None	⇑ with ⇑ age	None
ACTB	None	⇓in MHS+ and MHS-	None	None
DTNA	None	⇓in MHS – compared to MHS+	⇑ with ⇑ age	Age:Phenotype No ⇑ with ⇑ age in MHS-
SNTB1	None	None	⇑ with ⇑ age	Age:Phenotype No ⇑ with ⇑ age in MHS-
CAPN3	None	⇓in MHS-	⇑ with ⇑ age	Age:Phenotype No ⇑ with ⇑ age in MHS-
CAV1	None	None	⇓ with ⇑ age	None
KCNA1	None	None	None	Age:Phenotype ⇑ with ⇑ age in MHS-

*Defined as comparison with MHN unless specified otherwise. Green shading denotes where TaqMan® result was consistent with result from Array data, red shading denotes where TaqMan® result was not consistent with Array data.

It is clear that not all results were confirmed by the TaqMan® validation. This could suggest that the method of selecting the genes of interest from the array data was not ideally suited to this process. The gene that showed the most consistent results when validated using TaqMan® was *UNC13*. This gene was ranked as having the largest AIC difference (ΔAIC -49) in the model comparison, indicating that it may have been better to choose a larger AIC cut off than -10 to avoid falsely including genes that were showing age-phenotype expression differences.

Only two pathways of the 881 identified from the list of genes defined as being important in relation to MH phenotype were comprehensively interrogated in this chapter. The Affymetrix data represents a wealth of information and could be analysed further to explore additional genes of interest with a specific focus on MH. One avenue that has not been explored in the analysis of the array data is network analysis (Schäfer & Strimmer, 2005; Lowes *et al.*, 2017). This would involve quantitative modelling of the direct interactions between genes, and has the potential to highlight a number of different features such as sub-groups, interrelated groups and the density (the extent of the connections within the group) of the gene network (Nair *et al.*, 2014). This method would be valuable for exploring other aspects of genetic complexity that are associated with MH susceptibility, such as relationships between genes responsible for calcium handling in skeletal muscle, rather than simply examining them in isolation.

Many of the major differences in gene expression in the groups with different MH phenotypes were related to differences in expression between the MHS+ and MHS- groups. The distinction between MHS+ and MHS- is specifically related to whether (MHS+) or not (MHS-) a causative, diagnostic variant in *RYR1* has been identified. The process of determining presence of an *RYR1* variant has been augmented over the course of this project and since many of the samples were identified. Initially, the process involved determining whether an individual was from a family carrying a diagnostic variant in *RYR1* and subsequently screening for that variant. Samples with no family history of a diagnostic variant were also sequenced for a panel of diagnostic variants (varying between 5 and 13 depending on sample and timing). More recently samples with no detected diagnostic variant are sent for next generation sequencing of

RYR1 and *CACNA1S* and for research purposes samples are also processed using Haloplex to determine novel variants in a panel of 50 candidate genes including *RYR1* and *CACNA1S*. It is possible that with further characterisation of *RYR1* variants that the classification used here may no longer be of value or meaningful.

The MHS- samples in the Affymetrix data (n=18) were identified and processed in 2007. Five have family members with the 7300G>A variant (the most common associated with MH in the UK population) but in these individuals that variant was not found. Three have none of the diagnostic *RYR1* variants and have since been screened using Haloplex. The remaining (n=10) are from families with no causative variant, three are from families with a non-functionally characterised *RYR1* variant that was not identified and the remaining seven are from families with no variant in *RYR1* detected through sequencing of the gene.

Of the MHS- samples in the TaqMan® data (n=22), 13 are from families with no causative variant that have been screened for the diagnostic *RYR1* mutations with no further follow up. Three have been assigned to screening with Haloplex and have, since this project started, had uncharacterised novel variants identified in *CACNA1S*. The remaining six samples have had *RYR1* and *CACNA1S* screened using NGS with no variants in either gene found. It is clear that the MHS- category is somewhat arbitrary due to the underlying genetic complexity of the samples. Despite no evidence of a diagnostic variant, it is possible that many have another, as yet uncharacterised variant that may be causative of MH. It is also important to acknowledge the genetic complexity of the MHS+ category. Despite all exhibiting a diagnostic *RYR1* variant, these have been shown to have a range of reaction severities in the IVCT (Carpenter

et al., 2009b). It could be argued that individuals with different variants may exhibit different expression profiles. An ideal experiment would utilise a specific variant in *RYR1* that is known to be causative of MH and this serve as the basis for comparison with a group that definitively does not have that variant or any others, providing a scenario whereby the variables for all other variants are controlled.

The methods used in this chapter represent only a small number of ways to investigate differential gene expression in skeletal muscle. The Affymetrix data was obtained in 2008, with more recent developments in next-generation sequencing, RNA-Seq is perhaps a more exhaustive means of investigating differential expression. This technique uses largely the same sample preparation methods as Affymetrix arrays, however also provides the full sequence information for the samples processed. This would enable investigation of novel variants alongside differential gene expression.

4 Basal oxidative phosphorylation and expression of genes implicated in mitochondrial dysfunction in malignant hyperthermia and in the context of ageing

4.1 Introduction

Normal skeletal muscle contraction is dependent on calcium and ATP and is therefore reliant on effective function of calcium channels and their associated proteins as well as mitochondria. This chapter focuses on the role of mitochondria in ageing and *RYR1* related myopathies. It will also examine changes in expression levels of genes involved in mitochondrial dysfunction that have been implicated in human ageing.

4.1.1 Mitochondrial energy metabolism

Mitochondria are the cellular powerhouse, responsible for the producing the majority of ATP required to drive cellular functions that require energy. In skeletal muscle these functions include EC coupling and subsequently cross-bridge cycling (summarised in detail in chapter 1.1) and active calcium transport (Pietrangelo *et al.*, 2015). When EC coupling is impaired (a feature of aged and myopathic muscle) there is reduction in the supply of calcium ions to the skeletal muscle contractile apparatus, resulting in reduced specific force (Delbono *et al.*, 1995).

Oxidative phosphorylation (OXPHOS) is the pathway through which mitochondria generate ATP and is reliant upon the electron transport chain (ETC) (Bratic & Trifunovic, 2010) (). The ETC is a series of complexes (I-IV) that transfers electrons

from electron donors to electron acceptors. The complexes couple this electron transfer with the transfer of protons across the inner mitochondrial membrane. The substrates required for this process (NADH and $FADH_2$) are formed during glycolysis, fatty-acid oxidation and the citric acid cycle. These substrates donate electrons to the ETC. These functionally coupled complexes are located in the mitochondrial inner membrane (MIM). As the electrons are transferred through the ETC, protons (H^+) are driven across the MIM at three of the ETC complexes (I, III and IV) (Mailloux & Harper, 2012). This proton flux generates kinetic energy that is harnessed by complex V, driving the generation of ATP.
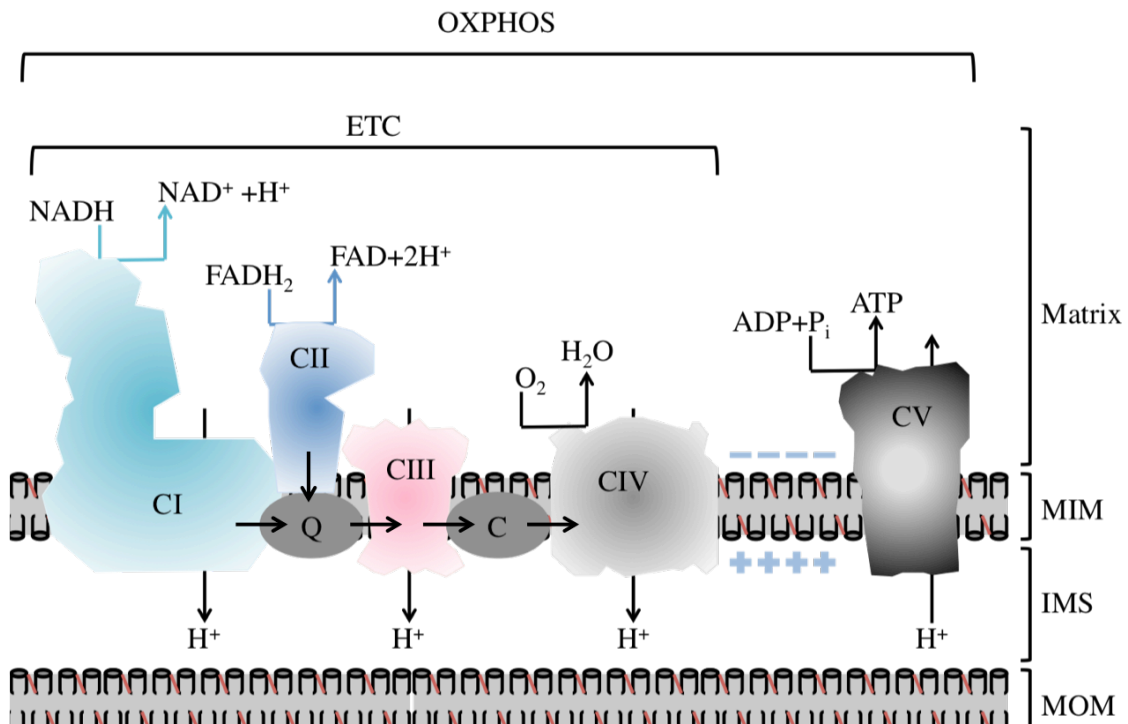
Figure 4.1 Schematic of mitochondrial oxidative phosphorylation (OXPHOS) (adapted from, Koopman *et al.*, 2013). Five multi-subunit complexes comprise OXPHOS system residing in the mitochondrial inner membrane (MIM): Complex I-NADH dehydrogenase, Complex II-Succinate dehydrogenase, Complex III-cytochrome C reductase, Complex IV- cytochrome C oxidase and Complex V-ATP synthase. Complex I and Complex II oxidise NADH and FAH_2 respectively. Electrons are derived from oxidation of these compounds and transported to the Q junction (electron carrier Q_{10}). Electrons are transported from Complex III *via* cytochrome-C. Complexes I-IV make up the electron transport chain (ETC). The energy derived from the flow of electrons through the ETC establishes an electrochemical gradient *via* the efflux of H^+ ions from the matrix across the MIM into the inter membrane space (IMS)(occurring at Complex 1, III and IV). Flow of H^+ ions back into the matrix is coupled to ATP generation by Complex V, each ATP molecule produced requires the Complex V mediated backflow of 2.7 H^+ ions (Watt *et al.*, 2010).

Complex I oxidises NADH. NADH is produced through the tricarboxylic cycle, decarboxylation of pyruvate and β-oxidation of fatty acids. Through this oxidation rection electrons are donated to Co-enzyme Q_{10} ($CoQ_{10,}$) (shown in Figure 4.1 as 'Q'). This complex is the largest in the ETC, initially appearing to consist of 45 subunits (Carroll *et al.*, 2006) though more recently it has been proposed that one of the subunits (NDUFA4) actually appears to be a component of complex IV (Balsa *et al.*, 2012). It is organised into a lipophilic arm, embedded in the MIM, and a hydrophilic arm that protrudes into the matrix, resulting in an L-shaped structure (Clason *et al.*, 2010). Complex II (succinate dehydrogenase), like Complex I, has a region that protrudes into the matrix that oxidises $FADH_2$, transferring the released electrons to CoQ_{10}, and a region embedded in the MIM that catalyses succinate into fumarate (Brière *et al.*, 2005). CoQ_{10} can receive electrons donated by other enzymes (Koopman *et al.*, 2010).

The convergent electron flux through complex I and complex II is received by complex III (Cytochrome C reductase) *via* CoQ_{10}. Cytochrome C (shown as 'C' in Figure 4.1) transfers electrons from complex III to complex IV (cytochrome C oxidase) where the electrons are donated to O_2 to form H_2O. Approximately 95% of inspired oxygen in humans is consumed by complex IV (Ferguson-Miller *et al.*, 2012). At complexes I, III and IV the energy released by the electron transport drives the efflux of protons (H^+) through the MIM, resulting in a trans-MIM proton motive force consisting of an electric charge and pH difference across the MIM (Mailloux & Harper, 2012, Figure 4.1). This energy is coupled to the formation of ATP from ADP and inorganic phosphate (P_i) at complex V (ATP synthase). Complex V is a molecular machine consisting of two components, one that can utilise the proton motive force to

generate ATP and one that can use ATP to fuel the transport H$^+$ across the MIM (Okuno *et al.*, 2011; Watanabe *et al.*, 2011).

4.1.2   Alterations in mitochondrial content and function

The pathophysiology of MH is notably complex in a manner that is also evident in skeletal muscle ageing. Alterations and abnormalities in the mitochondria of skeletal muscle may provide insight into these complexities.

Mitochondria in healthy skeletal muscle exist as two distinct subpopulations, one localised within a few microns of the plasma membrane (subsarcolemmal) and the other found within the myofibril distributed along the contractile proteins (Lanza & Nair, 2010). The ability to sustain muscular work during contraction is directly related to the volume and density of the mitochondria (Chance *et al.*, 1985). Mitochondrial content has been shown to decrease with age (Conley *et al.*, 2000; Welle *et al.*, 2003; Menshikova *et al.*, 2006), and it is posited that this reduction holds partial responsibility for the age-related declines in skeletal muscle function.

Altered mitochondrial content is also a feature of certain myopathies associated with *RYR1* variants, such as central core disease. CCD is characterised histologically by regions of muscle fibres that lack mitochondria (Dubowitz & Pearse, 1960). Knocking out calsequestrin in mice has also shown that this causes core formation with a similar presentation to those shown in CCD (Paolini *et al.*, 2015). It is also important to note that in the calsequestrin null mice, the cores were primarily observed in old mice (14-27 months) and more rarely seen in age-matched WT mice (Paolini *et al.*, 2015). Cores are a feature of skeletal muscle from individuals expressing the Y522S mutation in

RYR1 that is implicated in MH and CCD (Chelu *et al.*, 2006). These cores are a striking feature of some, but not all MH-inducing mutations, begging the question of why this discrepancy? It has been proposed that the cores may be the result of chronically elevated calcium resulting in damage to the mitochondria (MacLennan & Zvaritch, 2011) or potentially caused by increased oxidative/nitrosative stress by reactive oxygen and nitrogen species (Durham *et al.*, 2008; Lanner *et al.*, 2012; Manno *et al.*, 2013).

Cores are notably not present in all myopathic muscle or indeed in all aged muscle, therefore other factors altering mitochondrial function must be investigated. It was first suggested in 1971 that the uncoupling of OXPHOS could aid in explaining the metabolic disturbances observed in MH (Wilson *et al.*, 1971). This has since been demonstrated in the R163C mouse model, reporting altered bioenergetics in skeletal muscle from these rodents under normal conditions (Giulivi *et al.*, 2011). Maximal respiratory capacity has shown to be compromised in T4826I mice (Yuen *et al.*, 2012). These models have not been examined in the context of ageing. There have been some rodent studies simply examining age-related uncoupling of OXPHOS, though the results are contradictory. Some have demonstrated increased mitochondrial efficiency with age (Iossa *et al.*, 2004), whereas others show reduced coupling in aged mice using an *in vivo* approach (Marcinek *et al.*, 2005). Data for human tissue OXPHOS and ageing is limited (Peterson *et al.*, 2012), studies have shown that ATP turnover is lower in elderly compared to young adults (Johannsen *et al.*, 2012) supporting earlier work indicating uncoupling of mitochondrial function with age (Amara *et al.*, 2007).

There is clearly a picture of potential similarities between the basal metabolic rates of myopathic and aged muscle with respect to mitochondrial function. Further investigation is needed to better understand these aspects and how they may interact. This chapter aims to investigate the potential for compromised OXPHOS capacity in MH skeletal muscle, in the context of age, MH status and sex. Additionally, age-related changes in gene expression will be considered using a panel of genes implicated in mitochondrial dysfunction and ageing.

4.2   Materials and Methods

4.2.1   Sample information

Excess tissue from patient muscle biopsies from the IVCT was subjected to high-resolution respirometry (HRR) to evaluate oxidative phosphorylation capacity. The samples comprise a ~5cm long by 1cm wide by 0.5cm thick section of *vastus medialis* muscle obtained from a patient under local anaesthesia by a member of the MH diagnostic team. The HRR titration protocol is outlined in section 4.2.3. Muscle biopsies are conducted by the Leeds MH group on a weekly basis with the typical aim of processing 3 patients each week. Of those 3 weekly patients, a total number of 90 patients had excess muscle biopsy tissue which was made available for HRR over the course of this project (Table 4.1).

Table 4.1 Sample information for muscle biopsies used in mitochondrial respirometry assays

Sex	Male	Female
MHN	18 (11-83)*	45 (12-66)*
MHS	17 (12-71)*	10 (14-46)*

*Age ranges in years are displayed in bracket

The use of excess muscle tissue is covered by the ethical approval assigned to the MH diagnostic unit and all patients have the option to opt-out of their muscle biopsy material being used for additional scientific research (Appendices A and B).

The first 30 samples were processed using a simplified version of the HRR protocol, where complex IV activity was not quantified. This only permits for normalisation using the flux control ratio (full details in 4.2.4). The remaining 60 samples were processed using the full protocol allowing for normalisation with the flux control ratio (FCR) and calculation of % maximum OXPHOS capacity. Therefore 90 samples were

170

used in the flux control ratio normalisation and 60 were used in the % maximum

OXPHOS capacity normalisation (Table 4.2).

Table 4.2 Sample information according to different normalisation processes

Normalisation	FCR		%MAX OXPHOS	
Sex	Male	Female	Male	Female
MHN	18 (11-83)*	45 (12-66)*	15 (11-83)*	28 (12-65)*
MHS	17 (12-71)*	10 (14-46)*	11 (12-71)*	6 (20-61)*

*Age ranges in years are displayed in brackets

I carried out storage and transportation of all samples. Dr John Boyle completed initial

HRR processing in 2013-2014 processing approximately 40 samples, as I was

occupied with attempts to devise muscle energetics experiments during this time. I

then took over HRR processing in 2015 and processed the remaining samples. I

completed all data handling, normalisation and statistical analysis for all the samples

processed. Data obtained by me and Dr Boyle was compared to establish any

significant differences that might be related to different experimenters but no

difference was observed. As such, the data was combined.

Tissue from patients undergoing IVCT is also routinely stored for RNA extraction by

the Leeds MH group. Additional tissue samples from patients subjected to HRR in this

chapter also underwent TaqMan® gene expression analysis (detailed in section 4.2.6).

14 samples that underwent mitochondrial HRR did not have additional muscle tissue

available for RNA extraction, therefore a subset of available samples was processed

(Table 4.3).

Table 4.3 Sample information for TaqMan® gene expression analysis.

Sex	Male	Female
MHN	15 (11-83)*	37 (12-66)*
MHS	15 (12-71)*	9 (14-46)*

*Age ranges in years are displayed in brackets

4.2.2   Sample handling and preparation

During storage and transportation, muscle samples (*vastus medialis*) were kept in 1ml

BIOPS solution (2.77mM CaK$_2$EGTA + 7.23mM K$_2$EGTA, 0.1μM free calcium,

20mM imidazole, 20mM taurine, 50mM K$^+$-MES, 0.5mM dithiothreitol, 6.56mM

MgCl$_2$, 5.77mM ATP, 15mM phosphocreatine, at pH 7.1) in a 1.5ml eppendorf tube

on ice. Dissection of the muscle sample was carried out under a light microscope at

x3 magnification, on ice in chilled BIOPS, using fine forceps. Any dead tissue

(apparent as pale in appearance, healthy muscle tissue is red) was removed along with

any non-muscle tissue (such as capillaries, connective tissue and adipose tissue)

attached to the sample. The sample was dissected until individual fibre bundles were

visible (Figure 4.2).
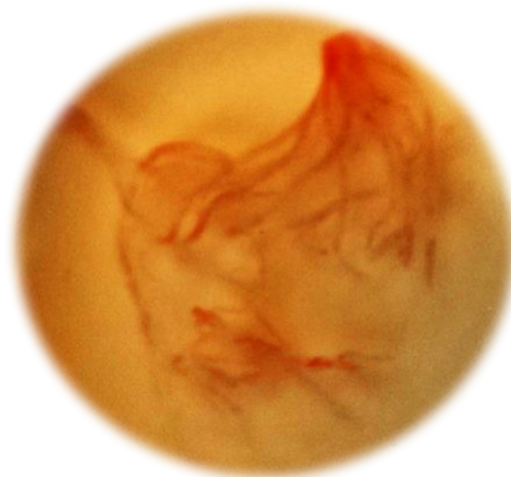
Figure 4.2 Example of dissected muscle biopsy sample showing small fibre bundles.

Following dissection, the sample was placed into 1ml fresh BIOPS in a 1.5ml

eppendorf tube and chemically permeabilised using saponin (50μg/ml). Saponin acts

as a detergent that selectively permeabilises the sarcolemma while retaining the

structural integrity of the inner and outer mitochondrial membranes as well as other

extracellular components (Figure 4.3).
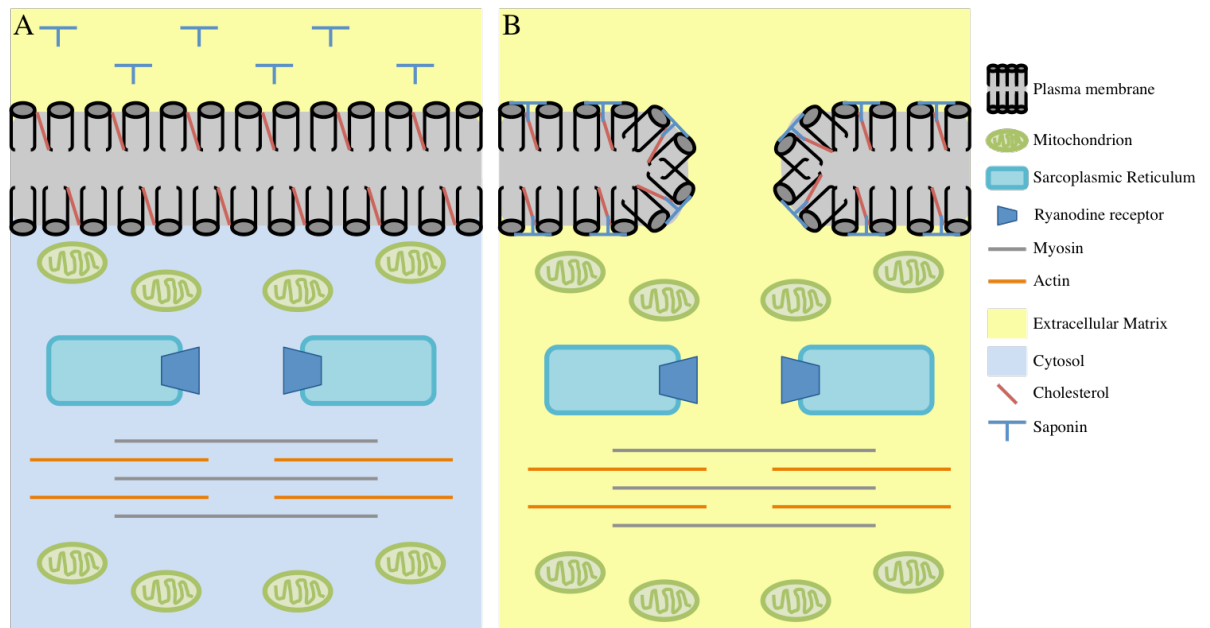
Figure 4.3 Effect of saponin on muscle tissue. A: schematic of an aspect of the muscle cell depicting the intact plasma membrane (sarcolemma) with saponin added the extracellular matrix. B: schematic of how saponin selectively binds to cholesterol in the plasma membrane creating pores that permit addition of compounds that can interact with the still intact mitochondria (adapted from, Kuznetsov *et al.*, 2008).

This makes the mitochondria accessible to subsequent titrations of exogenous components while best preserving their *in vivo* state (Kuznetsov *et al.*, 2008). Procedures that involve isolation of mitochondria have a number of disadvantages, including; requiring large quantities of cells or tissue for optimal yield (Frezza *et al.*, 2007), introducing defects in normal mitochondrial properties (Piper *et al.*, 1985) and altering normal mitochondrial interactions (Saks *et al.*, 1998; Milner *et al.*, 2000). Dissected fibre bundles were then blotted using filter paper to remove excess BIOPS and wet weight determined prior to conducting respirometry.

4.2.3   High-resolution respirometry

A high-resolution respirometer (HRR), Oxygraph-2k (Oroboros Instruments, Innsbruck, Austria) with two 2ml chambers was used (S). This permitted simultaneous duplicate measurements of the same sample. Chambers were filled with 2.2ml mitochondrial respirator media (MiRO5) (0.5mM EGTA, 3mM $MgCl_2$, 60mM K^+-lactobionate, 20mM taurine, 10mM KH_2PO_4, 20mM HEPES, 110mM sucrose, and 1g/L bovine serum albumin at pH 7.1). Calibration of respirometers with MiRO5 and at air saturation was conducted daily.

Respiratory states were induced by sequential titration of substrates, inhibitors and uncouplers to the closed chambers by Hamilton microsyringe. A Peltier temperature controller maintained chamber temperature at 37°C for the duration of experiments. Oxygen levels were maintained in the normoxic range (~150μM) by reoxygenation *via* syringe.

First, NADH-related substrates were added to stimulate complex I respiration (10mM glutamate, 1mM malate, 5mM pyruvate). After stabilisation of the O_2 flux signal, ADP (2.5mM) was added to measure ADP stimulated respiration. Then, mitochondrial membrane integrity was evaluated by the addition of cytochrome C (10μM). This action should not affect O_2 flux in undamaged mitochondria (Gnaiger, 2013). This step represents the first quality control step in the experiment. Maximal respiration with convergent flow of electrons through complex I and II was measured through addition of succinate (10mM). This was followed by addition of 1μl increments of FCCP (uncoupler of complex I and II) until no further increase in respiratory rate was observed. This process permits determination of the maximal ETC capacity in an

174
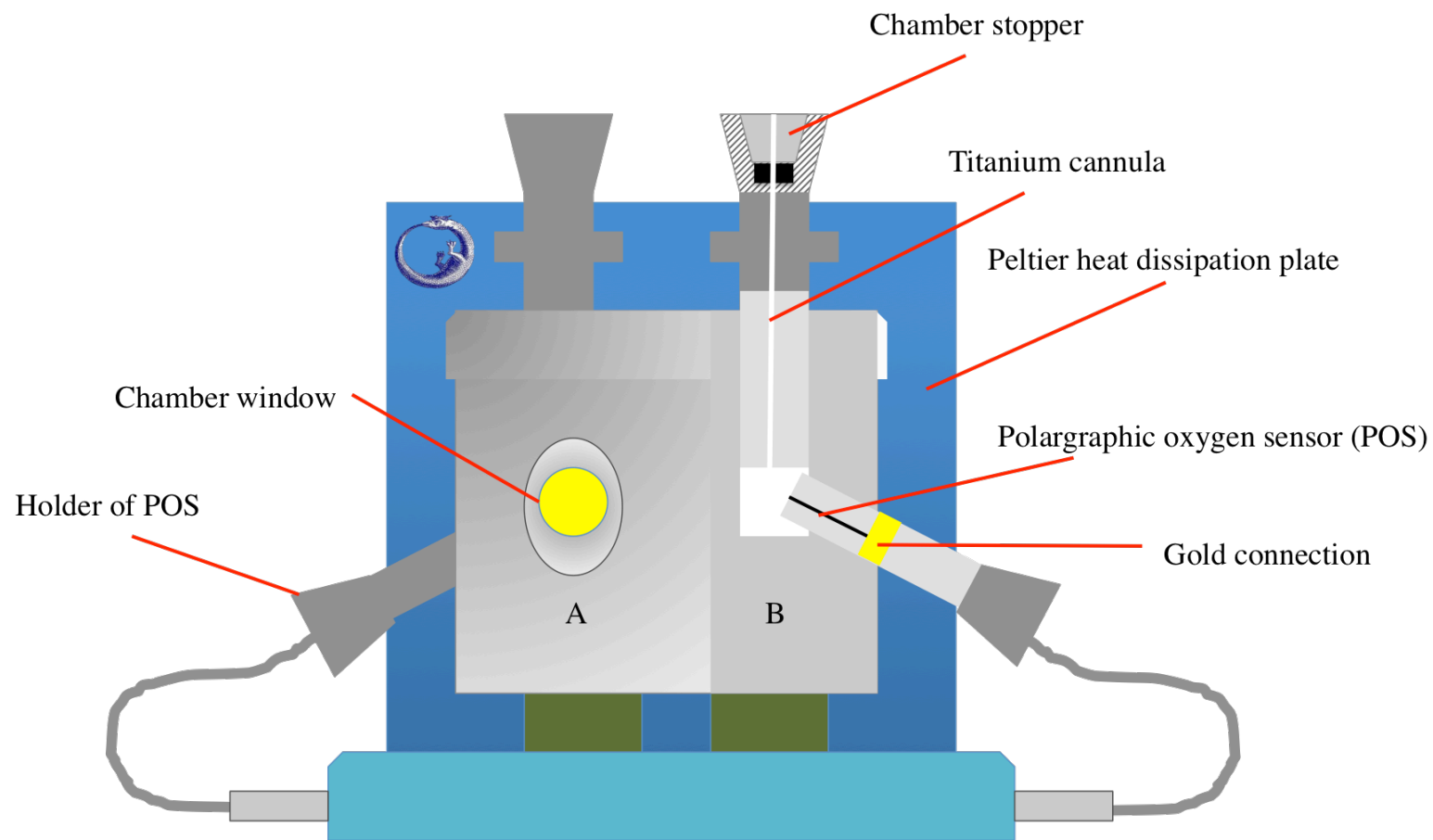
Figure 4.4. Schematic of HRR Oxygraph-2k equipment. Intact appearance is shown (chamber A), demonstrating the window into the chamber, alongside cross section (chamber B) to illustrate the oxygen sensor within the chamber and the way titanium cannula used to allow titration of chemicals into the chamber. Both chambers are housed in a copper block (insulated and temperature-regulated). Peltier thermopiles are in contact between the copper block and the Peltier heat dissipation plate. Figure adapted from OROBOROS©.

uncoupled state. Titration to an optimum concentration was conducted as beyond this point FCCP can inhibit respiration.

Rotenone (0.25μM) was then added to inhibit complex I to measure complex II respiration alone. Subsequently, complex III was inhibited with antimycin A (12.5μM) for estimation of residual, non-mitochondrial, oxygen consumption. In later experiments an extra step was added, Ascorbate (2.5mM) and TMPD (0.5mM) titration, to activate complex IV. These substrates act as artificial electron donors to reduce cytochrome c and determine OXPHOS capacity as an estimate of mitochondrial mass. The experiment was terminated by the addition of azide (20mM). This final step is the second quality control measure as it confirms that the O_2 flux measured during the experiment is due to real mitochondrial function and not transient O_2 flux by the respirometer. Mass-specific O_2 flux (steady-state O_2 flux normalised to sample wet fibre mass, pmol/s) was recorded using DATLAB (Oroboros) (Figure 4.5).

All respiratory states measured were adjusted for instrumental background of the polargraphic oxygen sensors and residual oxygen consumption. Complex IV activity was corrected for the autooxidation of ascorbate and TMPD by subtraction of the chemical background coefficient. This protocol is carried out in Excel® (macro supplied by Oroboros).
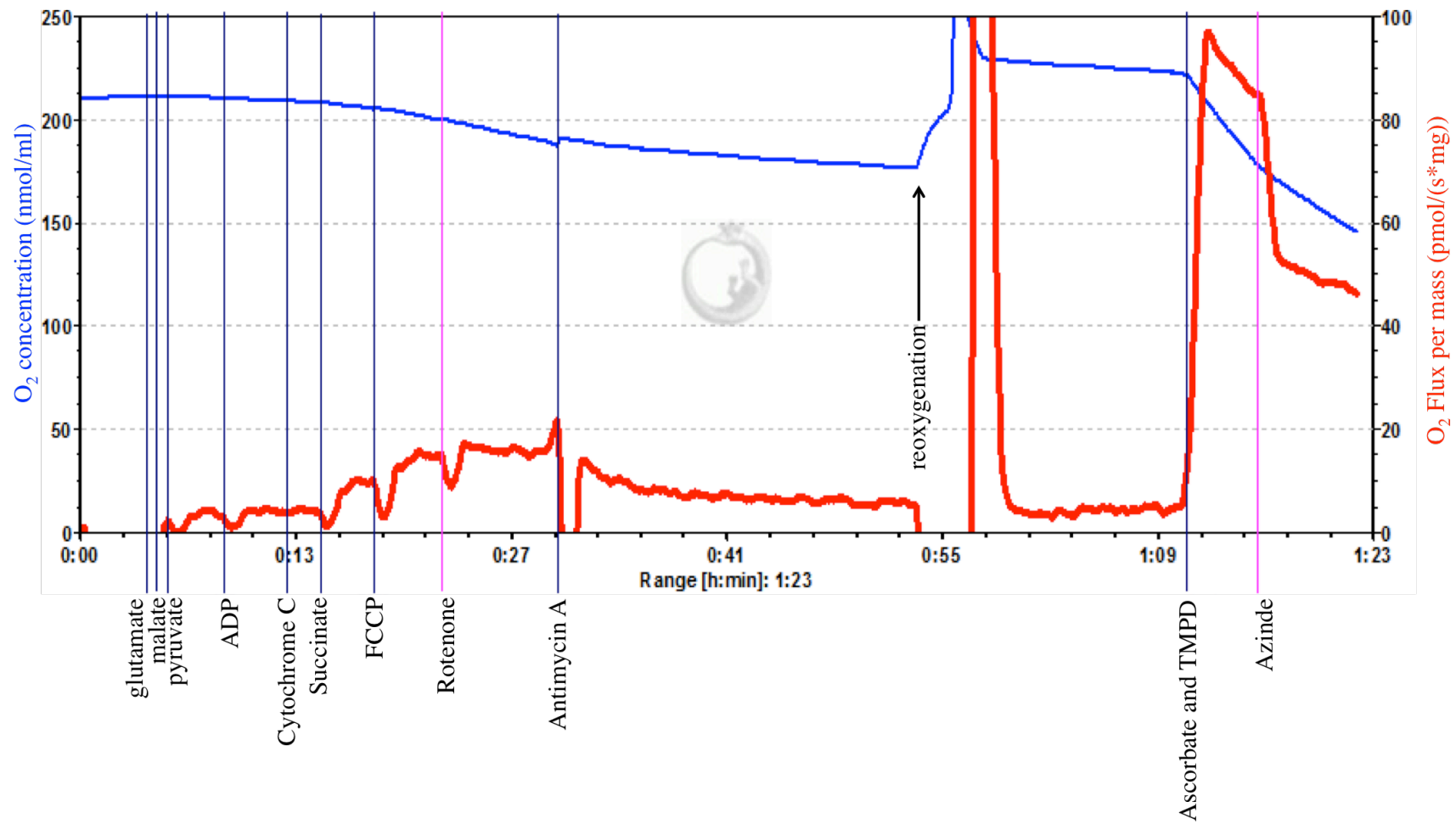
Figure 4.5 Example HRR trace (OROBOROS, DatLab software). Left hand axis is O_2 concentration (blue line), right hand axis is O_2 flux (red line). Annotation outlines titration protocol and reoxygenation

4.2.4 Normalisation of mitochondrial oxygen consumption

Following data processing in Excel® the O_2 flux for the different parts of the ETC are presented as a ratio of the maximum flux in an uncoupled state relative to convergent electron flow through complexes I and II. This is one approach to internal normalisation of mitochondrial oxygen consumption, known as the flux control ratio (FCR). It expresses respiratory control independent of mitochondrial content (Gnaiger, 2014).

Complex IV activity has recently been reported as being strongly associated with muscle OXPHOS capacity in humans (Larsen *et al.*, 2012). As measuring complex IV activity through the addition of TMPD and ascorbate provides a measure of OXPHOS capacity as an estimate of mitochondrial mass this metric was also used as an alternative means of internal normalisation by expressing the raw O_2 flux for each aspect of the ETC as a percentage of the O_2 flux through complex IV, termed %MAX OXPHOS capacity.

4.2.5 Statistical analysis of FCR and %MAX OXPHOS capacity data

The resulting normalised data was tabulated in Excel® and exported to the statistical package RStudio 3.2.2 for analysis. Linear models were designed to test for effects of age, sex and MH status on each of the measured aspects of the ETC (complex I basal, complex I ADP stimulated, complex II, complex I+II coupled, complex I+II uncoupled, membrane integrity and complex IV). Then 3-way ANOVA was performed on the linear models that enabled examination of all individual, pair-wise and the 3-way interaction of the independent variables. To account for multiple-

testing, Bonferroni correction of p values was applied to correct for the 6 aspects of the ETC measured, and both sets of p values presented in the results. Graphical illustration of results was completed in Microsoft® Excel® for Mac 2011 (version 14.6.4).

4.2.6   Gene expression analysis of mitochondrial genes in human ageing

RNA extraction, cDNA synthesis and Taqman® assays were all carried out using the same process outlined in chapter 3 (3.2.2, 3.2.5 and 3.2.6 respectively). The panel of genes were identified based on a commercial available Array produced by Qiagen (RT^2 Profiler^{TM} PCR Array Human Ageing). The array itself comprises 84 genes altered during ageing, covering categories such as genomic instability, telomere attrition, transcriptional regulation and epigenetic alterations. These categories are clearly related to human ageing as a whole but do not address the aspect that is the focus of this chapter. However, the array does include a cohort of 9 genes considered to be implicated in mitochondrial dysfunction in ageing (Table 4.4).

Table 4.4 Genes implicated in mitochondrial dysfunction in ageing (compiled from, QIAGEN, 2016).

Gene ID	Role
MRPL43	Mammalian ribosomal protein L43, aids in protein synthesis within the mitochondrion.
NDUFB11	NADH: ubiquinone oxidoreductase subunit B11, a component of mitochondrial complex I.
POLRMT	Mitochondrial RNA polymerase, responsible for mitochondrial gene expression and provides RNA primers to initiation and replication of the mitochondrial genome.
SIRT1 SIRT3 SIRT6	Members of the sirtuin family (class I), NAD-dependent enzymes. In humans they are suggested to function as intracellular regulatory proteins with mono-ADP-ribosyltransferase activity and play a role in RNA repair and inflammation.
TFAM	Transcription factor A, a key mitochondrial transcription factor also involved in mitochondrial DNA replication and repair. Polymorphisms are associated with Alzheimer's and Parkinson's disease.
TFB1M TFB2M	Transcription factor B1 and 2, necessary for mitochondrial gene expression.

Reference genes, B2M, GAPDH and TBP were used for normalisation and the same method applied as chapter 3 (3.2.7). Statistical analysis also followed the same method as chapter 3 (3.2.8). Graphical illustration of results was completed in Microsoft© Excel© for Mac 2011 (version 14.6.4).

4.3 Results

4.3.1 Flux Control Ratio

All samples processed were subjected to internal normalisation of O_2 consumption using the flux control ratio. This expresses the various respiratory states induced by the HRR protocol as a ratio of the maximum flux in the uncoupled state of electron flow through complex I and II. All chamber replicates for each sample were included in analysis. It was therefore possible to visualise possible differences in the FCR of the different aspects of the ETC between MHS and MHN samples (Figure 4.6) controlled for age and sex.
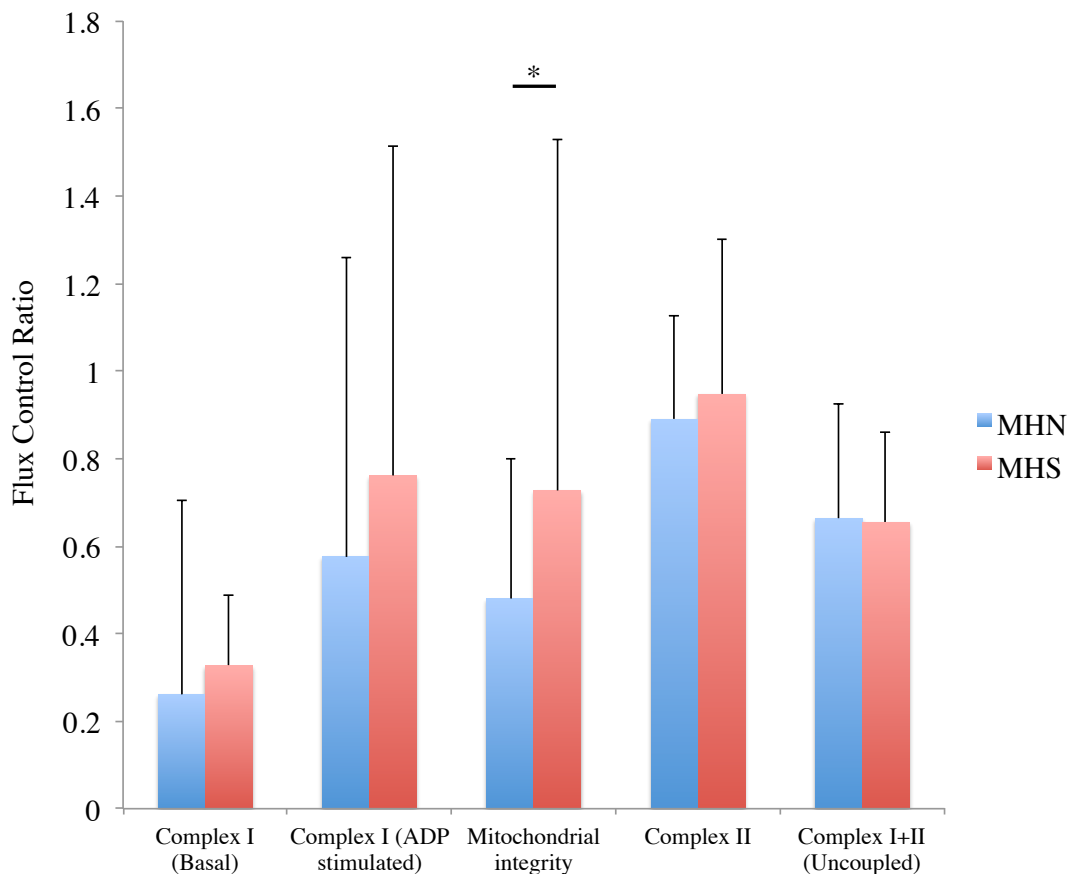
Figure 4.6 Flux control ratios measured in skeletal muscle samples from MHN (n=63) and MHS (n=27). Data is presented as means with error bars showing standard deviation. *p<0.05.

181

Basal activity of complex I was slightly elevated in MHS samples, though this was not statistically significant when compared to MHN using ANOVA. Following addition of ADP, activity of complex I was stimulated in both MHN and MHS samples, with a greater increase observed in MHS samples than in MHN though when comparing the FCR means for MHS and MHN at this stage in the ETC there was no significant difference. With the addition of cytochrome C to test mitochondrial integrity there was a marked increase in FCR observed in MHS samples. When compared to MHN, this was statistically significant, $p=0.015$. However, following Bonferroni correction, $p=0.09$. Upon inhibition of complex I and stimulation of complex II activity the FCR was found to be very similar when comparing MHS and MHN samples, both close to 0.9. Measuring complex I and complex II uncoupled activity was also similar when examining MHS and MHN samples.

No significant differences were observed when comparing FCR in males and females for any aspect of the ETC measured except for complex I&II uncoupled activity (Figure 4.7). FCR of complex I and II uncoupled activity was significantly lower in females, $p=0.0001$ (corrected $p=0.0006$).
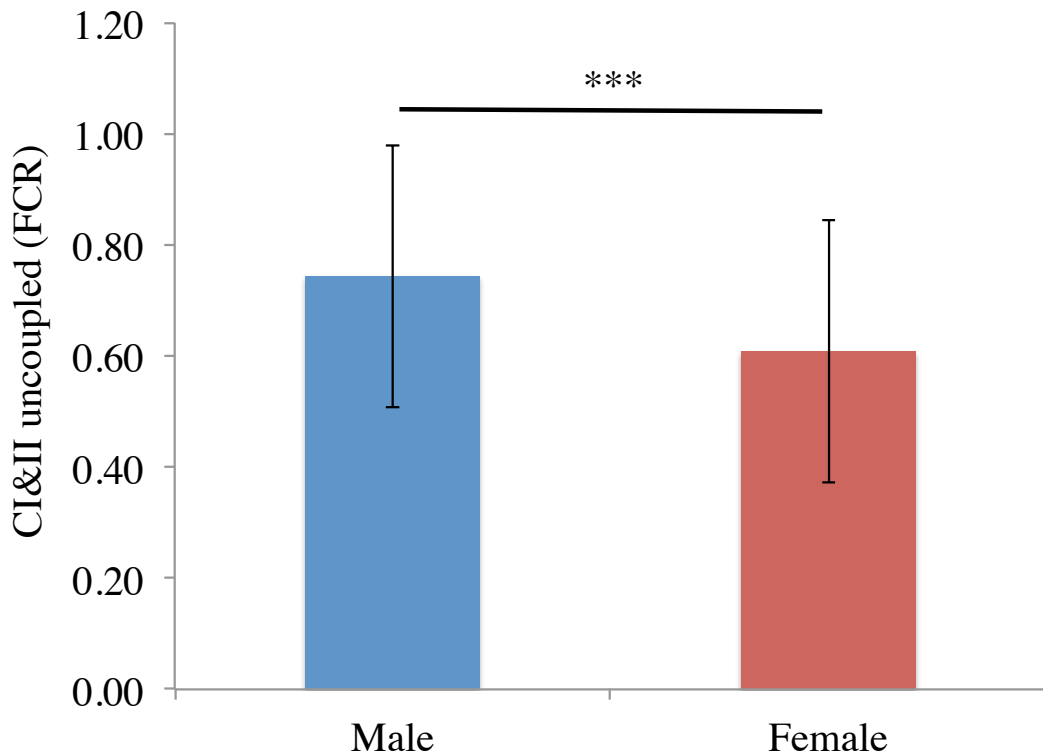
Figure 4.7 Differences between males (n=35) and females (n=55) for Complex I&II uncoupled activity (FCR). Error bars are standard deviation, ***p<0.001.

Age alone was found to have no effect on FCR for any aspect of the ETC measured. When the combined effect of age and sex was considered there was an increase in the FCR for complex I&II uncoupled activity in females with increasing age whereas in males the FCR for this aspect of the ETC decreased with increasing age. This result was statistically significant, p=0.029. However following Bonferroni correction this result is not significant.

The interaction between sex and MH status was also found to have a significant effect on complex I&II uncoupled activity when normalised using the FCR, p=0.005 (0.03 with Bonferroni correction). Specifically, there was a significant increase in activity of this aspect of the ETC in MHN males, compared with MHN females, MHS females

and MHS males (Figure 4.8). The rate of complex I&II uncoupled activity in these three groups was similar and reduced compared to that shown in the MHN males group. It was lowest in MHN females.
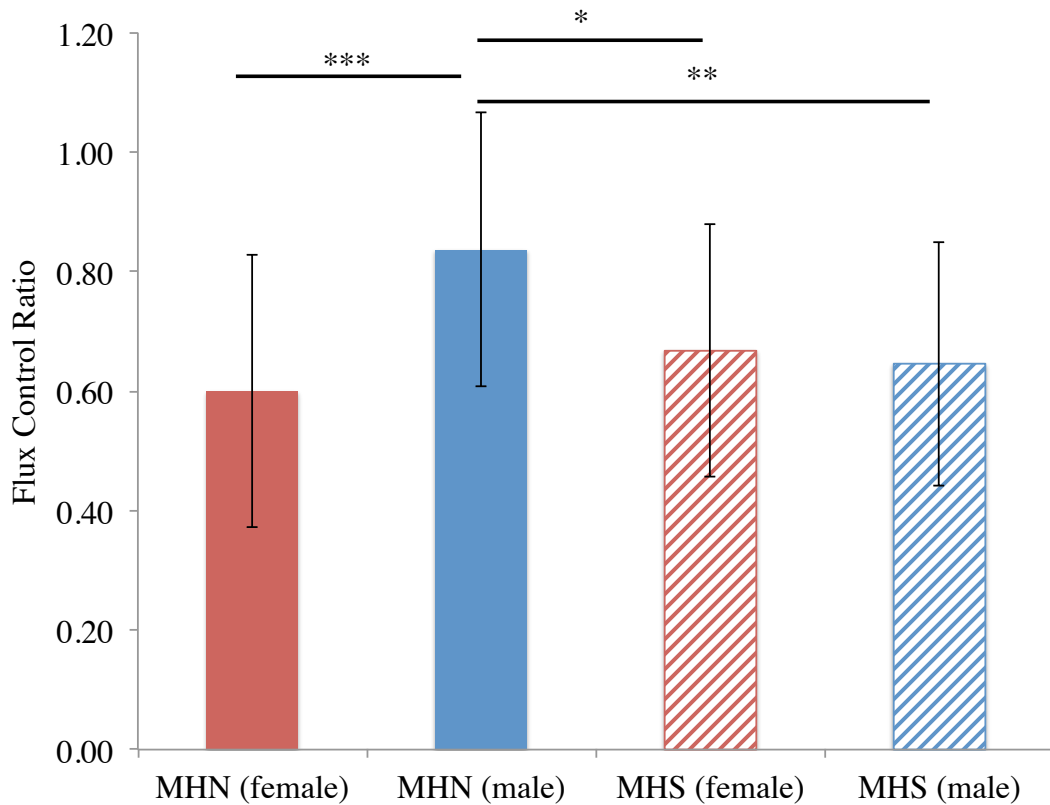
Figure 4.8 Mean complex I&II uncoupled activity, normalised using FCR for groups of MH status separated by gender. ***$p<0.001$, **$p<0.01$, *$p<0.05$. Error bars are standard deviation.

4.3.2   Complex IV and maximum OXPHOS capacity

Maximal complex IV activity was measured by the inhibition of the other complexes and the addition of ascorbate and TMPD that acts as an artificial electron donor to complex IV. This measurement was completed on a reduced number of samples as it was introduced part way through the sample processing, n=60. Raw O_2 flux through complex IV is very highly associated with maximal OXPHOS capacity and therefore can be used as an indicator of this (Larsen *et al.*, 2012). In MHN samples, the mean

complex IV activity was just below 70pmol/(s*mg) whereas in MHS samples, mean

complex IV activity was closer to 50pmol/(s*mg) (Figure 4.9). However, this result

was not statistically significant.
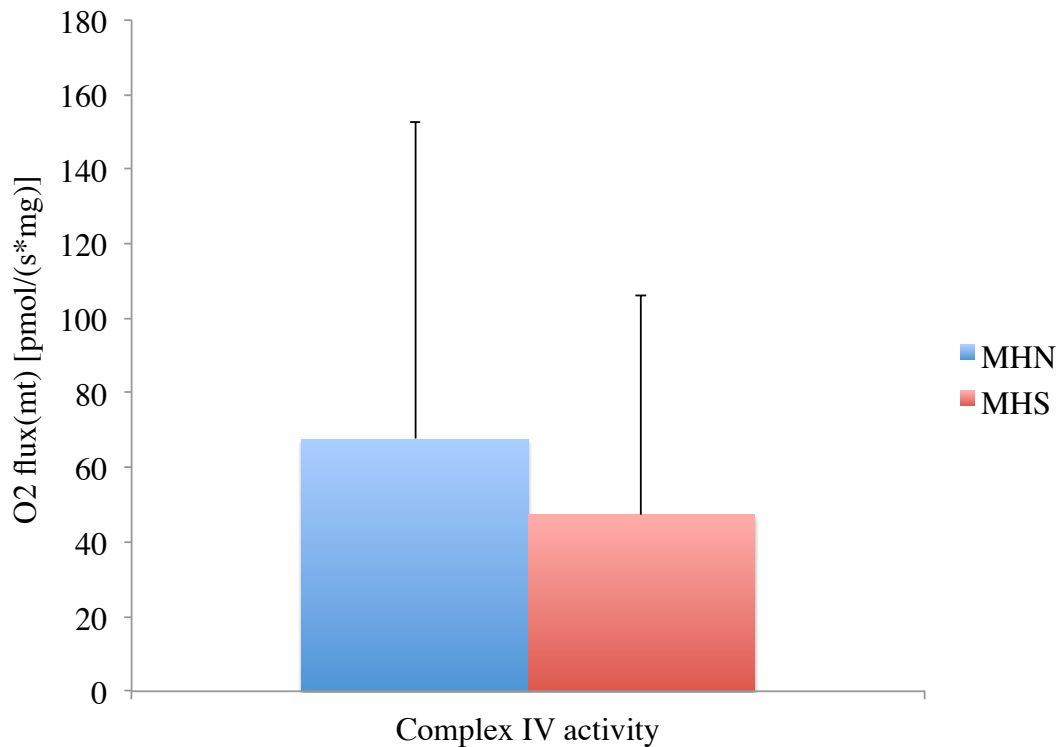
Figure 4.9 Maximum mitochondrial complex IV activity (OXPHOS CAPACITY) in MHN (n=43) and MHS (n=17) individuals. Data is presented as mean with error bars showing standard deviation.

As complex IV activity can be used as an indicator of maximal OXPHOS capacity it

was also used as an alternate means of internally normalising the respiratory states

induced throughout the HRR protocol. By examining the data through this process it

is clear that MHS and MHN samples have consistently similar levels of mitochondrial

OXPHOS capacity at each aspect measured (Figure 4.10).
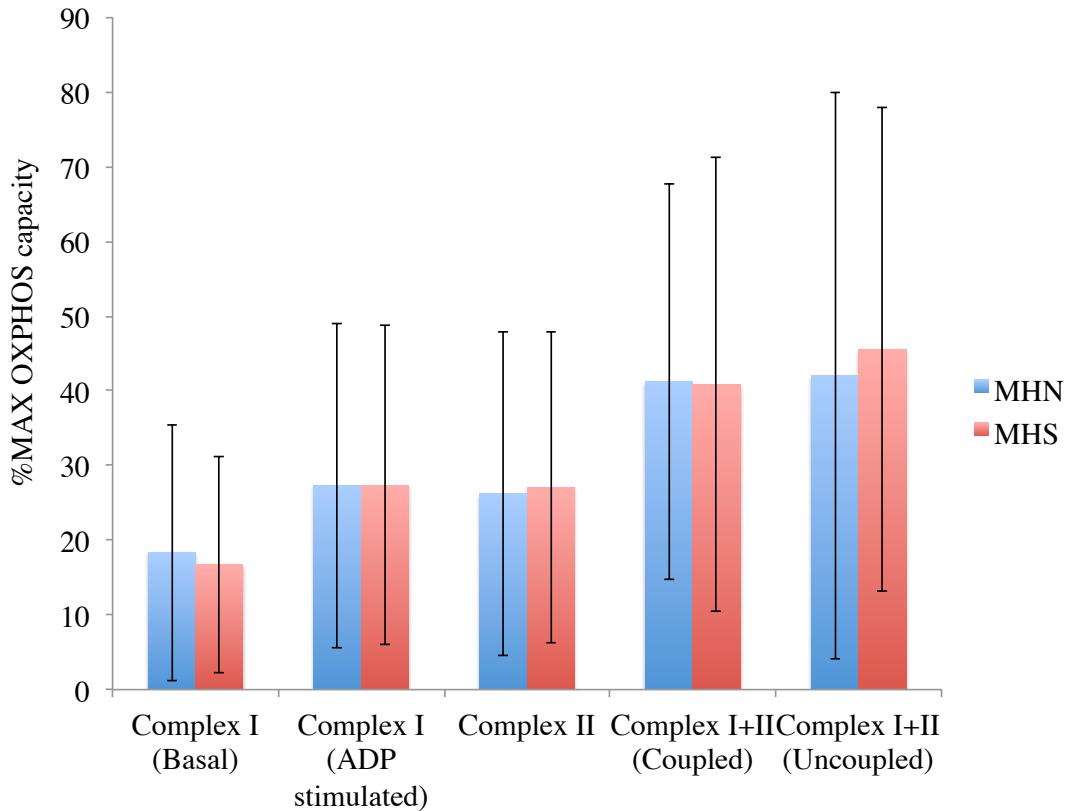
Figure 4.10 O2 flux during the different measured respiratory states expressed as a percentage of the maximum OXPHOS capacity. Data is presented as means with error bars showing standard deviation.

Statistical analysis was also carried out to determine the potential effects of sex and age on the respiratory rates in each aspect of the OXPHOS pathway. As variables independently, neither sex nor age was found to have an effect on the measurements from the HRR protocol. However, when considering the interaction between age and sex differences were observed. Complex I basal and complex I ADP stimulated activity was shown to increase with age in males, whereas in female's activity of this aspect of the OXPHOS pathway decreased, $p=0.029$ and $p=0.021$ respectively. However, Bonferroni correction of these p values showed them to be non-significant.

4.3.3 Gene expression analysis of mitochondrial genes in human ageing

A cohort of genes implicated in human ageing was chosen for analysis, using the samples that underwent HRR. Owing to availability of tissue, only 76 of the 90 samples that underwent HRR were analysed using TaqMan® gene expression analysis for the genes implicated in human ageing. Data was analysed factoring in age, sex and MH status as possible predictor variables and also considering the possible pairwise and three-way interactions between these variables. Following this rigorous analysis it was found that none of the genes in the cohort showed differential expression according to the variables previously defined. One exception was *TFB2M* that showed significantly lower expression in females compared to males, $p=0.038$ (Figure 4.11). However, with Bonferroni correction this p value is no longer significant, $p=0.342$.
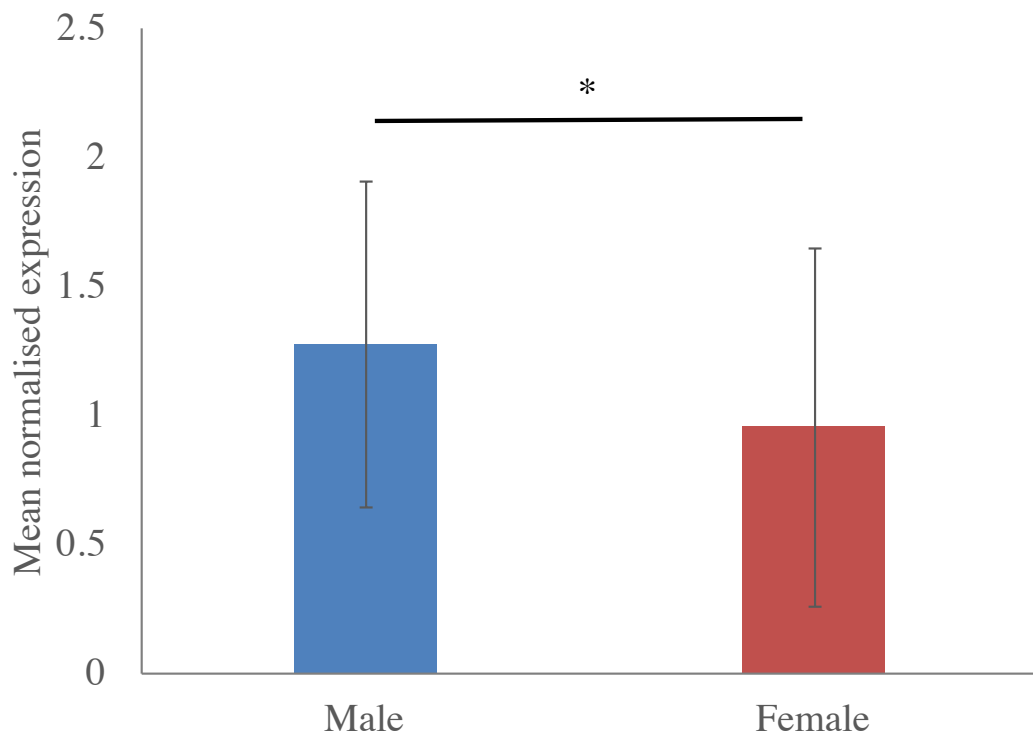
Figure 4.11 *TFB2M* Expression in skeletal muscle , error bars show standard deviation, *$p<0.05$.

187

4.4 Discussion

4.4.1 Mitochondrial oxidative phosphorylation capacity

This chapter has addressed the question of whether there is evidence of altered or abnormal mitochondrial function in malignant hyperthermia susceptible skeletal muscle in the context of age. This was examined through the use of high-resolution respirometry to quantify alterations in OXPHOS capacity of muscle samples derived from patients. These biopsy samples were obtained from patients that had not been exposed to any triggering agents and therefore the measurements represent an assessment of the basal metabolic activity of the mitochondria. It may be of interest in future work to examine the potential for altered mitochondrial function in MH susceptible muscle following application of caffeine and halothane, to determine whether these substrates alter the basal bioenergetics of the mitochondria in both normal and susceptible muscle.

Quality control of experimental procedure was ensured by using the cytochrome c assays to establish and deficit in mitochondrial membrane integrity and termination of the experiment using azide to confirm that measurements made were really due to mitochondrial activity and not random noise. Quality control of mitochondrial data is currently the subject of a European Cooperation in Science and Technology (COST) initiative called MITOEAGLE (COST, 2017). MITOEAGLE aims to improve knowledge of mitochondrial function in health and disease related to evolution, age, gender, lifestyle and environment. It is working towards establishing protocols to standardise mitochondrial assays so that data from all labs can be directly compared. The fact that two experimenters carried out the assays in this chapter and no

differences were observed in the data obtained suggests that the protocol used is robust and reliable.

It has been indicated, by a study using R163C (implicated in MH, CCD and EHI) knock-in mice, that in addition to other changes in mitochondrial function, there is a reduction in basal OXPHOS capacity that is associated with this variant (Giulivi *et al.*, 2011). The approach used with the R163C mice used isolated mitochondria and therefore the results may not be directly comparable to the information obtained from permeabilised muscle fibres used in this chapter. Age-related changes in mitochondrial OXPHOS capacity have also been identified and this chapter sought to investigate the potential for an age-related decline in mitochondrial OXPHOS in the context of MH susceptibility.

Findings from this investigation have highlighted that the FCR for mitochondrial integrity is significantly higher in MHS muscle compared with MHN. This provides evidence for possibly compromised mitochondria in MHS individuals, suggesting that they might be leakier. However, all other aspects of the OXPHOS pathway for this metric (FCR) were unaffected by MH status, showing similar levels to that of MHN muscle. This could indicate possible compensatory mechanisms in the MH mitochondria to account for the loss of membrane integrity.

Recent findings by Larsen et al (2012) suggest that complex IV activity is strongly associated with the oxidative capacity of skeletal muscle, and therefore respiratory states were also normalised to maximal complex IV activity. By this method, the difference in respiratory activity between MHN and MHS phenotypes is also

negligible. This analysis was not performed on the same number of samples as the FCR cohort, owing to adopting this altered method partway into sample processing. It would clearly be desirable to make more measurements of this type on additional samples to derive a more representative sample set. At present, the data encompasses only 18 MHS samples, but 42 MHN which could be affecting the results.

In light of the information that complex IV activity is an accurate marker of OXPHOS (Larsen *et al.*, 2012) then these results suggest the total OXPHOS capacity of MHS muscle mitochondria is lowered compared to MHN. However, this result was not statistically significant. This may be due to the small sample size of the MHS group and if there were more samples it would reduce the residual error in the mean and may make the result significant. It is clear however, that the individual aspects of the OXPHOS pathway don't differ between MHN and MHS muscle, indicating that relative to this reduced total OXPHOS capacity, the mitochondrial are still functioning in a similar manner. This possibly lowered total OXPHOS capacity in human MH skeletal muscle is also in line with findings from an MH-susceptible mouse model that complex IV activity was significantly reduced in skeletal muscle mitochondria of R163C mice (Giulivi *et al.*, 2011).

The findings of this study contradict those reported from experiments using mitochondria extracted from skeletal muscle of R163C mice, where state 3 oxygen uptake rates with both NAD and FAD-linked substrates were significantly lower than values obtained for wild-type animals (Giulivi et al., 2011). However, in the data from this chapter, there were no observed differences in MHS and MHN skeletal muscle from human biopsies. These contrasting observations could simply reflect a species-

specific difference that is additionally confounded by the potential for the human samples to represent a number of different *RYR1* variants possibly not even including the R163C variant. R163C is implicated in CCD as well as MH and is defined by a reduction to oxidative activity (Brislin & Theroux, 2013), and therefore this mutation is likely to present with reduced oxidative capacity of skeletal muscle whereas this may not be the case for other MH genotypes. These differing results may also be related to the fact the R163C mouse experiments were carried out on isolated mitochondrial populations, rather than in permeabilised tissue, suggesting that the results of that study may not be reflective of the *in vivo* state of the mitochondria.

In this *in situ* preparation it is only possible to look at the activity of the total mitochondrial population (Kuznetsov *et al.*, 2008). It may be more relevant to look at subpopulations within the skeletal muscle. For instance, in the knock-in mouse line that expresses *RYR1* variant T4826I, mitochondria are seen to redistribute to subsarcolemmal regions and are often found to be surrounded by accumulations of amorphous electron-dense material (Yuen *et al.*, 2012). This may suggest mitochondria in this region are more likely to be more physiologically compromised. If this translates to human MH, and pathological alterations affect mitochondrial subpopulations differently, using HRR alone could underestimate OXPHOS abnormalities. Confocal imaging has provided evidence of functional heterogeneity of mitochondrial subpopulations (Kuznetsov *et al.*, 2006). Oxidative state, reflected by intensity of flavoprotein autofluorescence, was significantly increased in the subsarcolemmal subpopulation compared with intermyofibrillar mitochondria. This higher oxidative state of subsarcolemmal mitochondria correlated with the higher levels of resting calcium in this subpopulation. Further work in this area could utilise

a fluorescent-imaging approach in conjunction with HRR to identify potential subsets of pathologically altered human mitochondria.

Altered resting calcium levels are another feature of MH that may be of interest due to altered ryanodine receptor function (Lyfenko *et al.*, 2004; Eltit *et al.*, 2012). It is also a feature of muscle ageing whereby the receptor has been shown to become leaky and thus elevate resting calcium levels (Wang et al., 2012). Considering the signalling properties of calcium within skeletal muscle has been shown to extend to stimulation of the ETS in skeletal muscle (Glancy *et al.*, 2013) it seems imperative to study mitochondrial respiration in their relevant environment. Higher mitochondrial calcium levels were excluded as the cause of mitochondrial dysfunction in R163C mice since chelation of free Ca^{2+} with EGTA did not significantly alter state 3 oxygen uptake (Giulivi *et al.*, 2011). However, preparations of isolated mitochondria which eliminate a functioning cytoplasm lose the pathological consequences of increased Ca^{2+}. Additionally, there is a loss of organelle interaction in isolated mitochondria, and therefore any interactions between functionally-altered SR and mitochondria will be absent. Although the permeabilised tissue preparation utilised within this study more closely resembles the integrated cellular system of an intact cell (i.e. basic interactions with cytoskeleton and organelles are present), in both this preparation and that of the isolated mitochondria the full influence of any changes to resting $[Ca^{2+}]$ are lost. It is therefore likely that the OXPHOS activity observed in these preparations is not a fully accurate representation of skeletal muscle mitochondria of MHS *in vivo*.

There are factors regarding the protocol itself which may alter the HRR measurements obtained. For example, the preparation of the fibres is subjective and even having been

performed by one individual does not guarantee dissection to the same level. The time between surgical removal of biopsy specimens to analysis in the laboratory also appears to influence basal mitochondrial activity. Variables such as these are hard to standardise and in such a varied cohort factors which may affect the respiratory activity of the tissue are more likely result in exaggerated differences in the parameters being measured. While there was every attempt to minimise transport and storage time and to ensure consistency in dissection, it is not possible to fully eliminate these variables as having an influence on the results. In hindsight, it might have been helpful to more accurately record the time of biopsy relative to time of sample processing for mitochondrial respirometry to accurately quantify any potential effects of transport and storage time. Future work could focus on developing the means to carry out the mitochondrial measurements on location at St James's Hospital where the biopsies take place. This would reduce transport time and reduce the variation in storage and processing time.

Previous work looking at gender alone showed no differences between the genders in relation to the different aspects of the OXPHOS pathway in gastrocnemius muscle samples (Thompson *et al.*, 2014). This is reflected by the results of this chapter.

4.4.2   *Gene expression differences in HRR muscle samples*

Of the genes identified for analysis that were cited as being implicated in human ageing and mitochondrial dysfunction, none demonstrated age related changes in expression when investigated in this cohort of samples. There were also no observed differences in expression between MHS and MHN samples or between males and females, with the exception of *TFB2M* which showed a very week effect of MH status

on expression and could be a chance finding. There was no effect of any pairwise interaction of age, sex or MH status or indeed the 3-way interaction. This result could indicate that these genes were perhaps not the right choice for investigation in these samples, and that there may be other as yet investigated genes that are altered in their expression with respect to mitochondrial function. Alternatively, due to the fact no change in mitochondrial function was observed in these samples (apart from in relation to the age-sex interaction for complex I activity) then it is reasonable to expect no changes in gene expression for this cohort of genes.

Further work is required to put the results of this chapter into the wider context of MH susceptibility and ageing. Examination of mitochondrial OXPHOS in triggered skeletal muscle will provide useful comparison of the data shown here and enable us to better understand the evidence of compromised mitochondria in MH skeletal muscle. Additionally, evaluation of gene expression in skeletal muscle that has been exposed to triggering agents would serve as a useful comparison to the investigation carried out here on un-triggered skeletal muscle.

5 Development of a system for quantifying the effect of age on skeletal muscle energetics

5.1 Introduction

5.1.1 Muscle mechanical performance

An essential function of skeletal muscle is to produce force that powers locomotion. Force can be produced when the muscle is held at a constant length (isometric contraction) or be actively shortened to produce mechanical work, or stretched to absorb mechanical energy. The rate of work production is termed the mechanical power output. Force, work and power determine an animal's locomotor performance.

An isolated muscle can be mechanically activated *in vitro* by the application of an electrical stimulus. Under isometric conditions a single stimulus elicits a twitch, during which muscle force rapidly increases and then returns to the resting state. A train of stimuli, delivered at an appropriate frequency, causes mechanical summation where tension is developed further before relaxation occurs. If stimulation is of a high enough frequency, a plateau is observed and the muscle is considered to be in tetanus. The level of force produced during an isometric contraction is largely determined by the sarcomere length. Sarcomere length determines the degree of overlap between the actin and myosin filaments and hence the number of cross-bridges that can form. When the overlap is optimised, maximal isometric force is produced (Gordon *et al.*, 1966). Optimum *in vitro* sarcomere length corresponds with optimum muscle length *in vivo* (Rome *et al.*, 1988; James *et al.*, 1995). Isotonic contractions occur when the length of the muscle changes but tension remains constant. This is exhibited in

concentric contractions where the force produced by the muscle exceeds the force applied and the muscle will shorten, and in eccentric contractions whereby the length of the muscle increases due to the force of the load exceeding the force produced by the muscle.

While isometric and isotonic contractions provide fundamental information concerning the intrinsic physiological properties of the muscle, they do not represent the way in which many muscles function *in vivo*. In normal locomotion, many muscles undergo cycles of contraction, with distinct power generating and recovery phases, and undergo a range of length trajectories and activation patterns. In 1985, a new technique, based on an earlier study from 1959, was pioneered that enabled muscle physiologists to quantify skeletal muscle function *in vitro* using *in vivo*-like conditions, the 'work loop technique' (Josephson, 1985). Using this method, a muscle can be subjected to a cyclical length change and phasic stimulation resulting in force generation (Figure 5.1A-D). Muscle power can be determined as the product of force and velocity (length change) and muscle work is established by dividing power by cycle frequency.
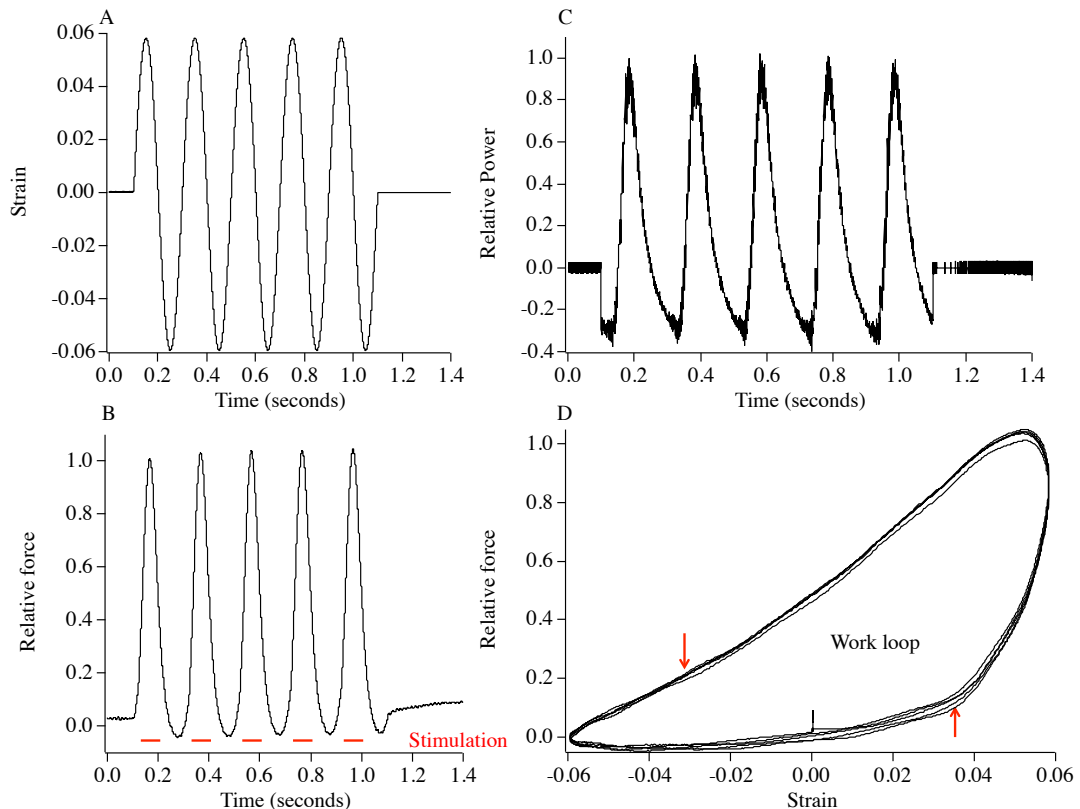
Figure 5.1 Illustration of the work loop technique used to measure muscle work output. Data derived from mouse soleus muscle at 9Hz cycle frequency A: Sinusoidal length trajectory trace, muscle had a mean fibre length of 10.6mm (L_0). B: Force production while the muscle is stimulated (stimulation initiated 20ms prior to the start of shortening and lasted for 22ms) undergoing the length change shown in A, force normalised relative to maximum force generated during the first cycle. C: Power produced during each cycle of work. D: Plot of force against strain showing a series of work loops for the data from in A-C. Upward pointing arrow indicates the start of stimulation and downward pointing arrow indicates the end of stimulation.

5.1.2 The energetic cost of muscle contraction

All muscles convert chemical energy into mechanical work. The first step in this process involves the production of ATP by oxidative metabolism in the mitochondria, from fuels such as glucose, the efficiency of this process is referred to as the 'oxidative recovery efficiency'(E_r). The second step concerns the hydrolysis of ATP by the cross-bridges in the myofibrils (myosin ATP cycle) to produce mechanical work (Smith *et al.*, 2005), termed 'myofibrillar efficiency' (E_i) (Figure 5.2).
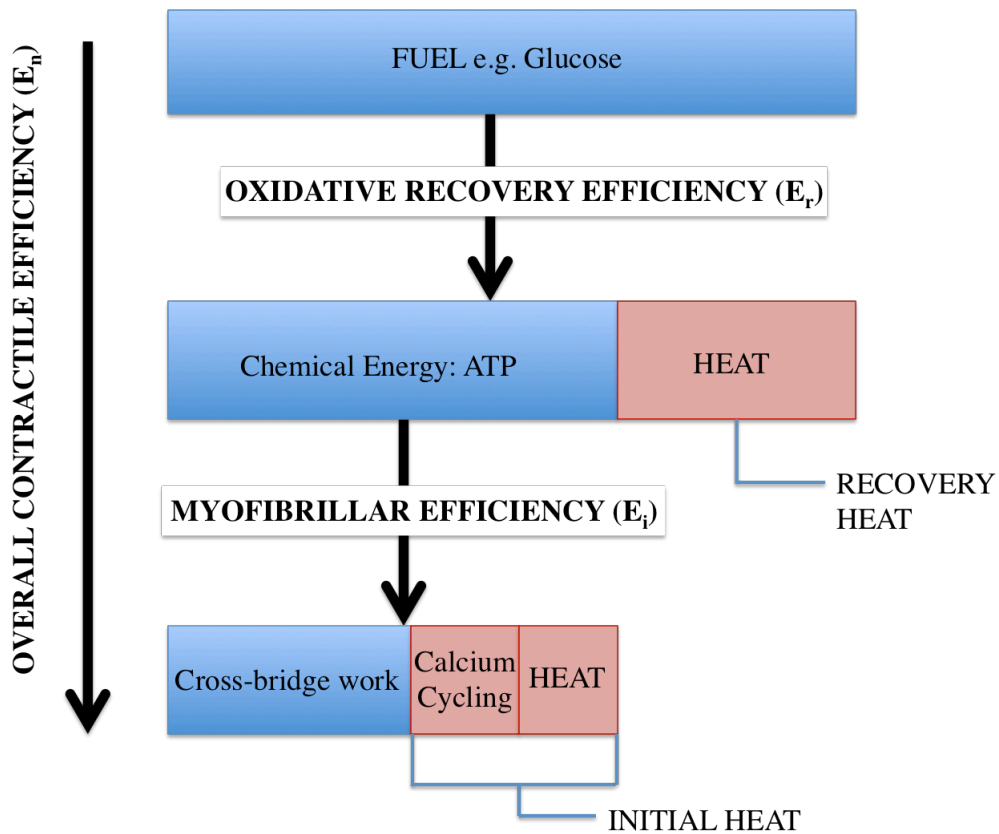
Figure 5.2. Energy cascade during muscle contraction. Initial heat: heat produced during the contraction, associated with the non-contractile processes and the inefficiencies of the cross bridges. Recovery heat: heat produced following the contraction, associated with the oxidative recovery processes.

At each step the process of energy transfer is not completely efficient, and some of the energy is lost as heat. There are also some processes that consume ATP that are required to support the contraction, but that produce no mechanical work, such as calcium cycling; as a result, this energy consumption is ultimately given off as heat and represents an inefficiency in the transduction of chemical energy into mechanical work. Through the measurement of initial heat (H_i) produced during the contraction, recovery heat (H_r) produced after the contraction and net mechanical work (W), it is possible to quantify the oxidative recovery and myofibrillar efficiencies and as a result, the net mechanical efficiency (E_n).

$$E_i = W/(W+H_i \qquad E_n = W/(W+H_i+H_r \qquad E_r = E_n/E_i$$

Combination of the work-loop technique and myothermic measurements (obtained using metal-film thermopiles) has previously been used to quantify muscle energetics in mice (Table 5.1), but has yet to be specifically utilised on aged mice, mice expressing *RYR1* variants or on human skeletal muscle.

Table 5.1 Summary of myothermic work carried out in mice to date

Strain	Age	Authors
Swiss	4-8 weeks	(Barclay *et al.*, 1993)
Swiss	Adult*	(Barclay, 1994)
Swiss	Adult*	(Barclay *et al.*, 1995)
Swiss	Adult*	(Barclay, 1996)
C57BL/6 C57BL/6 x CBA	not specified	(Curtin *et al.*, 2002)
Swiss	Adult*	(Barclay & Weber, 2004)
Swiss	Adult*	(Barclay *et al.*, 2010)
CD1	5-9 weeks	(Holt & Askew, 2012)

*definition of Adult is not specified

It has been indicated that there is a reduction in net efficiency of ATP production in aged skeletal muscle due to the decrease in the volume of ATP produced per unit of O_2 consumed (Marcinek *et al.*, 2005; Amara *et al.*, 2008). This uncoupling of oxidative phosphorylation is due to an increase in the proton leak through the inner mitochondrial membrane and has a significant physiological impact on exercise performance (Brand, 2000; Conley *et al.*, 2007; Amara *et al.*, 2007). Compromised basal oxidative phosphorylation has also been identified in mouse models of MH (Giulivi *et al.*, 2011). These alterations in mitochondrial function may be related to elevated intracellular calcium concentration (Yang *et al.*, 2007). Elevated calcium levels are a feature of both aged and myopathic muscle, attributed to increased leak through the RyR1 owing to mutations in *RYR1* and *CACNA1S* (Yang *et al.*, 2007; Beqollari *et al.*, 2015) in the case of myopathies, or age related oxidative damage to the RyR1 (Puzianowska-Kuznicka & Kuznicki, 2009). The combination of the work

loop technique and myothermic measurements represents a unique way in which to examine the consequences of impaired calcium handling and uncoupling of mitochondrial oxidative phosphorylation on skeletal muscle energetics. It is hypothesised that the impaired calcium handling will affect the recovery capacity of the muscle and ultimately also impact the ability for the muscle to efficiently produce mechanical work.

This chapter will present the development of new thermopile equipment, and preliminary data from old and young wild type mice highlighting the performance of the equipment and some indication of potential alterations in skeletal muscle efficiency associated with age. It represents the foundation for future work that will focus on utilising wild type mice in conjunction with mouse lines expression *RYR1* and *CACNA1S* variants to investigate the effect of these variants on skeletal muscle efficiency with age.

5.2   Materials and Methods

5.2.1   Measurement of heat production in skeletal muscle

Determining energy output by quantifying heat production during muscle contraction is a valuable, non-destructive, tool for understanding muscle energetics (Woledge *et al.*, 1985). A metal-film thermopile can be used to measure temperature change and this information converted into a measure of heat output.

The metal film thermopile used in this apparatus is made from vacuum deposited antimony and bismuth onto a film substrate (manufactured and supplied by Dr C. J. Barclay). The arrangement of these substances means that alternate thermocouples (the active junctions) lie in the centre of the thermopile, with remaining couples (reference junctions) located at the edges (Figure 5.3). The reference junctions are clamped into a frame and maintained at a constant temperature by a Peltier temperature control unit (custom built device with Peltier heat pumps, capable of regulating the temperature of muscle chamber to with 0.01 degrees).

During muscle contraction, heat is generated as a by-product of force generation. This raises the temperature of the active junctions on the thermopile and is measured as a voltage output according to the thermoelectric effect. The magnitude of this voltage output is determined by the temperature difference between the two locations and the Seebeck coefficient (α).

201
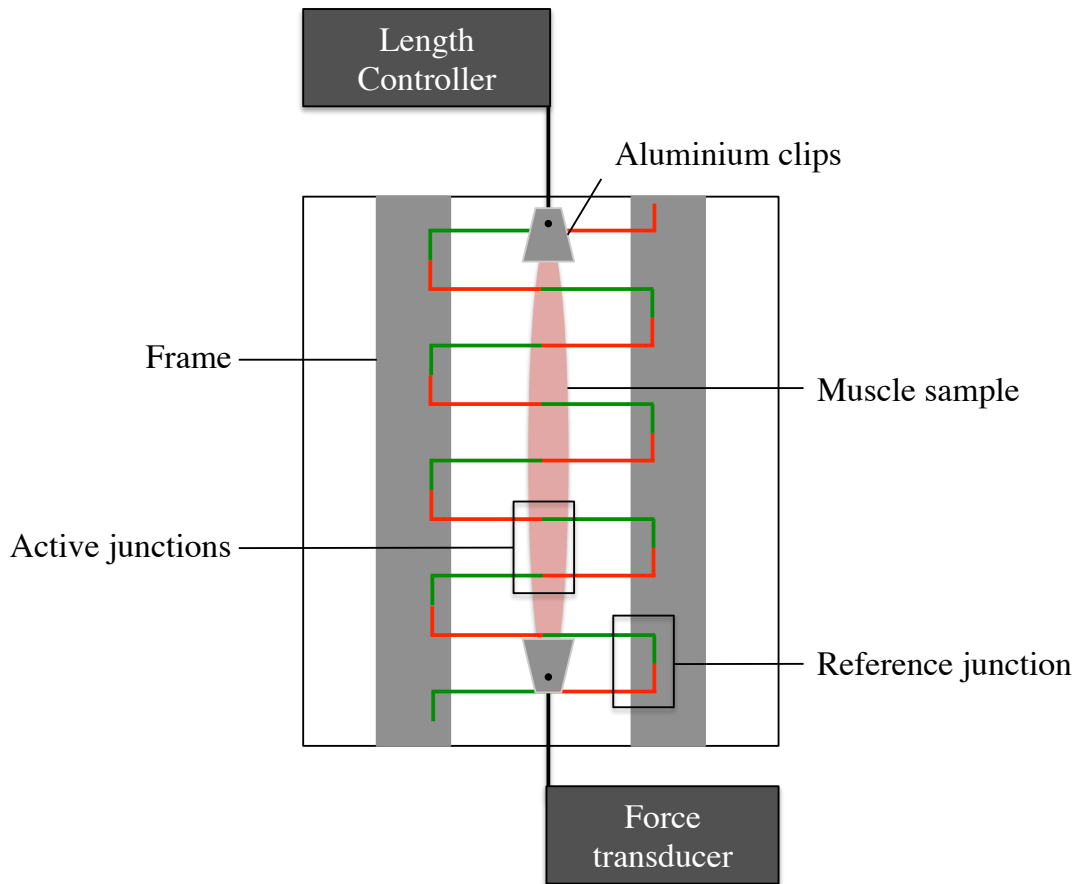
Figure 5.3 Schematic of thermopile apparatus showing muscle attached to the length controller and force transducer while resting on the thermopile. All thermopile apparatus is enclosed in brass block.

5.2.2 *Thermopile calibration*

In order to determine the temperature change from the voltage output from the thermopile, the Seebeck coefficient of the thermopile is required. This can be calculated from the rate of change of the thermopile output and the heat capacity of the thermopile immediately following a period of Peltier heating, i.e the heating and cooling of alternate junctions in response to a small, known current being passed through the thermopile (Kretzschmar & Wilkie, 1972; Kretzschmar & Wilkie, 1975). All calibration measurements were carried out at room temperature (21°C).

This was achieved by placing 10 different sized silver blocks (mass range 40.7-180.4mg) in turn on the active region of the thermopile (3 replicates for each block were performed at random). This active region was heated by passing a current (I) (1021 DC Current Source, Time Electronics Ltd., Botany Industrial Estate, Kent) of 100μA through the thermopile for 200 seconds (sufficient time to reach steady-state temperature). Thermopile output was amplified by a factor of 2000 (Low noise voltage preamplifier model SR560, Stanford Research Systems, Cambridge Technology Inc, MA, USA) and recorded onto a PC at 1000Hz using a PowerLab (ADI INSTRUMENTS). A single exponential curve was fitted using the equation $V = V_0 \exp(-t/tau)$, where V is thermopile output (in Volts), V_0 is a constant, t is the time and tau is the time constant. The initial rate of cooling (dV_0/dt) was calculated by multiplying V_0 by *invTau*. Curve fitting excluded the first second of data as this represents the change in temperature at the reference junctions not cooling in the active region of the thermopile (Kretzschmar & Wilkie, 1972). The relationship between the heat capacity of the silver blocks and the inverse rate of cooling was then be plotted (Figure 5.4).
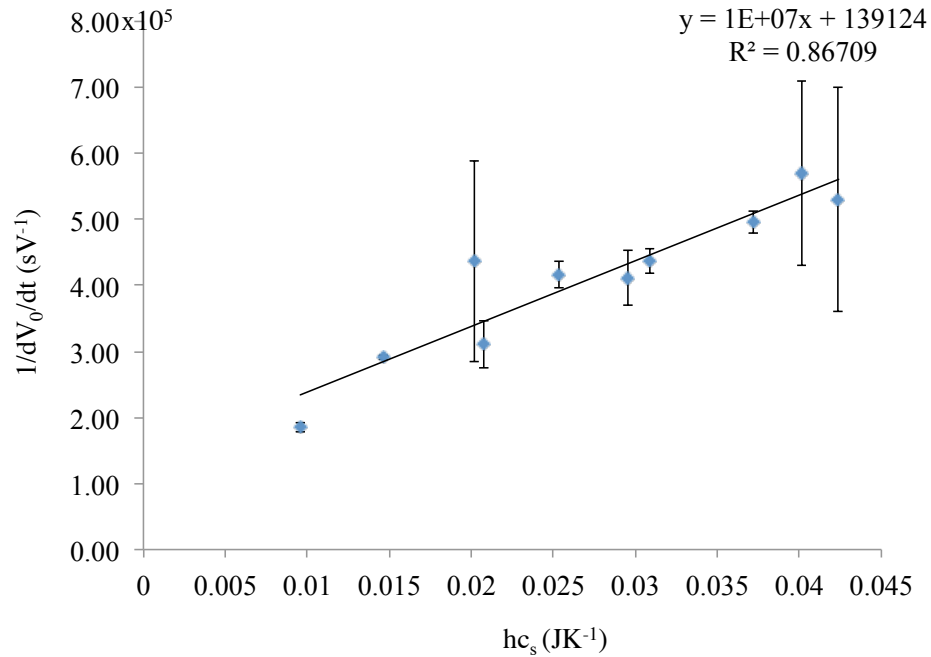
Figure 5.4 Relationship between heat capacity of silver blocks (hc_s) and the mean (n=3 for each block) inverse rate of thermopile cooling ($1/dV_0/dt$). Error bars show standard deviation.

The gradient of the line (m) is given by $ITn^2\alpha^2$, where I (Amperes) is the current passed through the thermopile, T is the environmental temperature (K), n is the number of thermocouples in the active region (16 in this thermopile) and α is the Seebeck coefficient ($\mu VK^{-1}couple^{-1}$). Therefore, given that the gradient of the line is m=$1x10^7$ the equation can be used to determine that α=115 $\mu VK^{-1}couple^{-1}$ for this thermopile.

5.2.3 Muscle preparation

Assessment of apparatus function and preliminary data was performed on isolated soleus muscles from young (Age=6 weeks, n=3) and old (Age=100 weeks, n=3) female C57BL/6 mice. Lower limbs were made available to us as excess from another project in the Faculty of Biological Sciences (FBS) that did not utilise this tissue. Animals were housed and maintained according to local requirements and killed by

cervical dislocation, in accordance with the Code of Practice for the humane killing of animals in Schedule 1 of the UK Animals (Scientific Procedures) Act 1986. Skin was removed from the hind limbs and legs removed at the hip joint and placed in chilled (4°C), oxygenated (95% O_2, 5% CO_2) Krebs-Henseleit solution (117mM NaCl, 4.7mM KCl, 2.5mM $CaCl_2$, 1.2mM $MgSO_4$, 24.8mM $NaHCO_3$, 1.2mM KH_2PO_4, 11.1mM $C_6H_{12}O_6$, pH 7.4). Soleus muscles were dissected out leaving the proximal and distal tendons attached. Aluminium foil clips were attached to the ends of the preparation (without damaging the muscle fibres) so that it could be attached to the experimental apparatus.

5.2.4 *Experimental Protocol*

The muscle was mounted onto the thermopile apparatus at approximately resting length and allowed to recover and thermoequilibrate at 37°C for 30 minutes whilst being irrigated with oxygenated Ringer's solution. It was attached at one end to a high-speed length controller (series 305B Aurora Scientific Inc., Ontario, Canada) and the other to a force transducer (model 404, Aurora Scientific, London, Ontario, Canada). Muscle activation was achieved through stimulation *via* platinum wire electrodes with stimuli generated by a muscle stimulator (S48; Grass, W. Warwick, USA) and the current amplified using a stimulus isolation unit (UISO model 236; Hugo Sachs Elektronik, March-Hugstetten, Germany). A series of isometric twitches were performed at a range of muscle lengths (increments varying by 0.5mm) to optimise length. The length at which twitch force was maximal was used in subsequent mechanical measurements, expressed as a measure of fibre length by multiplying by 0.85, known ratio of fibre length:muscle length (Askew & Marsh, 1997), and was

defined as L_0. Tetanic force was not measured in order to prevent the muscle becoming too fatigued to perform cycles of work.

The work loop technique was then used to measure net mechanical power output of the muscle during a series of sinusoidal length changes at cycle frequencies of 1, 3, 5, 7 and 9Hz with a constant length change of ±6% of fibre length (Table 5.2).

Table 5.2 Stimulation parameters for different cycle frequencies, used for both old and young mice

Cycle Frequency (Hz)	Phase* (ms)	Train Duration (ms)
1	-25	470
3	-25	120
5	-20	45
7	-20	30
9	-20	22

*Phase is defined as the time stimulation occurs before peak length.

The soleus muscle from young mice (6 weeks) has previously been shown to be capable of generating net positive power across this range of cycle frequencies (James et al., 1995; Askew and Marsh, 1997). It was expected that the optimum cycle frequency of soleus muscles from old mice would shift to lower cycle frequencies, compared with young mice. However, as no data exist on the performance of soleus muscle from old mice during cyclical contractions from which the event of this shift could be determined, the same frequency range was used for both young and old mice. Initial mechanical efficiency (E_i) was calculated by dividing the total work performed by the muscle (mJ) by the sum of the total work (mJ) and heat produced during the contraction (mJ).

5.3   Results

5.3.1   Basic mechanical properties

All results obtained from experiments with animals are reported in accordance with the ARRIVE guidelines (Kilkenny *et al.*, 2010). Old mice (100 weeks) were on average larger than young mice (6 weeks), with a higher total body mass (Table 5.3). However, the mass of the soleus muscle in young and old mice appears similar. This could indicate a greater relative soleus muscle mass in young mice. Optimum length, L_0 was also similar in old and young mice (Table 5.3).

Table 5.3 Mechanical properties of young and old mouse soleus muscle

Age	6 weeks			100 weeks		
Mouse	1	2	3	1	2	3
Total body mass (g)	20.35	19.06	20.35	31.6	32.6	26.9
Muscle mass (mg)	10.38	9.06	9.85	10.1	12.78	11.77
L_0 (mm)	13.5	11	11.75	11.5	13.5	13.75
P_0 Isometric twitch stress (Ncm^{-2})	57.49	35.52	37.61	24.31	21.03	26.45
Estimated* isometric tetanic stress (Ncm^{-2})	479.07	296.01	313.37	202.56	175.24	220.41
Twitch rise time (ms)	22.2	17.9	14.3	26.3	23.7	25.4
Half relaxation time (ms)	27.1	25.4	23.1	50.7	66.4	57.8

*based on twitch:tetanus ratio of 012 (Askew & Marsh, 1997)

 Isometric twitch and estimated isometric tetanic stress was higher in young mice than in old animals (Table 5.3). The time taken for a twitch to peak (twich rise time) was consistent between young and old mice. However, there was a marked difference in half relaxation time with old mice appearing to take over twice as long to relax after peak force generation compared to young mice (Table 5.3).

5.3.2   Power-frequency relationship

In all the young mouse soleus muscle tested, peak power production occurred at 3Hz with power rapidly declining at frequencies above and below this frequency (Figure 5.5). In old mouse soleus muscle, the peak power production appeared to be at 1Hz,

the lowest frequency studied, with rapid decline in power at frequencies above 1Hz. It is unknown what the optimal cycle frequency for maximum net power generation was in old mouse soleus as frequencies below 1 Hz were not studied. None of the old mouse muscle was capable of generating similar power at 3Hz when compared to the young mice.
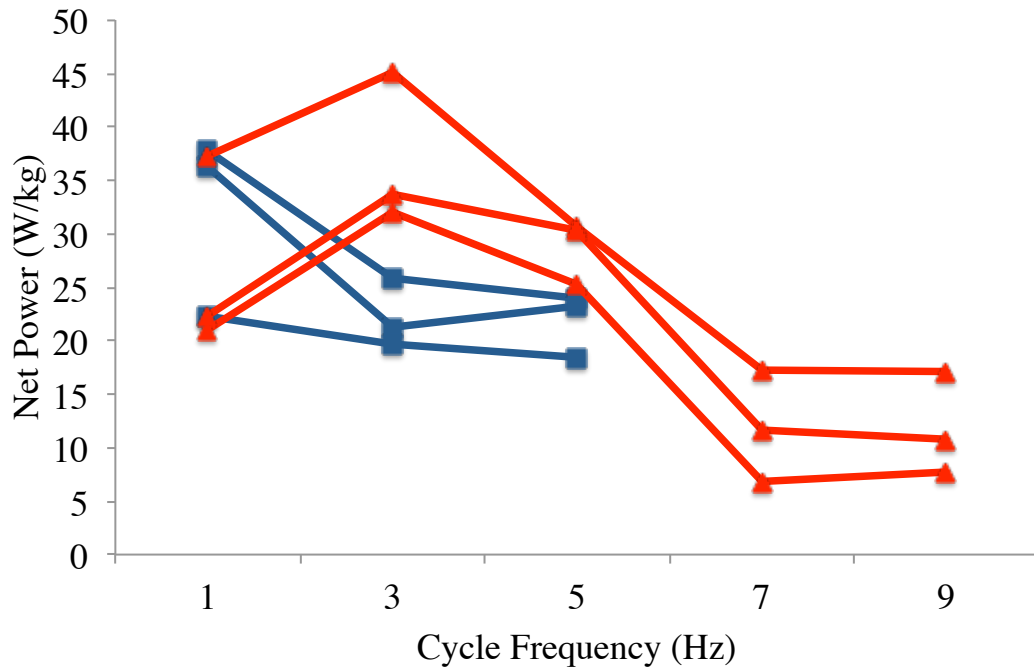
Figure 5.5 Mechanical net power output of soleus muscle from old (100 weeks, blue lines) and young (6 weeks, red lines) mice as a function of cycle frequency.

5.3.3   *Heat production*

The new thermopile apparatus was capable of detecting heat production in skeletal muscle, whereby it was observed that with successive contractions there was sustained heat production (attributed to inefficiencies in the cross bridge cycle) and evidence of continued heat production following cessation of contraction that can be attributed to the recovery processes such as regeneration of ATP (Figure 5.6).
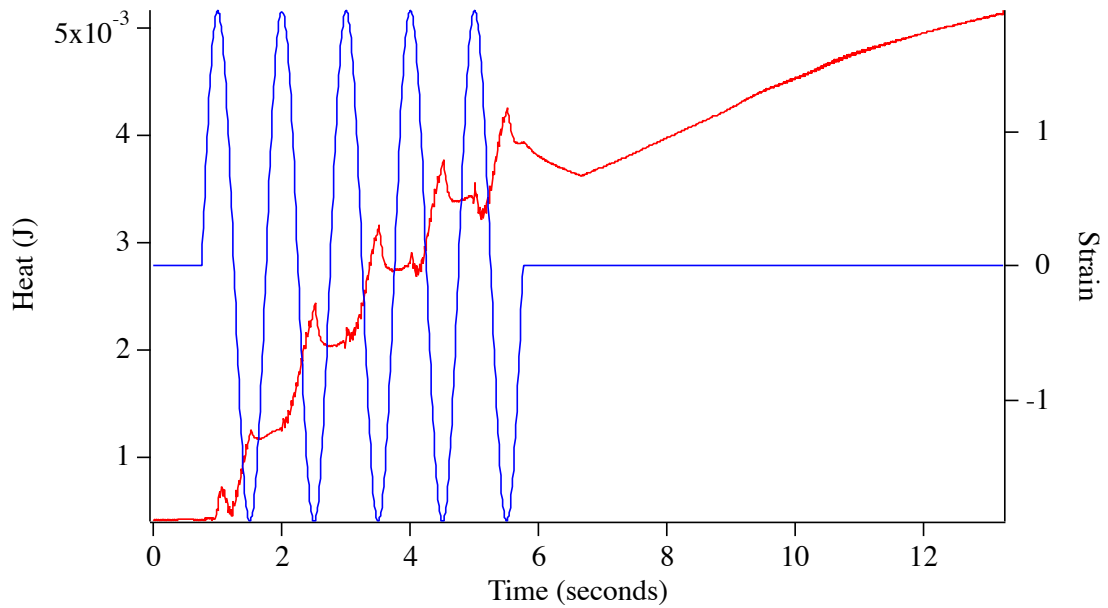
Figure 5.6 Example of heat production (red trace) during cyclical length change (blue trace) in mouse soleus muscle.

5.3.4 Initial mechanical efficiency

A range (1-9Hz) of frequencies were used on the soleus muscle from the young mice. This same range was applied to the soleus muscles from the old mice, however, at the higher cycle frequencies (7 and 9Hz) the muscle was incapable of generating net positive work and power and these data are excluded from the analysis.

Despite the apparent increased power production at a cycle frequency of 1Hz in old soleus muscle, this translates to a similar level of mechanical efficiency at this frequency as observed in young soleus muscle (Figure 5.7).
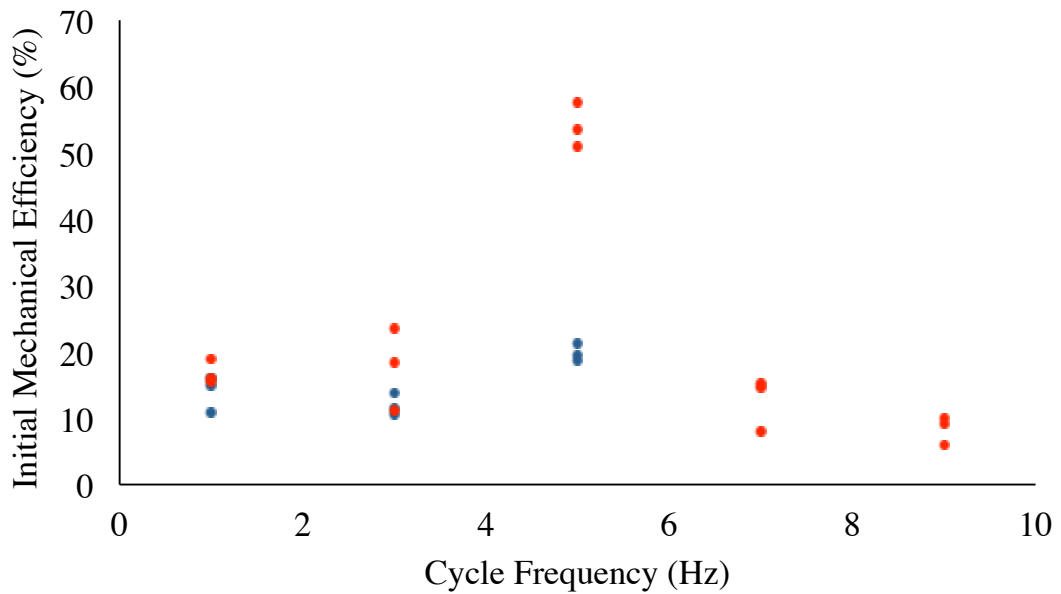
Figure 5.7 Initial mechanical efficiency of old (n=3, blue dots) and young (n=3, red dots) soleus muscle across range of frequencies studied.

There is clearly no overlap between the efficiency of old and young soleus muscle at 5Hz, with young mice demonstrating efficiency as high as 57% (young mouse 1) (Figure 5.7). Efficiency in young muscle is lowest at 9Hz. In old muscle, initial mechanical efficiency is lowest at 3Hz (10.6%, old mouse 3), though this cannot be directly compared to the range of frequencies examined in young muscle as the old soleus muscle did not complete successful cycles at 7 and 9Hz.

5.4   Discussion

Fundamentally, this work represents very preliminary data that was generated primarily to test the functionality of the thermopile apparatus that has been developed. With such low n values (n=3 for old and young mice) and only using female mice, interpretation of the results should be done with caution.

Previous work on mouse soleus muscle has used adult mice, generally defined as aged between 4 and 9 weeks (Table 5.1). The mechanical properties identified in this project (Table 5.3) appear consistent with previously reported values on mice of a similar age to the young mice used here. Holt and Askew (2012) reported a maximum isometric stress of $47.1 Ncm^{-2}$ in mouse soleus muscle. Results of this work found maximum isometric stress to be 35.52, 37.61 and $57.49 Ncm^{-2}$ in each of the young mice. This limited sample number appears to be close to what has been previously observed, though additional replicates would be necessary to make the results more reliable and make proper comparisons.

Preliminary data indicates that this new thermopile apparatus is functioning and capable of measuring heat during muscle contractions. It is important to acknowledge the limited sample size in interpreting the data obtained, however it clearly shows that this set-up is capable of detecting heat production in isolated skeletal muscles.

The observed differences in the power-frequency curve between old and young soleus muscle indicate an age-related shift in power production relative to cycle frequency. This is characterised by old muscle producing more power at 1Hz, whereas young muscle produces more power at 5Hz. This finding could indicate a slowing of the

muscle (Vmax and relaxation), the consequences of which is a reduction in the optimum frequency for power generation. This is because for a given frequency, when the strain is held constant, the shortening velocity represents a higher fraction of the Vmax and because of the force-velocity effects this results in lower forces. Also, the slowing of relaxation means that for a given frequency the muscle will be sub-maximally activated for a greater fraction of the cycle but may also resulted in increased force during relaxation, which reduces net mechanical work.

The increase in power at this frequency in old muscle demonstrates a similar level of efficiency as observed in young mice though young mouse soleus elicits lower power at 1Hz. This suggests that old muscle is relatively more efficient at producing power at 1Hz than young muscle. However, at 5Hz, old mouse soleus muscle is producing marginally less power but at a considerably reduced mechanical efficiency, indicating that at higher frequencies aged muscle is less efficient at producing work. This finding is consistent with changes in muscle phenotype with age towards more slow twitch fibres that will have a lower optimal frequency (Barclay, 1996; He *et al.*, 2000; Barclay & Weber, 2004).

The level of initial efficiency produced in young mouse soleus muscle at 5Hz is similar to that previously reported in adult (6-8 weeks) female mice in earlier work using sinusoidal length changes. However the efficiencies measured at all other cycle frequencies were considerably lower (Barclay, 1994). The higher frequencies used in this study (1-9Hz) are perhaps not optimal for the majority slow-twitch soleus muscle and as such may not be relevant for future study. These differences could also be

attributed to the small sample size in these experiments, and so with additional replicates there may be more consistent results.

Future work using this equipment will involve the assessment of contractile and oxidative recovery efficiency in three age groups of mice, young (6-8 weeks), adult (10-12 months) and old (18-20 months) mice to better ascertain the effects of age on these contractile properties. The cycle frequency range for old soleus muscle should also be extended to incorporate lower cycle frequencies in order to determine the optimum frequency for maximum net power output, allowing initial efficiency to be compared at the optimum frequency for each age group.

Preliminary data suggests that different frequencies will demonstrate differences in contractile efficiency in aged skeletal muscle compared to young, with a shift towards greater efficiency at lower frequencies with increasing age. Future investigations will also be made on mouse lines expressing *RYR1* and *CACNA1S* variants as well as a CASQ1-null mouse model. It is hypothesised that the impaired calcium handling in these strains will have an effect on the contractile efficiency of the muscle, and also on the oxidative recovery efficiency due to the detrimental effect of raised intracellular calcium concentration on mitochondria. The soleus will be used, as in the preliminary study presented here, along with the EDL in order to provide an insight into the comparison between slow and fast-twitch skeletal muscle efficiency alterations with age.

6   General Discussion

The studies presented in this thesis explored muscle ageing and how factors such as calcium handling and mitochondrial function are involved in the manifestation of conditions linked with variants in *RYR1*.

6.1   *The relevance of skeletal muscle development in muscle ageing and myopathic conditions*

The efflux of calcium from the SR is central to the control of skeletal muscle EC coupling. This process is dependent on normal functioning of RyR1 to ensure coordinated calcium release. Calcium is also a key component of muscle development, involved in migration, fusion and differentiation of myoblasts and growth of skeletal muscle (Berchtold *et al.*, 2000; Gehlert *et al.*, 2015). Pathway analysis of Affymetrix array data from skeletal muscle samples (Chapter 3), showed that aspects of the 'development role of HDAC and calcium/calmodulin-dependent kinase (CaMK) in control of skeletal myogenesis' pathway may also be implicated in skeletal muscle ageing and MH. This illustrates the importance of considering components of skeletal muscle development in conjunction with the process of skeletal muscle ageing and manifestation of myopathies. Calmodulin kinase II (CaMKII), part of the CaMK pathway, is also involved in phosphorylation of the RyR1 (Gehlert *et al.*, 2015). CaMKII responds to increased levels of Ca^{2+} ions in the SR (mediated by SERCA), and contributes to phosphorylation of RyR1 increasing channel activity and open probability. It may be relevant to consider the possibility that skeletal muscle ageing is related to the consequences of dysregulation of muscle development.

214

In addition to its crucial role in muscle contraction, more recently, RyR1 has been found to have an important non-contractile role in muscle organ development. This has been established through studying RyR1-null mice and the data shows that mice lacking this protein display differential expression of genes encoding muscle-specific structural and contractile proteins, suggesting that RyR1-mediated calcium signalling is important for normal muscle development and differentiation (Filipova *et al.*, 2016). The next step would be to investigate how models of *RYR1* variants, implicated in MH, might be implicated in the process of muscle development. This could be investigated through using cultured human myoblasts that can be differentiated into myotubes *in vitro*, from patients at the Leeds MH Unit that are MHS and MHN, to determine the impact of *RYR1* variants on muscle cell development and differentiation. It would also be useful to study the muscle structure of the *unc-68* knock-out strain CB540 using the approach used in this thesis to determine if lacking a functional ryanodine receptor has an impact on myosin fibre arrangement.

6.2   Muscle structure in and ageing and myopathic conditions

It is well understood that as humans age there is loss of muscle mass and evidence of compromised muscle structure that leads to impaired muscle function (Faulkner *et al.*, 2007). While there is no direct study of skeletal muscle ultra-structure in humans with *RYR1* variants, there is data to support changes in microscopic structure in mouse lines expressing *RYR1* variants, with the presence of core regions in skeletal muscle that lack mitochondria together with Z-line streaming suggesting disorganisation of sarcomeric structure (Zvaritch *et al.*, 2009; Yuen *et al.*, 2012).

C. elegans lines expressing eight different *unc-68* variants (equivalent to human *RYR1* variants) causative of four human myopathic conditions have been established. All variant strains demonstrated an altered response to halothane compared to the wild-type control, indicating a similar phenotypic response to that observed in humans. This makes them a viable means of studying these conditions in this model system with a view to setting a precedent for further translational research. As the only alteration present in these strains was in *unc-68,* the altered phenotype can be attributed to the presence of the variant. In addition to providing phenotypic characterisation of these strains, the impact of the variants on the muscle structure in these worms was been examined, by crossing the variant strains with a strain expressing gfp-myosin. This has created an additional cohort of *C. elegans* lines that can be used for direct visualisation of muscle fibre arrangement. Results have shown that the progressive disorganisation of nematode muscle, that has been well established in these worms, is also observed in strains expressing *unc-68* variants, but that the onset of fibre disorganisation is earlier (Herndon *et al.*, 2002). Some strains demonstrated disorganisation occurring as early as day 4 of adulthood. This indicates the crucial importance of normal ryanodine receptor function in muscle ageing, and that when a variant in the ryanodine receptor is present it will result in premature ageing of skeletal muscle.

Under normal resting conditions, worms with *unc-68* variants display no discernible differences in normal locomotion. However, with advanced age there is accelerated degeneration of skeletal muscle structure in the variant strains compared to wild-type. This suggests that there could be a consequence of the altered *unc-68* on the maintenance of muscle structure. Future work could test for any effect on calcium

transients in these strains expressing *unc-68* variants to determine if there is a direct involvement of calcium handling on maintenance of muscle structure. Data also indicated greater disorganisation of myosin fibres in the vulva and tail regions compared with the head. This could inform study of *C. elegans* locomotion and suggests that the head region may be subject to enhanced muscle cell development compared to the vulva and tail regions, perhaps because it is of more importance in driving movement of these nematodes. Neuronal control of movement is also relevant in relation to skeletal muscle ageing, though not considered a component of this thesis, the manifestation of action potentials and coordination of muscle contraction by the nervous system is an important factor in skeletal muscle ageing. Mechanisms of neuronal dysregulation could also be easily studied using the *C. elegans* models developed in order to better understand the nervous system's role in muscle ageing.

6.3   *Muscle ageing and quality of life*

The economic impact of an ageing population is characterised by the increased cost of healthcare in older age groups (House of Commons, 2015). A large portion of this assessment involves the cost of treating injuries from falls that result as a consequence of compromised muscle function. This study has shown that *unc-68* variants result in accelerated decline of skeletal muscle structure in *C. elegans,* supporting the notion that muscle calcium homeostasis is important in the ageing process. However, the results are a conservative estimate of muscle structure decline, owing to the necessity for including live worms in analysis. This work has been expanded by a senior research associate and in a new PhD project investigating muscle ageing in *C. elegans.* New work has included assessment of lifespan in the variant strains (Ferreira, Shaw and Hope, unpublished data) as well as analysis of healthspan (Graham, Shaw, Hope,

unpublished data). It will be interesting to ascertain whether worms with these variants have compromised longevity and any alterations in the quality of life, generally characterised by their ability to move towards a food source. This further study will provide information on mechanisms that could have a considerable impact in improving human health. As people are living longer in the 21st century it is imperative that research is carried out to better understand how to improve the healthspan of the ageing population.

6.4 Muscle ageing: a consequence of reduced mobility

The question of why muscle ageing occurs is a key component of understanding sarcopenia. It is clearly a process that involves a number of factors, and research from different perspectives often tries to underpin a principle underlying component. Exercise physiologists have indicated that with the right type of training, the impairments of skeletal muscle function that are characteristic of advancing age can be offset (Short *et al.*, 2004; Broskey *et al.*, 2014). This has led some researchers to suggest that the reason our muscle begins to decline is because humans become less active. This notion implies that there is a conscious choice to move less, or that there is a habitual drive towards inactivity due to people becoming too busy for exercise, they train less and then as a consequence training is uncomfortable. There is clear evidence for decreased muscle protein synthesis with disuse of skeletal muscle (de Boer *et al.*, 2007). Immobilisation can induce anabolic resistance in human myofibrillar protein synthesis (MPS), exemplified by the finding that increasing blood amino acid levels offset this decline in MPS but do not fully reverse it (Glover *et al.*, 2008). Effectively, it is possible to generate an elderly muscle phenotype in young individuals through making them immobile. However, the fact that resistance training

218

or aerobic exercise can offset some of the declines in muscle function observed with age is confounded by the fact that there is evidence to suggest that even elite athletes demonstrate the same rates of muscle power decline as healthy, age-matched, untrained controls (Pearson *et al.*, 2002). This indicates that, even with sustained training and healthy exercise, there are still underlying mechanisms at work that result in skeletal muscle ageing. Evidence from *C. elegans* models also refutes the notion that muscle ageing is the result of reduced mobility. Data in this thesis (Chapter 2) supports pre-existing work that there is steady decline of muscle structure with increasing age yet these animals still move in a wild-type manner.

6.5 *Mitochondrial involvement in muscle ageing and MH*

Loss of mitochondria is a feature of skeletal muscle ageing, a phenomenon that is also a feature of *RYR1* myopathies. Mitochondria produce ATP, which is, along with calcium, central to the energetic capacity of skeletal muscle. It must be produced and readily available for cross-bridge formation and rapidly re-synthesised following contractions. Supply of ATP can be raised through exercise training regimes that results in an increase in muscle performance (Conley, 2016). It has been shown that a decrease in mitochondrial coupling is a factor in the reduced mechanical performance of elderly compared to adult muscle in humans (Conley *et al.*, 2013). This project has evaluated mitochondrial oxidative phosphorylation in human skeletal muscle biopsies. Findings have shown a sex-specific alteration in mitochondrial OXPHOS, characterised by increased oxygen flux with age in complex I of the electron transport chain in males, but decreased flux in with age in females. There is also corresponding data that suggests there is loss of mitochondrial membrane integrity with increasing age in males, thereby reducing the capacity for mitochondria to produce ATP. The

difference between men and women could be related to hormonal differences between the subjects. Indeed, receptors for glucocorticoids, oestrogens, androgens and thyroid hormones have been detected in mitochondria and these receptors may play a role in cell survival and apoptosis (Psarra & Sekeris, 2008).

Results demonstrated altered levels of mitochondrial number in MH skeletal muscle (though not statistically significant), exemplified by a reduction in O_2 flux through complex IV of the electron transport chain. This ties in with skeletal muscle phenotypes that have been observed in mouse models of MH, such as the presence of core regions in the muscle fibres that lack mitochondria (Quane *et al.*, 1994). The reason for these changes in mitochondrial content and OXPHOS capacity remain unclear. They may be attributed to impairment of calcium handling in skeletal muscle. However, in MH muscle these deficiencies in calcium homeostasis are typically evident only in the presence of triggering agents. It would be worthwhile utilising the resource of muscle biopsies at the Leeds MH Unit to investigate mitochondrial OXPHOS in muscle that has been exposed to halothane and caffeine, in order to establish if the mishandling of calcium that is characteristic of MH has a direct impact on ATP production.

The thermopile apparatus that has been developed as part of this project will also provide a new means to investigate the efficiency of ATP generation following muscle contraction. The changes in mitochondrial function that have been characterised in muscle ageing can be examined in the context of muscle work production to determine how these alterations in mitochondrial function impact mechanical performance.

6.6 Calcium handling

Genes encoding proteins involved in calcium handling in skeletal muscle have been investigated in this project (Chapter 3). Expression of both *ORAI1* and *CASQ1* significantly decreases with increasing age. This could reflect involvement of these aspects of the calcium handling apparatus in skeletal muscle ageing. Follow up experiments should examine the consequences of this altered gene expression at the protein level.

Expression of genes involved in calcium handling in mitochondria has also shown changes with age, with decreased expression of *MICU1* and increased expression of *MCU* with increasing age. The next step in understanding the consequences of this altered expression profile is to ascertain protein expression and perhaps examine calcium transients in the mitochondria.

A feature of calcium handling in skeletal muscle that has not been examined in this thesis is the role of SERCA. It is responsible for the reuptake of calcium into the SR during EC coupling in order to bring about muscle relaxation (Rossi & Dirksen, 2006). Impaired calcium handling, leading to aberrant calcium signal transduction is a well reported feature of skeletal muscle disorders (Chemaly *et al.*, 2013). Over-expression of SERCA isoforms has been shown to ameliorate the symptoms of muscular dystrophy as well as preventing the swelling of mitochondria that is associated with this condition (Goonasekera *et al.*, 2011). SERCA pump expression and activity is also shown to be reduced in ageing (Periasamy & Kalyanasundaram, 2007). The action of SERCA is an active process, requiring ATP to pump Ca^{2+} ions against the concentration gradient back into the SR. Therefore, the involvement of mitochondrial

ATP production of obviously key to activity of SERCA. This study has shown altered mitochondrial integrity in MH susceptible skeletal muscle, indicating there is impairment of ATP production. This is likely to have additional consequences on the other active processes in skeletal muscle, such as SERCA. Activity of SERCA has been shown to be inadequate during an MH episode, though this is likely due to the rapid depletion of ATP that occurs because RyR1 remains in an open state and so no matter what Ca^{2+} is taken back up into the SR it will continue to be released (Rosenberg *et al.*, 2015).

6.7 *Fibre type composition in ageing muscle and MH*

This project has not concerned changes in muscle fibre type with age in humans, as the shift in muscle fibre type with age towards a slower fibre type is well characterised (Lexell, 1995). It has also been established that the efficiency of slow muscles is higher compared with fast muscles (Barclay, 1996; Barclay & Weber, 2004). As such it might be reasonable to hypothesise that with age there might be an increase in contractile efficiency accompanied by a reduction in oxidative recovery efficiency. Results in this thesis, using the predominantly slow twitch soleus muscle, demonstrate that there are differences in contractile efficiency across a range of frequencies, with older soleus muscle operating most efficiently at low (1Hz) frequencies while young soleus muscle operates most efficiently at 5Hz. It will be important to supplement these results with study of muscles that express a majority of fast fibres, such as EDL, to understand if there is an effect of age in the efficiency of this muscle fibre type.

The overarching aim of this study was to study skeletal muscle energetics in the context of *RYR1* variants and ageing. This has been achieved through successfully

establishing and charactering *C. elegans* models for myopathic conditions caused by *RYR1* variants and demonstrating that the muscle in these models displays accelerated muscle ageing. It has also highlighted the importance of genes involved in calcium homeostasis, mitochondrial function and other disorders affecting skeletal muscle in muscle ageing and the pathophysiology of MH. A new thermopile apparatus has been developed, providing the means to quantify the efficiency of skeletal muscle function. Preliminary data has demonstrated that there is reduced efficiency in aged mice compared to young. Future work using this apparatus will also involve the study of mouse lines expressing *RYR1* variants and a *CASQ1*-null mutant. This will provide the means to study the involvement of various aspects of calcium handling in skeletal muscle and how they impact muscle efficiency in ageing. Overall, this project has provided a framework for future research in skeletal muscle ageing in the context of *RYR1* variants. Future research will be able to build upon the information gathered in this thesis to expand understanding of the role of calcium handling in muscle ageing as well as utilising differential expression data to better understand the complexity of MH genetics.

References

ADACHI, R. & KAGAWA, H. 2003. Genetic analysis of ryanodine receptor function in Caenorhabditis elegans based on unc-68 revertants. *Molecular Genetic Genomics*, **269**, 806.

ADAMS, B.A., TANABE, T., MIKAMI, A., NUMA, S. & BEAM, K.G. 1990. Intramembrane charge movement restored in dysgenic skeletal muscle by injection of dihydropyridine receptor cDNAs. *Nature*, **346**, 569–572.

AHERN, C.A., VALLEJO, P., MORTENSON, L. & CORONADO, R. 2001. Functional analysis of a frame-shift mutant of the dihydropyridine receptor pore subunit (α 1S) expressing two complementary protein fragments. *BMC Physiology*, **1**, 1–11.

ALIZADEH, A.A., EISEN, M.B., DAVIS, R.E., MA, C., LOSSOS, I.S., ROSENWALD, A., BOLDRICK, J.C., SABET, H., TRAN, T., YU, X., POWELL, J.I., YANG, L., MARTI, G.E., MOORE, T., HUDSON, J., LU, L., LEWIS, D.B., TIBSHIRANI, R., SHERLOCK, G., CHAN, W.C., GREINER, T.C., WEISENBURGER, D.D., ARMITAGE, J.O., WARNKE, R., LEVY, R., WILSON, W., GREVER, M. R., BYRD, J.C., BOTSTEIND, D., BROWN, P.O. & STAUDT, L.M. 2000. Distinct types of diffuse large B-cell lymphoma identified by gene expression profiling. *Nature*, **403**, 503–511.

ALLEN, G.C., LARACH, M.G. & KUNSELMAN, A.R. 1998. The sensitivity and specificity of the caffeine-halothane contracture test: A report from the north american malignant hyperthermia registry. *Anesthesiology*, **88**, 579–588.

ALTUN, Z.F. & HALL, D.H. 2009. Muscle system: Somatic Muscle. *WormAtlas* Available at: http://www.wormatlas.org/hermaphrodite/musclesomatic/MusSomaticframeset.html [Accessed September 9, 2016].

AMARA, C.E., SHANKLAND, E.G., JUBRIAS, S.A., MARCINEK, D.J., KUSHMERICK, M.J. & CONLEY, K.E. 2007. Mild mitochondrial uncoupling impacts cellular aging in human muscles in vivo. *Procedings of the National Academy of Science*, **104**, 1057–1062.

ANDERSSON, D.C., BETZENHAUSER, M.J., REIKEN, S., MELI, A.C., UMANSKAYA, A., XIE, W., SHIOMI, T., ZALK, R., LACAMPAGNE, A. & MARKS, A.R. 2011. Ryanodine receptor oxidation causes intracellular calcium leak and muscle weakness in aging. *Cell Metabolism*, **14**, 196–207.

ARANAKE, A., MASHOUR, G.A. & AVIDAN, M.S. 2013. Minimum alveolar concentration: Ongoing relevance and clinical utility. *Anaesthesia*, **68**, 512–522.

ASKEW, G.N. & MARSH, R.L. 1997. The effects of length trajectory on the mechanical power output of mouse skeletal muscles. *Journal of Experimental Biology*, **200**, 3119–3131.

AZHER, S.N. & JANKOVIC, J. 2005. Camptocormia: pathogenesis, classification, and response to therapy. *Neurology*, **65**, 355–359.

BALABAN, R.S., NEMOTO, S. & FINKEL, T. 2005. Mitochondria, oxidants, and aging. *Cell*, **120**, 483–495.

BALOG, E.M., FRUEN, B.R., SHOMER, N.H. & LOUIS, C.F. 2001. Divergent effects of the malignant hyperthermia-susceptible Arg(615)-->Cys mutation on the Ca(2+) and Mg(2+) dependence of the RyR1. *Biophysical Journal*, **81**, 2050–2058.

BALSA, E., MARCO, R., PERALES-CLEMENTE, E., SZKLARCZYK, R., CALVO, E.,

LANDZURI, M.O. & ENRIQUEZ, J.A. 2012. NDUFA4 is a subunit of complex IV of the mammalian electron transport chain. *Cell Metabolism*, **16**, 378–386.

BARCLAY, C.J. 1994. Efficiency of fast- and slow-twitch muscles of the mouse performing cyclic contractions. *The Journal of Experimental Biology*, **193**, 65–78.

BARCLAY, C.J. 1996. Mechanical efficiency and fatigue of fast and slow muscles of the mouse. *Journal of Physiology*, **497**, 781–794.

BARCLAY, C.J., ARNOLD, P.D. & GIBBS, C.L. 1995. Fatigue and heat production in repeated contractions of mouse skeletal muscle. *The Journal of Physiology*, **488**, 741–752.

BARCLAY, C.J., CONSTABLE, J.K. & GIBBS, C.L. 1993. Energetics of fast- and slow-twitch muscles of the mouse. *The Journal of Physiology*, **472**, 61–80.

BARCLAY, C.J. & WEBER, C.L. 2004. Slow skeletal muscles of the mouse have greater initial efficiency than fast muscles but the same net efficiency. *Journal of Physiology*, **559**, 519–533.

BARCLAY, C.J., WOLEDGE, R.C. & CURTIN, N. A. 2010. Is the efficiency of mammalian (mouse) skeletal muscle temperature dependent? *The Journal of Physiology*, **588**, 3819–3831.

BARRIENTOS, G.C., FENG, W., TRUONG, K., MATTHAEI, K.I., YANG, T., ALLEN, P.D., LOPEZ, J.R. & PESSAH, I.N. 2012. Gene dose influences cellular and calcium channel dysregulation in heterozygous and homozygous T4826I-RYR1 malignant hyperthermia-susceptible muscle. *The Journal of Biological Chemistry*, **287**, 2863–2876.

BAUGHMAN, J.M., PEROCCHI, F., GIRGIS, H.S., PLOVANICH, M., BELCHER-TIMME, C.A., BOGORAD, R.L., KOTELIANSKY, V. & MOOTHA, V.K. 2011. Integrative genomics identifies MCU as an essential component of the mitochondrial calcium uniporter. *Nature*, **476**, 341–345.

BBC NEWS. 2015. SAS selection deaths: Coroner delivers neglect conclusion. *BBCNEWS* Available at: http://www.bbc.co.uk/news/uk-wales-33512416 [Accessed January 16, 2015].

BEARD, N.A., LAVER, D.R. & DULHUNTY, A.F. 2004. Review: Calsequestrin and the calcium release channel of skeletal and cardiac muscle. *Progress in Biophysics and Molecular Biology*, **85**, 33–69.

BELLINGER, A.M., REIKEN, S., DURA, M., MURPHY, P.W., DENG, S.-X., LANDRY, D.W., NIEMAN, D., LEHNART, S.E., SAMARU, M., LACAMPAGNE, A. & MARKS, A.R. 2008. Remodeling of ryanodine receptor complex causes "leaky" channels: a molecular mechanism for decreased exercise capacity. *Proceedings of the National Academy of Sciences of the United States of America*, **105**, 2198–2202.

BEQOLLARI, D., ROMBERG, C.F., FENG, W., LOPEZ, J.R., LAVORATO, M., PERNI, S., HOPKINS, P.M., FRANZINI-ARMSTRONG, C., PESSAH, I.N., ALLEN, P.D., BEAM, K.G. & BANNISTER, R.A. 2015. Calcium channel dysfunction in a mutant mouse model of malignant hyperthermia(CaV1.1 R174W). *Biophysical Journal*, **108**, 504a.

BEQOLLARI, D., ROMBERG, C.F., MEZA, U., PAPADOPOULOS, S. & BANNISTER, R.A. 2014. Differential effects of RGK proteins on L-type channel function in adult mouse skeletal muscle. *Biophysical Journal*, **106**, 1950–1957.

BERCHTOLD, M.W., BRINKMEIER, H. & MUNTENER, M. 2000. Calcium ion in skeletal muscle: its crucial role for muscle function, plasticity and disease. *Physiological Reviews*, **80**, 1215–1265.

BERGSTROM, D.A. & TAPSCOTT, S.J. 2001. Molecular distinction between

specification and differentiation in the myogenic basic helix-loop-helix transcription factor family. *Molecular and Cellular Biology*, **21**, 2404–2412.

BERRIDGE, M.J., LIPP, P. & BOOTMAN, M.D. 2000. The versatility and universality of calcium signalling. *Nature Reviews Molecular Cell Biology*, **1**, 11–21.

BONCOMPAGNI, S., LOY, R.E., DIRKSEN, R.T. & FRANZINI-ARMSTRONG, C. 2010. The I4895T mutation in the type 1 ryanodine receptor induces fiber-type specific alterations in skeletal muscle that mimic premature aging. *Aging Cell*, **9**, 958–970.

BONCOMPAGNI, S., ROSSI, A.E., MICARONI, M., HAMILTON, S.L., DIRKSEN, R.T., FRANZINI-ARMSTRON, C. & PROSAI, F. 2009. Characterization and temporal development of cores in a mouse model of malignant hyperthermia. *Proceedings of the National Academy of Sciences of the United States of America*, **106**, 21996–22001.

BOUCHAMA, A. & KNOCHEL, J.P. 2002. Heat Stroke. *New England Journal of Medicine*, **346**, 1978–1988.

BOYD, W.A., MCBRIDE, S.J., RICE, J.R., SNYDER, D.W. & JONATHAN, H. 2011. A high-throughput method for assessing chemical toxicity using a caenorhabditis elegans reproduction assay. *Toxicology and Applied Pharmacology*, **245**, 153–159.

BRAND, M.D. 2000. Uncoupling to survive? The role of mitochondrial inefficiency in ageing. *Experimental Gerontology*, **35**, 43–49.

BRATIC, I. & TRIFUNOVIC, A. 2010. Mitochondrial energy metabolism and ageing. *Biochimica et Biophysica Acta - Bioenergetics*, **1797**, 961–967.

BREDT, D.S. 2003. Nitric oxide signaling specificity — the heart of the problem. *Journal of Cell Science*, **116**, 9–15.

BRIÈRE, J.-J., FAVIER, J., EL GHOUZZI, V., DJOUADI, F., BÉNIT, P., GIMENEZ, A.-P. & RUSTIN, P. 2005. Succinate dehydrogenase deficiency in human. *Cellular and Molecular Life Sciences*, **62**, 2317–2324.

BRISLIN, R.P. & THEROUX, M.C. 2013. Core myopathies and malignant hyperthermia susceptibility: a review. *Paediatric Anaesthesia*, **23**, 834–841.

BROOKS, S. V. & FAULKNER, J.A. 1988. Contractile properties of skeletal suscles from young adult and aged mice. *The Journal of Physiology*, **404**, 71–82.

BROOME, C.S., KAYANI, A.C., PALOMERO, J., DILLMAN, W.H., MESTRIL, R., JACKSON, M.J. & MCARDLE, A. 2006. Effect of lifelong overexpression of HSP70 in skeletal muscle on age-related oxidative stress and adaptation after nondamaging contractile activity. *The FASEB Journal*, **20**, 1549–1551.

BROSKEY, N.T., GREGGIO, C., BOSS, A., BOUTANT, M., DWYER, A., SCHLUETER, L., HANS, D., GREMION, G., KREIS, R., BOESCH, C., CANTO, C. & AMATI, F. 2014. Skeletal muscle mitochondria in the elderly: Effects of physical fitness and exercise training. *Journal of Clinical Endocrinology and Metabolism*, **99**, 1852–1861.

BROWN, D. 2015. SAS deaths "were a result of catalogue of gross failures by MoD." *The Times* Available at: https://www.thetimes.co.uk/article/sas-deaths-were-a-result-of-catalogue-of-gross-failures-by-mod-9xs9ggw0gvq [Accessed January 17, 2015].

BUCK, E., ZIMAYNI, I., ABRAMSON, J.J. & PESSAH, I.N. 1992. Rynanodine stablizes multiple conformational states of the skeletal muscle calcium release channel. *Journal of Biological Chemistry*, **267**, 23560–23567.

BURKE, G., HILLIER, C., COLE, J., SAMPSON, M., BRIDGES, L., BUSHBY, K., BARRESI, R. & HAMMANS, S.R. 2010. Calpainopathy presenting as foot drop in a 41 year

old. *Neuromuscular Disorders*, **20**, 407–410.

CAMPBELL, K.P., KNUDSON, C.M., IMAGAWA, T., LEUNG, A.T., SUTKO, J.L., KAHL, S.D., RAAB, C.R. & MADSON, L. 1987. Identification and characterization of the high affinity [3H]ryanodine receptor of the junctional sarcoplasmic reticulum Ca2+ release channel. *Journal of Biological Chemistry*, **262**, 6460–6463.

CAPACCHIONE, J.F. & MULDOON, S.M. 2009. The relationship between exertional heat illness, exertional rhabdomyolysis, and malignant hyperthermia. *Anesthesia and Analgesia*, **109**, 1065–1069.

CARGNELLO, M. & ROUX, P.P. 2011. Activation and function of the MAPKs and their tubstrates, the MAPK-activated protein kinases. *Microbiology and Molecular Biology Reviews*, **75**, 50–83.

CARPENTER, D., RINGROSE, C., LEO, V., MORRIS, A., ROBINSON, R.L., HALSALL, P.J., HOPKINS, P.M. & SHAW, M.-A. 2009a. The role of CACNA1S in predisposition to malignant hyperthermia. *BMC Medical Genetics*, 104–114.

CARPENTER, D., ROBINSON, R.L., QUINNELL, R.J., RINGROSE, C., HOGG, M., CASSON, F., BOOMS, P., … HOPKINS, P.M. 2009b. Genetic variation in RYR1 and malignant hyperthermia phenotypes. *British Journal of Anaesthesia*, **103**, 538–548.

CARROLL, J., FEARNLEY, I.M., SKEHEL, J.M., SHANNON, R.J., HIRST, J. & WALKER, J.E. 2006. Bovine complex I is a complex of 45 different subunits. *Journal of Biological Chemistry*, **281**, 32724–32727.

CARSANA, A. 2013. Exercise-induced rhabdomyolysis and stress-induced malignant hyperthermia events, association with malignant hyperthermia susceptibility, and RYR1 gene sequence variations. *The Scientific World Journal*, **2013**, 1–6.

CHAMBERS, J.M., CLEVELAND, W.S., KLEINER, B. & TUKEY, P.A. 1983. Graphical methods for data analysis. *Graphical methods for data analysis*. Wadsworth & Brookes/Cole.

CHANCE, B., LEIGH, J.S., CLARK, B.J., MARIS, J., KENT, J., NIOKA, S. & SMITH, D. 1985. Control of oxidative metabolism and oxygen delivery in human skeletal muscle: a steady-state analysis of the work/energy cost transfer function. *Proceedings of the National Academy of Sciences of the United States of America*, **82**, 8384–8388.

CHELU, M.G., GOONASEKERA, S.A., DURHAM, W.J., TANG, W., LUECK, J.D., RIEHL, J., PESSAH, I.N., ZHANG, P., BHATTACHARJEE, M.B., DIRKSEN, R.T. & HAMILTON, S.L. 2006. Heat- and anesthesia-induced malignant hyperthermia in an RyR1 knock-in mouse. *The FASEB journal : official publication of the Federation of American Societies for Experimental Biology*, **20**, 329–330.

CHEMALY, E.R., BOBE, R., ADNOT, S., HAJJAR, R.J. & LIPSKAIA, L. 2013. Sarco (endo) plasmic reticulum calcium atpases (SERCA) isoforms in the normal and diseased cardiac, vascular and skeletal muscle. *Journal of Cardiovascular Diseases & Diagnosis*, **1**, 1–6.

CHEN, Y.-J., SPENCE, H.J., CAMERON, J.M., JESS, T., ILSLEY, J.L. & WINDER, S.J. 2003. Direct interaction of beta-dystroglycan with F-actin. *Biochemical Journal*, **375**, 329–337.

CHUNG, L. & NG, Y.Y.-C. 2006. Age-related alterations in expression of apoptosis regulatory proteins and heat shock proteins in rat skeletal muscle. *Biochimica et Biophysica Acta (BBA)-Molecular Basis of Disease*, **1762**, 103–109.

CLASON, T., RUIZ, T., SCHAGGER, H., PENG, G., ZICKERMANN, V., BRANDT, U., MICHEL, H. & RADERMACHER, M. 2010. The structure of eukaryotic and prokaryotic complex I. *Journal of Structural Biology*, **169**, 81–88.

CONLEY, K.E. 2016. Mitochondria to motion: optimizing oxidative phosphorylation to improve exercise performance. *The Journal of Experimental Biology*, **219**, 243–249.

CONLEY, K.E., JUBIAS, S.A., AMARA, C.E. & MARCINEK, D.J. 2007. Mitochondrial dysfunction: impact on exercise performance and cellular aging. *Exercise and Sport Medicine Reviews*, **35**, 43–49.

CONLEY, K.E., JUBRIAS, S.A. & ESSELMAN, P.C. 2000. Oxidative capacity and ageing in human muscle. *The Journal of Physiology*, **526**, 203–210.

CONLEY, K.E., JUBRIAS, S. a, CRESS, M.E. & ESSELMAN, P. 2013. Exercise efficiency is reduced by mitochondrial uncoupling in the elderly. *Experimental Physiology*, **98**, 768–777.

COST. 2017. Mitochondrial mapping: Evolution-Age-Gender-Lifestyle-Environment. *European Cooperation in Science and Technology* Available at: http://www.cost.eu/COST_Actions/ca/CA15203 [Accessed April 10, 2017].

CROWDER, C.M., SHEBESTER, L.D. & SCHEDL, T. 1996. Behavioural effects of volatile anesthetics in Caenorhabditis elegans. *Anesthesiology*, **85**, 901–912.

CSORDAS, G., GOLENAR, T., SEIFERT, E.L., KAMER, K.J., SANCAK, Y., PEROCCHI, F., MOFFAT, C., WEAVER, D., PEREZ, S.F., BOGORAD, R., KOTELIANSKY, V., ADIJANTO, J., MOOTHA, V.K. & HAJNICZKY, G. 2013. MICU1 controls both the threshold and cooperative activation of the mitochondrial Ca2+ uniporter. *Cell Metabolism*, **17**, 976–987.

CULLY, T.R. & LAUNIKONIS, B.S. 2016. Leaky ryanodine receptors delay the activation of store overload-induced Ca2+ release, a mechanism underlying malignant hyperthermia-like events in dystrophic muscle. *Americal Journal of Physiology-Cell Physiology*, **310**, C673–C680.

CURTIN, N. a, CLAPHAM, J.C. & BARCLAY, C.J. 2002. Excess recovery heat production by isolated muscles from mice overexpressing uncoupling protein-3. *The Journal of Physiology*, **542**, 231–235.

CUTHBERTSON, D., SMITH, K., BABRAJ, J., LEESE, G., WADDELL, T., ATHERTON, P., WACHERHAGE, H., TAYLOR, P.M. & RENNIE, M.J. 2005. Anabolic signaling deficits underlie amino acid resistance of wasing, aging muscle. *The FASEB Journal*, **19**, 422–424.

D'ADAMO, M.C., IMBRICI, P., SPONCICHETTI, F. & PESSIA, M. 1999. Mutations in the KCNA1 gene associated with episodic ataxia type-1 syndrome impair heteromeric voltage-gated K+ channel function. *The FASEB Journal*, **13**, 1335–1345.

DAINESE, M., QUARTA, M., LYFENKO, A.D., PAOLINI, C., CANATO, M., REGGIANI, C., DIRKSEN, R.T. & PROTASI, F. 2009. Anesthetic- and heat-induced sudden death in calsequestrin-1-knockout mice. *The FASEB Journal*, **23**, 1710–1720.

DAURY, L., BUSSON, M., TOURKINE, N., CASAS, F., CASSAR-MALEK, I., WRUTNIAK-CABELLO, C., CASTELLAZZI, M. & CABELLO, G. 2001. Opposing functions of ATF2 and Fos-like transcription factors in c-Jun-mediated myogenin expression and terminal differentiation of avian myoblasts. *Oncogene*, **20**, 7998–8008.

DAVIS, M., BROWN, R., DICKSON, A., HORTON, H., JAMES, D., LAING, N., MARSTON, R., NORGATE, M., PERLMAN, D., POLLOCK, N. & STOWELL, K. 2002. Malignant hyperthermia associated with exercise-induced rhabdomyolysis or congenital abnormalities and a novel RYR1 mutation in New Zealand and Australian pedigrees. *British Journal of Anaesthesia*, **88**, 508–515.

DAVIS, M.R., HAAN, E., JUNGBLUTH, H., SEWRY, C., NORTH, K., MUNTONI, F., KUNTZER, T., LAMONT, P., BANKIER, A., TOMLINSON, P., SANCHEZ, A., WALSH,

P., NAGARAJAN, L., OLEY, C., COLLEY, A., GEDEON, A., QUINLIVAN, R., DIXON, J., HAMES, D., MULLER, C.R. & LAING, N.G. 2003. Principal mutation hotspot for central core disease and related myopathies in the C-terminal transmembrane region of the RYR1 gene. *Neuromuscular Disorders*, **13**, 151–157.

DE BOER, M.D., SELBY, A., ATHERTON, P., SMITH, K., SEYNNES, O.R., MAGANARIS, C.N., MAFFULLI, N., MOVIN, T., NARICI, M. V & RENNIE, M.J. 2007. The temporal responses of protein synthesis, gene expression and cell signalling in human quadriceps muscle and patellar tendon to disuse. *The Journal of Physiology*, **585**, 241–251.

DE MAGALHÃES, J.P., CURADO, J. & CHURCH, G.M. 2009. Meta-analysis of age-related gene expression profiles identifies common signatures of aging. *Bioinformatics*, **25**, 875–881, 10.1093/bioinformatics/btp073.

DELBONO, O. 2002. Molecular mechanisms and therapeutics of the deficit in specific force in ageing skeletal muscle. *Biogerontology*, **3**, 265–270.

DELBONO, O., O'ROURKE, K.S. & ETTINGER, W.H. 1995. Excitation-calcium release uncoupling in aged single human skeletal muscle fibres. *Journal of Membrane Biology*, **148**, 211–222.

DENBOROUGH, M.A., FOSTER, J.F.A., LOVELL, R.R.H., MAPLESTONE, P.A. & VILLIERS, J.D. 1962. Anaesthetic deaths in a family. *British Journal of Anaesthesia*, **34**, 395–396.

DIRKSEN, R.T. & AVILA, G. 2002. Altered ryanodine receptor function in central core disease: leaky or uncoupled Ca(2+) release channels? *Trends in Cardiovascular Medicine*, **12**.

DIRKSEN, R.T. & AVILA, G. 2004. Distinct effects on Ca2+ handling caused by malignant hyperthermia and central core disease mutations in RyR1. *Biophysical Journal*, **87**, 3193–3204.

DOHERTY, T.J. 2003. Aging and sarcopenia. *Journal of Applied Physiology*, **4**, 1717–1727.

DOLPHIN, A.C. 1999. L-type calcium channel modulation. *Advances in Second Messenger and Phosphoprotein Research*, **33**, 153–177.

DOS REMEDIOS, C.G., LIEW, C.C., ALLEN, P.D., WINSLOW, R.L., VAN EYK, J.E. & DUNN, M.J. 2003. Genomics, proteomics and bioinformatics of human heart failure. *Journal of Muscle Research and Cell Motility*, **24**, 251–260.

DRISCOLL, M. & YU, S.M. 2011. EGF Signalling comes of age: promotion of healthy aging in C. elegans. *Experimental Gerontology*, **46**, 129–134.

DUBOWITZ, V. & PEARSE, A.G. 1960. Oxidative enzymes and phosphorylase in central-core disease of muscle. *Lancet*, **2**, 23–24.

DUKE, A.M., HOPKINS, P.M., CALAGHAN, S.C., HALSALL, J.P. & STEELE, D.S. 2010. Store-operated calcium entry in malignant hyperthermia-susceptible human skeletal muscle. *Journal of Biological Chemistry*, **285**, 25645.

DURHAM, W.J., ARACENA-PARKS, P., LONG, C., ROSSIE, A.E., GOONASEKERA, S.A., BONCOMPAGNI, S., GALVAN, D.L., GILMAN, C.P., BAKER, M., SHIROKOVA, N., PROTASI, F., DIRKSEN, R. & HAMILTON, S.L. 2008. RyR1 s-nitrosylation underlies environmental heat stroke and sudden death in Y522S RyR1 knock-in mice. *Cell*, **133**, 53–65.

EFREMOV, R.G., LEITNER, A., AEBERSOLD, R. & RAUNSER, S. 2015. Architecture and conformational switch mechanism of the ryanodine receptor. *Nature*, **517**, 39–43.

EISNER, V., CSORDAS, G. & HAJNOCZKY, G. 2013. Interactions between sarco-endoplasmic reticulum and mitochondria in cardiac and skeletal muscle - pivotal

roles in Ca(2)(+) and reactive oxygen species signaling. *Journal of Cell Ccience*, **126**, 2965–2978.

ELLIS, F.R., KEANEY, N.P., HARRIMAN, D.G., KYEI-MENSAH, K. & TYRRELL, J.H. 1972. Screening for malignant hyperpyrexia. *British Medical Journal*, **3**, 559–561.

ELTIT, J.M., BANNISTER, R.A., MOUA, O., ALTAMIRANO, F., HOPKINS, P.M., PESSAH, I.N., MOLINSKI, T.F., LÓPEZ, J.R., BEAM, K.G. & ALLEN, P.D. 2012. Malignant hyperthermia susceptibility arising from altered resting coupling between the skeletal muscle L-type Ca2+ channel and the type 1 ryanodine receptor. *Proceedings of the National Academy of Sciences of the United States of America*, **109**, 7923–7928.

EMHG. 2016. European malignant hyperthermia group: Causative RYR1 mutations Available at: http://www.emhg.org/genetics/mutations-in-ryr1/ [Accessed September 23, 2016].

ENGLAND, J. & LOUGHNA, S. 2013. Heavy and light roles: Myosin in the morphogenesis of the heart. *Cellular and Molecular Life Sciences*, **70**, 1221–1239.

ESTÈVE, E., ELTIT, J.M., BANNISTER, R.A., LIU, K., PESSAH, I.N., BEAM, K.G., ALLEN, P.D. & LÓPEZ, J.R. 2010. A malignant hyperthermia–inducing mutation in RYR1 (R163C): alterations in Ca2+ entry, release, and retrograde signaling to the DHPR. *The Journal of General Physiology*, **135**, 619–628.

FABER, P.W., ALTER, J.R., MACDONALD, M.E. & HART, A.C. 1999. Polyglutamine-mediated dysfunction and apoptotic death of a Caenorhabditis elegans sensory neuron. *Proceedings of the National Academy of Sciences*, **96**, 179–184.

FALK, M.J., KAYSER, E.B., MORGAN, P.G. & SEDENSKY, M.M. 2006. Mitochondrial complex I function modulates volatile anesthetic sensitivity in C. elegans. *Current Biology*, **16**, 1641–1615.

FAULKNER, J.A., LARKIN, L.M., CLAFLIN, D.R. & BROOKS, S. V. 2007. Age-related changes in the structure and function of skeletal muscles. *Clinical and Experimental Pharmacology and Physiology*, **34**, 1091–1096.

FENG, H., CRAIG, H.L. & HOPE, I.A. 2012. Expression pattern analysis of regulatory transcription factors in Caenorhabditis elegans. *In* Deplancke, B. & Gheldof, N., eds. *Gene Regulatory Networks: Methods and Protocols, Methods in Molecular Biology*. Springer Science and Business Media, 23–50.

FERGUSON-MILLER, S., HISER, C. & LIU, J. 2012. Gating and regulation of the cytochrome c oxidase proton pump. *Biochimica et Biophysica Acta*, **1817**, 489–494.

FERREIRO, A., MONNIER, N., ROMERO, N.B., LEROY, J.P., BONNEMANN, C., HAENGGELI, C.A., STRAUB, V., VOSS, W.D., NIVOCHE, Y., JUNGBLUTH, H., LEMAINQUE, A., VOIT, T., LUNARDI, J., FARDEAU, M. & GUICHENEY, P. 2002. A recessive form of central core disease, transiently presenting as multi-minicore disease, is associated with a homozygous mutation in the ryanodine receptor type 1 gene. *Annals of Neurology*, **51**, 750–759.

FESKE, S. 2007. Calcium signalling in lymphocyte activation and disease. *Nature Review of Immunology*, **7**, 690–702.

FESKE, S., GWACK, Y., PRAKRIYA, M., SRIKANTH, S., PUPPEL, S.H., TANASA, B., HOGAN, P.G., LEWIS, R.S., DALY, M. & RAO, A. 2006. A mutation in Orai1 causes immune deficiency by abrogating CRAC channel function. *Nature*, **441**, 179–185.

FILIPOVA, D., WALTER, A.M., GASPAR, J.A., BRUNN, A., LINDE, N.F., ARDESTANI,

M.A., DE, M., HESCHELER, J. & PFITZER, G. 2016. Gene profiling of embryonic skeletal muscle lacking type I ryanodine receptor Ca 2 + release channel. 1–14.

FILL, M. & COPELLO, J.A. 2002. Ryanodine receptor calcium release channels. *Physiological Reviews*, **82**, 893–922.

FINKEL, T., MENAZZA, S., HOLMSTRÖM, K.M., PARKS, R.J., LIU, J., SUN, J., LIU, J., PAN, X. & E., M. 2015. The ins and outs of mitochondrial calcium. *Circulation Research*, **116**, 1810–1819.

FISHER, J., PITERMAN, N., HUBBARD, E.J., STERN, M.J. & HAREL, D. 2005. Computational insights into Caenorhabditis elegans vulval development. *Proceedings of the National Academy of Sciences*, **102**, 1951–1956.

FISZER, D., SHAW, M.-A., FISHER, N.A., CARR, I.M., GUPTA, P.K., WATKINS, E.J., ROIZ DE SA, D., KIM, J.H. & HOPKINS, P.M. 2015. Next generation sequencing of RYR1 and CACNA1S in malignant hyperthermia and exertional heat illness. *Anesthesiology*, **122**, 1033–1046.

FITTIPALDI, S., DIMAURO, I., MERCATELLI, N. & CAPOROSSI, D. 2014. Role of exercise-induced reactive oxygen species in the modulation of heat shock protein response. *Free Radical Research*, **48**, 52–70.

FITTS, R.H. 2008. The cross-bridge cycle and skeletal muscle fatigue. *Journal of applied physiology*, **104**, 551–558.

FONG, A.P. & TAPSCOTT, S.J. 2013. Skeletal muscle programming and re-programming. *Current opinion in genetics & development*, **23**, 568–573.

FREZZA, C., CIPOLAT, S. & SCORRANO, L. 2007. Organelle isolation: functional mitochondria from mouse liver, muscle and cultured fibroblasts. *Nature protocols*, **2**, 287–295.

FRICKE, B., LINTS, R., STEWART, G., DRUMMOND, H., DODT, G., DRISCOLL, M. & VON DURING, M. 2000. Epithelial Na+ channels and stomatin are expressed in rat trigeminal mechanosensory neurons. *Cell and Tissue Research*, **299**, 327–334.

GARIGAN, D., HSU, A.L., FRASER, A.G., KAMATH, R.S., ABRINGET, J. & KENYON, C. 2002. Genetic analysis of tissue aging in Caenorhabditis elegans: A role for heat-shock factor and bacterial proliferation. *Genetics*, **161**, 1101–1112.

GEHLERT, S., BLOCH, W. & SUHR, F. 2015. Ca2+ dependent regulations and signaling in skeletal muscle: from electro-mechanical coupling to adaptation. *International Journal of Molecular Sciences*, **16**, 1066–1095.

GENAGE. 2013. NFKB1 (Homo sapiens) Available at: http://genomics.senescence.info/genes/entry.php?hgnc=NFKB1 [Accessed November 12, 2013].

GENE CARDS. 2013. MICU1: mitochondrial calcium uptake 1 Available at: http://www.genecards.org/cgi-bin/carddisp.pl?gene=MICU1 [Accessed October 13, 2013].

GIULIVI, C., ROSS-INTA, C., OMANSKA-KLUSEK, A., NAPOLI, E., SAKAGUCHI, D., BARRIENTOS, G., ALLEN, P.D. & PESSAH, I.N. 2011. Basal bioenergetic abnormalities in skeletal muscle from ryanodine receptor malignant hyperthermia-susceptible R163C knock-in mice. *The Journal of Biological Chemistry*, **286**, 99–113.

GLANCY, B., WILLIS, W.T., CHESS, D.J. & BALABAN, R.S. 2013. Effect of calcium on the oxidative phosphorylation cascade in skeletal muscle mitochondria. *Biochemistry*, **52**, 2793–2809.

GLASS, D., VIÑUELA, A., DAVIES, M.N., RAMASAMY, A., PARTS, L., KNOWLES, D., BROWN, A.A., … SPECTOR, T.D. 2013. Gene expression changes with age in skin, adipose tissue, blood and brain. *Genome Biology*, **14**, R75–R75.

GLATT, S.J., EVERALL, I.P., KREMEN, W.S., CORBEIL, J., ŠÁŠIK, R., KHANLOU, N., HAN, M., LIEW, C.-C. & TSUANG, M.T. 2005. Comparative gene expression analysis of blood and brain provides concurrent validation of SELENBP1 up-regulation in schizophrenia. *Proceedings of the National Academy of Sciences of the United States of America*, **102**, 15533–15538.

GLENN, C., CHOW, D., DAVID, L., COOKE, C., GAMI, M., ISER, W., HANSELMAN, K., GOLDBERG, I. & WOLKOW, C. 2004. Behavioural deficits during early stages of aging in Caenorhabditis elegans result from locomotory deficits possibly linked to muscle frailty. *The Journals of Gerontology Series A: Biological Sciences and Medical Sciences*, **59A**, 1251–1260.

GLOVER, E.I., PHILLIPS, S.M., OATES, B.R., TANG, J.E., TARNOPOLSKY, M. a, SELBY, A., SMITH, K. & RENNIE, M.J. 2008. Immobilization induces anabolic resistance in human myofibrillar protein synthesis with low and high dose amino acid infusion. *The Journal of Physiology*, **586**, 6049–6061.

GNAIGER, E. 2013. Cytochrome c control factor. *Bioblast* Available at: http://www.bioblast.at/index.php/Cytochrome_c_control_factor [Accessed August 6, 2016].

GNAIGER, E. 2014. Flux control ratio. *Bioblast* Available at: http://www.bioblast.at/index.php/Flux_control_ratio [Accessed August 6, 2016].

GOEMAN, J.J. 2010. L1 penalized estimation in the Cox proportional hazards model. *Biometrics journal*, **52**, 70–84.

GOONASEKERA, S. a, LAM, C.K., MILLAY, D.P., SARGENT, M. a, HAJJAR, R.J., KRANIAS, E.G. & MOLKENTIN, J.D. 2011. Mitigation of muscular dystrophy in mice by SERCA overexpression in skeletal muscle. *Journal of Clinical Investigation*, **121**, 1044–1052, 10.1172/JCI43844DS1.

GORDON, A.M., HUXLEY, A.F. & JULIAN, F.J. 1966. The variation in isometric tension with sarcomere length in vertebrate muscle fibres. *The Journal of Physiology*, **184**, 170–192.

GÖRLACH, A., BERTRAM, K., HUDECOVA, S. & KRIZANOVA, O. 2015. Calcium and ROS: A mutual interplay. *Redox Biology*, **6**, 260–271.

GUELLICH, A., NEGRONI, E., DECOSTRE, V., DEMOULE, A. & COIRAULT, C. 2014. Altered cross-bridge properties in skeletal muscle dystrophies. *Frontiers in Physiology*, **5**, 1–9.

HALSALL, P.J., CAIN, P.A. & ELLIS, F.R. 1979. Retrospective analysis of anaesthetics received by patients before susceptibility to malignant hyperpyrexia was recognized. *British Journal of Anaesthesia*, **51**, 949–954.

HAMADA, T., SAKUBE, Y., AHNN, J., KIM DO, H. & KAGAWA, H. 2002. Molecular dissection, tissue localization and Ca2+ binding of the ryanodine receptor of Caenorhabditis elegans. *Journal of Molecular Biology*, **324**, 123–135.

HARRINGTON, L.A. & HARLEY, C.B. 1988. Effect of vitamin E on lifespan and reproduction in Caenorhabditis elegans. *Mechanisms of Ageing and Development*, **43**, 71–78.

HART, J.D. & DULHUNTY, A.F. 2000. Nitric oxide activates or inhibits skeletal muscle ryanodine receptors depending on its concentration, membrane potential and ligand binding. *Journal of Membrane Biology*, **173**, 227–236.

HARTMAN, P.S. 1987. Caffeine Resistant Mutants of Caenorhabditis elegans. *Genetical Research*, **49**, 105–110.

HARTMAN, P.S., ISHII, N., KAYSER, E.B., MORGAN, P.G. & SEDENSKY, M.M. 2001. Mitochondrial mutations differentially affect aging, mutability and anesthetic sensitivity in Caenorhabditis elegans. *Mechanisms of Ageing and Development*,

122, 1187–1201.

HAYASHI, Y., SAWA, Y., NISHIMURA, M., FUKUYAMA, N., ICHIKAWA, H., OHTAKE, S., NAKAZAWA, H. & MATSUDA, H. 2004. Peroxynitrite, a product between nitric oxide and superoxide anion, plays a cytotoxic role in the development of post-bypass systemic inflammatory response. *European Journal of Cardio-thoracic Surgery*, **26**, 276–280.

HE, F. 2011. Making males of C. elegans. *Bio-protocol*, e58.

HE, Z., BOTTINELLI, R., PELLEGRINO, M.A., FERENCZI, M.A. & REGGIANI, C. 2000. ATP consumption and efficiency of human single muscle fibers with different myosin isoform composition. *Biophysical journal*, **79**.

HERNDON, L.A., SCHMEISSNER, P.J., DUDARONEK, J.M., BROWN, P.A., LISTNER, K.M., SAKANO, Y., PAUPARD, M.C., HALL, D.H. & DRISCOLL, M. 2002. Stochastic and genetic factors influence tissue-specific decline in ageing C. elegans. *Nature*, **419**, 808–814.

HODGKIN, J. 2015. Wormbase: UNC-68. *Wormbase: UNC-68* Available at: http://www.wormbase.org/species/c_elegans/gene/WBGene00006801#0-9e-3.

HOLT, N.C. & ASKEW, G.N. 2012. The effects of asymmetric length trajectories on the initial mechanical efficiency of mouse soleus muscles. *Journal of Experimental Biology*, **215**, 324–330.

HOPKINS, P.M. 2007. Is there a link between malignant hyperthermia and exertional heat illness? *British Journal of Sports Medicine*, **41**, 283–284.

HOPKINS, P.M. 2000. Malignant hyperthermia: advances in clinical management and diagnosis. *British Journal of Anaesthesia*, **85**, 118–128.

HOPKINS, P.M., ELLIS, F.R. & HALSALL, P.J. 1991. Evidence for related myopathies in exertional heat stroke and malignant hyperthermia. *Lancet*, **338**, 1491–1492.

HORINOUCHI, T., HIGASHI, T., HIGA, T., HARADA, T. & MIWA, S. 2012. Different binding property of STIM1 and its novel splice variant STIM1L to Orai1, TRPC3 and TRPC6 channels. *Biochemical and Biophysical Research Communications*, **428**, 252–258.

HOUSE OF COMMONS. 2015. Key issues for the new Parliament 2015 Available at: http://www.parliament.uk/business/publications/research/key-issues-parliament-2015/ [Accessed December 9, 2015].

HUANG, D.W., SHERMAN, B.T. & LEMPICKI, R.A. 2008. Systematic and integrative analysis of large gene lists using DAVID bioinformatics resources. *Nature Protocols*, **4**, 44–57.

HUGHES, V.A., FRONTERA, W.R., WOOD, M., EVANS, W.J., DALLAL, G.E., ROUBENOFF, R. & FIATARONE SINGH, M.A. 2001. Longitudinal muscle strength changes in older adults: influence of muscle mass, physical activity, and health. *The Journals of Gerontology Series A: Biological Sciences and Medical Sciences*, **56**, 209–217.

HWANG, C.Y., KIM, K., CHOI, J.Y., BAHN, Y.J., LEE, S.M., KIM, Y.K., LEE, C. & KWON, K.S. 2014. Quantitative proteome analysis of age-related changes in mouse gastrocnemius muscle using mTRAQ. *Proteomics*, **14**, 121–132.

IOSSA, S., MOLLICA, M.P., CRESCENZO, R. & TASSO, R. 2004. Efficiency and age-induced insulin resistance. *Diabetes*, **53**, 2861–2866.

JAMES, R.S., ALTRINGHAM, J.D. & GOLDSPINK, D.F. 1995. The mechanical properties of fast and slow twitch muscles of the mouse in relation to their locomotory function. *Journal of Experimental Biology*, **198**.

JAMES, R.S., WILSON, R.S. & ASKEW, G.N. 2004. Effects of caffeine on mouse skeletal muscle power output during recovery from fatigue. *Journal of Applied*

Physiology, **96**, 545–552.

JIMENEZ-MORENO, R., WANG, Z., GERRING, R.C. & DELBONO, O. 2008. Sarcoplasmic reticulum calcium release declines in muscle fibres from aging mice. *Biophysical Journal*, **94**, 3178–3188.

JINEK, M., CHYLINSKI, K., FONFARA, I., HAUER, M., DOUDNA, J.A. & CHARPENTIER, E. 2012. A programmable dual-RNA – guided DNA endonuclease in adaptive bacterial immunity. *Science*, **337**, 816–822.

JOHANNSEN, D.L., CONLEY, K.E., BAJPEYI, S., PUNYANITYA, M., GALLAGHER, D., ZHANG, Z., COVINGTON, J., SMITH, S.R. & RAVUSSIN, E. 2012. Ectopic lipid accumulation and reduced glucose tolerance in elderly adults are accompanied by altered skeletal muscle mitochondrial activity. *The Journal of Clinical Endocrinology and Metabolism*, **97**, 242–250.

JOSEPHSON, D. 1985. Mechanical power output from striated-muscle during cyclic contraction. *Journal of Experimental Biology*, **114**, 493–512.

JOZSI, A.C., DUPONT-VERSTEEGDEN, E.E., TAYLOR-JONES, J.M., EVANS, W.J., TRAPPE, T.A., CAMPBELL, W.W. & PETERSON, C.A. 2000. Aged human muscle demonstrates an altered gene expression profile consistent with an impaired response to exercise. *Mechanisms of Ageing and Development*, **120**, 45–56.

JUNGBLUTH, H. 2007. Central core disease. *Orphanet Journal of Rare Diseases*, **2**, 1–9, 10.1186/1750-1172-2-25.

JUNGBLUTH, H., DAVIS, M.R., MULLER, C., COUNSELL, S., ALLSOP, J., CHATTOPADHYAY, A., MESSINA, S., MERCURI, E., LAING, N.G., SEWRY, C.A., BYDDER, G. & MUNTONI, F. 2004. Magnetic resonance imaging of muscle in congenital myopathies associated with RYR1 mutations. *Neuromuscular Disorders*, **14**.

JUNGBLUTH, H., LILLIS, S., ZHOU, H., ABBS, S., SEWRY, C., SWASH, M. & MUNTONI, F. 2009. Late-onset axial myopathy with cores due to a novel heterozygous dominant mutation in the skeletal muscle ryanodine receptor (RYR1) gene. *Neuromuscular Disorders*, **19**, 344–347.

JUNGBLUTH, H., MULLER, C.R., HALLIGER-KELLER, B., BROCKINGTON, M., BROWN, S.C., FENG, L., CHATTOPADHYAY, A., MESSINA, S., MERCURI, E., LAING, N.G., SEWRY, C.A., BYDDER, G. & MUNTONI, F. 2002. Autosomal recessive inheritance of RYR1 mutations in a congenital myopathy with cores. *Neurology*, **59**.

KALETTA, T. & HENGARTNER, M.O. 2006. Finding function in novel targets: C. elegans as a model organism. *Nature Reviews Drug Discovery*, **5**, 387–399.

KATIKI, L.M., FERREIRA, J.F.S., ZAJAC, A.M., MASLER, C., LINDSAY, D.S., CHAGAS, A.C.S. & AMARANTE, A.F.T. 2011. Caenorhabditis elegans as a model to screen plant extracts and compounds as natural anthelmintics for veterinary use. *Veterinary Parasitology*, **182**, 264–268.

KAYO, T., ALLISON, D.B., WEINDRUCH, R. & PROLLA, T.A. 2001. Influences of aging and caloric restriction on the transcriptional profile of skeletal muscle from rhesus monkeys. *Proceedings of the National Academy of Sciences*, **98**, 5093–5098.

KAYSER, E.-B., MORGAN, P.G. & SEDENSKY, M.M. 2004. Mitochondrial complex I function affects halothane sensitivity in Caenorhabditis elegans. *Anesthesiology*, **101**, 365–372.

KAYSER, E.B., HOPPEL, C.L., MORGAN, P.G. & SEDENSKY, M.M. 2003. A mutation in mitochondrial complex I increases ethanol sensitivity in Caenorhabditis elegans. *Alcoholism: Clinical and Experimental Research*, **27**, 584–592.

KAYSER, E.B., MORGAN, P.G., HOPPEL, C.L. & SEDENSKY, M.M. 2001.

Mitochondrial expression and function of GAS-1 in Caenorhabditis elegans. *Journal of Biological Chemistry*, **276**, 20551–20558.

KAYSER, E.B., MORGAN, P.G. & SEDENSKY, M.M. 1999. GAS-1: A mitochondrial protein controls sensitivity to volatile anesthetics in the nematode Caenorhabditis elegans. *Anesthesiology*, **90**, 545–554.

KILKENNY, C., BROWNE, W.J., CUTHILL, I.C., EMERSON, M. & ALTMAN, D.G. 2010. Improving Bioscience Research Reporting: The ARRIVE Guidelines for Reporting Animal Research. *PLoS Biology*, **8**, e1000412, 10.1371/journal.pbio.1000412.

KIM, U. JIN, SHIZUYA, H., DE JONG, P.J., BIRREN, B. & SIMON, M.I. 1992. Stable propagation of cosmid sized human DNA inserts in an F factor based vector. *Nucleic Acids Research*, **20**, 1083–1085, 10.1093/nar/20.5.1083.

KIVILUOTO, S., DECUYPERE, J.-P., DE SMEDT, H., MISSIAEN, L., PARYS, J.B. & BULTYNCK, G. 2011. STIM1 as a key regulator for Ca(2+)homeostasis in skeletal-muscle development and function. *Skeletal Muscle*, **1**, 16.

KLEIN, A., JUNGBLUTH, H., CLEMENT, E., LILLIS, S., ABBS, S., MUNOT, P., PANE, M., … MUNTONI, F. 2011. Muscle magnetic resonance imaging in congenital myopathies due to ryanodine receptor type 1 gene mutations . *Archives of Neurology*, **68**, 1171–1179.

KONE, B.C. 2000. Protein–protein interactions controlling nitric oxide synthases. *Acta Physiologica Scandinavica*, **168**, 27–31.

KOOPMAN, W.J., NIJTMANS, L.G., DIETEREN, C.E., ROESTENBERG, P., VALSECCHI, F., SMEITINK, J.A. & WILLEMS, P.H. 2010. Mammalian mitochondrial complex I: biogenesis, regulation and reactive oxygen species generation. *Antioxidant redox signalling*, **12**, 1431–1470.

KOOPMAN, W.J.H., DISTELMAIER, F., SMEITINK, J.A. & WILLEMS, P.H. 2013. OXPHOS mutations and neurodegeneration. *The EMBO Journal*, **32**, 9–29.

KOVACHEVA, E.L., SINHA HIKIM, A.P., SHEN SINHA, I., R. & SINHA-HIKIM, I. 2010. Testosterone supplementation reverses sarcopenia in aging through regulation of myostatin, c-Jun NH(2)-terminal kinase, notch, and Akt signaling pathways. *Endocrinology*, **151**, 628–638.

KRAEVA, N., ZVARITCH, E., ROSSI, A.E., GOONASEKERA, S.A., ZAID, H., FRODIS, W., KRAEV, A., DIRKSEN, R.T., MACLENNAN, D.H. & RIAZI, S. 2013. Novel excitation-contraction uncoupled RYR1 mutations in patients with central core disease. *Neuromuscular Disorders*, **23**, 120–132.

KRAYTSBERG, Y., KUDRYAVTSEVA, E., MCKEE, A.C., GEULA, C., KOWALL, N.W. & KHRAPKO, K. 2006. Mitochondrial DNA deletions are abundant and cause functional impairment in aged human substantia nigra neurons. *Nature Genetics*, **38**, 518–520.

KRETZSCHMAR, K. & WILKIE, D.R. 1972. New method for absolute heat measurement, utilizing Peltier effect. *Journal of Physiology*, **224**, 18P–21P.

KRETZSCHMAR, K. & WILKIE, D.R. 1975. Use of peltier effect for simple and accurate calibration of thermoelectric devices. *Proceedings of the Royal Society B-Biological Sciences*, **190**, 315–321.

KUZNETSOV, A. V., TROPPMAIR, J., SUCHER, R., HERMANN, M., SAKS, V. & MARGREITER, R. 2006. Mitochondrial subpopulations and heterogeneity revealed by confocal imaging: Possible physiological role? *Biochimica et Biophysica Acta - Bioenergetics*, **1757**, 686–691.

KUZNETSOV, A. V, VEKSLER, V., GELLERICH, F.N., SAKS, V., MARGREITER, R. & KUNZ, W.S. 2008. Analysis of mitochondrial function in situ in permeabilized

muscle fibers, tissues and cells. *Nature Protocols*, **3**, 965–976.

KWEE, L.C., LIU, Y., HAYNES, C., GIBSON, J.R., STONE, A., SCHICHMAN, S.A., KAMEL, F., NELSON, L.M., TOPOL, B., VAN DEN EEDEN, S.K., TANNER, C.M., GRASSO, D.L., LAWSON, R., MURALIDHAR, S., ODDONE, E.Z., SCHMIDT, S. & HAUSER, M.A. 2012. A high-density genome-wide association screen of sporadic ALS in US veterans. *PLOS One*, **7**, 1–12.

LANG, T., STREEPER, T., CAWTHON, P., BALDWIN, K., TAAFFE, D.R. & HARRIS, T.B. 2010. Sarcopenia: etiology, clinical consequences, intervention, and assessment. *Osteoporosis International*, **21**, 543–559.

LANNER, J.T., GEORGIOU, D.K., DAGNINO-ACOSTA, A., AINBINDER, A., CHENG, Q., JOSHI, A.D., CHEN, Z., … HAMILTON, S.L. 2012. AICAR prevents heat-induced sudden death in RyR1 mutant mice independent of AMPK activation. *Nature Medicine*, **18**, 244–251.

LANNER, J.T., GEORGIOU, D.K., JOSHI, A.D. & HAMILTON, S.L. 2010. Ryanodine receptors: structure, expression, molecular details, and function in calcium release. *Cold Spring Harbor Perspectives in Biology*, **2**, 1–21.

LANZA, I.R. & NAIR, K.S. 2010. Regulation of skeletal muscle mitochondrial function: genes to proteins. *Acta Physiologica*, **199**, 529–547.

LARACH, M.G. 1989. Standardization of the caffeine halothane muscle contracture test. *Anaesthesia & Analgesia*, **69**, 511–515.

LARSEN, S., NIELSEN, J., HANSEN, C.N., NIELSEN, L.B., WIBRAND, F., STRIDE, N., SCHRODER, H.D., BOUSHEL, R., HELGE, J.W., DELA, F. & HEY-MOGENSEN, M. 2012. Biomarkers of mitochondrial content in skeletal muscle of healthy young human subjects. *The Journal of Physiology*, **590**, 3349–3360.

LAUNIKONIS, B.S., BARNES, M. & STEPHENSON, D.G. 2003. Identification of the coupling between skeletal muscle store-operated Ca2+ entry and the inositol trisphosphate receptor. *Proceedings of the National Academy of Sciences*, **100**, 2941–2944.

LAUNIKONIS, B.S. & RIOS, E. 2007. Store-operated Ca2+ entry during intracellular Ca2+ release in mammalian skeletal muscle. *Journal of Physiology*, **583**, 81–97.

LEE, C.K., KLOPP, R.G., WEINDRUCH, R. & PROLLA, T.A. 1999. Gene expression profile of aging and its retardation by caloric restriction. *Science*, **285**, 1390–1393.

LEE, E.C., YU, D., MARTINEZ DE VELASCO, J., TESSAROLLO, L., SWING, D.A., COURT, D.L., JENKINS, N.A. & COPELAND, N.D. 2001. A highly efficient Escherichia coli-based chromosome engineering system adapted for recombinogenic targeting and subcloning of BAC DNA. *Genomics*, **73**, 56–65.

LEWIS, C.M., LEVINSON, D.F., WISE, L.H., DELISI, L.E., STRAUB, R.E., HOVATTA, I., WILLIAMS, N.M., SCHWAB, S.G., PULVER, A.E., FARAONE, S.V., BRZUSTOWICZ, L.M., KAUFMANN, C.A., GARYER, D.L., GURLING, H.M.D., LINDHOLM, E., COON, H., MOISES, H.W., BYERLEY, W., SHAW, S.H., MESEN, A., SHERRINGTON, R., O'NEILL, F.A., WALSH, D., KENDLER, K.S., EKELUND, J., PAUNIO, T., LONNQVIST, J., PELTONEN, L., O'DONOVAN, M.C., OWEN, M.J., WILDENAUER, D.B., MAIER, W., NESTADT, G., BLOUIN, J.-L., ANTNARAKIS, S.E., MOWRY, B.J., SILVERMAN, J.M., CROWE, R.R., CLONINGER, C.R., TSUANG, M.T., MALASPINA, D., HARKAVY-FRIEDMAN, J.M., SVRAKIC, D.M. BASSETT, A.S., HOLCOMB, J., KALSI, G., MCQUILIN, A., BRYNJOLFSON, T., SIGMUNDSSON, T., PETURSSON, H., JAZIN, E., ZOEGA, T. & HELGASON, T. 2003. Genome scan meta-analysis of schizophrenia and bipolar disorder, part II: Schizophrenia. *American Journal of Human Genetics*, **73**, 34–48.

LEWIS, R.S. 2007. The molecular choreography of a store-operated calcium channel. *Nature*, **446,** 284–287.

LEXELL, J. 1995. Human aging, muscle mass, and fibre type composition. *Journals of Gerontology - Series A Biological Sciences and Medical Sciences*, **50**, 11–16.

LEXELL, J., TAYLOR, C.C. & SJOSTROM, M. 1988. What is the cause of the ageing atrophy? Total number, size and proportion of different fiber types studied in whole vastus lateralis muscle from 15- to 83-year-old men. *Journal of Neurological Science*, **84**, 275–294.

LIEWLUCK, T. & GOODMAN, B.P. 2012. Late-onset axial myopathy and camptocormia in a calpainopathy carrier. *Journal of Clinical Neuromuscular Disease*, **13**, 209–213.

LINDLE, R.S., METTER, E.J., LYNCH, N.A., FLEG, J.L., FOZARD, J.L., TOBIN, J., ROY, T.A. & HURLEY, B.F. 1997. Age and gender comparisons of muscle strength in 654 women and men aged 20–93 years. *Journal of Applied Physiology*, **83**, 1581–1587.

LINDSAY, A.R., MANNING, S.D. & WILLIAMS, A.J. 1991. Monovalent cation conductance in the ryanodine receptor-channel of sheep cardiac muscle sarcoplasmic reticulum. *The Journal of Physiology*, **439**, 463–480.

LINK, C.D. 1995. Expression of human b-amyloid peptide in transgenic Caenorhabditis elegans. *Proceedings of the National Academy of Sciences*, **92**, 9368–9372.

LINK, C.D. 2001. Transgenic invertebrate models of age-associated neurodegenerative diseases. *Mechanisms of Ageing and Development*, **122**, 1639–1649.

LIOCHEV, S.I. 2013. Reactive oxygen species and the free radical theory of aging. *Free Radical Biology and Medicine*, **60**, 1–4.

LIOU, J., KIM, M.L., HEO, W.D., JONES, J.T., MYERS, J.W., FERRELL, J.E.J. & MEYER, T. 2005. STIM is a Ca2+ sensor essential for Ca2+-store-depletion-triggered Ca2+ influx. *Current Biology*, **15**, 1235–1241.

LOGAN, C. V, SZABADKAI, G., SHARPE, J.A., PARRY, D.A., TORELLI, S., CHILDS, A.-M., KRIEK, M., … SHERIDAN, E. 2014. Loss-of-function mutations in MICU1 cause a brain and muscle disorder linked to primary alterations in mitochondrial calcium signaling. *Nature Genetics*, **46**, 188–193.

LOSETH, S., VOERMANS, N.C., TORBERGSEN, T., LILLIS, S., JONSRUD, C., LINDAL, S., KAMSTEEG, E.-K., LAMMENS, M., BROWMAN, M., DEKOMIEN, G., MADDISON, P., MUNTONI, F., SEWRY, C., RADUNOVIC, A., DE VISSER, M., STRAUB, V., VAN ENGELEN, B. & JUNGBLUTH, H. 2013. A novel late-onset axial myopathy associated with mutations in the skeletal muscle ryanodine receptor (RYR1) gene. *Journal of Neurology*, **260**, 1504–1510.

LOWE, D.A., SUREK, J.T., THOMAS, D.D. & THOMPSON, L. V. 2001. Electron paramagnetic resonance reveals age-related myosin structural changes in rat skeletal muscle fibres. *American Journal of Physiology-Cell Physiology*, **280**, 540–547.

LOWE, D.A., THOMAS, D.D. & THOMPSON, L. V. 2002. Force generation, but not myosin ATPase activity, declines with age in rat muscle fibres. *American Journal of Physiology-Cell Physiology*, **283**, 187–192.

LOWES, D.A., GALLEY, H.F., MOURA, A.P.S. & WEBSTER, N.R. 2017. Brief isoflurane anaesthesia affects differential gene expression, gene ontology and gene networks in rat brain. *Behavioural Brain Research*, **317**, 453–460.

LU, J., MCKINSEY, T.A., ZHANG, C.-L. & OLSON, E.N. 2000. Regulation of skeletal myogenesis by association of the MEF2 transcription factor with class II histone

deacetylases. *Molecular Cell*, **6**, 233–244.

LYFENKO, A.D. & DIRKSEN, R.T. 2008. Differential dependence of store-operated and excitation-coupled Ca2+ entry in skeletal muscle on STIM1 and Orai1. *The Journal of Physiology*, **586**, 4815–4824.

LYFENKO, A.D., GOONASEKERA, S.A. & DIRKSEN, R.T. 2004. Dynamic alterations in myoplasmic Ca2+ in malignant hyperthermia anc central core disease. *Biochemcial and Biophysical Research Communications*, **322**, 1256–1266.

MA, J. & LIEW, C.C. 2003. Gene profiling identifies secreted protein transcripts from peripheral blood cells in coronary artery disease. *Journal of Molecular Cell Cardiology*, **35**, 993–998.

MACKENZIE, A.E., KORNELUK, R.G., ZORZATO, F., FUJII, J., PHILLIPS, M., ILES, D., WIERINGA, B., LEBLOND, S., BAILLY, J. & WILLARD, H.F. 1990. The human ryanodine receptor gene: its mapping to 19q13.1, placement in a chromosome 19 linkage group, and exclusion as the gene causing myotonic dystrophy. *American journal of human genetics*, **46**, 1082–1089.

MACLENNAN, D.H. & WAYNE CHEN, S.R. 2010. Ryanodine Receptors. *In* Bradshaw, R.A. & Dennis, E.A., *eds. Handbook of Cell Signalling*. Elsevier, 927–936.

MACLENNAN, D.H. & WONG, P.T. 1971. Isolation of calcium-sequestering protein from sarcoplasmic reticulum. *Procedings of the National Academy of Science*, **68**, 1231–1235.

MACLENNAN, D.H. & ZVARITCH, E. 2011. Mechanistic models for muscle diseases and disorders originating in the sarcoplasmic reticulum. *Biochimica et Biophysica Acta - Molecular Cell Research*, **1813**, 948–964.

MAHJNEH, I., MARCONI, G., PAETAU, A., SAARINEN, A., SALMI, T. & SOMER, H. 2002. Axial myopathy – an unrecognised entity. *Journal of Neurology*, **249**, 730–734.

MAILLOUX, R.J. & HARPER, M.E. 2012. Mitochondrial proticity and ROS signaling: Lessons from the uncoupling proteins. *Trends in Endocrinology and Metabolism*, **23**, 451–458.

MAMMUCARI, C., GHERARDI, G., ZAMPARO, I., RAFFAELLO, A., BONCOMPAGNI, S., CHEMELLO, F., CAGNIN, S., BRAGA, A., ZANIN, S., PALLAFACCHINA, G., ZENTILIN, L., SANDRI, M., DE STEFANI, D., PROTASI, F., LANFRANCHI, G. & RIZZUTO, R. 2015. The mitochondrial calcium uniporter controls skeletal muscle trophism in vivo. *Cell Reports*, **10**, 1269–1279.

MANNO, C., FIGUEROA, L., ROYER, L., POUVREAU, S., LEE, C.S., VOLPE, P., NORI, A., ZHOU, J, MEISSNER, G., HAMILTON, S. L. & RÍOS, E. 2013. Altered Ca2+ concentration, permeability and buffering in the myofibre Ca2+ store of a mouse model of malignant hyperthermia. *The Journal of physiology*, **591**, 4439–4457.

MARCINEK, D.J., SCHENKMAN, K.A., CIESIELSKI, W.A., LEE, D. & CONLEY, K.E. 2005. Reduced mitochondrial coupling in vivo alters cellular energetics in aged mouse skeletal muscle. *Journal of Physiology*, **569**, 467–473.

MARIOL, M.C., WALTER, L., BELLEMIN, S. & GIESELER, K. 2013. A rapid protocol for integrating extrachromosomal arrays with high transmission rate into the C. elegans genome. *Jove-Journal of Visualized Experiments*, **82**, e50773.

MARON, B.J., DOERER, J.J., HAAS, T.S., TIERNEY, D.M. & MUELLER, F.O. 2009. Sudden deaths in young competitive athletes: Analysis of 1866 deaths in the United States, 1980–2006. *Circulation*, **119**, 1085–1092.

MARYON, E.B., ROBERTO, C. & ANDERSON, P. 1996. unc-68 encodes a ryanodine receptor involved in regulating C. elegans body-wall muscle contraction. *The Journal of Cell Biology*, **134**, 885–893.

MCARDLE, A., DILLMANN, W.H., MESTRIL, R., FAULKNER, J.A. & JACKSON, M.J.

2004. Overexpression of HSP70 in mouse skeletal muscle protects against muscle damage and age-related muscle dysfunction. *FASEB Journal*, **18**, 355–357.

McCarthy, T. V, Healy, J.M., Heffron, J.J., Lehane, M., Deufel, T., Lehmann-Horn, F., Farrall, M. & Johnson, K. 1990. Localization of the malignant hyperthermia susceptibility locus to human chromosome 19q12-13.2. *Nature*, **343**, 562–564.

McCarthy, T. V, Quane, K.A. & Lynch, P.J. 2000. Ryanodine receptor mutations in malignant hyperthermia and central core disease. *Human Mutation*, **15**, 410–417.

McKinsey, T.A., Zhang, C.L. & Olson, E.N. 2002. MEF2: a calcium-dependent regulator of cell division, differentiation and death. . *Trends in Biochemical Sciences*, **27**, 40–47.

McLeod, M., Breen, L., Hamilton, D.L. & Philp, A. 2016. Live strong and prosper: the importance of skeletal muscle strength for healthy ageing. *Biogerontology*, **17**, 1–14.

Meissner, G. 1994. Ryanodine receptor/calcium release channels and their regulation by endogenous effectors. *Annual reviews of physiology*, **56**, 485–508.

Meissner, G. & Lu, X. 1995. Dihydropyridine receptor-ryanodine receptor interactions in skeletal muscle excitation-contraction coupling. *Bioscience Reports*, **15**, 399–408.

Melé, M., Ferreira, P.G., Reverter, F., Deluca, D.S., Monlong, J., Sammeth, M., Young, T.R., Goldmann, J.M., Pervouchine, D.D., Sullivan, T. J., Johnson, R., Segre, A.V., Djebali, S., Niarchou, A., Wright, F.A., Deluca, D.S., Gelfand, E., Trowbridge, C.A., Maller, J.B., Tukianinen, T., Lek, M., Ward, L.D., Kheradpour, P., Iriarte, B., Meng, Y., Palmer, C.D., Esko, T., Winckler, W., Hirschhorn, J.N., Kellis, M., Macarthur, D.G., Getz G., Shabalin, A.A. & Li, G. 2015. The human transcriptome across tissues and individuals. *Science*, **348**, 660–665.

Menshikova, E. V., Ritov, V.B., Fairfull, L., Ferrell, R.E., Kelley, D.E. & Goodpaster, B.H. 2006. Effects of exercise on mitochondrial content and function in aging human skeletal muscle. *The Journals of Gerontology. Series A, Biological sciences and medical sciences*, **61**, 534–540.

Mian, O.S., Thom, J.M., Ardigo, L.P., Narici, M. V & Minetti, A.E. 2006. Metabolic cost, mechanical work and efficiency during walking in young and older men. *Acta Physiologica*, **186**, 127–139.

Michelucci, A., Paolini, C., Canato, M., Wei-lapierre, L., Pietrangelo, L., Marco, A. De, Reggiani, C., Dirksen, R.T. & Protasi, F. 2016. Antioxidants Protect Calsequestrin-1 Knockout Mice. *Critical Care Medicine*, 603–617.

Milner, D.J., Mavroidis, M., Weisleder, N. & Capetanaki, Y. 2000. Desmin cytoskeleton linked to muscle mitochondrial distribution and respiratory function. *Journal of Cell Biology*, **150**, 1283–1297, 10.1083/jcb.150.6.1283.

Ministry of Defence. 2013. Climatic injuries in the Armed Forces: prevention and treatment. *Joint Service Protocol*.

Monnier, N., Krivosic-Horber, R., Payen, J.-F., Kozak-Ribbens, G., Nivoche, Y., Adnet, P., Reyford, H. & Lunardi, J. 2002. Presence of two different genetic traits in malignant hyperthermia families. *Anesthesiology*, **97**, 1067–1074.

Monnier, N., Romero, N., Lerale, J., Landrieu, P., Nivoche, Y., Qi, D., MacLennan, D.H., Fardeau, M. & Lunardi, J. 2000. An autosomal dominant

congenital myopathy with cores and rods is associated with a neomutation in the RYR1 gene encoding the skeletal muscle ryanodine receptor. *Human Molecular Genetics*, **9**, 2599–2608.

MONNIER, N., ROMERO, N.B., LERALE, J., LANDRIEU, P., NIVOCHE, Y., FARDEAU, M. & LUNARDI, J. 2001. Familial and sporadic forms of central core disease are associated with mutations in the C-terminal domain of the skeletal muscle ryanodine receptor. *Human Molecular Genetics*, **10**, 2581–2592, 10.1093/hmg/10.22.2581.

MORESI, V., MARRONCELLI, N., COLETTI, D. & ADAMO, S. 2015. Regulation of skeletal muscle development and homeostasis by gene imprinting, histone acetylation and microRNA. *Biochimica et Biophysica Acta - Gene Regulatory Mechanisms*, **1849**, 309–316.

MORGAN, P.G. & CASCORBI, H.F. 1985. Effect of Anesthetics and a Convlusant on Normal and Mutant Caenorhabditis elegans. *Anesthesiology*, **62**, 738–744.

MORGAN, P.G., KAYSER, E.-B. & SEDENSKY, M.M. 2007. C. elegans and volatile anesthetics. The C. elegans Research Community, *ed. Worm-Book* Available at: http://www.wormbook.org/chapters/www_anesthetics/anesthetics.html [Accessed January 13, 2015].

MORGAN, P.M. & CARSCOBI, H.F. 1985. Effect of anaesthetics and a convulsant on normal and mutant Caenorhabditis elegans. *Anaesthesiology*, **62**, 738–744.

MORI, M.X., ERICKSON, M.G. & YUE, D.T. 2004. Functional stoichiometry and local enrichment of calmodulin interacting with Ca(2+) channels. *Science*, **304**, 432–435.

MORRIS, S. 2015. Defence minister apologises for SAS test march deaths. *The Guardian*.

MOUGEOLLE, A., POUSSARD, S., DECOSSAS, M., LAMAZE, C., LAMBERT, O. & DARGELOS, E. 2015. Oxidative stress induces caveolin 1 degradation and impairs caveolae functions in skeletal muscle cells. *PLoS ONE*, **10**, 1–19.

MOURKIOTI, F. & ROSENTHAL, N. 2008. NF-kB signaling in skeletal muscle: Prospects for intervention in muscle diseases. *Journal of Molecular Medicine*, **86**, 747–759.

MURRAY, M.P., DUTHIE, E.H.J., GAMBERT, S.R., SEPIC, S.B. & MOLLINGER, L.A. 1985. Age-related differences in knee muscle strength in normal women. . *The Journals of Gerontology Series A: Biological Sciences and Medical Sciences*, **40**, 275–280.

NAIR, J., GHATGE, M., KAKKAR, V. V. & SHANKER, J. 2014. Network analysis of inflammatory genes and their transcriptional regulators in coronary artery disease. *PLoS ONE*, **9**, 1–12.

NAIR, K.S. 2005. Aging muscle. *American Journal of Clinical Nutrition*, **81**, 953–963.

NARAYANAN, N., JONES, D.L., XU, A. & YU, J.C. 1996. Effects of aging on sarcoplasmic reticulum function and contraction duration in skeletal muscles of the rat. *American Journal of Physiology - Cell Physiology*, **271**, C1032–C1040.

NCBI. 2016. PDE1A Available at: http://www.ncbi.nlm.nih.gov/gene/5136 [Accessed July 21, 2016].

NELSON, T.E. 1990. Porcine malignant hyperthermia: Critical temperatures for in vivo and in vitro responses. *Anesthesiology*, **73**, 449–454.

NICHOLAS, W.L. 1984. The biology of free living nematodes. *Clarendon Press*, 31–53.

NIH. 2016. The genotype-tissue expression project Available at: https://www.genome.gov/27543767/genotypetissue-expression-project-gtex/

[Accessed August 2, 2016].

NIH NEWS. 2010. NIH launches genotype-tissue expression project. *National Human Genome Research Institute* Available at: https://www.genome.gov/27541670/2010-release-nih-launches-genotypetissue-expression-project/ [Accessed July 27, 2016].

NISHIO, H., SATO, T., FUKUNISHI, S., TAMURA, A., IWATA, M., TSUBOPI, K. & SUZUKI, K. 2009. Idenditification of malignant hyperthermia-susceptible ryanodine receptor type 1 gene (RYR1) mutations in a child who died in a car after exposure to a high environmental temperature. *Legal Medicine*, **11**, 142–143.

NONET, M.L., SAIFEE, O., ZHAO, H., RAND, J.B. & WEI, L. 1998. Synaptic transmission deficits in Caenorhabditis elegans synaptobrevin mutants. *Journal of Neuroscience*, **18**, 70–80.

NORD. 2015. National organisation for rare disorders: Central core disease Available at: http://rarediseases.org/rare-diseases/central-core-disease/ [Accessed January 15, 2015].

OFFICE FOR NATIONAL STATISTICS. 2015. UK population at its oldest ever in mid-2014. *The National Archives* Available at: http://webarchive.nationalarchives.gov.uk/20160105160709/http://www.ons.gov.uk/ons/rel/pop-estimate/population-estimates-for-uk--england-and-wales--scotland-and-northern-ireland/mid-2014/sty-ageing-of-the-uk-population.html [Accessed January 8, 2016].

OKUNO, D., IINO, R. & NOJI, H. 2011. Rotation and structure of FoF1-ATP synthase. *Journal of Biochemistry*, **149**, 655–664.

OLORUNSHOLA, K. V & ACHIE, L.N. 2011. Caffeine alters skeletal muscle contraction by opening calcium ion channels. *Current Research Journal of Biological Sciences*, **3**, 521–525.

ORDING, H., BRANCADORO, V., COZZOLINO, S., ELLIS, F.R., GLAUBER, V., GONANO, E.F., HALSALL, P.F., HARUNG, E., HEFFRON, J.J.A., HEYTENS, L., KOZAK-RIBBENS, G., KRESS, H., KRIVOSIC-HORBER, R., LEHMANN-HORN, F., MORTIER, W., NIVOCHE, Y., RANKLEV-TWETMAN, E., SIGUDSSON, S., SNOECK, M., STIEGLITZ, P., TEGAZZIN, V., URWYLER, A. & WAPPLER, F. 1997. In vitro contracture test for diagnosis of malignant hyperthermia following the protocol of the European Malignant Hyperthermia Group: results of testing patients surviving fulmiant MH and unrelated low-risk subjects. *Acta Anaesthesiologica Scandanavia*, **41**, 955–966.

ORTEGA, J.D. & FARLEY, C.T. 2007. Individual limb work does not explain the greater metabolic cost of walking in elderly adults. *Journal of Applied Physiology*, **102**, 2266–2273.

OZAWA, E. 2011. Regulation of phosphorylase kinase by low concentrations of Ca ions upon muscle contraction: the connection between metabolism and muscle contraction and the connection between muscle physiology and Ca-dependent signal transduction. *Proceedings of the Japan Academy, Series B*, **87**, 486–508.

PAN, Z., YANG, D., NAGARAJ, R.Y., NOSEK, T.A., NISHI, M., TAKESHIMA, H., CHENG, H. & MA, J. 2002. Dysfunction of store-operated calcium channel in muscle cells lacking mg29. *Nature Cell Biology*, **4**, 379–383.

PAOLINI, C., QUARTA, M., D'ONOFRIO, L., REGGIANI, C. & PROTASI, F. 2011. Differential effect of calsequestrin ablation on structure and function of fast and slow skeletal muscle fibers. *Journal of Biomedicine and Biotechnology*, 1–10.

PAOLINI, C., QUARTA, M., NORI, A., BONCOMPAGNI, S., CANATO, M., VOLPE, P., ALLEN, P.D., REGGIANI, C. & PROTASI, F. 2007. Reorganized stores and impaired

calcium handling in skeletal muscle of mice lacking calsequestrin-1. *The Journal of Physiology*, **583**, 767–784.

PAOLINI, C., QUARTA, M., WEI-LAPIERRE, L., MICHELUCCI, A., NORI, A., REGGIANI, C., DIRKSEN, R.T. & PROTASI, F. 2015. Oxidative stress, mitochondrial damage, and cores in muscle from calsequestrin-1 knockout mice. *Skeletal Muscle*, **5**, 1–17.

PARAEKH, A.B. & PUTNEY, J.W.J. 2005. Store-operated calcium channels. *Physiology Reviews*, **85**, 757–810.

PAYNE, A.M. & DELBONO, O. 2004. Neurogenesis of excitation-contraction uncoupling in aging skeletal muscle. *Exercise and Sport Science Reviews*, **32**, 36–40.

PAYNE, B.A.I. & CHINNERY, P.F. 2015. Mitochondrial dysfunction in aging: Much progress but many unresolved questions. *Biochimica et Biophysica Acta - Bioenergetics*, **1847**, 1347–1353.

PEARSON, S.J., YOUNG, A., MACALUSO, A., DEVITO, G., NIMMO, M.A., COBBOLD, M. & HARRIDGE, S.D. 2002. Muscle function in elite master weightlifters. *Medicine & Science in Sports and Exercise*, **34**, 1199–1206.

PERIASAMY, M. & KALYANASUNDARAM, A. 2007. SERCA pump isoforms: their role in calcium transport and disease. *Muscle and Nerve*, **35**, 430–442.

PETERSON, C.M., JOHANNSEN, D.L. & RAVUSSIN, E. 2012. Skeletal muscle mitochondria and aging: a review. *Journal of Aging Research*, 1–20.

PIETRANGELO, L., INCECCO, A.D., AINBINDER, A., MICHELUCCI, A., KERN, H., DIRKSEN, R.T., BONCOMPAGNI, S. & PROTASI, F. 2015. Age-dependent uncoupling of mitochondria from Ca 2 + release units in skeletal muscle. *Oncotarget, Advence Publications*, **6**, 1–14.

PIÉTRI-ROUXEL, F., GENTIL, C., VASSILOPOULOS, S., BAAS, D., MOUISEL, E., FERRY, A., VIGNAUD, A., … GARCIA, L. 2010. DHPR alpha1S subunit controls skeletal muscle mass and morphogenesis. *The EMBO journal*, **29**, 643–654.

PIPER, H.M., SEZER, O., SCHLEYER, M., SCHWARTZ, P., HIITTER, J.F., SPIECKERMANN, P.G., PIPER, H.M., SEZER, O. & SCHWARTZ, P. 1985. Development of ischemia-induced damage in defined mitochondrial subpopulations. *Journal of Molecular Cell Cardiology*, **17**, 885–896.

POWERS, S.K., DUARTE, J., KAVAZIS, A.N. & TALBERT, E.E. 2010. Reactive oxygen species are signalling molecules for skeletal muscle adaptation. *Experimental physiology*, **95**, 1–9.

PSARRA, A.M.G. & SEKERIS, C.E. 2008. Steroid and thyroid hormone receptors in mitochondria. *International Union of Biochemistry and Molecular Biology: Life*, **60**, 210–223.

PUZIANOWSKA-KUZNICKA, M. & KUZNICKI, J. 2009. The ER and ageing II: Calcium homeostasis. *Ageing Research Reviews*, **8**, 160–172.

QIAGEN. 2016. RT2 Profiler PCR Arrays: Human Aging Available at: https://www.qiagen.com/gb/search/rt2-profiler-pcr-arrays?catno=PAHS-178Z&cmpid=PR150810+PCR+Arrays+and+Aging+and+Neurodegeneration+I ntl&imm_mid=0d6642&s_cid=PR150810+PCR+Arrays+and+Aging+and+Neu rodegeneration&s_med=email&s_ce=iPost#geneglobe [Accessed June 8, 2016].

QUANE, K.A., KEATING, K.E., HEALY, J.M., MANNING, B.M., KRIVOSIC-HORBER, R., KRIVOSIC, I., MONNIER, N., LUNARDI, J. & MCCARTHY, T. V. 1994. Mutation screening of the RYR1 gene in malignant hyperthermia: detection of a novel Tyr to Ser mutation in a pedigree with associated central cores. *Genomics*, **23**, 236–239.

QUINLIVAN, R.M., MULLER, C.R., DAVIS, M., LAING, N.G., EVANS, G.A., DWYER, J., DOVE, J., ROBERTS, A.P. & SEWRY, C.A. 2003. Central core disease: clinical, pathological, and genetic features. *Archives of Disease in Childhood*, **88**, 1051–1056.

REID, M.B. 1998. Role of nitric oxide in skeletal muscle: synthesis, distribution and functional importance. *Acta Physiologica Scandinavica*, **162**, 401–409.

REIKEN, S., LACAMPAGNE, A., ZHOU, H., KHERANI, A., LEHNART, S.E., WARD, C., HUANG, F., GABURJAKOVA, M., GABURJAKOVA, J., ROSEMBLIT, N., WARREN, M.S., HE, K., YI, G., WANG, J., BURKHOFF, D., VASSORT, G. & MARKS, A.R. 2003. PKA phosphorylation activates the calcium release channel (ryanodine receptor)-in skeletal muscle: Defective regulation in heart failure. *Journal of Cell Biology*, **160**, 919–928.

RICHARDS, S.A. 2005. Testing ecological theory using the information-theoretic approach: examples and cautionary results. *Ecology*, **86**, 2805–2814.

ROBINSON, R., CARPENTER, D., SHAW, M.-A., HALSALL, J. & HOPKINS, P. 2006. Mutations in RYR1 in malignant hyperthermia and central core disease. *Human Mutation*, **27**, 977–989.

ROBINSON, R., HOPKINS, P., CARSANA, A., GILLY, H., HALSALL, J., HEYTENS, L., ISLANDER, G., JURKAT-ROTT, K., MUELLER, C. & SHAW, M.-A. 2003a. Several Interacting genes influence the malignant hyperthermia phenotype. *Human Genetics*, **112**, 217–218.

ROBINSON, R.L., ANETSEDER, M.J., BRANCADORO, V., VAN BROECKHOVEN, C., CARSANA, A., CENSIER, K., FORTUNATO, G., GIRRARD, T., HEYTENS, L., HOPKINS, P., JUKAT-ROTT, K., KOZAK-RIBBENS, G., KRIVOSIC, R., MONNIER, N., NIVOCHE, Y., OLTHOFF, D., RUEFFERT, H., SORRENTINO, V., TEGASSIN, V. & MUELLER, C. 2003b. Recent advances in the diagnosis of malignant hyperthermia susceptibility: how confident can we be of genetic testing? *European Journal of Human Genetics*, **11**, 342–348.

ROBINSON, R.L., BROOKS, C., BROWN, S.L., ELLIS, F.R., HALSALL, P.J., QUINNELL, R.J., SHAW, M.A. & HOPKINS, P.M. 2002. RYR1 mutations causing central core disease are associated with more severe malignant hyperthermia in vitro contracture test phenotypes. *Human Mutation*, **20**, 88–97.

ROBINSON, R.L., CURRAN, J.L., ELLIS, F.R., HALSALL, P.J., HALL, W.J., HOPKINS, P.M., ILES, D.E., WEST, S.P. & SHAW, M.-A. 2000. Multiple interacting gene products may influence susceptibility to malignant hyperthermia. *Annals of Human Genetics*, **64**, 307–320.

ROBINSON, R.L. & HOPKINS, P.M. 2001. A breakthrough in the genetic diagnosis of malignant hyperthermia. *British Journal of Anaesthesia*, **86**, 166–168.

ROME, L.C., FUNKE, R.P., ALEXANDER, R.M., LUTZ, G., ALDRIDGE, H., SCOTT, F. & FREEDMAN, M. 1988. Why animals have different muscle-fibre types. *Nature*, **335**, 824–827.

ROOYACKERS, O.E., ADEY, D.B., ADES, P.A. & NAIR, K.S. 1996. Effect of age in vivo rates of mitochondrial protein synthesis in human skeletal muscle. *Procedings of the National Academy of Science U S A*, **93**, 15364–15369.

ROSENBERG, H., DAVIS, M., JAMES, D., POLLOCK, N. & STOWELL, K. 2007. Malignant hyperthermia. *Orphanet Journal of Rare Diseases*, **2**, 1–14.

ROSENBERG, H., POLLOCK, N., SCHIEMANN, A., BULGER, T. & STOWELL, K. 2015. Malignant hyperthermia: A review. *Orphanet Journal of Rare Diseases*, **10**, 1–19.

ROSENBERG, P., HAWKINS, A., STIBER, J., SHELTON, J.M., HUTCHESON, K., BASSEL-

DUBY, R., SHIN, D.M., YAN, Z. & WILLIAMS, R.S. 2004. TRPC3 channels confer cellular memory of recent neuromuscular activity. *Proceedings of the National Academy of Sciences*, **101**, 9387–9392.

ROSSI, A.E., BONCOMPAGNI, S. & DIRKSEN, R.T. 2009. Sarcoplasmic reticulum-mitochondrial symbiosis: Bidirectional signaling in skeletal muscle. *Exercise and Sport Science Reviews*, **37**, 29–35.

ROSSI, E.A. & DIRKSEN, R.T. 2006. Sarcoplasmic reticulum: the dynamic calcium governor of muscle. *Muscle and Nerve*, **33**, 715–731.

ROSSI, R., BOTTINELLI, R., SORRENTINO, V. & REGGIANI, C. 2001. Response to caffeine and ryanodine re-ceptor isoforms in mouse skeletal muscles. . *American Journal of Cellular Physiology*, **281**, 585–594.

ROTH, S.M., FERRELL, R.E., PETERS, D.G., METTER, E.J., HURLEY, B.F. & ROGERS, M.A. 2002. Influence of age, sex, and strength training on human muscle gene expression determined by microarray. *Physiological Genomics*, **10**, 181–190.

ROYER, L. & RíOS, E. 2009. Deconstructing calsequestrin. Complex buffering in the calcium store of skeletal muscle. *Journal of Physiology*, **58713**, 3101–3111.

RYAN, T., SHARMA, P., IGNATCHENKO, A., MACLENNAN, D.H., KISLINGER, T. & GRAMOLINI, A.O. 2011. Identification of novel ryanodine receptor 1 (RyR1) protein interaction with calcium homeostasis endoplasmic reticulum protein (CHERP). *Journal of Biological Chemistry*, **286**, 17060–17068.

RYBAKOVA, I.N., HUMSTON, J.L., SONNEMANN, K.J. & ERVASTI, J.M. 2006. Dystrophin and utrophin bind actin through distinct modes of contact. *Journal of Biological Chemistry*, **281**, 9996–10001.

SÁENZ, A., LETURCQ, F., COBO, A.M., POZA, J.J., FERRER, X., OTAEGUI, D., CAMAÑO, P., … DE MUNAIN, A.L. 2005. LGMD2A: genotype–phenotype correlations based on a large mutational survey on the calpain 3 gene. *Brain*, **128**, 732–742.

SAKS, V.A., VEKSLER, V.I., KUZNETSOV, A. V, KAY, L., SIKK, P., TIIVEL, T., TRANQUI, L., OLIVARES, J., WINKLER, K., WIEDEMANN, F. & KUNZ, W.S. 1998. Permeabilized cell and skinned fiber techniques in studies of mitochondrial function in vivo. *Molecular and Cellular Biochemistry*, **184**, 81–100.

SAKUBE, Y., ANDO, H. & KAGAWA, H. 1997. An abnormal ketamine response in mutants defective in the ryanodine receptor gene RYR1 (unc-68) of Caenorhabditis elegans . *Journal of Molecular Biology*, **267**, 849–864.

SAMBUUGHIN, N., HOLLEY, H., MULDOON, S., BRANDOM, B.W., DE BANTEL, A.M., TOBIN, J.R., NELSON, T.E. & GOLDFARB, L.G. 2005. Screening of the entire ryanodine receptor type 1 coding region for sequence variants associated with malignant hyperthermia susceptibility in the North American population. *Anesthesiology*, **102**, 515–521.

SAMPIERI, A., D´IAZ-MUNOZ, M., ANTARAMIAN, A. & VACA, L. 2005. The foot structure from the type 1 ryanodine receptor is required for functional coupling to store-operated channels. *Journal of Biological Chemistry*, **280**, 24804–24815.

SANCHEZ, E.J., LEWIS, K.M., DANNA, B.R. & KANG, C. 2012. High-capacity Ca(2+) binding of human skeletal calsequestrin. *The Journal of Biological Chemistry*, **287**, 11592–11601.

SANDOW, A. 1952. Excitation-contraction coupling in muscular response. *Yale Journal of Biological Medicine*, **25**, 176–201.

SCHÄFER, J. & STRIMMER, K. 2005. An empirical Bayes approach to inferring large-scale gene association networks. *Bioinformatics*, **21**, 754–764.

SCORZETO, M., GIACOMELLO, M., TONIOLO, L., CANATO, M., BLAAUW, B., PAOLINI, C., PROTASI, F., REGGIANI, C. & STIENEN, G.J.M. 2013. Mitochondrial Ca2+-

handling in fast skeletal muscle fibers from wild type and calsequestrin-null mice. *PLoS ONE*, **8**, 1–12.

SEDENSKY, M.M., PUJAZON, M. A & MORGAN, P.G. 2006. Tail clamp responses in stomatin knockout mice compared with mobility assays in Caenorhabditis elegans during exposure to diethyl ether, halothane, and isoflurane. *Anesthesiology*, **105**, 498–502.

SERYSHEVA, I.I., LUDTKE, S.J., BAKER, M.L., CONG, Y., TOPF, M., ERAMIAN, D., SALI, A., HAMILTON, S.L. & CHIU, W. 2008. Subnanometer-resolution electron cryomicroscopy-based domain models for the cytoplasmic region of skeletal muscle RyR channel. *Proceedings of the National Academy of Sciences of the United States of America*, **105**, 9610–9615.

SHEN, L.-L., WANG, Y. & WANG, D.-Y. 2007. Involvement of genes required for synaptic function in aging control in C. elegans. *Neuroscience Bulletin*, **23**, 21–29.

SHEPHERD, S., ELLIS, F., HALSALL, J., HOPKINS, P. & ROBINSON, R. 2004. RYR1 mutations in UK central core disease patients: more than just the C-terminal transmembrane region of the RYR1 gene. *Journal of Medical Genetics*, **41**, 1–7.

SHIGENAGA, M.K., HAGEN, T.M. & AMES, B.N. 1994. Oxidative damage and mitochondrial decay in aging. *Proceedings of the National Academy of Sciences of the United States of America*, **91**, 10771–10778.

SHIRRAN, S., GARNAUD, P., DAFF, S., MCMILLAN, D. & BARRAN, P. 2005. The formation of a complex between calmodulin and neuronal nitric oxide synthase is determined by ESI-MS. *Journal of The Royal Society Interface*, **2**, 465–476.

SHORT, K.R., VITTONE, J., BIGELOW, M.L., PROCTOR, D.N. & NAIR, K.S. 2004. Age and aerobic exercise training effects on whole body and muscle protein metabolism. *Americal Journal of Physiology*, **286**, 92–101.

SHY, G.M. & MAGEE, K.R. 1956. A new congenital non-progressive myopathy. *Brain*, **79**, 610–619.

SINHA, B., KÖSTER, D., RUEZ, R., GONNORD, P., ABANKWA, D., STAN, R. V, BUTLER-BROWNE, G., Vedie, B., Johannes, L., Morone, N., Parton, R.G., Raposo, G., Lamaze, C. & Nassoy, P. 2011. Cells Respond to Mechanical Stress by Rapid Disassembly of Caveolae. *Cell*, **144**, 402–413.

SITSAPESAN, R. & WILLIAMS, A.J. 1990. Mechanisms of caffeine activation of single calcium-release channels of sheel cardiac sarcoplasmic reticulum. *The Journal of Physiology*, **423**, 425–439.

SMITH, N.P., BARCLAY, C.J. & LOISELLE, D.S. 2005. The efficiency of muscle contraction. *Progress in Biophysics and Molecular Biology*, **88**, 1–58.

STAMLER, J.S. & MEISSNER, G. 2001. Physiology of nitric oxide in skeletal muscle. *Physiological Reviews*, **81**, 209–237.

STEPHENSON, D.G. 2008. Caffeine-a valuable tool in excitation-contraction coupling research. *Journal of Physiology*, **586**, 695–696.

STIBER, J., HAWKINS, A., ZHANG, Z.S., WANG, S., BURCH, J., GRAHAM, V., WARD, C.C., … ROSENBERG, P. 2008. STIM1 signalling controls storeoperated calcium entry required for development and contractile function in skeletal muscle. *Nature Cell Biology*, **10**, 688–697.

STIERNAGLE, T. 2006. Maintenance of C. elegans. The C. elegans Research Community, *ed. Worm-Book* Available at: http://www.wormbook.org.

STROUSTRUP, N., ULMSCHNEIDER, B.E., NASH, Z.M., LOPEZ MOYADO, I.F., APFELD, J. & FONTANA, W. 2013. The C. elegtrans Lifespan Machine. *Nature Methods*, **10**, 1–15.

Su, J., Ekman, C., Oskolkov, N., Lahti, L., Ström, K., Brazma, A., Groop, L., Rung, J. & Hansson, O. 2015. A novel atlas of gene expression in human skeletal muscle reveals molecular changes associated with aging. *Skeletal Muscle*, **5**, 35.

Su, Z., Blazing, M.A., Fan, D. & George, S.E. 1995. The calmodulin-nitric oxide synthase interaction. Critical role of the calmodulin latch domain in enzyme activation. *The Journal of Biological Chemistry*, **270**, 29117–29122.

Sumner, W. A., Beqollari, D., Romberg, C., Scheele, M.P. & Bannister, R.A. 2013. Upregulation of RGK protein expression in aging mouse fast twitch skeletal muscle. *Biophysical Journal*, **104**, 289a–290a.

Takekura, H., Nishi, M., Noda, T., Takeshima, H. & Franzini-Armstrong, C. 1995. Abnormal junctions between surface membrane and sarcoplasmic reticulum in skeletal muscle with a mutation targeted to the ryanodine receptor. *Proceedings of the National Academy of Sciences of the United States of America*, **92**, 3381–3385.

Tang, Y., Gilbert, D.L., Glauser, T.A., Hershey, A.D. & Sharp, F.R. 2005. Blood gene expression profiling of neurologic diseases: A pilot microarray study. *Archives of Neurology*, **62**, 210–215.

Territo, P.R., French, S.A., Dunleavy, M.C., Evans, F.J. & Balaban, R.S. 2001. Calcium activation of heart mitochondrial oxidative phosphorylation: rapid kinetics of mVO2 , NADH, and light scattering. *Journal of Biological Chemistry*, **276**, 2586–2599.

Thompson, J.R., Swanson, S.A., Casale, G.P., Johanning, J.M., Papoutsi, E., Koutakis, P., Miserlis, D., Zhu, Z. & Pipinos, I.I. 2014. Gastrocnemius mitochondrial respiration: Are there any differences between men and women? **185**, 1–14.

Tibshirani, R. 1996. Regression shrinkage and selection via the Lasso. *Journal of the Royal Society Statistical Series B-Methodological*, **58**, 267–288.

Tinker, A., Lindsay, A.R. & Williams, A.J. 1992. A model for ionic conduction in the ryanodine receptor channel of sheep cardiac muscle sarcoplasmic reticulum. *The Journal of General Physiology*, **100**, 495–517.

Tissenbaum, H.A. & Guarente, L. 2002. Model organisms as a guide to mammalian aging. *Developmental Cell*, **2**, 9–19.

Tong, J., Oyamada, H., Demaurex, N., Grinstein, S., McCarthy, T. V & MacLennan, D.H. 1997. Caffeine and halothane sensitivity of intracellular calcium release is altered by 15 calcium release channel (ryanodine receptor) mutations associated with malignant hyperthermia and/or central core disease. *The Journal of Biological Chemistry*, **272**, 26332–26339.

Tripathy, A., Xu, L., Mann, G. & Meissner, G. 1995. Calmodulin activation and inhibition of skeletal muscle Ca2+ release channel (ryanodine receptor). *Biophysics Journal*, **69**, 106–119.

Trounce, I., Byrne, E. & Marzuki, S. 1989. Decline in skeletal muscle mitochondrial respiratory chain function: possible factor in ageing. *Lancet*, **1**, 637–639.

Tyrovolas, S., Koyanagi, A., Olaya, B., Ayuso-Mateos, J.L., Miret, M., Chatterji, S., Tobiasz-Adamczyk, B., Koskinen, S., Leonardi, M. & Haro, J.M. 2016. Factors associated with skeletal muscle mass, sarcopenia, and sarcopenic obesity in older adults: A multi-continent study. *Journal of Cachexia, Sarcopenia and Muscle*, **7**, 312–321.

United Nations. 2007. WHO global report on falls prevention in older age.

Community Health, 53.

UNITED NATIONS. 2012. World Population Prospects.

URWYLER, A., DEUFEL, T., MCCARTHY, T. & WEST, S. 2001. Guidelines for molecular genetic detection of susceptibility to malignant hyperthermia. *British Journal of Anaesthesia*, **86**, 283–287.

VALK, P.J., VERHAAK, R.G.W., BEIJEN, M.A., ERPELINCK, C.A., VAN WAALWIJK, B., VAN DOORN-KHOSROVANI, S., BOER, J.M., … DELWEL, R. 2004. Prognostically useful gene-expression profiles in acute myeloid leukemia. *New England Journal of Medicine*, **350**, 1617–1628.

VAN SWINDEREN, B., SAIFEE, O., SHEBESTER, L., ROBERSON, R., NONET, M.L. & CROWDER, C.M. 1999. A neomorphic syntaxin mutation blocks volatile-anesthetic action in Caenorhabditis elegans. *Proceedings of the National Academy of Sciences*, **96**, 2479–2484.

VANDESOMPELE, J., DE PRETER, K., PATTYN, F., POPPE, B., VAN ROY, B., DE PAEPE, A. & SPELEMAN, F. 2002. Accurate normalisation of real-time quantitative RT-PCR data by genomic averaging of multiple internal control genes. *Genome Biology*, **3**, 1–11.

VIG, M., DEHAVEN, W.I., BIRD, G.S., BILLINGSLEY, J.M., WANG, H., RAO, P.E., HUTCHINGS, A.B., JOUVIN, M.H., PUTNEY, J.W. & KINET, J.P. 2008. Defective mast cell effector functions in mice lacking the CRACM1 pore subunit of store-operated calcium release- activated calcium channels. *Nature Immunology*, **9**, 89–96.

VÖLKERS, M., DOLATABADI, N., GUDE, N., MOST, P., SUSSMAN, M.A. & HASSEL, D. 2012. Orai1 deficiency leads to heart failure and skeletal myopathy in zebrafish. *Journal of Cell Science*, **125**, 287–294.

WANG, L., ZHANG, L., LI, S., ZHENG, Y., YAN, X., CHEN, M., WANG, H., PUTNEY, J.W. & LUO, D. 2015. Retrograde regulation of STIM1-Orai1 interaction and store-operated Ca(2+) entry by calsequestrin. *Scientific reports*, **5**, 11349.

WANG, S., TRUMBLE, W.R., LIAO, H.J., WESSON, C.R., DUNKER, A.K. & KANG, C.H. 1998. Crystal structure of calsequestrin from rabbit skeletal muscle sarcoplasmic reticulum. *Nature Structural Biology*, **5**, 476–483.

WANG, Z.-M., TANG, S., MESSI, M.L., YANG, J.J. & DELBONO, O. 2012. Residual sarcoplasmic reticulum Ca2+ concentration after Ca2+ release in skeletal myofibers from young adult and old mice. *Pflügers Archiv - European Journal of Physiology*, **463**, 615–624.

WANG, Z.M., MESSI, M.L. & DELBONO, O. 2000. L-Type Ca(2+) channel charge movement and intracellular Ca(2+) in skeletal muscle fibers from aging mice. *Biophysical journal*, **78**, 1947–1954.

WATANABE, R., OKUNO, D., SAKAKIHARA, S., SHIMABUKURO, K., IINO, R., YOSHIDA, M. & NOJI, H. 2011. Mechanical modulation of catalytic power on F1-ATPase. *Nature Chemical Biology*, **8**, 86–92.

WATT, I.N., MONTGOMERY, M.G., RUNSWICK, M.J., LESLIE, A.G.W. & WALKER, J.E. 2010. Bioenergetic cost of making an adenosine triphosphate molecule in animal mitochondria. *Proceedings of the National Academy of Sciences of the United States of America*, **107**, 16823–16827.

WEISLEDER, N., BROTTO, M., KOMAZAKI, S., PAN, Z., ZHAO, X., NOSEK, T., PARNESS, J., TAKESHIMA, H. & MA, J. 2006. Muscle aging is associated with compromised calcuim spark signalling and segregated intracellular calcium release. *Journal of Cell Biology*, **174**, 639–645.

WEISS, R.G., O'CONNELL, K.M.S., FLUCHER, B.E., ALLEN, P.D., GRABNER, M. &

DIRKSEN, R.T. 2004. Functional analysis of the R1086H malignant hyperthermia mutation in the DHPR reveals an unexpected influence of the III-IV loop on skeletal muscle EC coupling. *American Journal of Physiology-Cell physiology*, **287**, C1094–C1102.

WELLE, S., BHATT, K., SHAH, B., NEEDLER, N., DELEHANTY, J.M. & THORNTON, C. A. 2003. Reduced amount of mitochondrial DNA in aged human muscle. *Journal of Applied Physiology*, **94**, 1479–1484.

WELLE, S., BHATT, K. & THORNTON, C.A. 2000. High-abundance mRNAs in human muscle: comparison between young and old. *Journal of Applied Physiology*, **89**, 297–304.

WELLE, S., BROOKS, A. & THORNTON, C.A. 2001. Senescence-related changes in gene expression in muscle: similarities and differences between mice and men. *Physiol Genomics*, **5**, 67–73.

WELLE, S., BROOKS, A.I., DELEHANTY, J.M., NEEDLER, N., BHATT, K., SHAH, B. & A., T.C. 2004. Skeletal muscle gene expression profiles in 20-29 year old and 65-71 year old women. *Experimental Gerontology*, **39**, 369–377.

WILSON, R.D., TRABER, D.L., ALLEN, C.R. & PRIANO, L.L. 1971. Malignant hyperpyrexia: a reexamination. *Southern Medical Journal*, **64**, 411–414.

WOLEDGE, R., CURTIN, N. & HOMSHER, E. 1985. *Energetic aspects of muscle contraction*. London: Academic Press.

WOOD, W.B. 1988. The nematode Caenorhabditis elegans. *The nematode Caenorhabditis elegans*. New York: Cold Spring Harbour Laboratory, pp. 1-16 pp.

WORMATLAS. 2006. Worm Atlas Available at: http://www.wormatlas.org/ver1/handbook/anatomyintro/anatomyintro.htm.

WU, S., IBARRA, M.C., MALICDAN, M.C., MURAYAMA, K., ICHIHARA, Y., KIKUCHI, H., NONAKA, I., NOGUCHI, S., HAYASHI, Y.K. & NISHINO, I. 2006. Central core disease is due to RYR1 mutations in more than 90% of patients. *Brain*, **129**, 1470–1480.

XIE, Z., DONG, Y., ZHANG, M., CUI, M.-Z., COHEN, R. a, RIEK, U., NEUMANN, D., SCHLATTNER, U. & ZOU, M.-H. 2006. Activation of protein kinase C zeta by peroxynitrite regulates LKB1-dependent AMP-activated protein kinase in cultured endothelial cells. *The Journal of biological chemistry*, **281**, 6366–6375.

XU, Q. & WU, Z. 2000. The insulin-like growth factor-phosphatidylinositol 3-kinase-Akt signaling pathway regulates myogenin expression in normal myogenic cells but not in rhabdomyosarcoma-derived RD cells. *The Journal of Biological Chemistry*, **275**, 36750–36757.

YAN, Z., BAI, X., YAN, C., WU, J., LI, Z., XIE, T., PENG, W., YIN, C.-C., LI, X., SCHERES, S.H.W., SHI, Y. & YAN, N. 2015. Structure of the rabbit ryanodine receptor RyR1 at near-atomic resolution. *Nature*, **517**, 50–55.

YANG, T., ESTEVE, E., PESSAH, I.N., MOLINSKI, T.F., ALLEN, P.D. & LOPEZ, J.R. 2007. Elevated resting [Ca(2+)](i) in myotubes expressing malignant hyperthermia RyR1 cDNAs is partially restored by modulation of passive calcium leak from the SR. *American Journal of Cellular Physiology*, **292**, C1591-8.

YANG, T., PH, D., RIEHL, J., PH, D., ESTEVE, E., PH, D., MATTHAEI, K.I. & PH, D. 2006. Pharmacologic and functional characterization of malignant hyperthermia in the R163C RyR1 knock-in. *Anesthesiology*, **105**, 1164–1175.

YANG, T., TA, T.A., PESSAH, I.N. & ALLEN, P.D. 2003. Functional defects in six ryanodine receptor isoform-1 (RyR1) mutations associated with malignant

hyperthermia and their impact on skeletal excitation-contraction coupling. *Journal of Biological Chemistry*, **278**, 25722–25730.

YANG T., TA, T.A., PESSAH, I.N. & ALLEN, P.D. 2003. Functional defects in six ryanodine receptor isoform-1 (RyR1) mutations associated with malignant hyperthermia and their impact on skeletal excitation-contraction coupling. *Journal of Biological Chemistry*, **278**, 25722–25730.

YASUKO, O., HIROKO, S., HIROYUKI, S., ISABELLE, R., TAKAOMI, C.S., JACQUES, S.B., SHOICHI, I. & S., K. 1998. Functional defects of a muscle-specific calpain, p94, caused by mutations associated with limb-girdle muscular dystrophy type 2A. *Journal of Biological Chemistry*, **273**, 17073–17078.

YOO, Y.-E. & KO, C.-P. 2011. Treatment with trichostatin A initiated after disease onset delays disease progression and increases survival in a mouse model of amyotrophic lateral sclerosis. *Experimental Neurology*, **231**, 147–159.

YU, D., ELLIS, H.M., LEE, E.C., JENKINS, N.A., COPELAND, N.G. & COURT, D.L. 2000. An efficient recombination system for chromosome engineering in Escherichia coli. *Proceedings of the National Academy of Sciences*, **97**, 5978–5983.

YUEN, B., BONCOMPAGNI, S., FENG, W., YANG, T., LOPEZ, J.R., MATTHAEI, K.I., GOTH, S.R., PROTASI, F., FRANZINI-ARMSTRONG, C., ALLEN, P.D. & PESSAH, I.N. 2012. Mice expressing T4826I-RYR1 are viable but exhibit sex- and genotype-dependent susceptibility to malignant hyperthermia and muscle damage (The FASEB Journal (2012) DOI:10.1096/fj.11-197582). *FASEB Journal*, **26**, 3587.

ZAHN, J., SONU, R., VOGEL, H., CRANE, E., MAZAN-MAMCZARZ, K., RABKIN, R., DAVIS, R.W., BECKER, K.G., OWEN, A.B. & KIM, S.K. 2006. Transcriptional profiling of aging in human muscle revelas a common aging signature. *Plos Genetics*, **2**, 1058–1069.

ZALK, R., CLARKE, O.B., DES GEORGES, A., GRASSUCCI, R.A., REIKEN, S., MANCIA, F., HENDRICKSON, W.A., FRANK, J. & MARKS, A.R. 2015. Structure of a mammalian ryanodine receptor. *Nature*, **517**, 44–49.

ZHAO, X., WEISLEDER, N., THORNTON, A., OPPONG, Y., CAMPBELL, R., MA, J. & BROTTO, M. 2008. Compromised store-operated calcium entry in aged skeletal muscle. *Aging Cell*, **7**, 561–568.

ZHOU, H., JUNGBLUTH, H., SEWRY, C.A., FENG, L., BERTINI, E., BUSHBY, K., STRAUB, V., ROPER, H., ROSE, M.R., BROCKINGTON, M., KINALI, M., MANZUR, A., ROBB, S., APPLETON, R., MESSINA, S., D'AMICO, A., QUINLIVAN, R., SWASH, M., MULLER, C.R., BROWN, S., TREVES, S. & MUNTONI, F. 2007. Molecular mechanisms and phenotypic variation in RYR1-related congenital myopathies. *Brain*, **130**, 2024–2036.

ZUO, L. & PANNELL, B.K. 2015. Redox characterization of functioning skeletal muscle. *Frontiers in Physiology*, **6**, 1–9.

ZUO, L., SHIAH, A., ROBERTS, W.J., CHIEN, M.T., WAGNER, P.D. & HOGAN, M.C. 2013. Low Po(2) conditions induce reactive oxygen species formation during contractions in single skeletal muscle fibers. *American Journal of Physiology - Regulatory, Integrative and Comparative Physiology*, **304**, R1009–R1016.

ZVARITCH, E., DEPREUX, F., KRAEVA, N., LOY, R.E., GOONASEKERA, S.A., BONCOMPAGNI, S., KRAEV, A., GRAMOLINI, A. O., DIRKSEN, R. T., FRANZINI-ARMSTRONG, C., SEIDMAN, C.E., SEIDMAN, J.G. & MACLENNAN, D.H. 2007. An Ryr1I4895T mutation abolishes Ca2+ release channel function and delays development in homozygous offspring of a mutant mouse line. *Proceedings of the National Academy of Sciences of the United States of America*, **104**, 18537–

18542.

ZVARITCH, E., KRAEVA, N., BOMBARDIER, E., MCCLOY, R.A., DEPREUX, F., HOLMYARD, D., KRAEV, A., SEIDMAN, C.E., SEIDMAN, J.G. & TUPLING, A.R. 2009. Ca2+ dysregulation in Ryr1(I4895T/wt) mice causes congenital myopathy with progressive formation of minicores, cores, and nemaline rods. *Procedings of the National Academy of Science*, **106**, 21813–21818.

Appendix A: Ethical approval for use of IVCT biopsy material

NHS

National Research Ethics Service

Leeds (East) Research Ethics Committee
Yorkshire and Humber REC Office
First Floor, Millside
Mill Pond Lane
Meanwood
Leeds
LS6 4RA

Telephone: 0113 3050166

30 November 2010

Professor Philip Hopkins
Professor of Anaesthesia, Honorary Consultant Anaesthetist
University of Leeds
Academic Unit of Anaesthesia
Clinical Sciences Department
St Jame's University Hospital
LS9 7TF

Dear Professor Hopkins

Study Title:	**Human tissues & genomics research in malignant hyperthermia**
REC reference number:	**10/H1306/70**

Thank you for your email of 17 and 30 November 2010, responding to the Committee's request for further information on the above research and submitting revised documentation.

Confirmation of ethical opinion

On behalf of the Committee, I am pleased to confirm a favourable ethical opinion for the above research on the basis described in the application form, protocol and supporting documentation as revised, subject to the conditions specified below.

Ethical review of research sites

The favourable opinion applies to all NHS sites taking part in the study, subject to management permission being obtained from the NHS/HSC R&D office prior to the start of the study (see "Conditions of the favourable opinion" below).

Conditions of the favourable opinion

The favourable opinion is subject to the following conditions being met prior to the start of the study.

Management permission or approval must be obtained from each host organisation prior to the start of the study at the site concerned.

For NHS research sites only, management permission for research ("R&D approval") should be obtained from the relevant care organisation(s) in accordance with NHS research governance arrangements. Guidance on applying for NHS permission for research is available in the Integrated Research Application System or at http://www.rdforum.nhs.uk.

I

Where the only involvement of the NHS organisation is as a Participant Identification Centre (PIC), management permission for research is not required but the R&D office should be notified of the study and agree to the organisation's involvement. Guidance on procedures for PICs is available in IRAS. Further advice should be sought from the R&D office where necessary.

Sponsors are not required to notify the Committee of approvals from host organisations.

It is the responsibility of the sponsor to ensure that all the conditions are complied with before the start of the study or its initiation at a particular site (as applicable).

Approved documents

The final list of documents reviewed and approved by the Committee is as follows:

Document	Version	Date
Protocol	1.0	18 August 2010
Response to Request for Further Information		
Participant Information Sheet: Parent Information sheet	2.0	16 August 2010
GP/Consultant Information Sheets	2	11 November 2010
Investigator CV	0.3	24 November 2005
Participant Consent Form: Patient Assent From	3.0	16 August 2010
Participant Consent Form: Genetics of malignant hyperthermia	2.2	11 November 2010
Participant Consent Form	4.0	16 August 2010
Letter to GP		21 June 2010
Patient assent form- genetics of malignant hyperthermia	3.2	11 November 2010
Evidence of insurance or indemnity		26 July 2010
Referees or other scientific critique report		17 August 2010
REC application		
Participant Information Sheet: Patient Information sheet (under 16years)	3.0	16 August 2010
Participant Information Sheet: Patient Information sheet	4.0	16 August 2010
Participant Consent Form: Genetics of malignant hyperthermia	4.2	11 November 2010
Participant Consent Form: Genetics of malignant hyperthermia	1.2	11 November 2008
Covering Letter		02 September 2010
Covering Letter		17 November 2010
Letter from Sponsor		27 August 2010
Research License form University of Leeds		
Family member letter	4.2	11 November 2010

Statement of compliance

The Committee is constituted in accordance with the Governance Arrangements for Research Ethics Committees (July 2001) and complies fully with the Standard Operating Procedures for Research Ethics Committees in the UK.

After ethical review

Now that you have completed the application process please visit the National Research Ethics Service website > After Review

You are invited to give your view of the service that you have received from the National Research Ethics Service and the application procedure. If you wish to make your views known please use the feedback form available on the website.

The attached document *"After ethical review – guidance for researchers"* gives detailed guidance on reporting requirements for studies with a favourable opinion, including:

- Notifying substantial amendments
- Adding new sites and investigators
- Progress and safety reports
- Notifying the end of the study

The NRES website also provides guidance on these topics, which is updated in the light of changes in reporting requirements or procedures.

We would also like to inform you that we consult regularly with stakeholders to improve our service. If you would like to join our Reference Group please email referencegroup@nres.npsa.nhs.uk.

10/H1306/70	Please quote this number on all correspondence

With the Committee's best wishes for the success of this project

Yours sincerely

Dr Carol Chu
Chair

Email: Charlene.morgan@leedspft.nhs.uk

Enclosures: "After ethical review – guidance for researchers" *SL- AR2*

Copy to: *Mrs Rachel De Souza*
Level 10, Room 10.110 Worsley Building
Clarendon Way
University of Leeds
LS2 9NL

Appendix B: Patient consent form for use of muscle biopsy tissue for research purposes

The Leeds Teaching Hospitals **NHS**
NHS Trust

Leeds Institute of Molecular Medicine   UNIVERSITY OF LEEDS

PATIENT CONSENT FORM

Malignant Hyperthermia Unit

Level 08, Clinical Sciences Building

St James's University Hospital

LEEDS LS9 7TF

(Version 1.2, 11.11.2010)

Genetics of malignant hyperthermia

Patient name: …..…………………………………..   Initials: ………

Date of Birth: ………………............………………….

Please initial each box

1. I confirm that I have read and understand the information sheet dated 11.11.2010 (version 1.2) for the above study. I have had the opportunity to consider the information, ask questions and have had these answered satisfactorily.

2. I understand that my participation is voluntary and that I am free to withdraw at any time without my medical care or legal rights being affected.

3. I understand that relevant sections of my medical notes and data collected during the study, may be looked at by individuals from the sponsor for the study or by regulatory bodies, where it is relevant to my taking part in this research. I give permission for these individuals to have access to my records. I also give permission for a copy of this consent form to be sent to the Sponsor for the study.

4. I understand that my tissues will be stored for the duration of this research. I consent to my tissues being retained at the end of the study for future research approved by the regulatory authorities.

5. I consent to samples of my tissues, with all personal information removed, being sent to laboratories in the UK, Europe or the USA.

6. I consent to the storage including electronic, of personal information for the purposes of this study. I understand that any information that could identify me will be kept strictly confidential and that no personal information will be included in the study report or other publication.

7. I agree to allow the use of any information or results arising from this study for healthcare and/or medical research purposes. I understand that my identity will remain anonymous.

8. I understand that I will be contacted if any results from the research may be to my clinical benefit or to the benefit of my relatives.

9.   I agree to take part in the study

Signatures:

Name of patient	Date	Signature
Name of Person taking Consent (if different from the Principal Investigator)	Date	Signature

(Original to be retained and filed in the site file, 1 copy to patient, 1 copy to be filed in patient's notes, 1 copy for Sponsor)

IV